

*Final Report*

***High Strength Steel Welding Research***

*Submitted to:*  
*Dr. George Yoder*  
*Office of Naval Research*  
*Arlington, Virginia 22217*

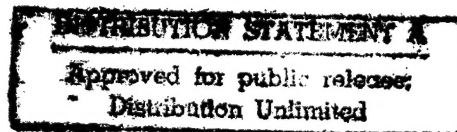
*Submitted by:*  
*Glen R. Edwards, David L. Olson and Stephen Liu*  
*Center for Welding, Joining and Coatings Research*  
*Colorado School of Mines*  
*Golden, Colorado 80401*

*Research Performed under Contract:*  
*N00014-95-1-0592*

*August 1998*

19981030 001

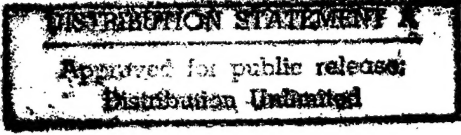
CSM



**CENTER FOR WELDING, JOINING  
AND COATINGS RESEARCH**

Colorado School of Mines  
Golden, Colorado 80401

Public reporting burden for this collection of information is estimated to average 1 hour per response, including the time for reviewing instructions, searching existing data sources, gathering and maintaining the data needed, and completing and reviewing the collection of information. Send comments regarding this burden estimate or any other aspect of this collection of information, including suggestions for reducing this burden to Washington Headquarters Services, Directorate for Information Operations and Reports, 1215 Jefferson Davis Highway, Suite 1204, Arlington, VA 22202-4302, and to the Office of Management and Budget, Paperwork Reduction Project (0704-0188), Washington, DC 20503. **DMS**

1. AGENCY USE ONLY (Leave blank)		2. REPORT DATE August, 1998		3. REPORT TYPE AND DATES COVERED Final:3/1/95 - 2/28/98	
4. TITLE AND SUBTITLE High Strength Steel Welding Research				5. FUNDING NUMBERS N00014-95-1-0542	
6. AUTHOR(S) Glen R. Edwards, David L. Olson, Stephen Liu					
7. PERFORMING ORGANIZATION NAMES(S) AND ADDRESS(ES) Colorado School of Mines Center for Welding, Joining and Coatings Research Golden, CO 80401				8. PERFORMING ORGANIZATION REPORT NUMBER MT-CWJCR-098-024	
9. SPONSORING / MONITORING AGENCY NAMES(S) AND ADDRESS(ES) Office of Naval Research Dr. George Yoder Arlington, Virginia 22217				10. SPONSORING / MONITORING AGENCY REPORT NUMBER	
11. SUPPLEMENTARY NOTES					
a. DISTRIBUTION / AVAILABILITY STATEMENT  ONR Seattle SEP 02 1998				12. DISTRIBUTION CODE	
13. ABSTRACT (Maximum 200 words) By optimizing the contents of microalloying elements and elements that promote dual precipitation, a family of welding consumables with excellent characteristics were developed. These electrodes were insensitive to moderate variations in chemical composition or cooling rate, had acceptable strength and impact toughness, and exhibited more uniform mechanical properties throughout the entire weldment cross-section, including the reheated weld zones. An electrode containing 1.25 wt. pct. Mn, 2 wt. pct. Ni, 0.5 wt. pct. Mo, and reduced nitrogen met the project mechanical property requirements (yield strength: 88 to 115 ksi; Charpy impact energy: 60 ft-lb at 0°F and 35 ft-lb at -60°F). Adding 1.0 wt. pct. Cu and 0.03 wt. pct. Nb as dual precipitation agents, a consumable with 0.03 wt. pct. C, 1.25 wt. pct. Mn, 0.28 wt. pct. Si, 1.5 wt. pct. Ni, 0.50 wt. pct. Mo, Ti between the 240 and 400 ppm range, and N below 80 ppm, also easily met the Navy requirements. To improve hydrogen management in high strength steel welding, CSM investigated the following three metallurgical practices: 1) use of fluoride additives to control hydrogen in arc welding plasmas, 2) adjustment of the martensite start temperature for hydrogen control, and 3) hydrogen trapping in high strength steel weldments. These concepts were incorporated in the design of innovative consumables for experimentation. Welding electrodes containing five percent cryolite, K <sub>3</sub> AlF <sub>6</sub> , reduced weld metal diffusible hydrogen content by approximately 25 percent. Results obtained using KF and MnF <sub>3</sub> additions were even more encouraging, with over 40 percent reduction of diffusible hydrogen content. The addition of 0.1 wt. pct. yttrium as hydrogen trap resulted in a fifty- percent reduction of diffusible hydrogen, from 6.7 ml to 3.1 H <sub>2</sub> /100g. Addition of 0.2 wt. pct. yttrium reduced the diffusible hydrogen content even more significantly, to 1 ml H <sub>2</sub> /100g. Hydrogen thermal desorption analysis (TDA) verified that rare earth oxides form deep hydrogen traps, which potentially prevent hydrogen atoms from reaching crack initiation sites during a thermal cycle.					
14. SUBJECT TERMS hydrogen trapping, fluoride additives, high strength steel welding, dual precipitation, welding consumables, hydrogen management, martensite start emperature, impact toughness				15. NUMBER OF PAGES ±200	
				16. PRICE CODE	
17. SECURITY CLASSIFICATION OF REPORT		18. SECURITY CLASSIFICATION OF THIS PAGE		19. SECURITY CLASSIFICATION OF ABSTRACT	
				20. LIMITATION OF ABSTRACT	



## Table of Contents

	Page
1) Statement of the Problem	4
a) Advanced Welding Consumables	5
i) Optimized HSLA Steel SMAW Consumable	5
ii) Dual Precipitation Strengthening	5
b) Hydrogen Management	6
i) Use of Fluorides to Control Hydrogen in Arc Welding Plasmas	6
ii) Adjustment of the Martensite Start Temperature for Hydrogen Control	6
iii) Hydrogen Trapping in High Strength Steel Weld Metals	7
2) Experimental Approach and Summary of the Most Important Results	8
a) Advanced Welding Consumables	8
i) Optimized HSLA Steel SMAW Consumable	8
(1) Materials and Testing	8
Electrodes and Test Weldments	8
Tensile and Charpy V-notch Impact Testing	9
Metallographic Characterization	9
(2) Results and Discussion	11
Mechanical Properties: Original Matrix	11
Mechanical Properties: Modified Compositions	11
Microstructure: Traditional Characterization	12
Microstructure: Characterization with LePera's Reagent	12
Fracture Propagation Control	13
ii) Dual Precipitation Strengthening	21
(1) Materials and Testing	21
Electrodes and Test Weldments	21
Mechanical Testing	22
Light and Electron Microscopy	22
(2) Results and Discussion	22
Effect of Dual Precipitation	22
Copper Precipitation in High Strength Steel Weldments	23
Electrical Resistance Measurements as a Function of Copper Precipitation	23
Weld Metal Microstructures	23
Mechanical Properties of Cu-Nb Enhanced High Strength Steel Welds	24
(3) Conclusions	25
b) Hydrogen Management	31
i) Use of Fluorides to Control Hydrogen in Arc Welding Plasmas	31
ii) Adjustment of the Martensite Start Temperature for Hydrogen Control	31

iii) Hydrogen Trapping in High Strength Steel Weld Metals	32
iv) Conclusions	33
3) List of Publications and Technical Reports	38
a) Advanced Welding Consumables	38
i) Optimized HSLA Steel SMAW Consumable	38
ii) Dual Precipitation Strengthening	38
b) Hydrogen Management	38
i) Use of Fluorides to Control Hydrogen in Arc Welding Plasmas	38
ii) Adjustment of the Martensite Start Temperature for Hydrogen Control	39
iii) Hydrogen Trapping in High Strength Steel Weld Metals	40

## HIGH STRENGTH STEEL WELDING RESEARCH

### 1. Statement of the Problem

The use of high strength steels in ships and submarines offers structural weight savings that can reduce cost or, alternatively, be used to increase payload or platform speed. Unfortunately, as the strength of the steel increases, acceptable welding operational envelopes become more restrictive and the steel weldments generally become more susceptible to degradation by hydrogen contamination. As a result, a complex array of strict welding production controls are currently necessary to circumvent the limitations of existing Navy high strength steel welding consumables. These controls significantly increase the cost of welding and underscore the need for weld metals whose properties and cracking resistance are independent of the techniques and conditions used to produce the weld.

The High Strength Steel Welding Research Program at CSM has contributed significantly toward enhancements in the fabrication of surface and undersea vessels. The program has shown ways to reduce acquisition, maintenance, and repair costs of HSLA steel structures of ship, submarine and commercial infrastructure by reducing or eliminating stringent welding requirements. The technical goals of this program have been elimination of pre- and post-weld heat treatments, improved hydrogen management, increased productivity associated with welding over expanded operating ranges, and reduced requirements for welder training and quality assurance. This research has developed consumables for SMA welding using three different concepts: 1) microalloying, 2) dual-phase precipitation, and 3) hydrogen gettering.

The primary objectives of this research were to improve the mechanical properties of multipass high strength steel weld metals, and to develop a family of high strength steel welding consumables capable of depositing robust weld metals that were insensitive to moderate variations in chemical composition or cooling rate, and more resistant to hydrogen-induced cracking. Cost savings will result from elimination of the preheating and postweld heat treatments, improved hydrogen management, increased productivity associated with welding over expanded operating ranges, and reduced requirements for welder training and quality assurance.

To achieve these goals, this research work focused upon two related areas:

1) Advanced Welding Consumables, and 2) Hydrogen Management.

## 1.a. Advanced Welding Consumables

The Advanced Welding Consumables effort has evaluated two concepts:

1) Optimized HSLA Steel Welding Consumables and 2) Dual Precipitation Strengthening.

### 1.a.i. Optimized HSLA Steel SMAW Consumable

The ability to produce high strength, high toughness, SMA welds using Ni-Mo-Ti electrodes based on a 1.5Mn, 3.0Ni, 0.5Mo composition (in wt.pct.) with low carbon and minor titanium additions, has been demonstrated for weld metals needing yield strengths in excess of 690 MPa (100 ksi). Optimal toughness was obtained at titanium levels of 30 ppm and 240 to 400 ppm. However, because of the relatively high alloy levels, the hardenability of these filler metals may result in higher than desired strength deposits with increasing concerns over hydrogen cracking susceptibility.

The goal of this task was to develop a leaner, lower strength (88 to 115 ksi yield) filler metal exhibiting high low temperature toughness and insensitivity to welding heat input. These consumables must be suitable for welding HSLA-80 and for undermatching applications with HSLA-100 and HY-100, without preheat/interpass requirements

### 1.a.ii. Dual Precipitation Strengthening

The economic fabrication of steel structures possessing yield strengths greater than 690 MPa (100 ksi) depends upon the development of adequate welding consumables suitable for high heat input processing. It is well known that welding of high strength steels does not consistently produce weldments with combined acceptable strength and toughness. At lower heat inputs, the minimum strength criterion can easily be achieved, but the weld metal generally exhibits poor toughness. Conversely at higher heat inputs, weld metal is produced with good toughness but poor strength. The resulting heat input window within which acceptable values for both strength and toughness can be achieved is severely restrictive. In multipass welding, the multiple thermal cycles can also result in mechanical property fluctuations in the reheated zones that must be minimized for consistent performance.

The goal of this task was to optimize copper and niobium additions to the filler metals such that the welds developed acceptable strength and impact toughness, as well as uniform mechanical properties throughout the entire weldment cross-section. To ensure these characteristics, this research work considered filler

metals containing alloying elements that promoted dual precipitation of  $\epsilon$ -copper and niobium carbide.

### 1.b. Hydrogen Management

To improve hydrogen management in high strength steel welding, CSM investigated three metallurgical practices developed to assist the design of welding consumables. The following three areas of investigation were :

- i. use of fluoride additives to control hydrogen in arc welding plasmas,
- ii. adjustment of the martensite start temperature for hydrogen control, and
- iii. hydrogen trapping in high strength steel weldments

#### *1.b.i. Use of Fluorides to Control Hydrogen in Arc Welding Plasmas*

To control hydrogen in the arc plasma, ingredients that decompose readily in the arc and react with hydrogen can be added to welding consumable fluxes. Selected fluorides have been evaluated, since they release fluorine gas, which has high affinity to react with hydrogen. This reaction decreases the hydrogen available to contaminate the weld pool. In addition, the reaction product, hydrogen fluoride gas (HF), has very low solubility in liquid steel, and thus will not affect the mechanical property of the weldment. Fluorides that will effectively remove hydrogen from the arc stream were identified through thermochemical calculations, as well as through experimental research on fluorides inserted into flux-cored welding electrodes.

#### *1.b.ii. Adjustment of the Martensite Start Temperature for Hydrogen Control*

During the cooling cycle, hydrogen atoms must migrate through a composite of different phases (austenite, ferrite or martensite) because of the compositional mismatch between weld metal and base metal. Complications arise because the time and temperature at which the weld metal and the base metal transform from austenite to lower transformation temperature products, such as martensite, are different. Hydrogen transport across these phases is critical because of the large difference in hydrogen solubility and diffusivity between austenite and ferrite or martensite. This investigation aimed to calculate hydrogen distribution across the weldment, through numerical modeling, for different values of martensite start temperatures of the weld metal and the heat affected zone (HAZ). Depending upon the actual martensite start temperatures and the difference between that of the weld metal and the HAZ, hydrogen can either be accumulated in the weld metal or in the HAZ. By properly selecting the consumable composition relative to the base metal, the optimal hydrogen distribution in a weldment can be achieved.

### *1.b.iii. Hydrogen Trapping in High Strength Steel Weld Metals*

Hydrogen cracking in high strength steel welding can still occur even though hydrogen contamination during the welding process is low. The primary cause of this problem is the presence of regions of high stress concentration, such as notches, grain boundaries, etc., which attract diffusible hydrogen and increase localized accumulation of hydrogen. These high stress concentration points can also behave as crack initiation sites.

Introduction of hydrogen traps to the weld metal is intended to prevent hydrogen localization by assuring that the hydrogen is trapped at finely distributed trap sites. In this way, hydrogen atoms are more uniformly distributed, without exceeding a critical level for cracking at any particular location. A potential trap must possess a high binding energy for hydrogen, so that it can quickly minimize diffusible hydrogen, either in single pass or in multipass welding.

Potential hydrogen traps, such as titanium or vanadium carbides and yttrium or neodymium oxides, were selected to experimentally demonstrate the effectiveness of hydrogen trapping in reducing diffusible hydrogen. TiC has been identified as a strong hydrogen trap site in wrought steel with a trap binding energy as high as 100 kJ/mole. Similarly, VC has been used to manage hydrogen in very high strength wrought steel. Neodymium and yttrium oxides have been calculated to have trap binding energies as high as 130 kJ/mole and show promise as weld metal traps.



## 2. Experimental Approach and Summary of the Most Important Results

### 2.a. Advanced Welding Consumables

A fundamental and systematic approach has been used to evaluate the effect of electrode formulation, weld metal chemical composition, as-deposited microstructure, heat input and interpass temperature on the mechanical properties of high strength steel weld metals.

#### 2.a.i. Optimized HSLA Steel SMAW Consumable

An experimental matrix of SMAW multipass weldments was fabricated, characterized and evaluated. Compositions of the welding consumables, based on a low carbon (< 0.06 wt. pct.) formulation, were systematically varied to provide data concerning the influence of weld metal composition and thermal history on weld metal microstructure, mechanical properties, and fracture behavior.

##### 2.a.i.1. Materials and Testing

###### *Electrodes and Test Weldments*

Experimental basic type electrodes were prepared to yield multipass SMA weld metals with nominal compositions ranging in alloy content from 2.0 to 3.0 wt. pct. nickel and 1.0 to 1.5 wt. pct. manganese. Nine compositions were evaluated. Both low heat input (1 kJ/mm with ambient preheat and interpass temperatures), and high heat input (2.2 kJ/mm with 150°C preheat and interpass temperatures) test weldments were produced. The welds were prepared in accordance with ISO 2560. Base plates were plain carbon steel. Since ISO 2560 does not address requirements for buttering of plates, the weld bevels were buttered according to the requirements of AWS 5.1 (Figure 2), with the electrodes to be tested.

All filler metals were fabricated to produce as-deposited welds containing between 240 and 400 ppm titanium. Research in C-Mn and 1.5Mn-3.0Ni-0.5Mo SMA welding consumables has demonstrated that optimal toughness is achieved within this range of titanium. Other alloying additions were controlled to the following limits: 0.5 wt. pct. molybdenum; 0.3 wt. pct. max. silicon. Copper, chromium, boron, niobium, aluminum, and vanadium were maintained at the lowest achievable levels. Nitrogen was targeted to remain below 100 ppm.

When ferro-titanium additions were made to the electrode covering, difficulty in maintaining as-deposited nitrogen levels below 100 ppm was encountered. With

as-deposited titanium levels ranging from 110 to 220 in the low heat input welds and 150 to 240 ppm in the high heat input welds, the feasibility of reducing nitrogen by making titanium metal additions to the electrode covering was investigated. Testing of welds fabricated with the 2.0Ni-1.25Mn electrode was repeated at both the low and high heat inputs with titanium metal in the electrode covering. Additionally, to further reduce the weld metal yield strength and optimize toughness, the 2.0Ni-1.25Mn electrode test welds were repeated with a reduced molybdenum content of 0.25 wt. pct. at both typical and low nitrogen levels.

Weld metal compositions were analyzed using a combination of spark emission spectroscopy, atomic absorption spectroscopy, and various Leco interstitial analyzers.

#### *Tensile and Charpy V-notch Impact Testing*

A full size (0.5 in. dia.) tensile specimen and fourteen full size Charpy V-notch specimens were machined from mid-plate for each of the test weldments. The tensile samples were tested at room temperature. The Charpy specimens were tested at different temperatures over a range from -196°C to room temperature to develop energy versus temperature transition curves. Tensile and Charpy V-notch testing was conducted in accordance with the requirements of ASTM A370.

The specified project goal was to develop SMA welding consumables that are capable of producing as-deposited multipass welds with a yield strength in the range of 88-115 ksi, a minimum of 20 percent elongation, and minimum Charpy V-notch impact toughness of 60 ft-lb (81 J) at 0°F and 35 ft-lb (48 J) at -60°F.

#### *Metallographic Characterization*

The strength and toughness of fabricated weldments is dependent upon the microstructure of the deposit. An understanding of the microstructural evolution in low alloy steel welds is necessary to correlate the effects of alloy content and thermal cycle as they relate to the properties of the deposited weld metal. Microstructural development involves a sequence of transformation reactions which include: inclusion formation, delta ferrite formation, austenite formation and transformation of austenite to the various decomposition products.

Normally, the microstructure formed within each austenite grain will be a complex mixture of two or more constituents. The identification and quantification of the various microstructural constituents was mainly done by light microscopy, and occasionally by scanning electron microscopy.

Metallographic samples were prepared from the fractured Charpy specimens. The Charpy specimens were sectioned mid-sample, perpendicular to the notch, and mounted so as to be viewed in the short transverse (through thickness) direction. Samples were prepared by grinding through 600 grit, then polishing through  $0.05\mu\text{m}$  alumina. When available, macrosections cut perpendicular to the welding direction were ground and polished through  $0.05\mu\text{m}$  alumina to allow for analysis of the top bead microstructures.

Initial characterization of the microstructures was based upon a 2 percent nital etch (2 percent nitric acid in ethanol). Optical characterization was conducted at magnifications up to  $2000\times$ , but most characterization was performed at  $1000\times$ . The characterization of the major constituents was based on the classification scheme developed by the International Institute of Welding (IIW), Sub-Commission IX-J. The IIW scheme classifies the microstructures into six major classifications: primary ferrite (PF), acicular ferrite (AF), ferrite with second phase (FS), ferrite carbide aggregate (FC), and martensite (M). This assessment scheme is only intended for the classification of major constituents in the microstructures.

Standard etching techniques for low alloy steels, such as nital, usually accent grain boundaries. Classification of the various constituents is based on features such as aspect ratio, relative lath size, number of parallel laths, or relative position in the structure. To aid in the identification of retained austenite and untempered martensite, collectively referred to as "M-A", LePera's reagent, a tint etchant based on sodium metabisulfite mixed with picric acid was used. After being polished, etched in 2 percent nital, and examined, the specimens were repolished and etched in LePera's Reagent. LePera's Reagent consists of a mixture of 1% sodium metabisulfite in distilled water, and 4% picric acid in ethyl alcohol, in a 1:1 volume ratio. In this study, a mixture with a volume ratio of 1:2 (4% picric acid:1% sodium metabisulfite) was found to be more effective for these alloys. The mixture must be prepared immediately before use, and then discarded. Etch times ranged from 30 to 60 seconds and were based upon the sample developing a uniform golden-tan color.

Area fractions of M-A constituent were determined by image analysis from optical photomicrographs taken at  $1000\times$  and compared to XRD results. Image analysis was performed by scanning the photomicrographs at 200 dpi and processing the digitized image with Adobe Photoshop. The specimens for XRD were prepared by standard polishing techniques followed by electropolishing to provide a stress-free surface. X-ray diffractograms were taken with a Phillips PW-1050 diffractometer operating in scan-step mode with  $\text{Cu-K}_\alpha$  radiation. The  $\text{K}_\beta$  was removed by graphite monochromator. The Rietveld program was used for structure refinement and determination of the lattice parameters.

Electron microscopy, both SEM and STEM were done on longitudinal sections, which were removed near the grip ends of the tensile specimens. Scanning electron microscopy was done on samples that were polished, etched in 2% nital, and gold sputter coated to enhance contrast. A wavelength dispersive X-ray (WDX) trace for iron, nickel, manganese, and molybdenum was performed on a selected sample which had been repolished but unetched. Foils for STEM were made by turning the end section of the tensile specimen by lathe down to 3 mm diameter. The 100  $\mu$ m discs were cut from the turned tensile specimens, ground to reduce thickness, and finally thinned in a twin-jet electropolisher with an electrolyte of 30 ml perchloric acid, 500 ml butyl alcohol, and 300 ml methyl alcohol. STEM was done using a Phillips CM200 scanning electron microscope with an accelerating voltage of 200 kV.

## 2.a.i.2. Results and Discussion

### *Mechanical Properties: Original Matrix*

Tensile and Charpy V-notch test results from the original test matrix are summarized in Figures 1 and 2. Charpy V-notch toughness significantly exceeded specified project requirements for all compositions at both heat inputs.

In the original test series, all electrode compositions met the project strength requirements at 2.2 kJ/mm heat input. At the low heat input (1 kJ/mm) one filler metal, nominal 1 Mn-2 Ni, met the project requirements and one other, nominal 1.25 Mn-2 Ni, was only slightly above (116,700 psi) the specified strength range.

### *Mechanical Properties: Modified Compositions*

To investigate whether the nominal 1.25 Mn-2 Ni, weld metal composition could be modified to meet the project yield strength requirements and to optimize toughness, the 2.0Ni-1.25Mn electrode test welds were repeated with a reduced molybdenum content of 0.25 wt. pct. at both typical and low nitrogen levels. These filler metals did not meet the minimum strength requirements at one of the two heat input conditions.

A reduced nitrogen version of the nominal 1.25 Mn-2 Ni-0.5 Mo electrode met the project strength requirements at both the high and low heat inputs. While a low nitrogen version of the nominal 1.0 Mn-2 Ni-0.5 Mo filler metal has not been produced nor tested, it is anticipated that this composition would not drop below the 88ksi minimum yield strength requirement.

The beneficial effect of reduced nitrogen is verified by the improvement in 70J transition temperature for both the original 1.25 Mn-2 Ni-0.5 Mo and the modified 1.25 Mn-2 Ni-0.25 Mo electrodes.

The mechanical properties of these modified compositions are summarized in Figure 3.

#### *Microstructure: Traditional Characterization*

As illustrated in Figures 4 and 5, microstructural characterization showed the expected trends with respect to primary ferrite. At the leaner compositions, approaching 2 Ni-1 Mn, primary ferrite approached 25 percent for the low heat input welds and 45 percent for the high heat input welds. In comparison, for the richest alloy compositions, primary ferrite levels were as low as 4 percent. While the trends in primary ferrite fractions were as expected, the absolute percentages were higher than anticipated, especially at the 1.5 Mn-3 Ni composition where essentially no primary ferrite was expected. The trends with respect to acicular ferrite and ferrite with second phase were much more complex. Acicular ferrite percentages ranged from 21 to 61 percent for the high heat input welds, and 27 to 70 percent for the low heat input welds. Ferrite with second phase ranged from 25 to 56 percent for the high heat input welds and 18 to 69 percent for the low heat input welds.

#### *Microstructure: Characterization with LePera's Reagent*

A tint etchant based on sodium metabisulfite (modified LePera's Reagent) was used to enhance specific microstructural features which are not revealed by traditional nital or picral etches. Traditional etchants usually accent grain boundaries and are not typically used in the identification of microphases such as retained austenite. LePera's Reagent aids in the differentiation of the structures by tinting bainite "dark brown", ferrite "tan" and tempered martensite "black". Retained austenite and untempered martensite are not affected by the sodium metabisulfite and are left "white".

Figure 6 shows a comparison of the results from etching in 2% nital and LePera's Reagent. Figure 6a shows the mid-weld structure of the high heat input weld based on nominal composition of 2.5 wt. pct. nickel and 1.25 wt. pct. manganese as revealed by etching in 2% nital. The nital etch clearly delineates the ferrite grain boundaries; however, due to the lack of contrast difference and fine size, the M-A microphase cannot be reliably identified, even when examined at magnifications up to 2000x. Figure 6b shows the structure from the same region of the weld after etching with LePera's Reagent. With LePera's Reagent, the

ferrite grain boundaries are not strongly etched but the M-A constituent is readily identified as "white" in the structure.

Table 1. Comparison of Percentage Retained Austenite Measured by XRD to Percentage M-A Determined by Optical Image Analysis.

Nominal Composition	Heat Input (KJ/mm)	XRD (percent)	Optical Image Analysis (percent)
2Ni-1Mn	2.2	1.8 - 2.1	1.2
3Ni-1.5Mn	2.2	0.5 - 0.6	0.7
2Ni-1Mn	1	1.7 - 2.0	0.8
3Ni-1.5Mn	1	1.7 - 2.0	0.7

The results of image analysis and XRD are given in Table 1 for four samples representing the range of alloys and heat inputs considered in the welding program. A comparison of the results shows reasonable agreement. All of the samples contained less than two percent retained austenite, with one exception. As expected the optical image analysis resulted in lower quantities of retained austenite than XRD due to the inability to optically resolve very fine grains or very thin films of M-A.

#### *Fracture Propagation Control*

Transition temperature and lower shelf Charpy specimen fracture surfaces were evaluated by scanning electron microscopy. No correlation was noted between the presence of a specific microstructural constituent (microphase, oxide) and fracture initiation, although oxide inclusions were often noted at initiation sites.

Comparison of the fracture facet size with the transition temperature revealed a relationship similar to that modeled by Cottrell, as shown in Figure 7. This relationship suggests that the fracture behavior of the weld metal compositions studied, in the as-welded condition, is propagation controlled and not dependent upon specific local brittle zones for fracture initiation.



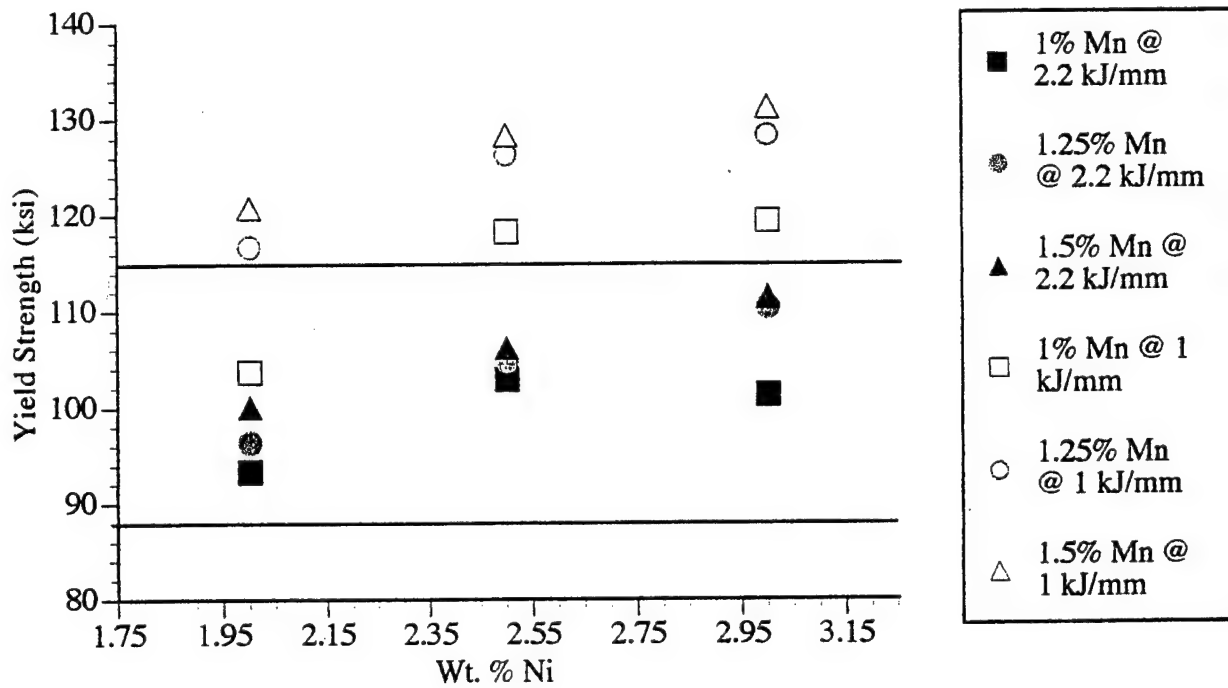
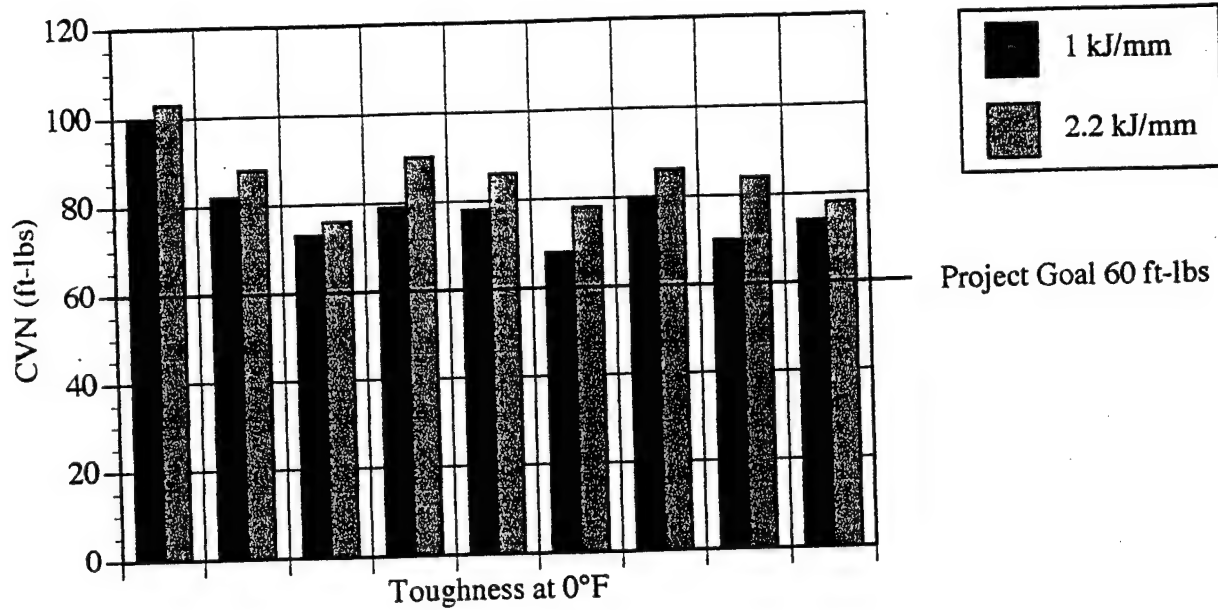
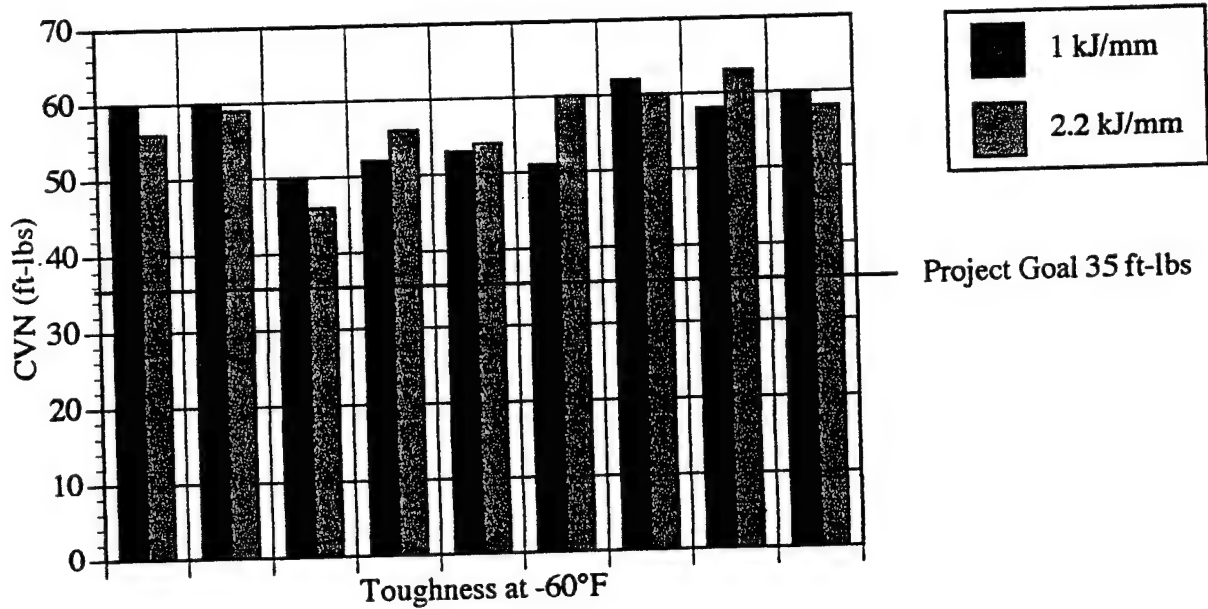


Figure 1: Summary of Yield Strengths for HSLA Steel SMAW Consumable

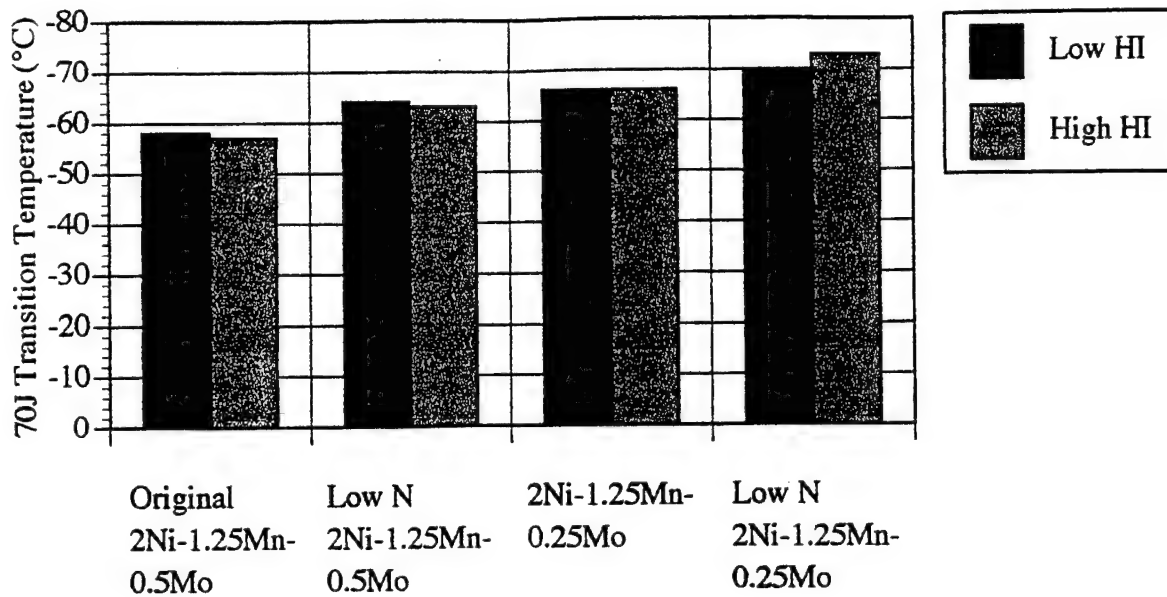


(a)

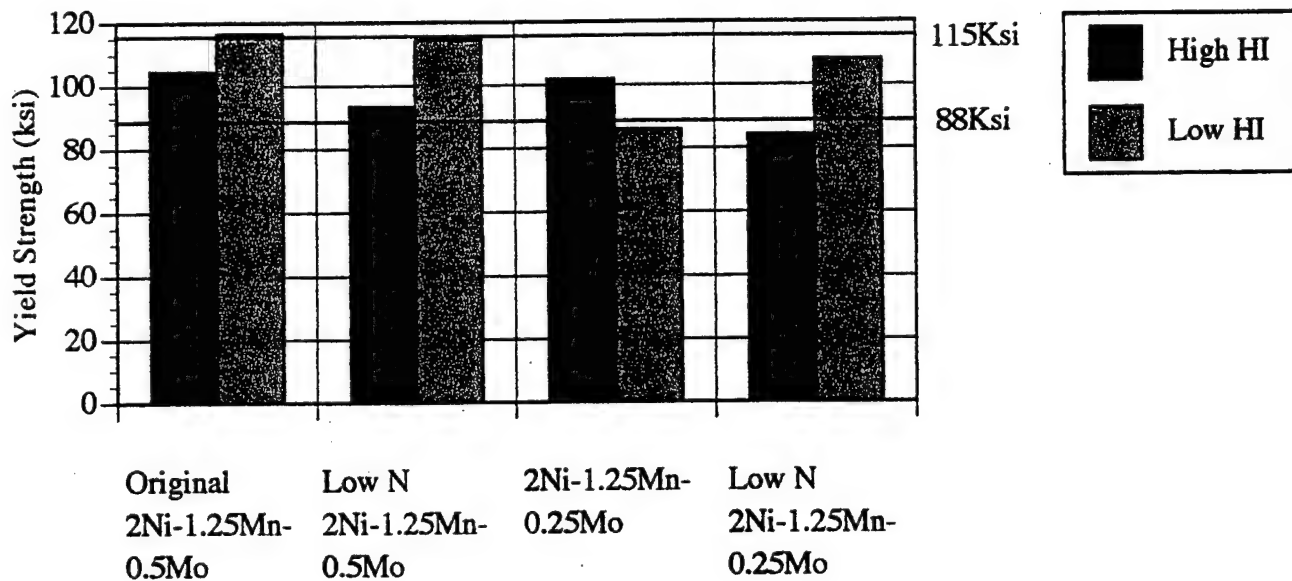


(b)

Figure 2: Summary of CVN energy for HSLA Steel SMAW Consumables at (a) 0°F and (b) -60°F



(a)



(b)

Figure 3: Summary of (a) 70J Transition Temperatures and (b) Yield Strength from Optimized HSLA Steel SMAW Consumables

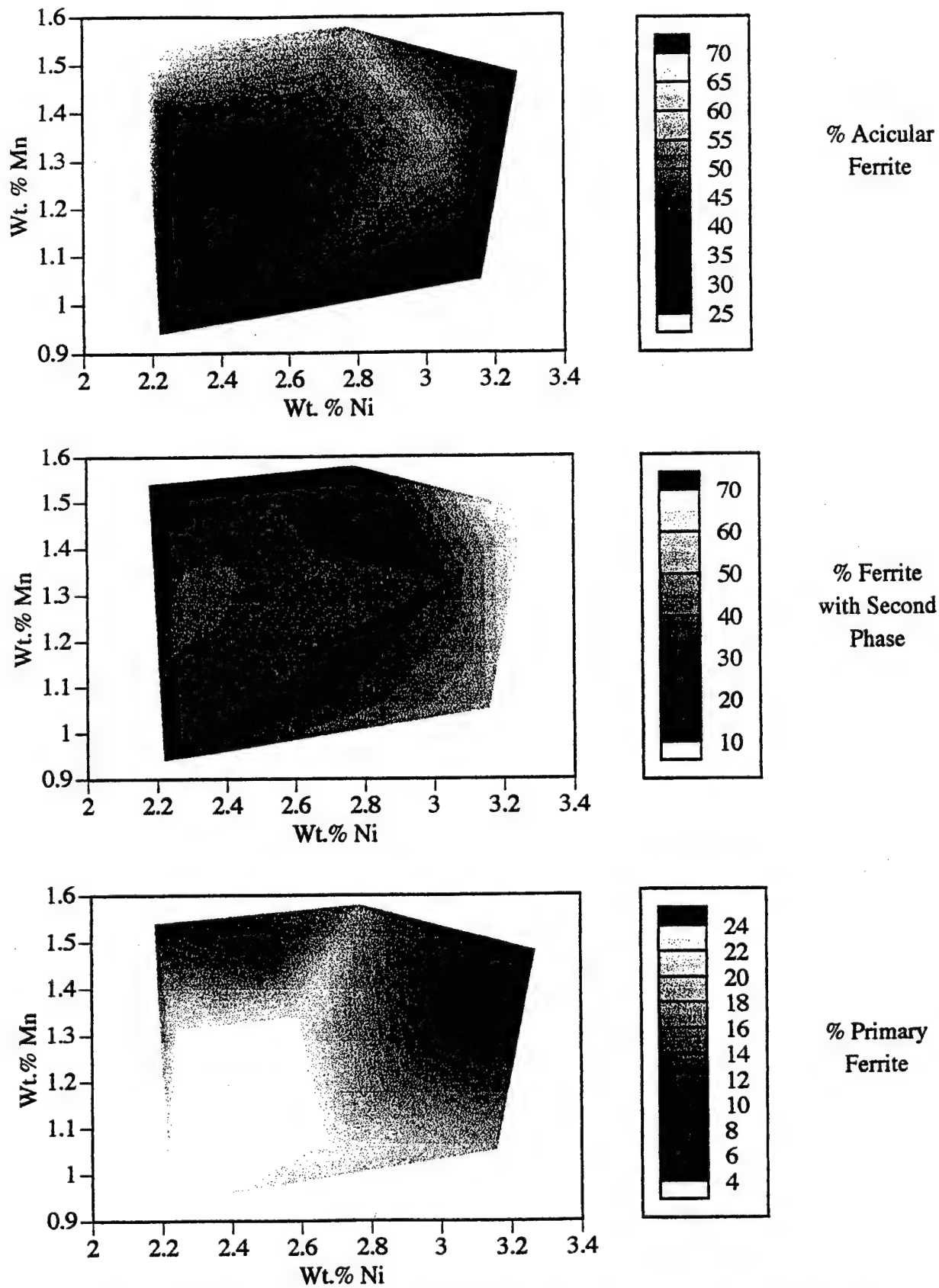


Figure 4: Summary of Major Microconstituents from Mid-Weld Microstructures from Low Heat Input Optimized HSLA Steel SMAW Consumables

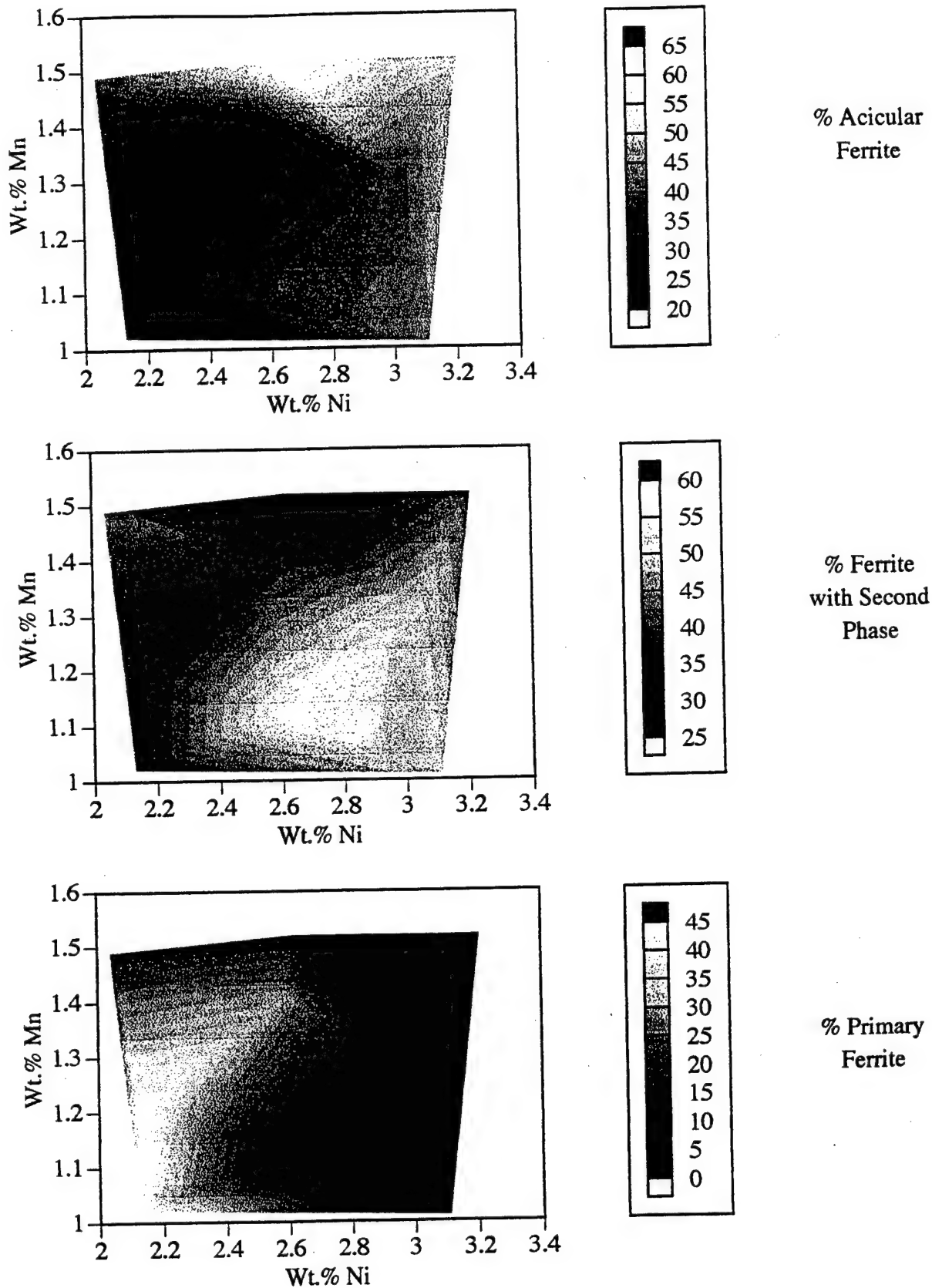
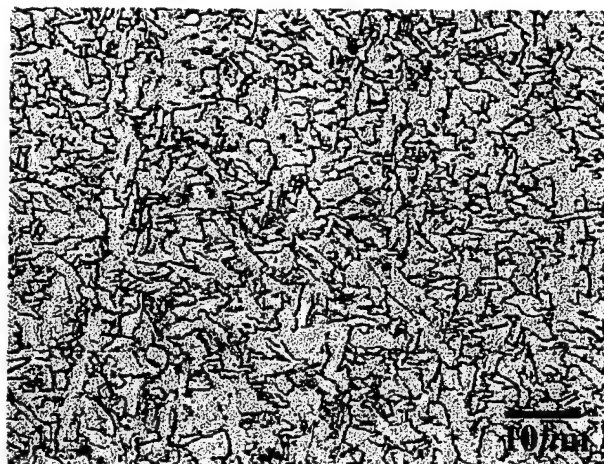
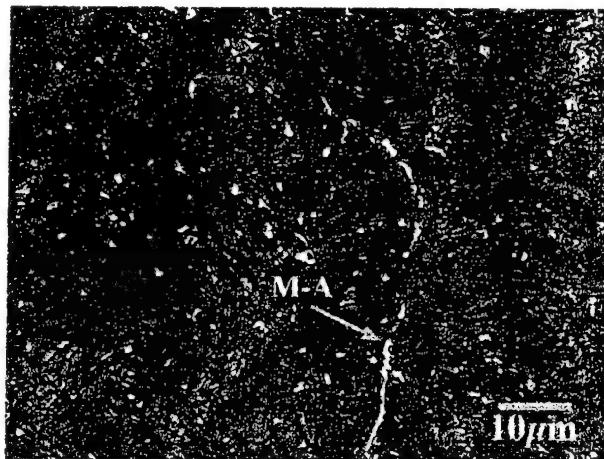


Figure 5: Summary of Major Microconstituents from Mid-Weld Microstructures from High Heat Input Optimized HSLA Steel SMAW Consumables



(a)



(b)

Figure 6. (a) Light micrograph showing weld metal microstructure as revealed by 2% nital and (b) as revealed by LePera's Reagent.



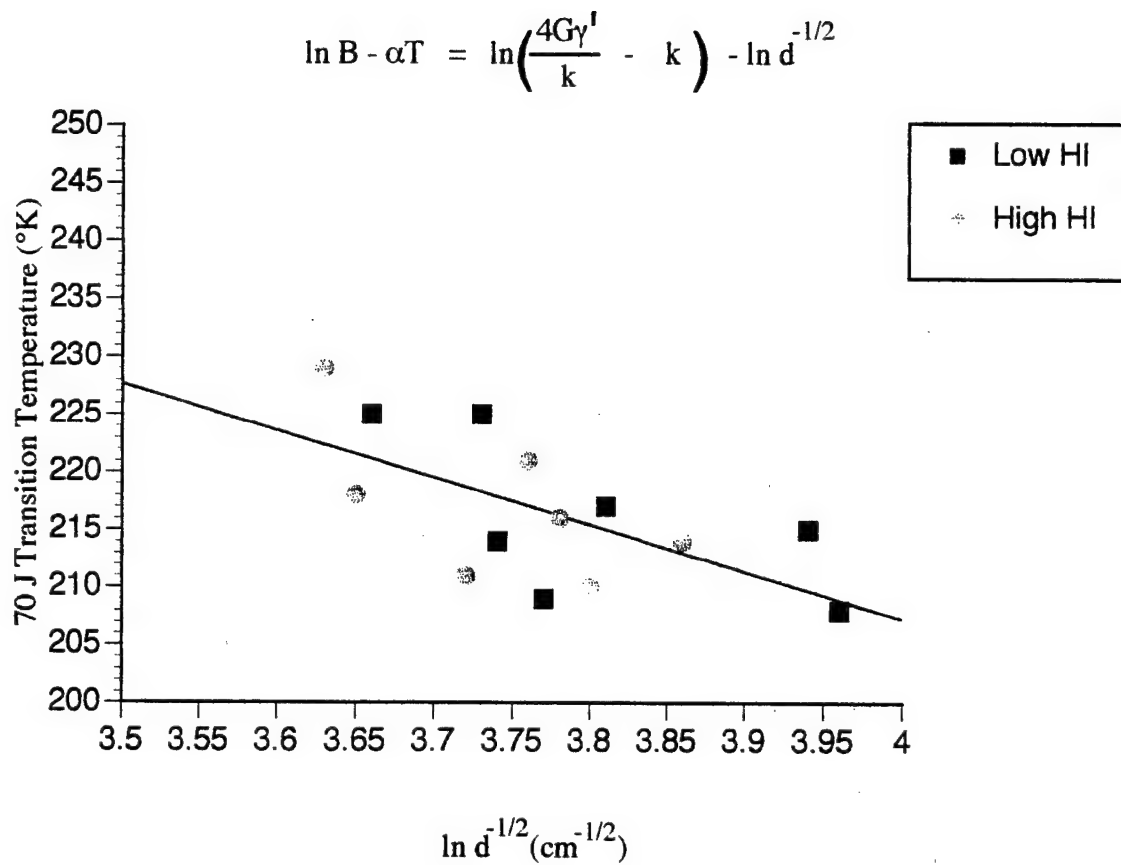


Figure 7: Comparison of Lower Shelf Charpy Sample Cleavage Facet Size versus 70 Joule Transition Temperature

## 2.a.ii. Dual Precipitation Strengthening

The goal of this task was to optimize copper and niobium additions in the filler metals such that the welds produced acceptable strength and impact toughness, and uniform mechanical properties throughout the entire weldment cross-section. To ensure these characteristics, this research work considered filler metals with alloying elements that promoted dual precipitation of  $\epsilon$ -copper and niobium carbide.

### 2.a.ii.1. Materials and Testing

#### *Electrodes and Test Weldments*

The effect of copper, as a single addition, was initially determined using GTAW and GMAW, while the effect of niobium was investigated using GMAW. The range of copper content varied between 0 and 5.5 wt. pct. and that of niobium, between 0 and 0.5 wt. pct. To characterize the combined effect of copper and niobium in multipass welding of high strength steels, additions of about 3.0 wt. pct. copper and about 0.06 wt. pct. niobium were made to the weld metal via experimental metal cored welding wires. The welds were evaluated with respect to their microstructure, austenite grain size, hardness, and chemical composition distribution. Isothermal heat treatments simulated the multiple thermal cycles experienced by the weldments. These welds were also used to examine the dual precipitation strengthening effect.

Subsequent to the GTAW, GMAW and MCAW experiments, the interim results were incorporated into the design matrix of experimental SMAW electrodes for the program. A total of three iterations of SMAW electrodes were produced for experimentation. Major elements in these electrodes included Ni, Mo, Cr, Nb, and Cu. The first batch of the welding electrodes consisted of twelve formulations with different levels of copper and niobium additions; i.e., 0 to 2.5 wt. pct. copper and 0 to 0.06 wt. pct. niobium. Chromium was removed from the second batch of electrode formulations, and the level of nickel and copper additions were adjusted to result in 1.0 to 3.0 wt. pct. and 1.0 to 2.0 wt. pct. in the weld metal, respectively. The niobium content was kept constant at 0.03 wt. pct. The third and final batch of electrodes had their carbon content lowered to 0.03 wt. pct. and the nitrogen content to 80 ppm. The nickel and copper contents of these welds were fine-tuned to the ranges of 1.0 to 2.2 wt. pct. and 0.8 to 1.0 wt. pct., respectively. To achieve the best combination of strength and toughness, the remaining composition was fixed at: 1.25 wt. pct. Mn, 0.28 wt. pct. Si, and 240 to 400 ppm Ti. The welds were fabricated using DCEP, and heat inputs of both 1.2 and 2.4 kJ/mm.

### *Mechanical Testing*

Tensile specimens were machined from the multipass weldments and tested at the rate of 0.2 in./min.

Standard full-size Charpy specimens were extracted from the multipass weldments. Impact tests were mainly conducted at -60°, -30°, and 0°F. Some extra specimens from selected weld specimens were also tested at -90°, 70°F and room temperature. The minimum mechanical property requirements are identical to those given in the "Optimized HSLA Steel SMAW Consumables" section.

Transverse cross-section hardness profiles were also obtained for each weld to determine any localized hardness fluctuations.

### *Light and Electron Microscopy*

Both light and electron microscopes were used to examine the bulk and fine microstructures of the welds produced. In particular, carbon extraction replicas were obtained to characterize the copper and niobium precipitates. Some thin foils were also prepared for high magnification observation of the precipitate-matrix relationship using TEM.

## 2.a.ii.2. Results and Discussion

### *Effect of Dual Precipitation*

The behavior of the weld metal that contained copper and niobium during multipass welding can be best illustrated by Figures 8 and 9. The data plotted in these figures were obtained using isothermal heat treatment simulation. In these figures, the hardness for the copper-enhanced and copper-niobium-enhanced weld metals were plotted as a function of the holding temperature and holding time. The shaded regions correspond to the intercritical reheated region of the weld metal. Notice that maximum softening in the reheated zone occurred at 675°C. Despite the fact that both the copper-enhanced and the copper-niobium-enhanced weld metal exhibited softening to some extent in this zone, the copper-enhanced weld metal showed a much higher susceptibility to weld metal softening than the copper-niobium-enhanced weld metal. As a result, significant hardness or strength fluctuations in the intercritical zone are not expected in the dual precipitation strengthened steel weld metals. The greater and more stable strengthening effect results from the dual precipitation of  $\epsilon$ -copper and niobium carbide, each with a different precipitation reaction kinetics.

### *Copper Precipitation in High Strength Steel Weldments*

A hardness survey was performed on the cross sections to determine the effect of copper additions. Hardness readings increased to around 380 HV500 at 2.6 wt. pct. copper following by a decrease, as illustrated in Figure 10. At zero copper addition, the hardness of the weld metal is most likely due to the solid-solution strengthening of nickel, chromium and molybdenum. The slight increase at around 0.4 wt. pct. copper addition is certainly due to a copper solid solution effect (copper was the only element added and at a concentration below the solubility limit). At concentrations exceeding the solubility limit, further increases in hardness must be due to copper precipitation and the dispersion of fine copper precipitates in the weld metal. Beyond 2.6 wt. pct., however, the copper precipitates coarsened, which increased the inter-precipitate spacing. TEM observations confirmed the interpretation above. The variation of average diameter of the copper precipitates as a function of copper additions is shown in Figure 11. Additionally, microanalyses showed that only at high copper concentrations were the precipitates predominately copper. At lower concentrations, the precipitates were found to contain some amounts of iron.

As illustrated in Figure 12, the precipitates were mostly spherical in shape. No rod-shaped precipitates, which would indicate the fourth stage of copper precipitation, were observed. The size of the precipitates and the spherical geometry seemed to indicate that the growth of the copper precipitates in the weld with 2.6 wt. pct. copper was at the late third stage of copper precipitation.

### *Electrical Resistance Measurements as a Function of Copper Precipitation*

Electrical resistivity measurement is an indirect but effective way to develop a picture of copper precipitation in a steel weldment. The resistivity of a weld specimen increases with the population of precipitates if the size of precipitates remains at a constant level. Figure 13 shows that electrical resistance of the weld metal increased with its copper content. Comparing Figure 10 with Figure 13, it is quite obvious that the resistance profile follows closely the hardness profile. When the copper precipitates coarsened to around 150 nm diameter, (such as those in the specimens with 2.6 wt. pct. copper content), the electrical resistance of the specimens decreased substantially.

### *Weld Metal Microstructures*

Light and electron microscopy work characterized the microstructure of the experimental welds. A total of six distinguishable microstructural features were identified which are: grain boundary ferrite (GBF), ferrite with second phase aligned (FS[A]), ferrite with second phase non-aligned (FS[NA]), acicular ferrite

(AF), granular bainite (GB), and martensite (M). Figure 14 shows typical microstructures observed in this program and Table 2 summarizes the quantitative findings.

Table 2. Quantitative Metallography of Welds made at 1.0 kJ/mm.

Weld	GBF	FS[A]	FS[NA]	AF	GB	M
A	2.3	14.2	3.1	55	22	3.4
B	0.5	17	10.2	35.8	25.6	10.8
C	0.5	37	7.5	21	32.5	12
D	2.9	30.9	0.6	40.5	17.3	7.7

Of the six microstructures, granular bainite was probably the most interesting one. It was identified using TEM as packets of ferrite laths or equiaxed ferrite crystals with interlath islands of martensite and retained austenite without cementite.

When the microstructural features were plotted as a function of copper content in the weld metal, the amounts of martensite, granular bainite and FS[A] varied in a trend consistent with changes in the hardness and electrical resistance, as indicated in Figure 15. The observed relationship seems to indicate that copper precipitation occurred more readily in the "hard" phases, suggesting nucleation sites such as dislocations and subgrain boundaries commonly found in these phases.

#### *Mechanical Properties of Cu-Nb Enhanced High Strength Steel Welds*

Based on the chemical composition of the experimental welds, it anticipated that, as the copper concentration increased, the strength would increase accordingly but the impact toughness would decrease. In fact, findings from the first iteration of experimental electrodes demonstrated just that, the inverse relationship of strength and toughness. Nevertheless, for the second and third batch of electrodes whose alloying contents were redesigned, the trend observed was completely different from the earlier batch. By optimizing the manganese, silicon and titanium content, adjusting the copper and nickel content, and by lowering both the carbon and nitrogen content, the impact toughness improved substantially, without significantly decreasing the yield strength (still around 110 ksi). Figures 16 and 17 show the Charpy impact energy as a function of testing temperature for the welds made using the third generation electrodes. All three formulations performed extremely well, producing welds at 2.0 kJ/mm that met the requirements imposed by the Navy (35 ft-lb/47.5 J at -60°F and 60 ft-lb/81 J at 0°F), Figure 16. Only the lower nickel filler metal produced welds at 1.0 kJ/mm which exhibited lower impact toughness, insufficient to meet the

81 J (60 ft-lb) at 0°F requirement. But the welds made by this electrode easily met the 48J (35 ft-lb) at -60°F requirement.

For 1 kJ/mm heat input, the 0.8Cu-2.3Ni-0.03Nb electrode produced welds with the best toughness. The performance of the 1Cu-1.5Ni-0.0Nb electrode was, however, quite comparable to that of the higher nickel electrode and also satisfied the Navy requirements. At higher heat input, 2 kJ/mm, the 1Cu-1.5Ni-0.03Nb electrode outperformed the other two electrodes. If one single composition was to be chosen for both heat inputs, for the sake of process simplicity, the 1Cu-1.5Ni-0.03Nb electrode is the clear winner. At 2kJ/mm heat input, the impact toughness values at 0 and -60°F were 48 and 81 percent higher than the minimum requirement, respectively. Equally, at 1 kJ/mm heat input, the impact toughness values exceeded the minimum requirement by 16 and 39 percent.

### 2.a.ii.3. Conclusions

The major conclusions of this research are:

- a. Dual precipitation using copper and niobium was found to be extremely effective in controlling the mechanical properties of high strength steel weld metals.
- b. High strength steel electrodes that contain copper and niobium can be optimized to produce weldments that meet the strength and impact toughness requirements imposed by the U.S. Navy.
- c. The optimized electrode composition contains: 0.03 wt. pct. C, 1.25 wt. pct. Mn, 0.28 wt. pct. Si, 1.5 wt. pct. Ni, 1.0 wt. pct. Cu, 0.50 wt. pct. Mo., 0.03 wt. pct. Nb, titanium between 240 and 400 ppm, and nitrogen below 80 ppm.
- d. At low copper content, the fine copper precipitates (of the order of 14 nm) are spherical. Increasing copper contents to beyond 2.5 wt. pct. coarsened the precipitates rapidly to around 150 nm.
- e. Electrical resistivity measurements can be used to non-destructively characterize copper precipitation in high strength steel welds, which indirectly indicates the strength and hardness of the weld metal.



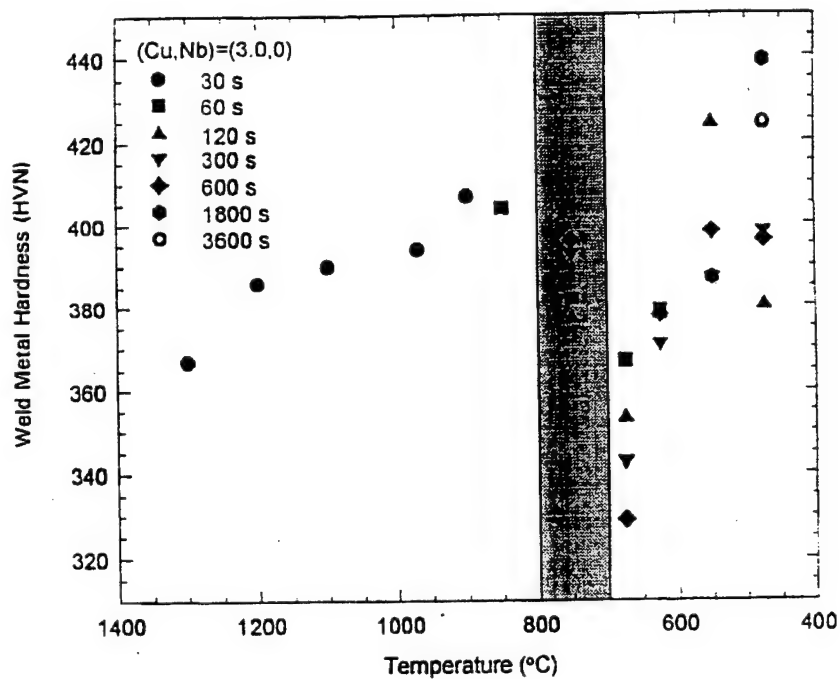


Figure 8. Substantial softening of the reheated zone as a result of multiple thermal cycle simulated using isothermal heat treatment.

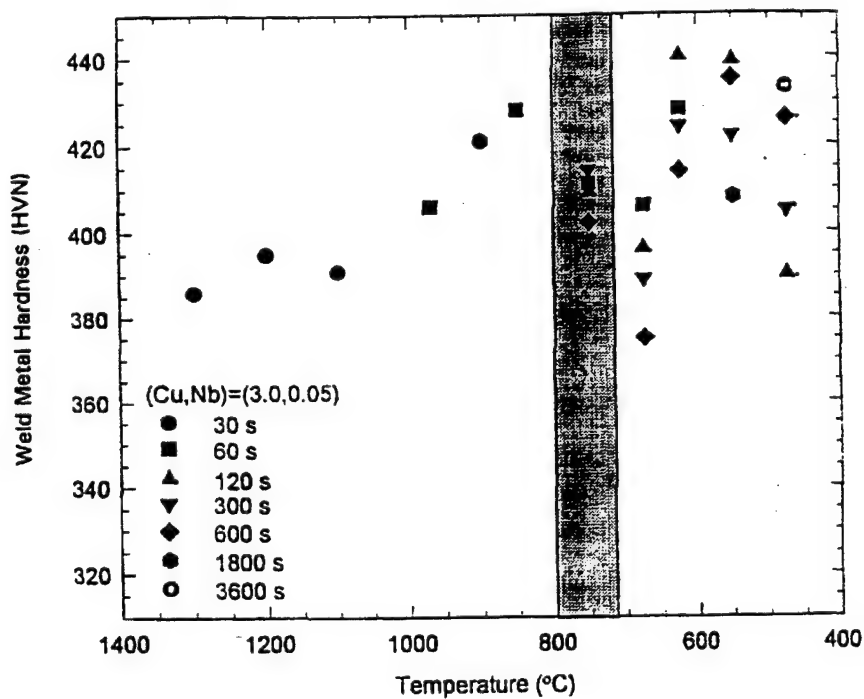


Figure 9. Minor softening of the reheated zone as a result of multiple thermal cycle simulated using isothermal heat treatment. The presence of Cu-Nb precipitates resisted the softening phenomenon.

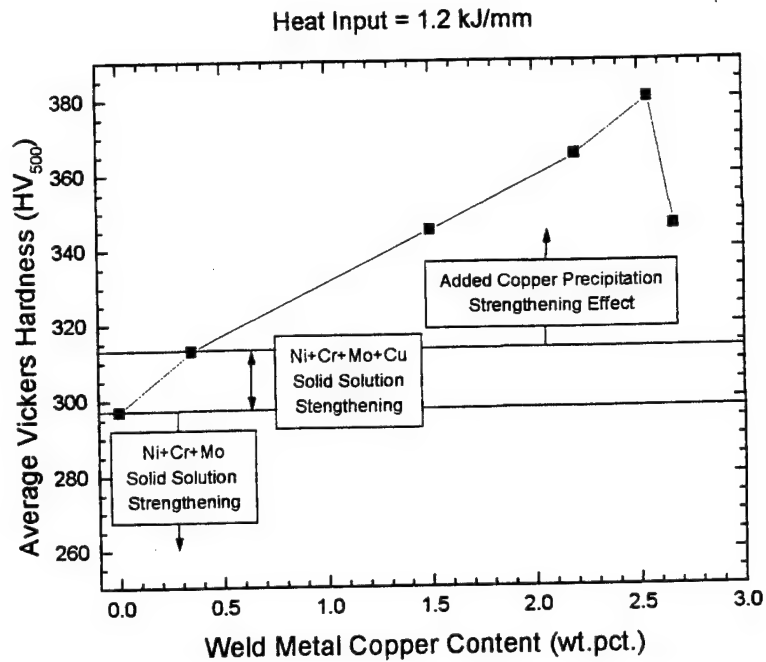


Figure 10. Weld hardness as a function of copper content. Copper precipitation only occurs after reaching the solubility limit.

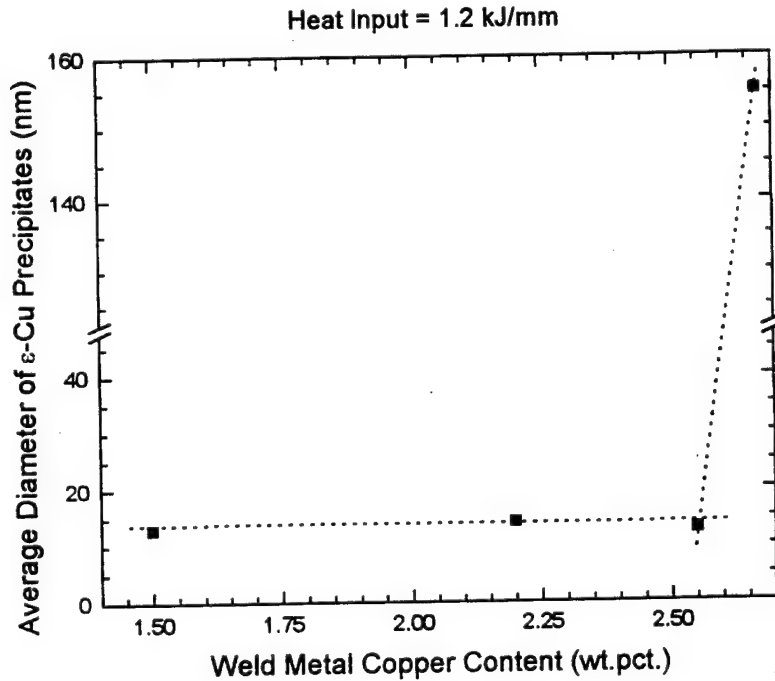


Figure 11. Diameter of copper precipitates as a function of weld metal copper content. Substantial coarsening occurred when copper content exceeded 2.5 wt. pct.

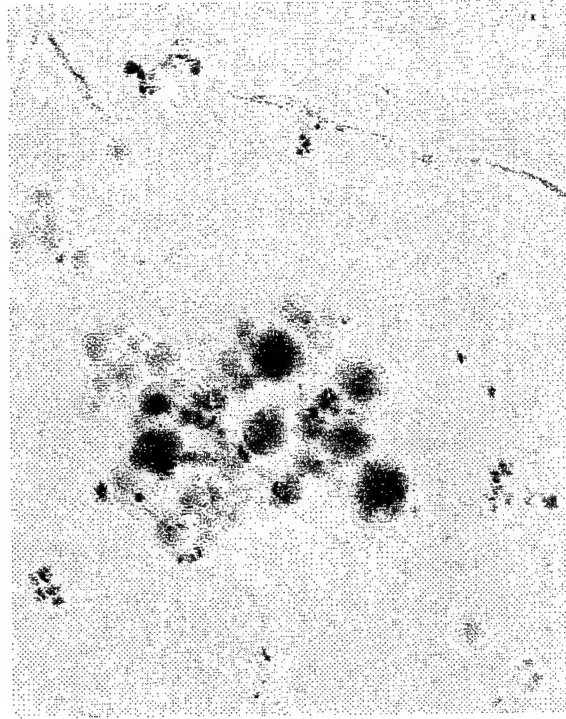


Figure 12. Carbon extraction replica with spherical  $\epsilon$ -copper precipitates.

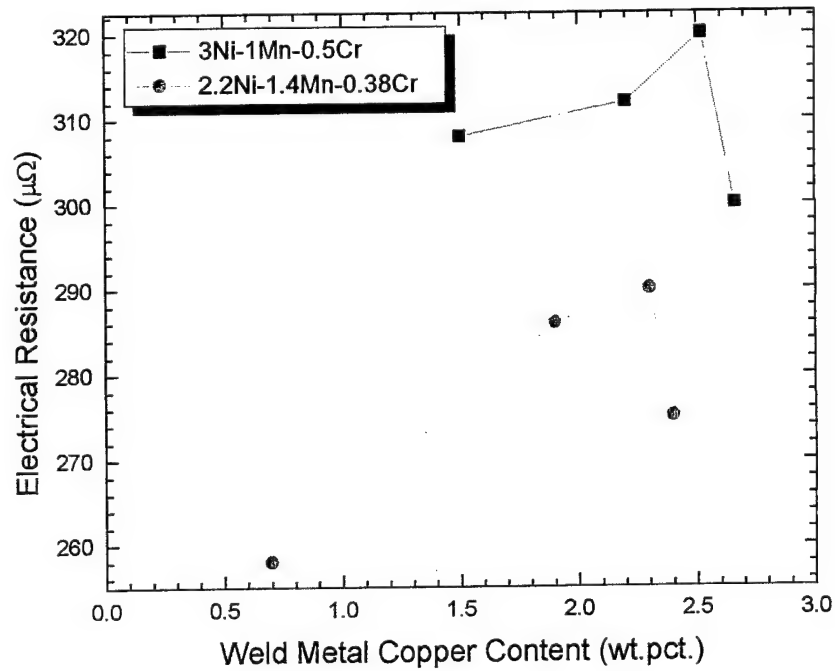


Figure 13. Weld metal electrical resistance as a function of copper content. Note the similar increasing trend as weld metal hardness with copper content.

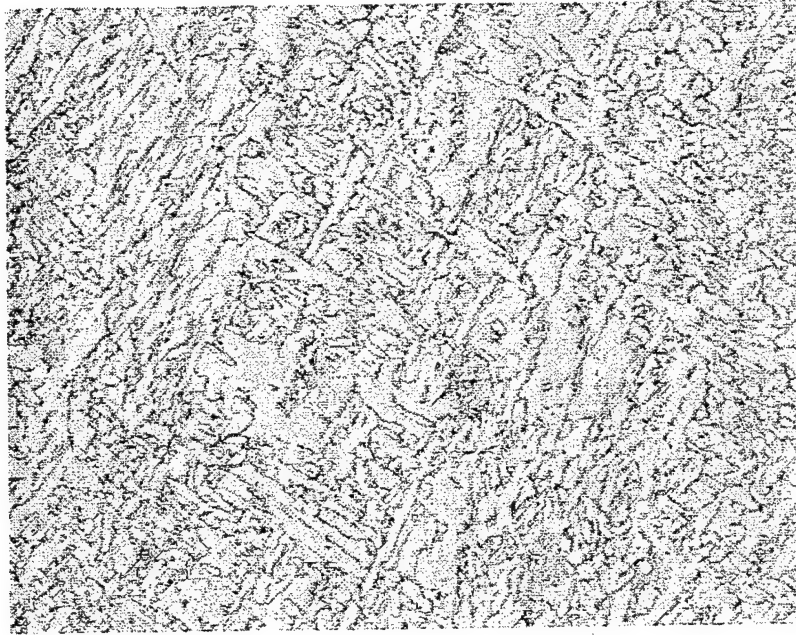


Figure 14. Typical light micrograph showing the different phases observed in the experimental high strength steel welds.

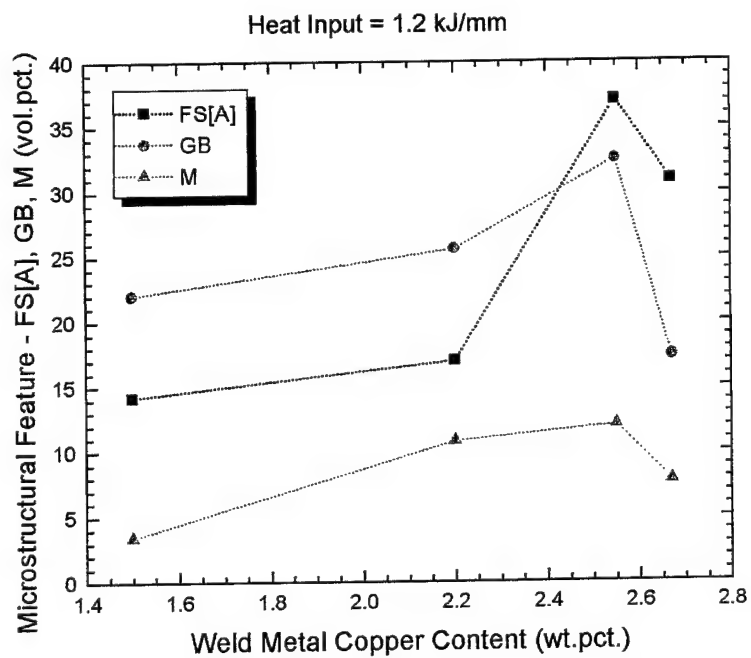


Figure 15. Major microstructural features in the high strength steel welds.

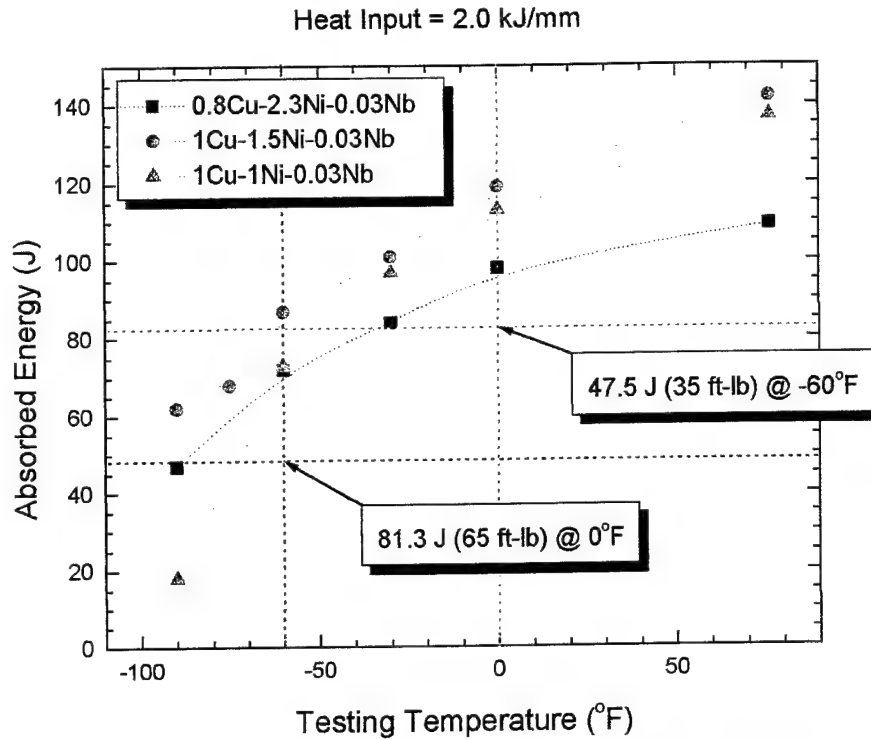


Figure 16. Charpy impact energy as a function of testing temperature for 2.0 kJ/mm welds. All satisfied the Navy requirements.

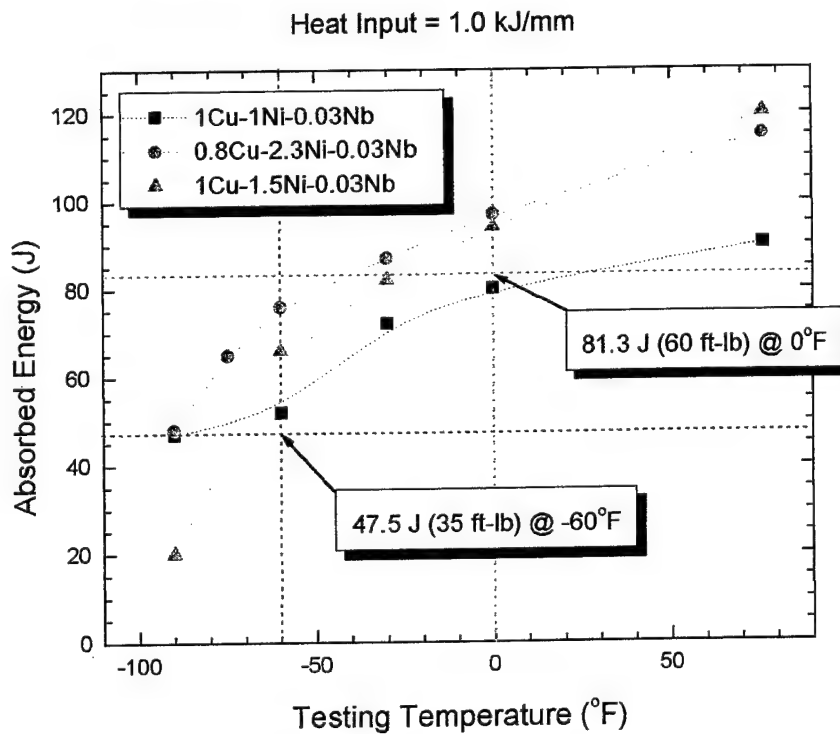


Figure 17. Charpy impact energy as a function of testing temperature for 1.0 kJ/mm welds. Except for one weld, all others satisfied the Navy requirements.

## 2.b. Hydrogen Management

### 2.b.i. Use of Fluorides to Control Hydrogen in Arc Welding Plasmas

Thermochemical calculations indirectly determined the effectiveness of selected fluorides. A fluoride is considered effective if the calculated ratio of  $p\text{HF}/p\text{H}_2$  is high, which means that a high concentration of fluorine gas is generated in the arc plasma, which in turn reduces abundant hydrogen when forming hydrogen fluoride gas. These calculations indicated that fluorides such as  $\text{K}_3\text{AlF}_6$ ,  $\text{KF}$ , and  $\text{MnF}_3$  would be more efficient than others (e.g.,  $\text{CaF}_2$ ,  $\text{KAlF}_4$ ,  $\text{AlF}_3$ ,  $\text{MnF}_2$ ) in lowering the hydrogen pickup in the weld pool.

In initial efforts, experimental flux-cored arc welding consumables containing cryolite,  $\text{K}_3\text{AlF}_6$ , were manufactured at CSM and used to verify the concept of hydrogen control by means of fluorine additions to the plasma. In welding experiments with  $\text{CO}_2\text{-H}_2$  (1 to 4 vol. pct.) shielding gas, a reduction of almost 25 percent in diffusible hydrogen, from 7.0 ml  $\text{H}_2$ /100g metal (without fluorine addition) to 5.4 ml  $\text{H}_2$ /100g metal, with five percent  $\text{K}_3\text{AlF}_6$  addition was achieved (Figure 18). Five percent  $\text{K}_3\text{AlF}_6$  was found to be optimum, since higher addition up to ten percent did not further reduce the diffusible hydrogen content. Notice that these results were obtained for the 4 vol. pct. hydrogen shielding gas. Typical atmospheric humidity, however, would be closer to one volume percent hydrogen in argon, which would result in weldments with around 2 ml/100g diffusible hydrogen content. The experimental work continued with demonstrating the performance of the other potential fluorides ( $\text{MnF}_3$  and  $\text{KF}$ ). As illustrated in Figure 19, among the results for the potential fluorides,  $\text{KF}$  showed the greatest reduction in diffusible hydrogen content, approximately 40 percent reduction in an argon atmosphere enriched with 4 vol. pct.  $\text{H}_2$ .

### 2.b.ii. Adjustment of the Martensite Start Temperature for Hydrogen Control

Hydrogen concentrations across the weldment were calculated to describe how the austenite-ferrite (or austenite-martensite) phase transformation in steel weldments affects the resulting hydrogen distribution. Two cases were considered. The first case is shown in Figure 20. Here, the austenite/martensite transformation in the weld metal occurred at a higher temperature than the transformation in the heat-affected zone. In this situation, diffusible hydrogen accumulated in the heat-affected zone just under the fusion line, and, as verified by experimental data, under-bead cracking occurred in the heat affected zone. In the alternate situation, shown in Figure 21, the martensite transformation in the heat-affected zone occurred at a higher temperature than in the weld metal. It is possible, in this case, that the major fraction of the initial diffusible hydrogen was

retained in the weld metal, and thus promoted crack initiation in the weld metal. To minimize the susceptibility to hydrogen assisted cracking, alloying additions to welding consumables must be selected to achieve a martensite start temperature which is slightly higher in the weld metal as compared to that temperature in the HAZ. Satisfying this condition is expected to alleviate the non-uniformity of hydrogen distribution in weldments, as well as to facilitate a maximum rate of hydrogen transport away from the weld metal to the base plate.

### 2.b.iii. Hydrogen Trapping in High Strength Steel Weld Metals

Experimental metal cored wire electrodes containing various trap additions were manufactured to demonstrate the hydrogen trapping concept. The performance of these trap additions has been demonstrated by diffusible hydrogen measurements of GMA welded samples, contaminated with a range of hydrogen gas content (from 0.1 to 3 vol. pct.) in the argon shielding gas. The most promising result is shown in Figure 22, for samples welded with yttrium-containing wire and 0.1 percent hydrogen contamination in the shielding gas. A fifty percent reduction of diffusible hydrogen was achieved by introducing 0.1 wt. pct. yttrium (Samples welded with wire not containing traps contained 6.7 ml  $H_2/100g$ ; these samples had 3.1  $H_2/100g$ ). Addition of 0.2 wt. pct. yttrium reduced the diffusible hydrogen content even more significantly to 1 ml  $H_2/100g$ . The hydrogen gas level of 0.1 percent mixed with the argon shielding gas produced weld hydrogen contents similar to that experienced at naval shipyards.

Characteristics of specific trap additions have been assessed through hydrogen thermal desorption analysis (TDA). This experimental apparatus analyzed the release of hydrogen from various trap sites in the weld sample during a constant heating rate. The methodology applied in this analysis provides an easy way to evaluate a specific weld metal trap without interference from other coexisting traps. As shown in Figure 23, both neodymium and yttrium were shown to form strong or deep trap sites; the TDA measurements clearly showed hydrogen release peaks at high temperature (around 800 to 900°C). Samples welded with trap free reference wires showed only TDA hydrogen release peaks from weak traps such as dislocations and grain boundaries (100 to 200 °C). Yttrium additions (Figure 23a) produced more impressive results because, during wire manufacturing, yttrium ( $Fe_2Y$ ) can be added in a much larger amount than neodymium ( $Nd_2Fe_{17}$ ). Inclusions containing these trap additions have been identified by X-ray diffraction measurements as well as by electron microscopy. These findings verified that rare earth oxides form deep hydrogen traps, which potentially prevent hydrogen atoms from reaching crack initiation sites during a thermal cycle. Particularly for multipass welding, the TDA results also imply



that, when not completely saturated, these traps can absorb released hydrogen from grain boundaries, which in turn can minimize the risk of intergranular hydrogen cracking.

#### 2.b.iv. Conclusions

Three hydrogen management steps can be effectively utilized to reduce the hydrogen content during the welding of high strength steels. Specialized consumables, containing either hydrogen trapping elements or complex fluoride additions, can be made. Alloying elements also can be added to force the  $M_s$  temperature of the weld metal to be slightly higher than that of the heat-affected zone. These methods for managing hydrogen offer promising practices for reducing the susceptibility to hydrogen assisted cracking, controlling the hydrogen distribution, and lowering the diffusible hydrogen content.

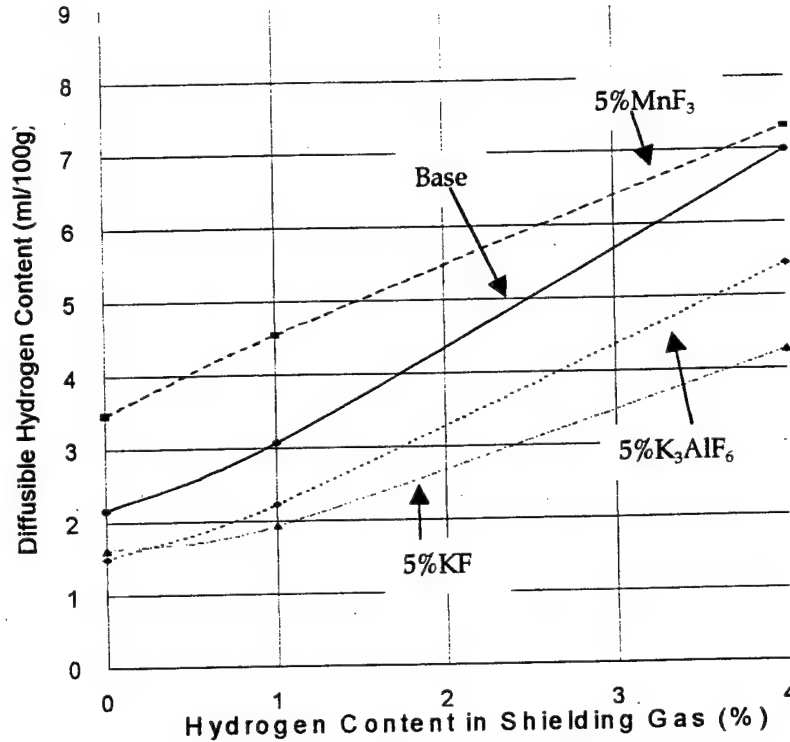


Figure 18. Diffusible hydrogen content as a function of hydrogen content in shielding gas with 5% K<sub>3</sub>AlF<sub>6</sub> and 10% K<sub>3</sub>AlF<sub>6</sub> content in flux.

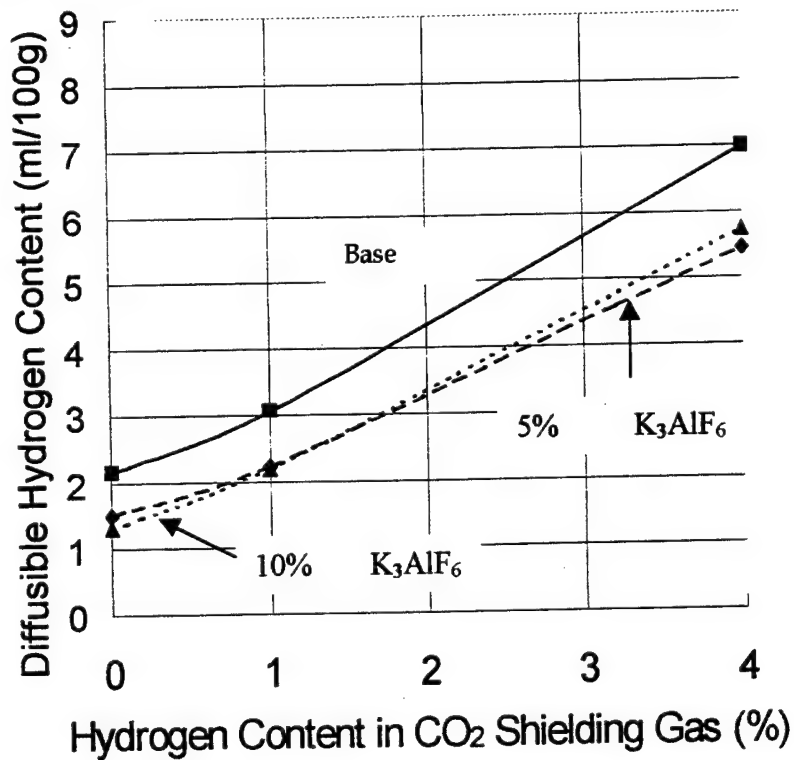


Figure 19. Effectiveness of KF and MnF<sub>3</sub> on diffusible hydrogen reduction comparing with K<sub>3</sub>AlF<sub>6</sub>.

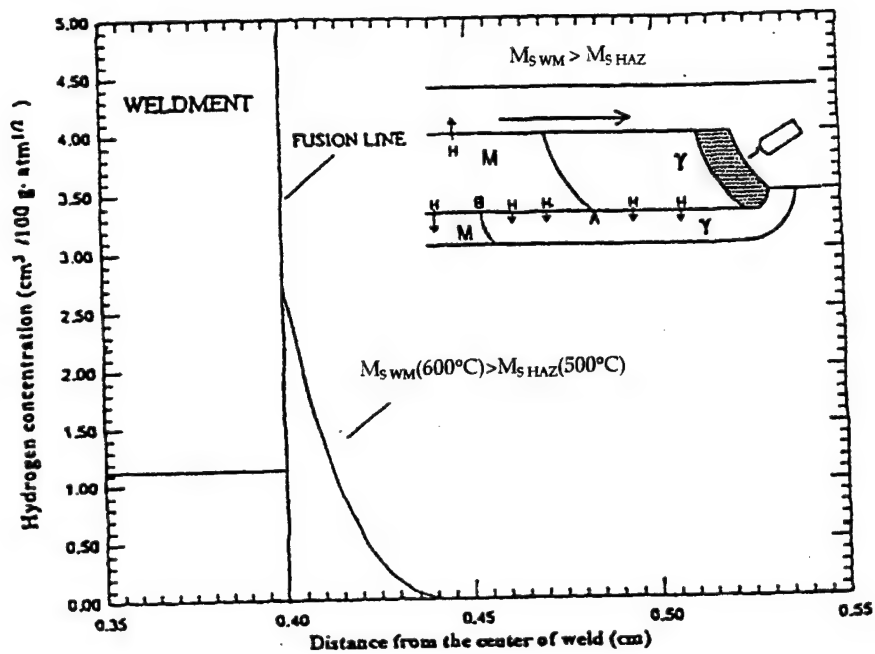


Figure 20. Hydrogen distributions across the fusion line of a steel weldment for  $M_{s \text{ WM}}(600^\circ\text{C}) > M_{s \text{ HAZ}}(500^\circ\text{C})$ .

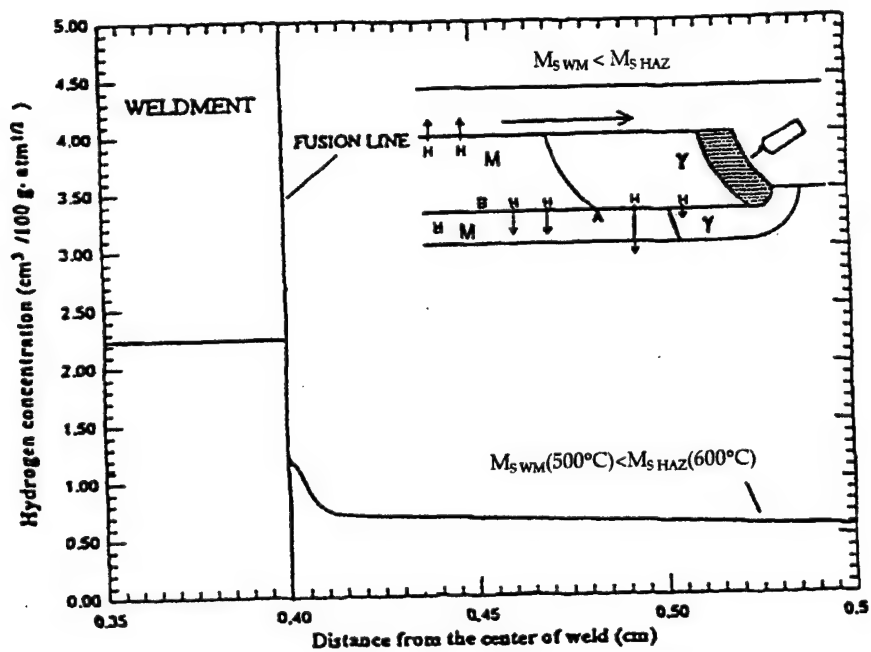


Figure 21. Hydrogen distributions across the fusion line of a steel weldment for  $M_{s \text{ WM}}(500^\circ\text{C}) < M_{s \text{ HAZ}}(600^\circ\text{C})$ .

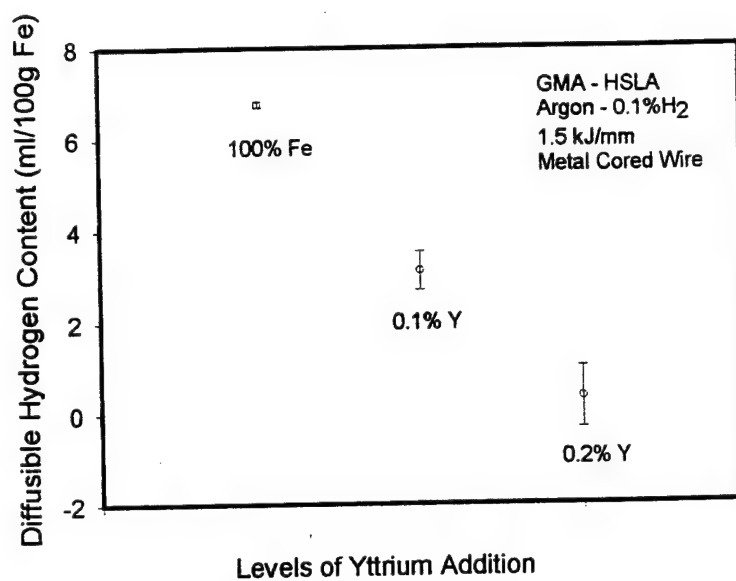


Figure 22. The reduction of diffusible hydrogen content in the weldment without traps and with two levels of yttrium traps. (0.1 and 0.2 wt. pct. of Y in the metal cored wire)

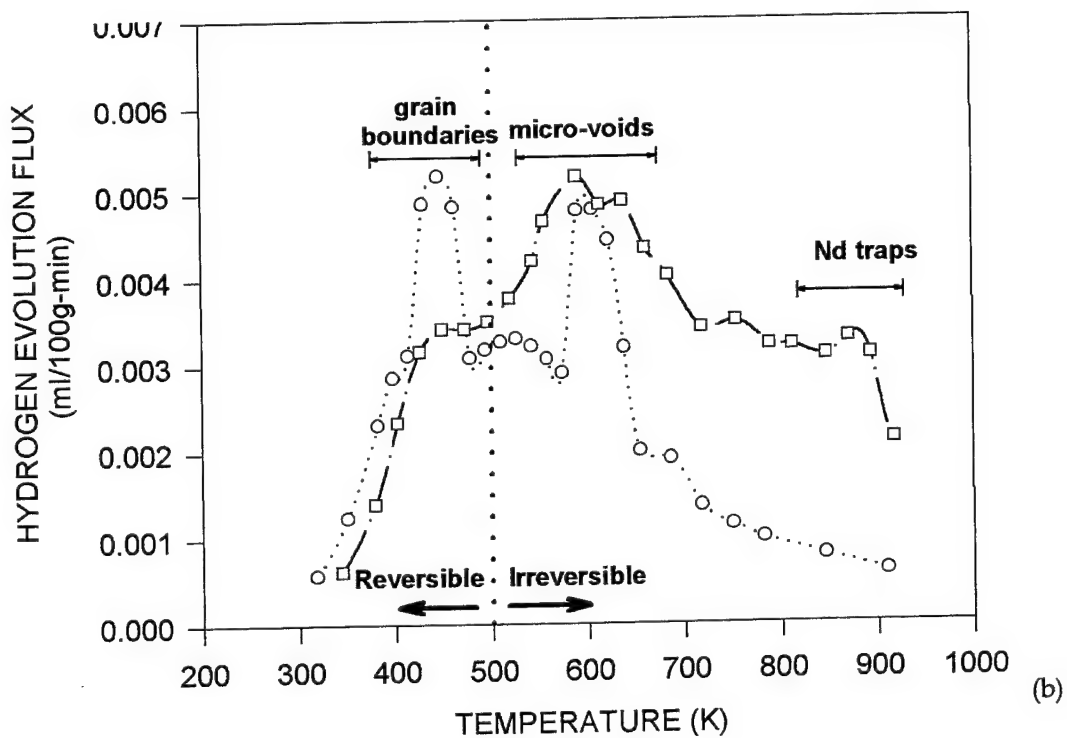
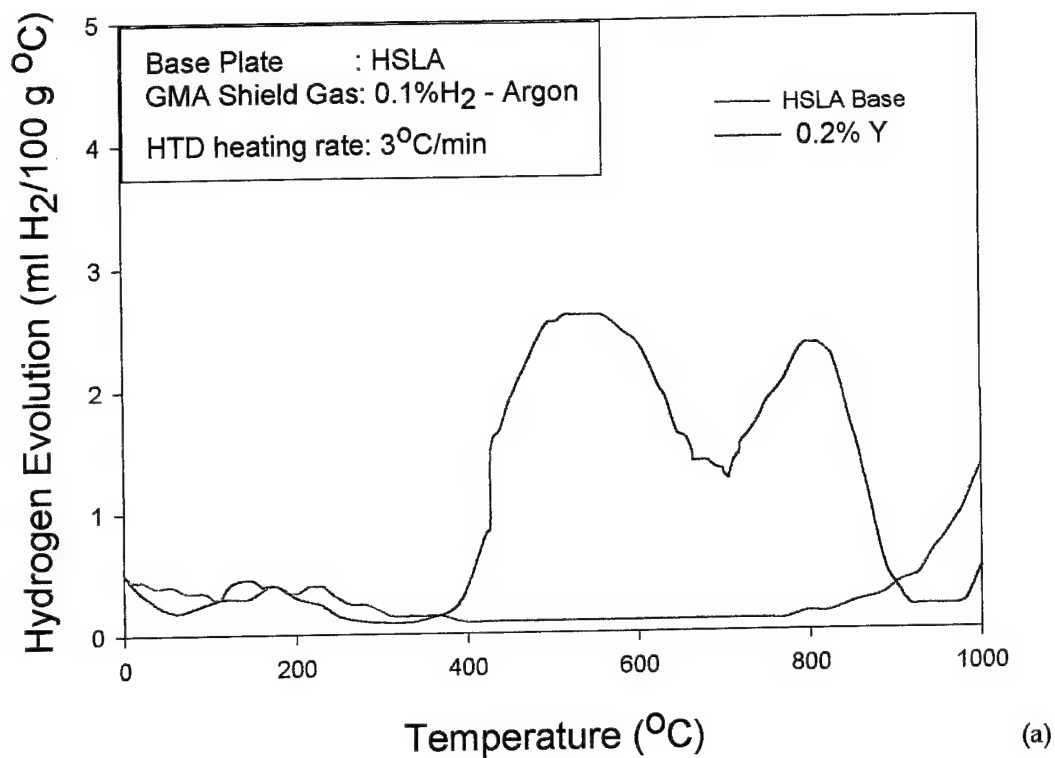


Figure 23. Evidence of the effectiveness of Yttrium and Neodymium hydrogen traps in high strength steel weldments from Thermal desorption analysis (TDA).

### 3. List of Publications and Technical Reports

#### 3.a. Advanced Welding Consumables

##### 3.a.i. Optimized HSLA Steel SMAW Consumable

- M.Q. Johnson, G.R. Edwards, and G.M. Evans, "The Effect of Thermal Cycles on the Microstructures and Mechanical Properties of High Strength Titanium Bearing Shielded Metal Arc Weld Metal," IIW-DOC.IX-1890-97.
- M.D. Clark and G.R. Edwards, "Microstructural and Fractographic Characterization of SMAW Filler Metal for HSLA 100 Steel," presented at the 79th Annual AWS Convention, Detroit, MI, April 26-29, 1998.
- M.D. Clark, G.R. Edwards and A. Landau, "Metallographic Techniques for Microstructural Characterization of SMAW Filler Metal for HSLA 100 Steel," presented at Trends in Welding Research 1998, Pine Mountain, GA, June 1-5, 1998.

##### 3.a.ii. Dual Precipitation Strengthening

- J. E. Ramirez, S. Liu, and D.L. Olson, "Synergistic Precipitation Strengthening Effect of Copper and Niobium in High Strength Steel Weld Metal", Abstracts of Papers – 75<sup>th</sup> AWS Welding Convention, pp. 91, Philadelphia, PA, April 1994.
- J. E. Ramirez, S. Liu, and D.L. Olson, "Dual-Precipitation Agent Selection for Minimizing Mechanical Property Fluctuation in the Reheated Weld Metal in Multipass High Strength Steel Welds", Abstracts of Papers – 76<sup>th</sup> AWS Welding Convention, pp. 107-108, Cleveland, Ohio, April 1995.
- J. E. Ramirez, S. Liu, and D.L. Olson, "Dual Precipitation Strengthening Effect of Copper and Niobium in High Strength Steel Weld Metal", Materials Science and Engineering A, A216, pp. 91-103, October, 1996.
- T. Yamaura and S. Liu, "Effect of Cu Content on Mechanical Properties in Multipass Cu-V Enriched High Strength Steel Weld Metal," Abstracts of Papers – 79<sup>th</sup> AWS Welding Convention, pp. 203-204, Detroit, Michigan, April 1998.

#### 3.b. Hydrogen Management

##### 3.b.i. Use of Fluorides to Control Hydrogen in Arc Welding Plasmas

- A.M. Pope and S. Liu, "Hydrogen Content of Underwater Wet Welds Deposited by Rutile and Oxidizing Electrodes", in Intl. Conf. Proc. on Offshore Mechanics and Arctic Engineering - Materials Engineering', ASME, Vol.111, pp.85-92, Florence, Italy, June 1996.

- S. Liu, "Recent Developments in High Strength Steel Welding: Strength, Toughness and Cracking Susceptibility", Keynote Address, Israeli Metallurgical Society - Annual Welding Convention, Tel Aviv, Israel, October 20, 1996.
- R.C. de Medeiros and S. Liu, "Effect of Oxidizing Electrodes and Polarity on Hydrogen Mitigation in Underwater Wet Welding", Abstracts of Papers - 78<sup>th</sup> AWS Annual Convention, pp. 122, Los Angeles, CA, April 13-17, 1997.
- K. Johnson and S. Liu, "Consumables for Arc Welding over Paint Primer", Abstracts of Papers - 78<sup>th</sup> AWS Annual Convention, pp. 138, Los Angeles, CA, April 13-17, 1997.
- M. Matsushita, S. Liu and D.L. Olson, "Effective Hydrogen Control by Means of Fluoride Additions in Flux Cored Arc Welding," Abstracts of Papers - 79<sup>th</sup> AWS Welding Convention, pp. 147-148, Detroit, Michigan, April 1998.
- K. Johnson, D.L. Olson, and S. Liu, "Hydrogen Control and Microstructural Refinement of Structural Steel Welds Using Fluoride-Containing FCAW Electrodes", in Intl. Conf. Proc. on Offshore Mechanics and Arctic Engineering - Materials Engineering', Omae98-2801, ASME, Lisbon, Portugal, July 1998.
- R.C. de Medeiros and S. Liu, "Effect of Slag Chemistry on Hydrogen Pickup in Underwater Wet Welds", Abstracts of Papers - 79<sup>th</sup> AWS, pp. 148, Detroit, MI, April 26-29, 1998.
- R.C. de Medeiros and S. Liu, "A Predictive Electrochemical Model for Weld Metal Hydrogen Pickup in Underwater Wet Welds", in Intl. Conf. Proc. on 'Offshore Mechanics and Arctic Engineering - Materials Engineering', Omae98-2211, ASME, Lisbon, Portugal, July 1998.

### *3.b.ii. Adjustment of the Martensite Start Temperature for Hydrogen Control*

- D.L. Olson and S. Liu, "Steel Weld Metal Composition Estimation including Diffusible and Residual Hydrogen Content", Abstracts of Papers - 77<sup>th</sup> AWS Welding Convention, pp. 97, Chicago, Illinois, April 1996.
- S. Liu and D.L. Olson, "The Effect of Altitude on Welding", in Conf. Proc. on 'Research Trends in Welding Science and Technology', pp. 347-352, Gatlinburg, Tennessee, June 1995, ASM Intl., 1996.
- D.L. Olson, S. Liu, W. Wang, R. Pieters, and S. Ibarra, "Martensite Start Temperature as a Weldability Index", in Conf. Proc. on 'Research Trends in Welding Science and Technology', pp. 615-620, Gatlinburg, Tennessee, June 1995, ASM Intl., 1996.
- W. Wang, R. Wong, S. Liu, D.L. Olson, "Use of Martensite Start Temperature for Hydrogen Control", in Conf. Proc. on 'Welding and



Weld Automation in Shipbuilding', pp. 17-31, Cleveland, Ohio, October 1995.

- W. Wang, S. Liu and D.L. Olson, "Consequences of Weld Undermatching and Overmatching: Non-Uniform Hydrogen Distribution", in Intl. Conf. Proc. on Offshore Mechanics and Arctic Engineering - Materials Engineering', ASME, Vol. III, pp. 403-409, Florence, Italy, June 1996.

### 3.b.iii. *Hydrogen Trapping in High Strength Steel Weld Metals*

- D.L. Olson, I. Maroef, C. Lensing, R.D. Smith, W.W. Wang, S. Liu, T. Wildeman, and M. Eberhart, "Hydrogen Management in High Strength Steel Weldments", in Proc. of the Joint Seminar on Hydrogen Management in Steel Weldments, Melbourne, Australia, October 23 (1996).
- I. Maroef, D.L. Olson, M. Eberhart, and C. Lensing, "Weld Metal Hydrogen Trapping", presented at the 77th Annual AWS Convention, Chicago, IL, April 21-25 (1996).
- D.L. Olson, "Application of Metallurgical Concepts to Develop Advanced High Strength Steel Welding Consumables", presented at the 8th Israeli Metallurgical Conference in Beer Shiva, Israel, March 18 (1997).
- C. Lensing, I. Maroef, and D.L. Olson, "Hydrogen Trapping in Hydrogen Management of Steel Welding", presented at the 78th Annual AWS Convention, Los Angeles, CA, April 13-17 (1997).
- D.L. Olson, I. Maroef, and C. Lensing, "The Role of Hydrogen Trapping in Hydrogen Management of Steel Welding", in Proc. of Indian National Welding Seminar 97", Bangalore, India, Dec. 11-13 (1997).
- I. Maroef, C. Lensing, and D.L. Olson, "Evaluation of Hydrogen Trapping for Hydrogen Management in Ferrous Alloy Welding", presented at the 79th Annual AWS Convention, Detroit, MI, April 26-30 (1998).
- Y.D. Park, A. Landau, G.R. Edwards, and D. L. Olson, "The Role of Retained Austenite in the Hydrogen Management of High Strength Steel Welds", presented at the Trends in Welding Research Conference, Callaway Gardens, Pine Mountain, Georgia, June 1-5 (1998).
- I. Maroef, D.L. Olson, and G.R. Edwards, "Hydrogen Assisted Cracking in High Strength Steel Weldments", in Intl. Conf. "Welding and Related Technologies for the 21<sup>st</sup> Century," Kiev, Ukraine, November 24-27 (1998).

# The Effect of Thermal Cycles on the Microstructures and Mechanical Properties of High Strength Titanium-Bearing Shielded Metal Arc Weld Metal

M.Q. Johnson<sup>1)</sup>, G.R. Edwards<sup>2)</sup>, G.M. Evans<sup>3)</sup>

## Abstract

The objective of this study was to determine the effect of thermal cycles, typical of those experienced while depositing multiple weld passes in shielded metal arc weldments, on the microstructures and properties of high strength titanium bearing weld metals. The effects of titanium, initial microstructure, and simulated thermal cycles on weld metal microstructures and properties were investigated. As-deposited low carbon-1.5Mn-0.5Mo-3Ni weld metals were produced with two interpass temperatures (to produce coarse and fine initial microstructures) and five titanium concentrations ranging from 0 to 420 ppm. These weld metals were subjected to thermal cycles simulating a range of heat affected zone regions. The microstructures and toughness of the as-deposited and thermally cycled welds were found to depend primarily on titanium concentration. For a given titanium concentration, complex changes in toughness as a function of thermal cycle peak temperature were measured and initial microstructure was found to only to have a minor effect on the toughness of thermally cycled weld metals.

## 1.0 Introduction

Multiple pass welds are fabricated by depositing layers of weld metal to fill a wide gap. The completed layers are reheated each time a new layer is deposited causing the various layers to undergo partial or complete reverse transformation to a different secondary microstructure. Other regions of the primary microstructure which do not reach sufficient temperature are tempered during welding. While considerable attention has been devoted to understanding microstructures in the as-welded regions (top bead) of mild steel weldments and factors governing the toughness of base metal heat affected zones, similar studies of the complex microstructures and properties found in multipass weld

---

1) Senior Research Engineer, EWI (formerly graduate student CSM), USA

2) Professor and Director of CWJCR, Colorado School of Mines, USA

3) Chief Metallurgist, Oerlikon Welding Ltd, Zurich, Switzerland.

metals are lacking. Many studies have associated large fractions of acicular ferrite in the top weld bead with high toughness in multipass weld metals although the correlation between the top bead microstructures and the properties measured in the heterogeneous reheated weld metal is uncertain.

The normal route to achieving high toughness in a multipass weld is to use a deposition sequence that minimizes the amount of primary weld metal. This technique is particularly helpful when the primary weld metal contains large fractions of coarse microconstituents such as aligned ferrite and/or grain boundary ferrite. It is unclear whether or not this approach is beneficial for higher strength weld metals or carefully optimized weld metals which contain a small fraction of grain boundary ferrite or aligned ferrite.

In many applications, weld metals with higher strengths than the base metal (overmatching) are used. Overmatching the strength of the weld metal relative to the base metal forces deformation to occur in the base metal. This situation is desirable since the base metal is likely to be tougher and have fewer defects than the weld metal. Recent developments in base metal production techniques have resulted in higher strength base metals with improved resistance to hydrogen assisted cracking. These improvements in base metal properties along with the desire to reduce production costs through reduction in preheat/interpass temperatures require development of high strength welding consumables which can effectively overmatch the base metal strength. For practical purposes, these consumables must have high strength, high toughness, and be robust (mechanical properties do not change significantly with minor changes in heat input or chemical composition).

This paper is part of a larger investigation of microstructure-property relationships in high strength shielded metal arc multipass weldments [1]. The objective of this study was to: 1) determine the relationship between as-deposited (primary) weld metal and reheated microstructures and properties, 2) identify any inherently brittle regions which may exist in a multipass weldment, and 3) evaluate the effect of titanium additions on primary and reheated weld metal microstructures and mechanical properties.

## **2.0 Experimental Procedure**

### **2.1 Weld Metal Preparation**

In order to study the effects of titanium concentration on microstructures and mechanical properties in greater detail, titanium additions of 0, 30, 90, 240, and 400 ppm were made to low carbon-1.5Mn-3Ni-0.5Mo weld metal. Titanium additions were made by the addition of pure titanium to the electrode coating.

Selection of these particular titanium concentrations were based on preliminary investigations [1,2] which revealed a strong dependence of toughness on titanium concentration.

For this study, specimens containing only primary (as-deposited) weld metal were produced so that the microstructure and toughness of non-transformed primary weld metal and weld metal subjected to thermal cycles simulating those encountered in a heat affected zone could be compared. In addition, welding procedures were varied to produce primary weld metal with both fine and coarse initial microstructures. Interpass temperatures of 25 °C and 240 °C were used to deposit weld metals with both fast and slow cooling rates thus producing both fine and coarse as-deposited microstructures.

One problem typically encountered when producing thermal simulation specimens from weld metal is the ability to produce a large enough specimen to provide meaningful mechanical test data. For this study, a special welding technique was used to provide enough primary weld metal for standard half-size (5-mm by 10-mm by 55-mm) Charpy specimens.

As shown in Figure 1, the Gleeble specimens were produced using a four-step process:

- 1.) In order to reduce dilution from the base metal, two 20-mm-thick plates were joined using the shielded metal arc process and multiple passes (approximately 27) at a nominal heat input of 1 kJ/mm.
- 2.) The weld reinforcement was removed and a U-groove with a width of 5-mm and depth of 6-mm was machined into the multiple-pass weld metal.
- 3.) A new top bead was deposited into the U-groove using a 5-mm diameter electrode at interpass temperatures of either 25 °C or 240 °C and a nominal heat input of 3.2 kJ/mm.
- 4.) The reheated weld metal produced in Step 1 was removed to produce a 5-mm by 10-mm by 95-mm specimen containing only as-deposited weld metal which was used for thermal simulation.

The time to cool between 800 °C and 500 °C ( $\Delta t_{8/5}$ ) was calculated to be 14 and 30 seconds respectively for the welds produced in Step 3.

## 2.2 Gleeble Simulation

Thermal cycles that a particular volume of weld metal would experience at different distances from the fusion line were calculated based on a Rosenthal thick plate solution [3,4], assuming a nominal welding heat input of 1 kJ/mm and an interpass temperature of 150 °C ( $\Delta t_{8/5} \sim 5.3$  s). As-deposited weld metals produced with the two interpass temperatures and the five titanium concentrations were subjected to thermal cycle simulating the following heat

affected zone regions: ICHAZ-intercritical heat-affected zone ( $Ac_1 < T_p < Ac_3$ ), FGHAZ -grain refined zone ( $T_p > Ac_3$ ), CGHAZ-grain-coarsened zone ( $T_p \gg Ac_3$ ), and ICGHAZ- intercritically heated grain-coarsened zone (a coarse-grained simulation followed by an intercritical simulation). Specifically, the samples were subjected to thermal cycles as shown in Figure 2 with peak temperatures of 850 °C (ICHAZ), 1050 °C (FGHAZ), 1150 °C (FGHAZ), 1350 °C (CGHAZ), and 1350 + 850 °C (ICGCHAZ).

## 2.3 Toughness Testing

Following simulation, the length of the test specimens (produced in Step 4 above) was reduced to produce standard half-size (5-mm by 10-mm by 55-mm) Charpy impact specimens. Approximately 10 samples were tested per titanium concentration/peak temperature were tested to produce full transition curves for both the as-deposited and simulated weld metals. Samples were notched such that crack propagation proceeded in the welding direction.

## 2.4 Metallography

The as-deposited and simulated weld metals were polished using standard metallographic methods, etched using 2 percent nital, and photographed at 800x. Quantitative metallography was performed according to the current guidelines of IIW-Commission IXJ [5]. Five microstructural features were quantified: PF (primary ferrite), AF (acicular ferrite), FS(A) (ferrite with aligned second phase), FS(NA) (ferrite with non-aligned second phase), and M (martensite).

## 3.0 Results and Discussion

### 3.1 Weld Metal Chemical Composition

The chemical compositions of the as-deposited welds are shown in Table 1. Samples produced at fast cooling rates (25 °C interpass temperature) are identified with an "F" (fine microstructure) followed by the titanium concentration in ppm. Similarly, samples produced with slow cooling rates (240 °C interpass temperature) are identified with a "C" (coarse microstructure) followed by the titanium concentration in ppm. For example, a weld containing 30 ppm titanium produced with an 25 °C interpass temperature would be designated as F30. As shown in Table 1, very little difference in chemical composition was observed for welds produced with the two different cooling rates. Consistent with the multipass welds described elsewhere [1], oxygen concentration decreased with increasing titanium. Other elements such as Al, Nb, B, Cu, and Cr were maintained at trace levels.

### 3.2 Weld Metal Microstructures

Increasing the interpass temperature from 25 °C to 240 °C resulted in coarser as-deposited microstructures which are shown in Figures 3 and 4. It is clear from Figures 3 and 4 that the slower cooling rates changed the relative size and nature of the as-welded microstructures. Welds produced with the 25 °C interpass temperature (fast cooling rate) had microstructures which were much more refined than weld metals produced using a higher interpass temperature of 240 °C (slower cooling rate). Figures 5a and 5b show the results of the quantitative metallography. Comparison of Figure 5a with 5b shows that the relative amount of the various microconstituents was strongly dependent on titanium concentration and that martensite replaced non-aligned ferrite when the interpass temperature was decreased. In both cases, a maximum amount of acicular ferrite was measured in weld metals containing approximately 30 ppm titanium.

Figures 6 and 7 show the as-welded and simulated microstructures found in titanium free welds produced with coarse and fine initial microstructures. Coarse martensitic and bainitic microstructures were observed in the simulated weld metals. Comparison of Figures 6 and 7 suggests that the initial microstructure had little influence on the reheated microstructures. Similarly, Figures 8 and 9 show the as-welded and simulated microstructures found in weld metals containing 30 ppm titanium with coarse and fine initial microstructures. In contrast to the titanium-free welds, these welds contained approximately 20 to 30 volume percent acicular ferrite which effectively refined the microstructures when compared to the titanium-free weld metal microstructures. Previous work [6] has suggested that the presence of acicular ferrite in higher strength weld metals improves toughness by the following mechanism: acicular ferrite first nucleates in the austenite grain interiors and upon further cooling, the remaining austenite within the acicular ferrite laths transforms to martensite thus refining the microstructure. This mixed microstructure provides a finer apparent grain size when compared to high strength microstructures which are entirely martensitic. The microstructures found in the simulated weld metals were similar to those found in multipass welds produced with a heat input of 1 kJ/mm and an interpass temperature of 25 °C.

Increasing titanium to approximately 100 ppm had a detrimental effect on the simulated weld metal microstructures with decreased amounts of acicular ferrite and increased amounts aligned ferrite. The microstructures in weld metals containing approximately 100 ppm titanium were similar to those of the titanium free weld metal shown in Figures 6 and 7. Further increases in titanium concentration to a level between 200 ppm and 420 ppm resulted in mixed acicular ferrite/low carbon martensite microstructures similar to the 30 ppm weld metals shown in Figures 8 and 9. These trends in microstructures were noted in



the as-deposited weld metals and in several other studies involving controlled variations of titanium [1,2,7,8].

It is clear that the addition of small amounts of titanium had a pronounced effect on as-welded and simulated weld metal microstructures. The addition of either 30 ppm or 200-420 ppm titanium promoted acicular ferrite formation in the as-welded and simulated weld metals. On the other hand, the microstructures of the titanium-free weld metals and weld metals containing approximately 100 ppm titanium contained mixed martensite/bainite microstructures with very little acicular ferrite. These trends are consistent with those observed in multipass welds produced with similar variations in titanium concentration [1]. While the beneficial effect of titanium is well recognized, the mechanism by which titanium promotes the formation of acicular ferrite is still a subject of great debate. The inclusions from these weld metals were characterized as part of a larger study [1]. While inclusion density decreased with increasing titanium (due to deoxidation), inclusion average size and size distribution remained essentially constant and independent of titanium concentration. Additionally, while the titanium concentration increased in the non-metallic inclusions increased with increasing weld metal titanium, no clear explanation was apparent to describe the microstructural and mechanical property changes (to be discussed) which depended strongly upon titanium.

### **3.3 Weld Metal Hardness**

The effect of thermal cycles and titanium concentration on weld metal hardness is summarized in Figures 10 and 11. Figure 10 shows Vickers hardness measurements for weld metals produced with a fine as-deposited microstructure and the hardness of weld metals subjected to thermal simulation. Similarly, the as-deposited and simulated weld metal hardnesses in weld metals produced with coarse initial microstructures are shown in Figure 11.

The hardness of the weld metals subjected to thermal cycles increased relative to the as-deposited weld metals. This increase in hardness was attributed to the faster cooling rate in the weld metal HAZ simulation and the resulting microstructural refinement. Excepting the hardness of welds produced with a coarse as-deposited microstructure, hardness increased with increasing titanium concentration. This increase in hardness with increasing titanium is consistent with hardness and tensile test results in multipass weld metals with similar variations in titanium concentration.

Careful inspection of Figure 10 and Figure 11 reveals higher hardness in both the as-deposited and simulated weld metals when welds were produced to yield a fine initial microstructure. The exception to this observation was weld metals produced with titanium concentrations of either 235 or 250 ppm which had different as-deposited hardness (the fine microstructure was harder) and comparable hardness in the simulated weld metals (once again, welds with fine



initial microstructures were slightly harder). The reason for the higher hardness measured in simulated weld metals produced with a fine initial microstructure is uncertain since the simulated microstructures and inclusion populations were similar.

### 3.4 Weld Metal Toughness

Toughness in the as-deposited and reheated weld metals was measured by breaking half size (5-mm by 10-mm by 55-mm) Charpy impact specimens over a wide range of temperatures to produce a full transition curve. The use of half-size specimens was necessary to obtain samples containing only primary weld metal (free of weld metal which has been reheated). When using sub-size impact specimens, the overall energy absorbed decreases relative to the energy absorbed in full size CVN specimens because of the reduced cross-sectional area. Additionally, a decrease in the tri-axial stress state at the notch in sub-size specimens causes more plasticity and a shift in the transition temperatures to lower temperatures. While absolute toughness values are not directly comparable between full and half size CVN results, the trends in toughness are expected to be the same.

As reviewed elsewhere [1], a model to reliably predict the toughness of a multipass weld metal given the toughness of the individual regions has not been developed. However, Chen et. al. [9-12] have suggested that the most brittle region in a multipass weld metal will control the toughness of the entire weldment (i.e. the weakest link controls the toughness). One of the objectives of the Gleeble simulation experiments was to identify potentially brittle regions in high strength steel weld metal and develop an understanding between the as-deposited and reheated weld metal toughness.

Impact energies measured at -80 °C in as-deposited welds and welds subjected to thermal cycles are shown in Figures 12 to 16. The data shown in these figures were taken from full transition curves. Figure 12 shows the toughness of titanium-free as-deposited welds and weld metals subjected to thermal cycles with increasing peak temperatures. Low toughness was measured in the as-deposited weld metals and essentially no change in toughness was measured when thermal cycles were applied. Although the reheated microstructures were substantially refined when compared to the as-welded microstructures, aligned ferrite microstructures were predominant and poor toughness persisted in these weld metals when thermal cycles were applied. When considering the effect of initial microstructure, no clear "memory" effect was evident in the titanium-free weld metals (i.e. the reheated weld metal toughness did not appear to depend on prior structure).

Toughness improved in both the as-deposited and thermally cycled weld metals with the addition of 30 ppm titanium as shown in Figure 13. Weld metals

receiving intercritical thermal cycles had toughness that was comparable to the toughness measured in the as-welded samples. Improvements in toughness were measured when FGHAZ, CGHAZ, and ICGHAZ thermal cycles were applied to the as-deposited weld metals. A slight "memory" effect in the toughness was apparent in weld metals containing 30 ppm titanium. The difference in toughness between the thermally cycled weld metals with fine and coarse initial microstructures was small when compared to the large differences in toughness measured by changing titanium concentration from 0 to 30 ppm. In weld metals containing 30 ppm titanium, weld metals with coarse initial microstructures maintained higher toughness when subjected to the various thermal cycles.

As shown in Figure 14, complex variations in toughness were measured in reheated weld metals containing approximately 100 ppm titanium. Improved toughness was measured in welds subjected to thermal cycles simulating ICHAZ, FGHAZ, and ICGHAZ regions. Toughness equivalent to the as-welded toughness was measured in weld metals receiving a CGHAZ thermal cycle. As previously mentioned, acicular ferrite formation in weld metals containing approximately 100 ppm titanium was retarded. Although the mechanism causing the decrease of acicular ferrite in weld metals with this titanium concentration is unknown, the dramatic effect on toughness is apparent. The results of this study suggest that for metals with primary microstructures which are predominantly aligned, that the toughness of multipass weld could be improved by depositing small weld beads or large shallow weld beads such that the amount of refined weld metal is maximized and the amount of primary and CGHAZ weld minimized. In weld metals containing approximately 100 ppm titanium, welds with a fine initial structure were tougher than welds with a coarse initial structure. This observation was essentially independent of the applied thermal cycle. The exact metallurgical phenomena responsible for this is uncertain although it is probable that this behavior can be linked to aspects of weld metal microstructure such as inclusion chemical composition or solidification segregation that do not change appreciably with the short thermal cycles experienced during welding.

As shown in Figure 15, high toughness was measured in the as-deposited weld metals containing 235 ppm titanium (coarse initial microstructure) and 250 ppm titanium (fine initial microstructure). The effect of thermal cycles on the properties of these weld metals was complex. Unlike weld metals containing 100 ppm titanium, increasing the titanium in these weld metals and subjecting them to an intercritical thermal cycle caused a significant decrease in toughness. This decrease in toughness was attributed to an increased fraction of M-A constituent that formed within the acicular ferrite laths during the intercritical thermal cycle. In weld metals subjected to thermal cycles with higher peak temperatures, the toughness was found to be equivalent to the as-welded toughness. Surprisingly, toughness of specimens subject to an ICGHAZ thermal cycle did not decrease. No clear dependence of initial microstructure was observed in weld metals containing 235 and 250 ppm titanium.

The toughness of as-deposited and thermally cycled weld metals containing 320 ppm titanium (coarse initial microstructure) and 420 ppm titanium (fine initial microstructure) are shown in Figure 16. The highest toughness was measured in both the as-welded and thermally cycled weld metals containing higher concentrations of titanium (320 and 420 ppm titanium). Slight improvements in toughness were measured in weld metals receiving thermal cycles with peak temperatures above 1050 °C. Surprisingly, the highest toughness was measured in weld metals receiving the ICGHAZ thermal cycle. The toughness of the as-welded and thermally cycled weld metals was independent of initial microstructure in these welds containing higher titanium concentrations.

Consistent with multipass welds produced in another part of this study [1], it is clearly evident that titanium has a first order effect on weld metal microstructures and toughness in these high strength steel weld metals. High toughness was measured in both as-welded and thermally cycled weld metals with titanium concentrations of either 30, approximately 235 ppm titanium, or more than 320 ppm titanium. Decreased toughness was measured in weld metals with titanium concentrations of either < 10 ppm titanium or approximately 100 ppm titanium. The effect of thermal cycle peak temperature was apparent in two instances: increased toughness in the 100 ppm titanium ICHAZ weld metals and decreased toughness found in the 235/250 ppm titanium ICHAZ weld metals. For the most part, the effect of initial microstructure on the toughness of thermally cycled welds can be considered a second order effect at best.

The results of this study were similar to those obtained by Cerjak et. al.[8] who, in a nearly identical study, investigated the effect of thermal cycles on lower strength C-1.5Mn weld metals containing either 0 ppm titanium or 28 ppm titanium. Although the microstructures in the two studies were substantially different, they also found improved toughness in weld metal containing 28 ppm titanium when compared to titanium-free weld metals. They reported that a peak temperature of 1000 °C provided optimal toughness for both weld metal compositions tested.

Shiga et.al. [13] reported that the toughness of reheated Ti-B weld metals was degraded by the application of thermal cycles and that the largest decreased in toughness occurred in welds subject to thermal cycles simulating a fine-grained thermal cycle ( $T_p = 1000-1100$  °C). They also observed that microstructures in welds receiving FGHAZ thermal cycles were coarser than as-deposited microstructures or microstructures found in weld metals subject to GGHAZ thermal cycles ( $T_p > 1200$  °C) which contained large proportions of acicular ferrite. The results of Shiga et. al. are similar to those reported by Huppi [14] who thermally cycled submerged arc C-Mn-Mo-Ti-B and C-Mn-Mo-Nb weld metals. Huppi reported that minimum toughness was measured at a peak thermal simulation temperature of approximately 1150 °C and that toughness improved with increasing peak temperature.

Chen et. al. [9-12] investigated the effect of thermal cycle peak temperatures in weld metals with variations in manganese concentrations ranging from 0.68 wt. pct. to 1.98 wt. pct. They found that the lowest toughness was measured in weld thermally cycled to peak temperatures above 1350 °C or those subjected to a double thermal cycle of 1350 °C + 850 °C.

It is interesting to note the results obtained in the various weld metal simulation studies. It should be noted that the thermal cycles employed by the different investigators were not all similar. In some studies (as in this study and the study by Cerjak et. al.[8]), the simulated thermal cycles were similar to an actual thermal cycle found in a weld heat affected zone. In other studies, a long hold time was imposed at the peak temperature. The differences in simulation technique, sample preparation, and weld metal chemical composition make it difficult to directly compare the results of the different studies.

Gleeble simulation has proven to be a suitable test method to evaluate microstructures and toughness of different regions found in multipass weldments. The trends in microstructure and mechanical properties measured in the thermally cycled weld metals were consistent with those measured in multipass weld metals with the same chemical compositions and similar cooling rates.

#### **4.0 Conclusions**

1. Similar to the multipass studies, this study showed that high toughness in both as-deposited and reheated weld metals containing titanium concentrations of either 30 ppm, or approximately 235 to 420 ppm titanium. Decreased toughness was measured in weld metals containing either less than 10 ppm titanium or approximately 100 ppm titanium. The trends in toughness measured in the as-deposited and reheated weld metals were consistent with those measured previously in high strength multipass welds and in lower strength C-Mn steel weld metals with similar variations in titanium concentration.
2. In general, the toughness of weld metals with high fractions of acicular ferrite in the as-welded condition improved with increasing peak temperature during simulation. In contrast, toughness of weld metals with high proportions of aligned microconstituents improved with intercritical and FGHAZ thermal cycles and decreased when CGHAZ thermal cycles were imposed.

3. For a given chemical composition, initial microstructure had only a second-order effect on the toughness of the thermally cycled weld metal when compared to the effect of titanium additions on weld metal toughness.
4. Gleeble simulation was proven to be a suitable test method to evaluate the microstructures and toughness of different heat affected zone regions found in multipass weld metals.

## 5.0 Acknowledgments

Author M.Q. Johnson gratefully acknowledges financial support from the AWS Fellowship Foundation and the Center for Welding, Joining, and Coatings Research (CWJCR), and Oerlikon Welding Limited who fabricated the test welds.

## 6.0 References

1. M.Q. Johnson: "Microstructure-Property Relationships in Titanium-Bearing High Strength Multipass Shielded Metal Arc Weldments", Ph.D. Thesis T-4769, Colorado School of Mines, Golden, CO.
2. G.M. Evans: *Weld J.*, **71**(1992), pp. 447s-454s
3. D. Rosenthal: *Weld J.*: **20**(1941), pp. 220s-234s.
4. D. Rosenthal: *Trans. ASME*: **68**(1946), pp. 849-866.
5. D.J. Abson: IIW Doc. IX-1533-88, (1988)
6. C.W. Ramsay: Ph.D. Thesis, Colorado School of Mines, Golden, Colorado, (1986) USA.
7. M. Kocak, B. Petrovski, G.M. Evans: "Effect of Nitrogen, Titanium, and Strain Ageing on the Toughness of Weld Metals", in Eurojoin 2, Proceeding, 2nd European Conf. on Joining Technology, Florence, Italy, May 16-18, 1994.
8. H. Cerjak, E. Letofsky, X. Pitoset, A. Seiringer, and G.M. Evans: "The Influence of the Microstructure on the Toughness of C-Mn Multi-run-weld metal", IIW-Doc. IX-1814-95.
9. J.H. Chen and C. Yan: *Materials Science and Technology*, **4**(1988)732-739
10. J.H. Chen, T.D. Xia, and C. Yan: *Weld. J.* **72**(1993)19-s to 27-s.
11. J.H. Chen, G.Z. Wang, Z. Wang, L. Zhu, and Y.Y. Gao: *Metall. Trans.*, **22A**(1991)2287
12. Y. Chen and J.H. Chen, Microstructure and Toughness of Local Brittle Zone of HSLA Steel Multipass Weld Metals, IIW DOC II-1233-94, or see *China Welding* **1**(1992)122-127
13. C. Shiga, N. Texuka, T. Yamaguchi, and J. Bosansky: "Evaluation in Reheated Ti-B Weld Metals With Microstructure Analysis", IIW Doc IX-1833-96.
14. G.S. Huppi: Colorado School of Mines Thesis T-3176, Golden, Colorado, (1986)

Table 1: Chemical composition of experimental weld metals.

Interpass Temp °C	Code	C wt.pct.	S wt.pct.	P wt.pct.	Mn wt.pct.	Si wt.pct.	Ni wt.pct.	Mo wt.pct.	Ti ppm	N ppm	O ppm	P <sub>em</sub> wt. pct.	Ti(Coat) %
25	F1	0.040	0.006	0.011	1.51	0.26	3.35	0.46	1	54	462	0.20	0
25	F30	0.037	0.006	0.011	1.50	0.27	3.30	0.46	30	49	339	0.21	0.5
25	F100	0.039	0.006	0.011	1.56	0.27	3.02	0.45	100	59	307	0.20	1.5
25	F250	0.045	0.005	0.010	1.49	0.34	3.09	0.46	250	59	234	0.21	4
25	F420	0.047	0.006	0.010	1.58	0.34	3	0.43	420	60	215	0.21	5.7
240	C1	0.035	0.007	0.009	1.52	0.27	3.25	0.43	1	74	407	0.20	0
240	C30	0.038	0.006	0.011	1.51	0.28	3.35	0.46	30	64	353	0.20	0.5
240	C110	0.037	0.006	0.010	1.39	0.27	3.01	0.43	110	60	321	0.19	1.5
240	C235	0.046	0.006	0.011	1.53	0.35	3.10	0.45	235	58	224	0.21	4
240	C320	0.048	0.007	0.010	1.56	0.33	3.08	0.45	320	56	205	0.20	5.7

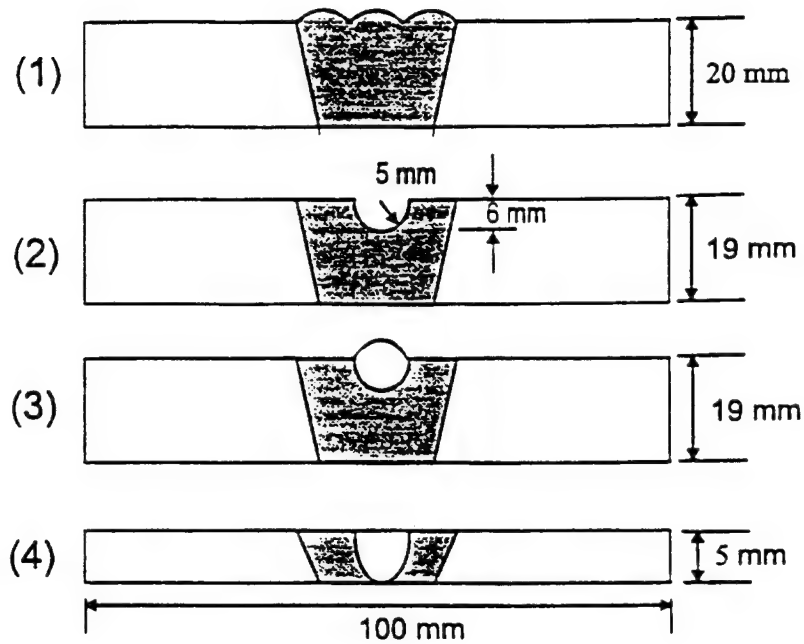


Figure 1: Production and extraction of the Gleeble test specimens.

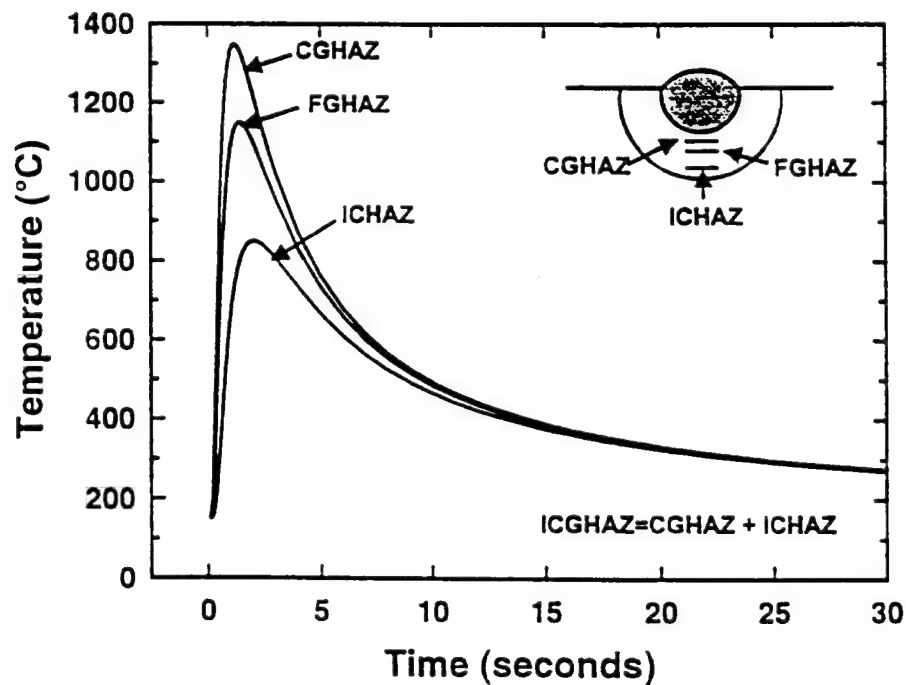


Figure 2: Thermal cycles used to simulate the following weld metal heat affected zone regions: CGHAZ-coarse grained heat affected zone, FGHAZ-fine grained heat affected zone, ICHAZ- intercritically heated heat affected zone and, ICGHAZ-intercritically heated coarse grained heat affected zone.



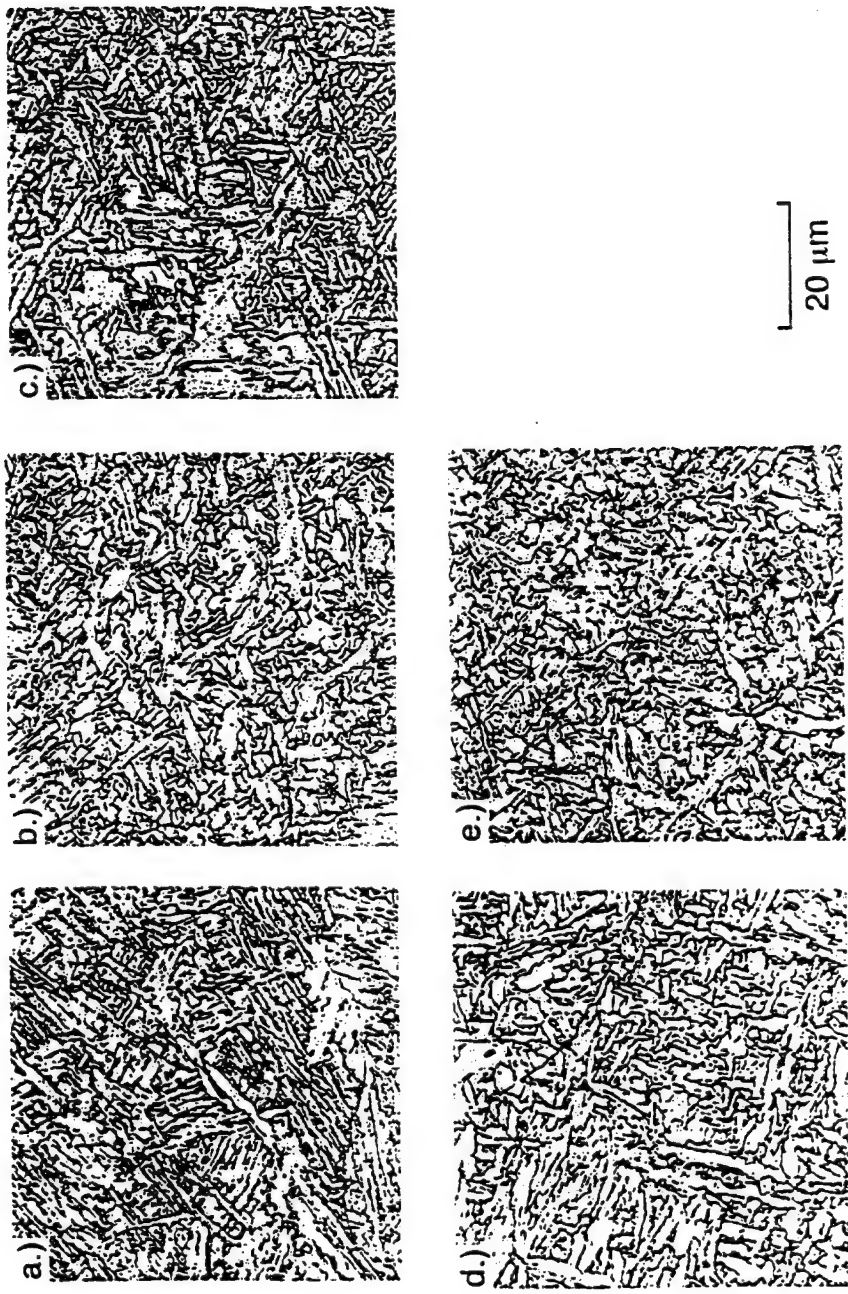


Figure 3: As-deposited weld metal microstructures in welds produced using fast cooling rates and a.) <10 ppm titanium, b.) 30 ppm titanium, c.) 100 ppm titanium, d.) 250 ppm titanium, and e.) 420 ppm titanium

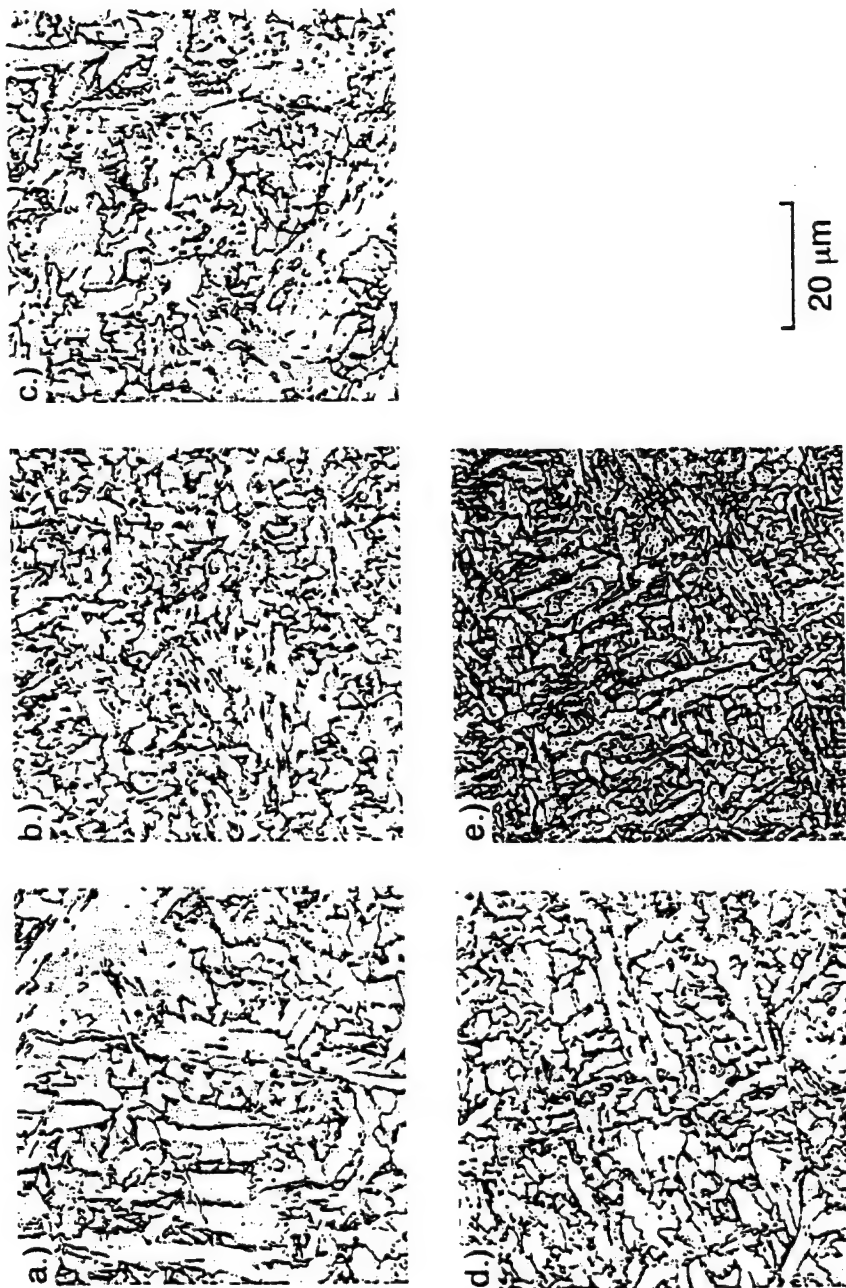
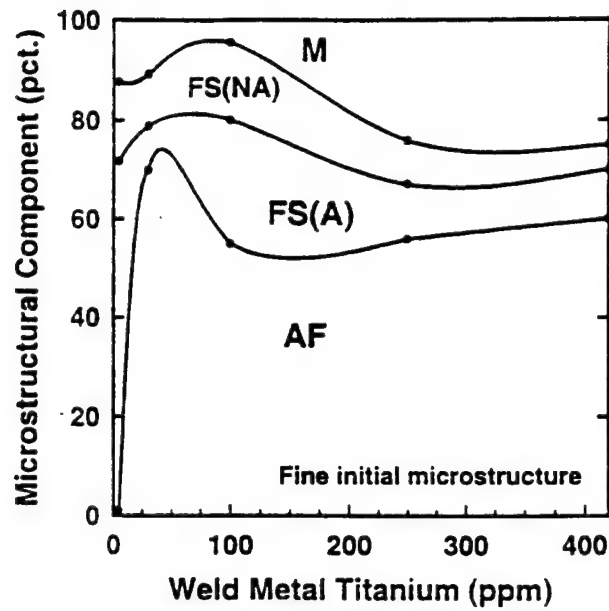
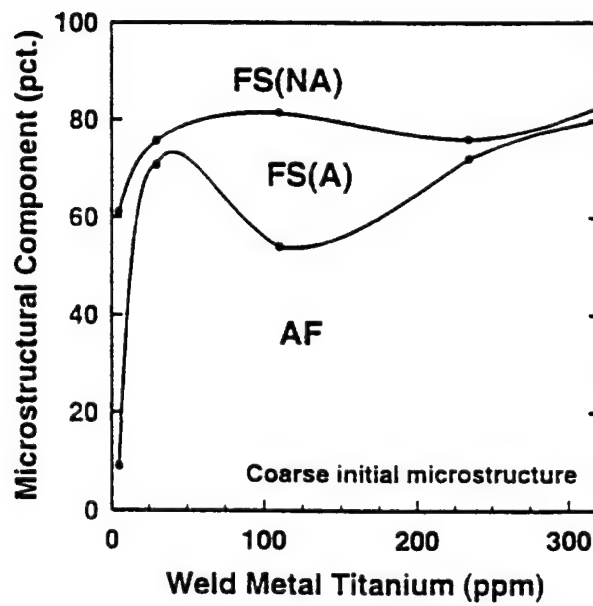


Figure 4: As-deposited weld metal microstructures in welds produced using slow cooling rates and a.) <10 ppm titanium, b.) 30 ppm titanium, c.) 110 ppm titanium, d.) 230 ppm titanium, and e.) 320 ppm titanium



a.)



b.)

Figure 5: Results of the quantitative metallography for the as-deposited weld metals produced with a.) fast cooling rates and b.) slow cooling rates.

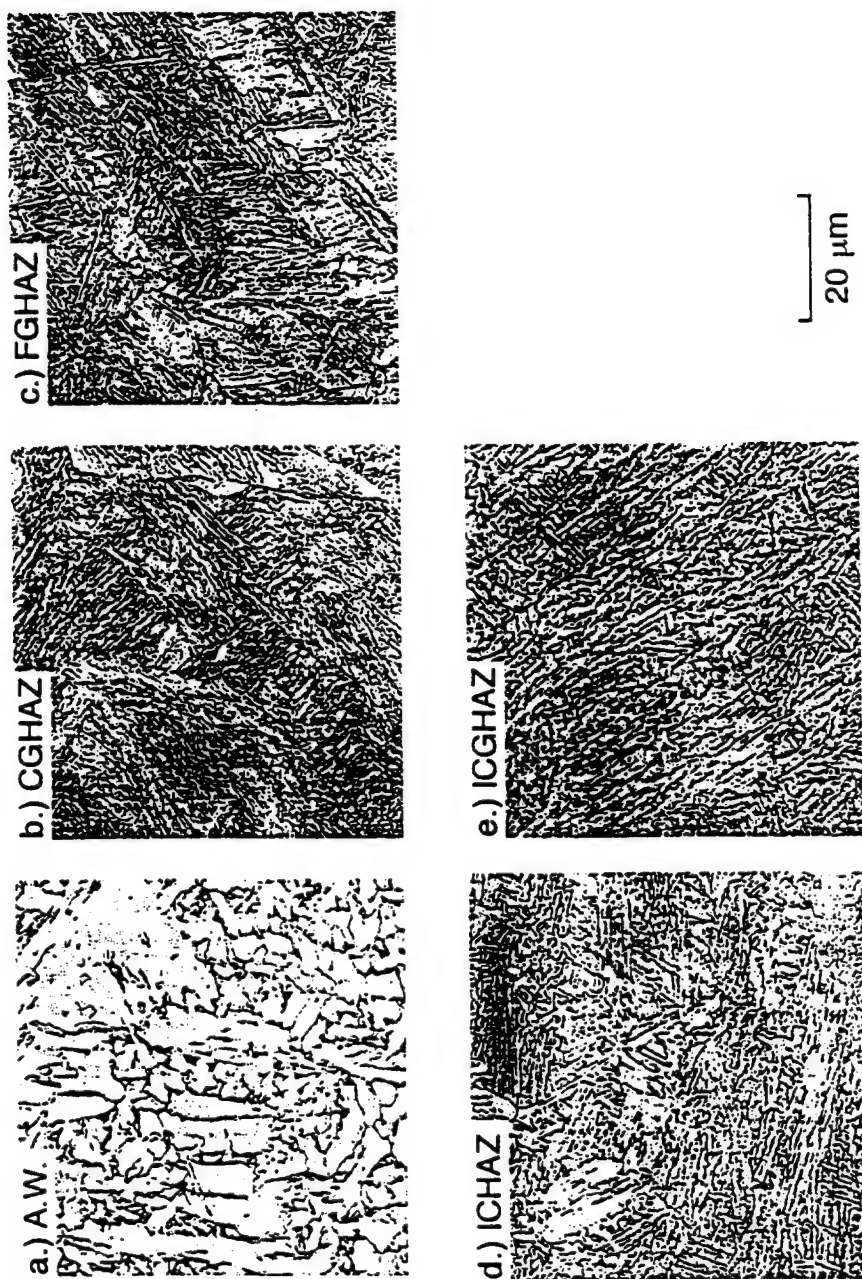


Figure 6: Simulated weld metal microstructures in titanium-free welds with coarse initial microstructures subjected to the following thermal cycles: a.) A.W.-as welded, b.) CGHAZ-coarse grained HAZ, c.) FGHAZ-fine grained HAZ, d.) ICHAZ- intercritically heated HAZ, and e.) ICGCHAZ-intercritically heated coarse grained HAZ.

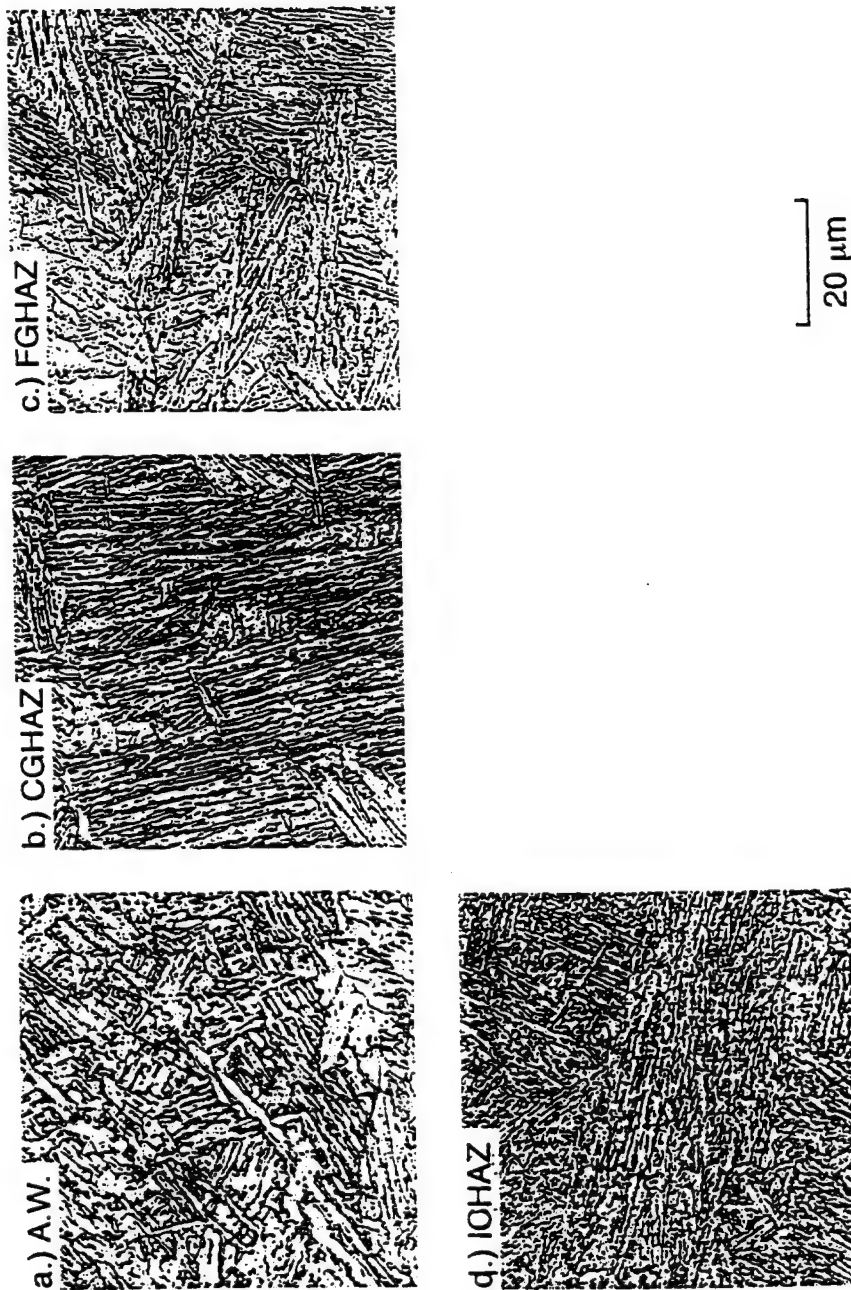


Figure 7: Simulated weld metal microstructures in titanium-free welds with fine initial microstructures subjected to the following thermal cycles: a.) A.W.-as welded, b.) CGHAZ-coarse grained HAZ, c.) FGHAZ-fine grained HAZ, d.) IOHAZ- intercritically heated HAZ.

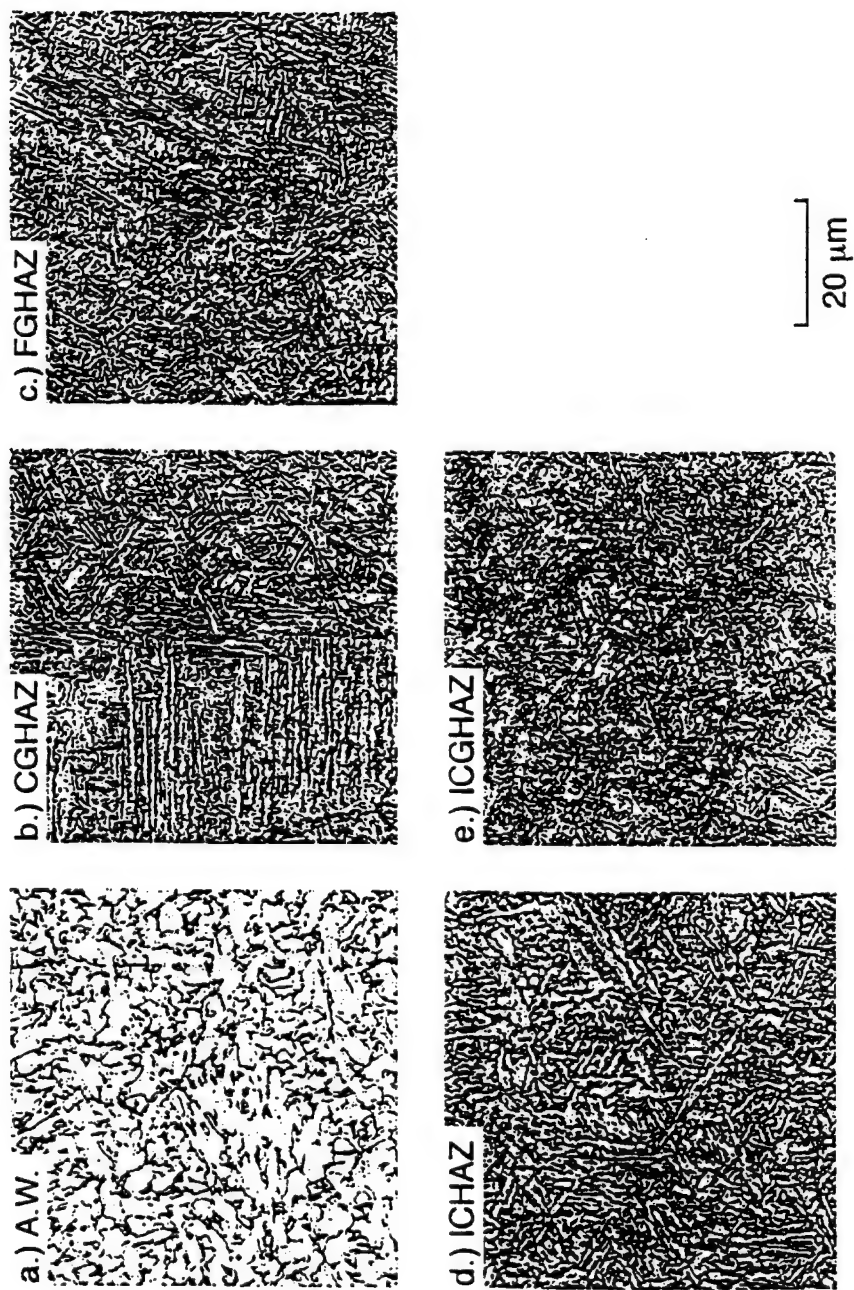


Figure 8: Simulated weld metal microstructures in welds containing 30 ppm titanium and coarse initial microstructures subjected to the following thermal cycles: a.) A.W.-as welded, b.) CGHAZ-coarse grained HAZ, c.) FGHAZ-fine grained HAZ, d.) ICHAZ-intercritically heated HAZ, and e.) ICGHAZ-intercritically heated grain coarsened HAZ.



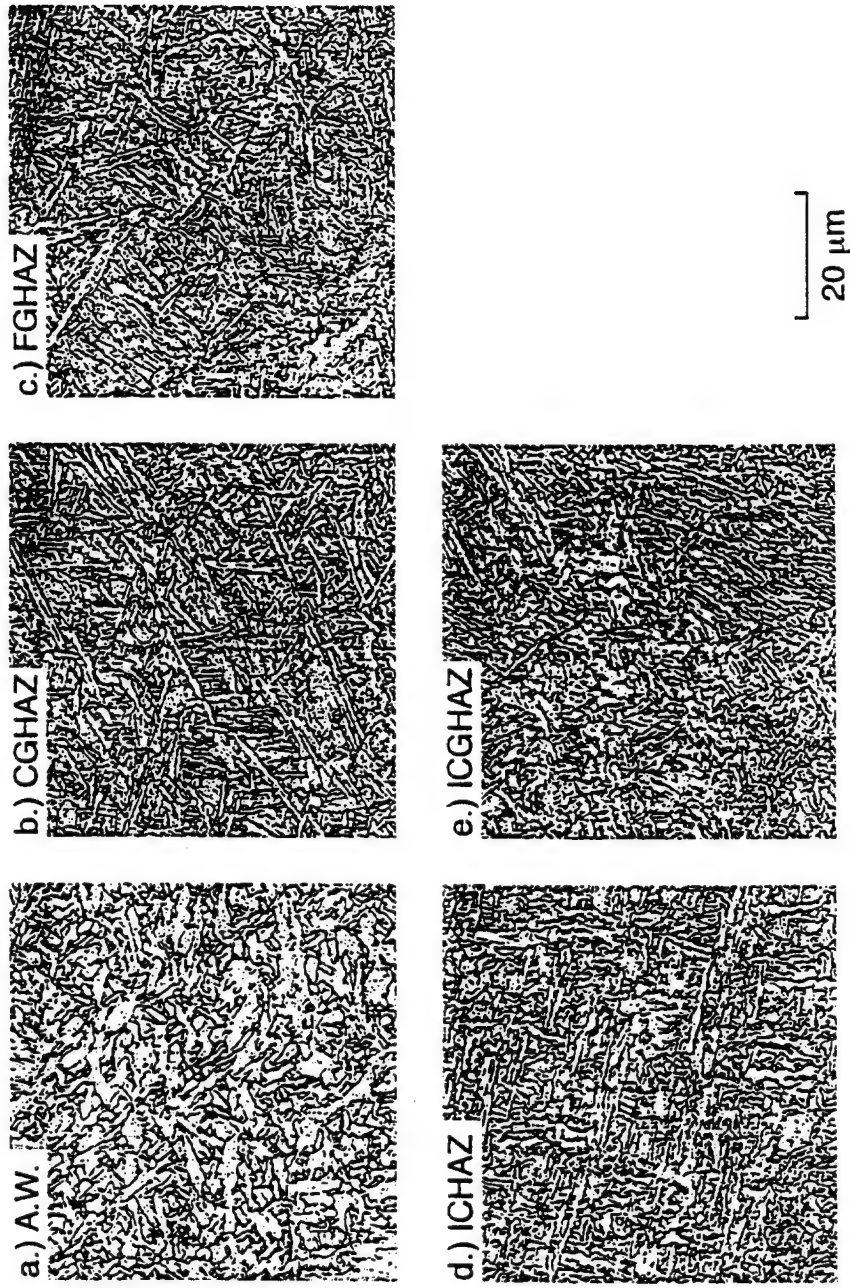


Figure 9: Simulated weld metal microstructures in welds containing 30 ppm titanium and fine initial microstructures subjected to the following thermal cycles: a.) A.W.-as welded, b.) CGHAZ-coarse grained HAZ, c.) FGHAZ-fine grained HAZ, d.) ICHAZ-intercritically heated HAZ, and e.) ICGHAZ-intercritically heated grain coarsened HAZ.

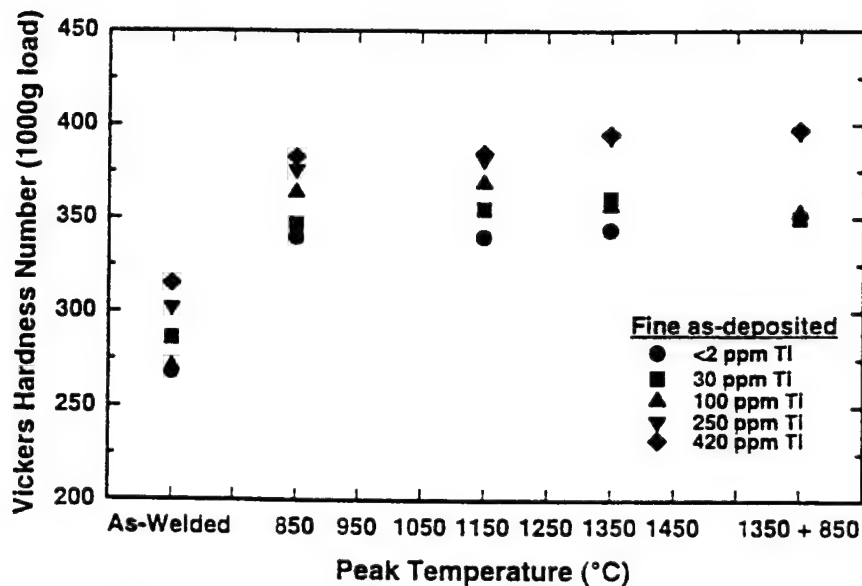


Figure 10: The effect of thermal cycles and titanium concentration on the hardness of as-deposited and simulated weld metals with fine initial microstructures.

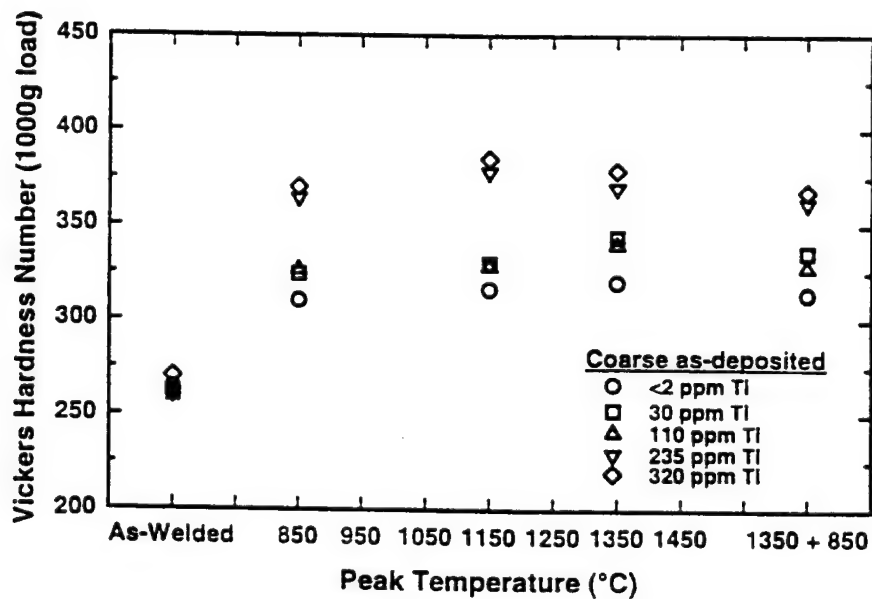


Figure 11: The effect of thermal cycles and titanium concentration on the hardness of as-deposited and simulated weld metals with coarse initial microstructures.



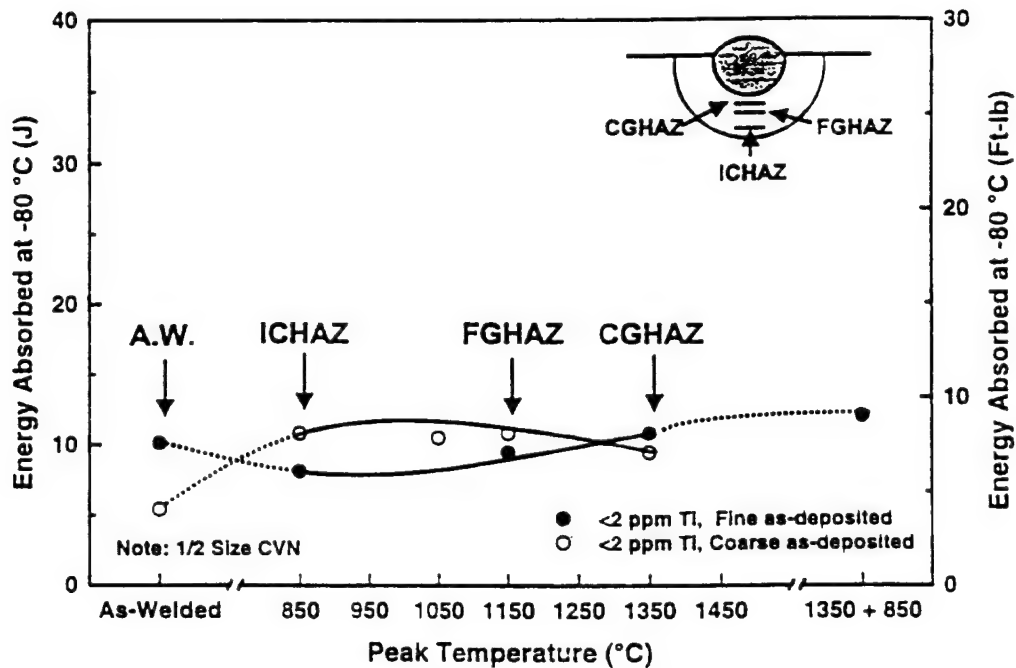


Figure 12: The effect of thermal cycles and initial microstructure on the toughness of titanium-free weld metals. Note: data taken from full transition curve using 1/2 size CVN specimens.

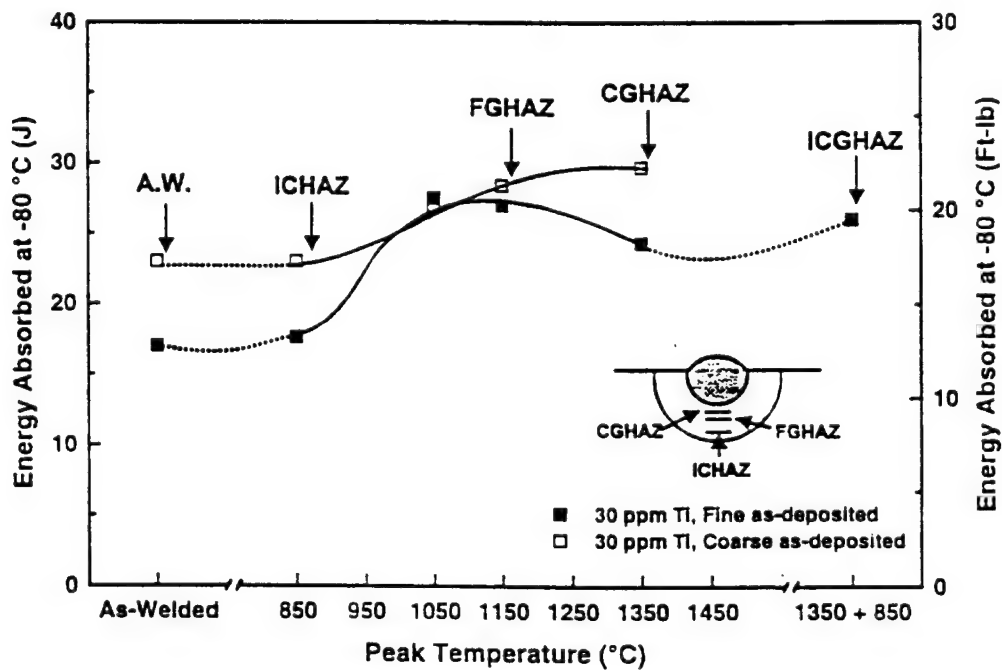


Figure 13: The effect of thermal cycles and initial microstructure on the toughness of weld metals containing 30 ppm titanium. Note: data taken from full transition curve using 1/2 size CVN specimens.

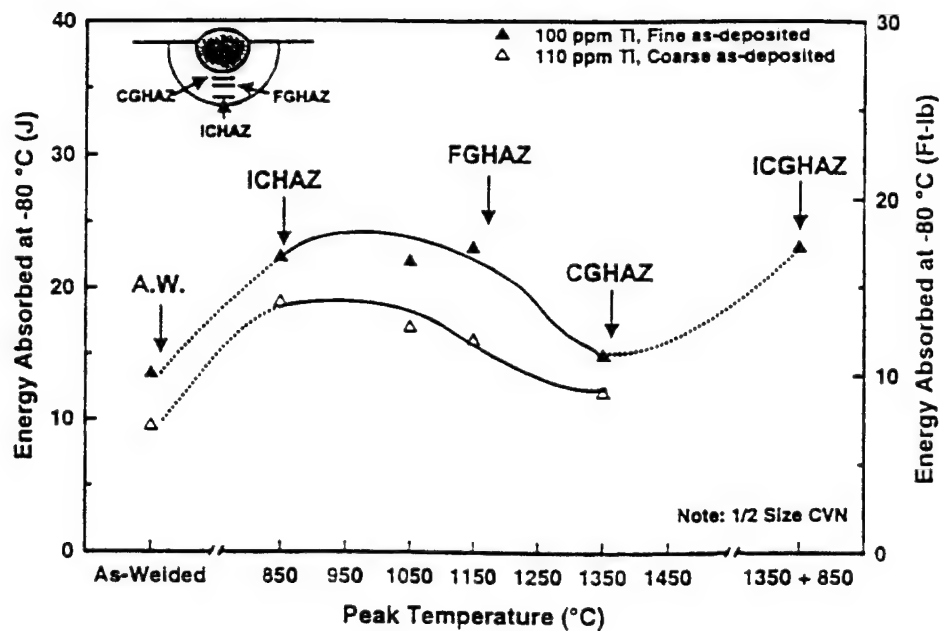


Figure 14: The effect of thermal cycles and initial microstructure on the toughness of weld metals containing 100 ppm titanium (fine initial microstructure) and 110 ppm titanium (coarse initial microstructure). Note: data taken from full transition curve using 1/2 size CVN specimens.

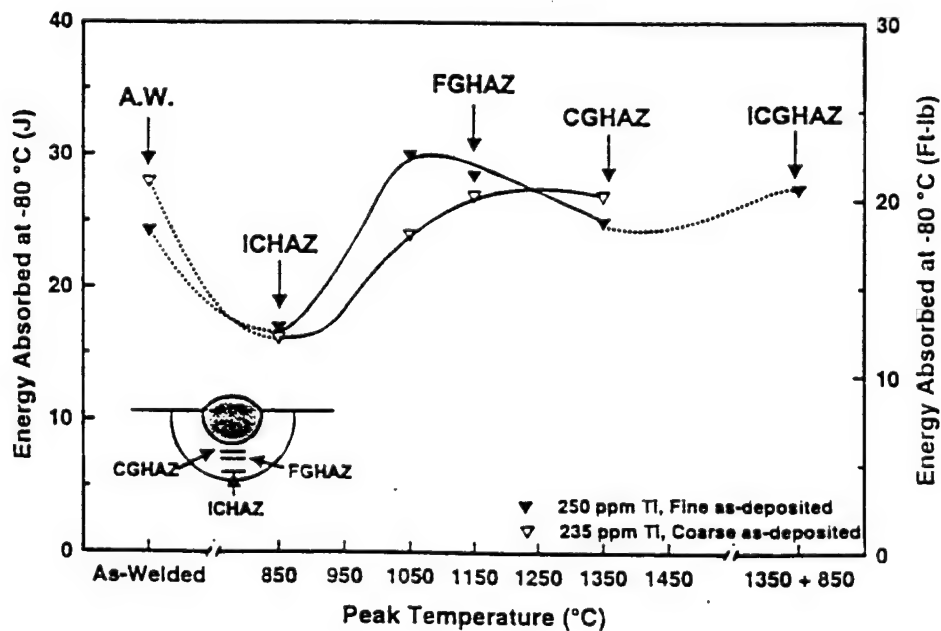


Figure 15: The effect of thermal cycles and initial microstructure on the toughness of weld metals containing 250 ppm titanium (fine initial microstructure) and 235 ppm titanium (coarse initial microstructure). Note: data taken from full transition curve using 1/2 size CVN specimens.

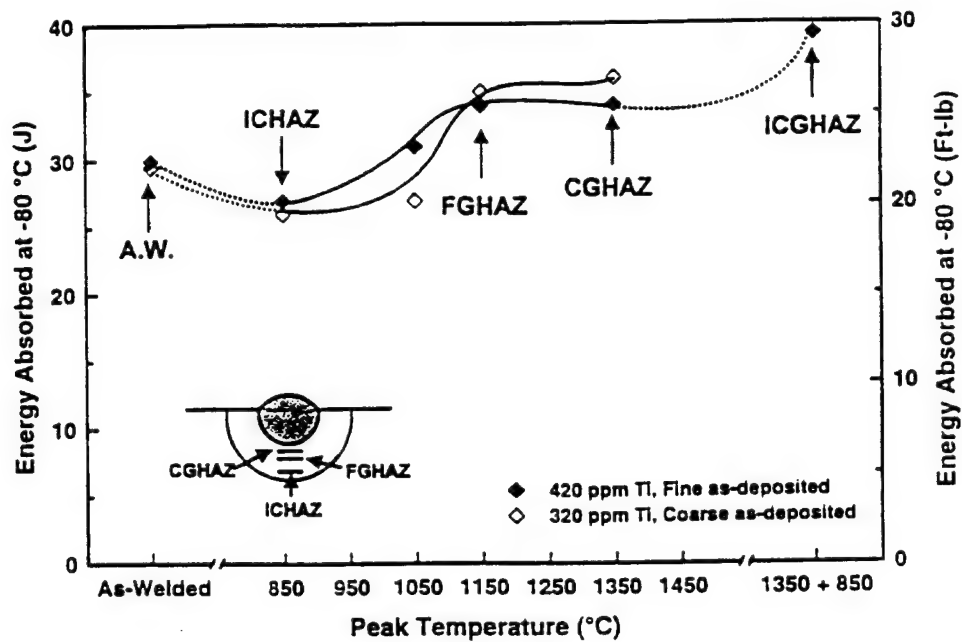


Figure 16: The effect of thermal cycles and initial microstructure on the toughness of weld metals containing 420 ppm titanium (fine initial microstructure) and 340 ppm titanium (coarse initial microstructure). Note: data taken from full transition curve using 1/2 size CVN specimens.

# **Microstructural and Fractographic Characterization of SMAW Filler Metal for HSLA 100 Steel**

by  
M. D. Clark  
G. R. Edwards

## Introduction

The implementation of high strength low alloy (HSLA) steels has resulted in substantial cost savings, primarily through the reduction or elimination of welding preheat requirements. However, weld metal cracking tendencies noted with overmatched shielded metal arc welding (SMAW) consumables have limited the possible savings.

This research was undertaken to improve the mechanical properties of multiple-pass, high strength steel weld metals, and to develop a high strength SMAW consumable capable of depositing a robust deposit that is insensitive to moderate variations in chemical composition or cooling rates.

The ability to produce high strength, high toughness, welds using SMA low C, 3%Ni-0.5%Mo-1.5%Mn electrodes with minor titanium additions, has been demonstrated for weld metals needing yield strengths in excess of 100 ksi (ref. 1). The goal of this program is to develop a leaner, lower strength (88 to 115 ksi yield) filler metal exhibiting good low temperature toughness and insensitivity to welding heat input.

## Procedure

Experimental SMAW consumables with as-deposited compositions ranging from 2.0 to 3.0 weight percent nickel and 1.0 to 1.5 weight percent manganese were prepared. In addition these welds contained 0.5 weight percent molybdenum, and 240 to 400 ppm titanium. Two sets of test welds were fabricated. "Low" heat input (1kJ/mm with ambient preheat and interpass temperatures) and "high" heat input (2.2 kJ/mm with 150°C preheat and interpass temperatures), test weldments were produced. Mechanical testing (tensile and Charpy V-notch impact), optical and scanning electron microstructural characterization of the reheated and top-bead microstructures was performed. Inclusions were characterized (size, size distribution and chemical composition) using optical microscopy, scanning electron microscopy, and scanning transmission electron microscopy. Fractographic characterization of Charpy V-notch specimens was performed by scanning electron microscopy.

## Results and Discussion

Mechanical testing demonstrated that the project goals for developing a robust, moderate strength (88-115 ksi), high CVN toughness filler metal have been met. At the high heat input (2.2 kJ/mm) all of the electrode compositions meet the project goal of 88 to 115 ksi. At the low heat input (1 kJ/mm) one filler metal, nominal 1% Mn-2% Ni, met the project requirements and one other, nominal 1.25% Mn-2% Ni, was only slightly above (116,700 psi) the specified strength range. Charpy V-notch toughness substantially exceeded the project goals of 60 ft-lbs at 0°F and 35 ft-lbs at -60°F.

A high level of toughness and insensitivity of mechanical properties to variations in heat input was observed in spite of high levels of primary ferrite in the microstructures. Correlation of transition region Charpy fracture characteristics with reheat and top bead microstructures, and oxide size and distribution, revealed those parameters which promoted microvoid nucleation and suppressed the initiation of cleavage fracture. The Charpy energy absorbed was compared to the length of the fibrous regions at the notch (the stretch zone width (SZW) and stable crack length (SCL)), and the brittle fracture zone. The absorbed energy was shown to correlate with the length of the fibrous region. The microstructural constituents associated with the initiation of brittle fracture were identified.

## Conclusion

A robust, moderate strength, high CVN toughness filler metal has been developed based on a nominal 1%Mn-2%Ni-0.5%Mo composition with 240 to 400 ppm titanium. Good impact toughness has been obtained in spite of relatively large fractions of both primary ferrite and ferrite with second phase observed in the microstructure. Microstructural characteristics which promote microvoid nucleation and correlate with the length of the Charpy V-notch fibrous zone have been identified.

## REFERENCES

1. M. Q. Johnson, "Microstructure-Property Relationships in Titanium-Bearing High Strength Multipass Shielded Metal Arc Weldments," PhD Thesis No. T-4769, August 1996, Colorado School of Mines.

# Metallographic Techniques for Microstructural Characterization of SMAW Filler Metal for HSLA 100 Steel

by

M. D. Clark

G. R. Edwards

A. Landau

## Abstract

To understand the nature of improvements in the mechanical properties of multiple-pass, high strength steel welds, it is necessary to accurately characterize the microstructures. Most studies have characterized top bead microstructures using one of several classification schemes. In this work, a tint etchant based on sodium metabisulfite is used to enhance specific microstructural features in SMA welds with as-deposited compositions ranging from 2.0 to 3.0 weight percent nickel and 1.0 to 1.5 weight percent manganese. Additionally, these welds contained 0.5 weight percent molybdenum, and 240 to 400 ppm titanium. Through a combination of etchants and etching procedures, using both optical and electron microscopy, the microstructures of these weldments were accurately characterized allowing for the correlation of mechanical properties to as-deposited microstructures.

## Introduction

The strength and toughness of fabricated weldments is dependent upon the microstructure of the deposit. An understanding of the microstructural evolution in low alloy steel welds is necessary to correlate the effects of alloy content and thermal cycle as they relate to the properties of the deposited weld metal. Microstructural development involves a sequence of reactions which include: inclusion formation, delta ferrite formation, austenite formation and transformation of austenite to the various decomposition products.

Normally, the microstructure formed within each austenite grain will be a complex mixture of two or more constituents. The identification and quantification of the various microstructural constituents is usually done by light optical and occasionally by scanning electron microscopy. The characterization of the major constituents is based on the classification scheme developed by the International Institute of Welding (IIW), Sub-Commission IXJ [1] or similar schemes.

Most welding studies quantify the relative volume fractions of microconstituents in the top bead of multiple pass welds while measuring the mechanical properties in the reheated weld

metal. Generally, only qualitative descriptions of the reheated microstructures are provided. Quantification of the reheated weld metal microstructures is difficult since the large thermal gradients produced during multiple pass welds result in correspondingly steep gradients in microstructure. The resulting as-deposited microstructures tend to be very fine, often approaching the resolution limits of optical microscopy. These structures are even difficult to quantify using the simplified IIW system. Additionally, the IIW system is only intended for the assessment of major constituents of the microstructure.

Tint etchants, based on sodium metabisulfite, have been used to aid in distinguishing the various microstructural constituents in dual- and triple-phase steels [2,3]. Standard etching techniques for low alloy steels, such as nital, usually accent grain boundaries. Classification of the various constituents is based on features such as aspect ratio, relative lath size, and number of parallel laths, or on relative position in the structure. By differentially staining the phases and structures with different crystallographic orientations, tint etchants aid in resolving the morphological features by improving resolution and contrast [4].

LePera's Reagent [5,6] is a tint etch which is based on sodium metabisulfite mixed with picric acid. This tint etch has been successfully used to aid in the microstructural analysis of HSLA 100 heat affected zone structures [7] and high strength steel weld metal microstructures [8]. LePera's Reagent aids in differentiation of the structures by tinting bainite "dark brown", ferrite "tan" and tempered martensite "black". Retained austenite and untempered martensite are not affected by the sodium metabisulfite and are left "white".

This paper discusses the application of LePera's Reagent to multiple pass SMA weld metal microstructures containing nominally 2.0 to 3.0 weight percent nickel and 1.0 to 1.5 weight percent manganese. LePera's Reagent was used to enhance contrast to aid in the identification of retained austenite and untempered martensite, collectively referred to as "M-A". The solidification structure was revealed through the use of a modification of LePera's Reagent. Finally, scanning electron microscopy (SEM), scanning transmission electron microscopy (STEM), and X-ray diffraction (XRD) were used to confirm the results of optical microscopy.

## Experimental Procedure

This work was performed as part of a program sponsored by the Office of Naval Research in the development of SMA consumables for multi-pass welding of HSLA 100 steel. A total of nine compositions have been evaluated with nominal compositions ranging from 1.0 to 1.5 weight percent manganese and 2.0 to 3.0 weight percent nickel. Other alloying additions were: 0.5 weight percent molybdenum; 0.3 maximum weight percent silicon; copper and chromium to lowest achievable levels; 0.06 maximum weight percent carbon; 240 to 400 ppm titanium; and a goal of nitrogen levels below 100 ppm. Test welds were prepared in accordance with ISO 2560 [9] using both low heat input (1 kJ/mm with ambient preheat and interpass temperatures), and high heat input (2.2 kJ/mm with a 150°C preheat and interpass temperatures).

Sections were removed from both mid-weld and the top bead (when available) and prepared for metallographic evaluation. The metallographic specimens were polished through 0.05  $\mu\text{m}$  alumina, etched in 2% nital and examined. The specimens were then repolished, etched in LePera's Reagent and examined. Since the nital etch interferes with the action of LePera's Reagent, the metallographic specimens were repolished from 0.25  $\mu\text{m}$  diamond through 0.05  $\mu\text{m}$  alumina prior to the use of LePera's Reagent. In addition, to remove any disturbed metal from the sample surface prior to using LePera's Reagent, the samples were etched in 4% picral, repolished with 0.05  $\mu\text{m}$  alumina long enough to remove the "frosted" appearance for three etching/polishing sequences. LePera's Reagent consists of a mixture of 1% sodium metabisulfite in distilled water, and 4% picric acid in ethyl alcohol, in a 1:1 volume ratio. In this study, a mixture with a volume ratio of 1:2 (4% picral:1% sodium metabisulfite) was found to be more effective for these alloys. The mixture must be prepared immediately before use, and then discarded. Etch times ranged from 30 to 60 seconds and were based upon the sample developing a uniform golden-tan color.

Area fractions of M-A constituent were determined by image analysis from optical photomicrographs taken at 1000x and compared to XRD results. Image analysis was performed by scanning the photomicrographs at 200 dpi and processing the digitized image with Adobe Photoshop (version 2.5.1). The specimens for XRD were prepared by standard polishing techniques followed by electropolishing to provide a stress-free surface. X-ray diffractograms were taken with a Phillips PW-1050 diffractometer operating in scan-step mode with Cu-K $\alpha$  radiation. The K $\beta$  was removed by graphite monochromator. The Rietveld program (version DBWS-9411PC) was used for structure refinement and determination of the lattice parameters.

Electron microscopy (both SEM and STEM) was done on longitudinal sections, which were removed near the grip ends of tensile specimens. Scanning electron microscopy was done on samples which were polished, etched in 2% nital, and gold sputter coated to enhance contrast. A wavelength dispersive X-ray (WDX) trace for iron, nickel, manganese, and molybdenum was performed on a selected sample which had been repolished and unetched. Foils for STEM were made by turning the end section of the tensile specimen by lathe down to 3 mm diameter. The 100  $\mu\text{m}$  discs were cut from the turned tensile specimens, ground to reduce thickness, and finally thinned in a twin-jet

electropolisher with an electrolyte of 30 ml perchloric acid, 500 ml butyl alcohol, and 300 ml methyl alcohol. STEM was done using a Phillips CM200 scanning electron microscope with an accelerating voltage of 200 kV.

## Results and Discussion

A comparison of the results from etching in 2% nital and LePera's Reagent is shown in Figure 1. Figure 1(a) shows the mid-weld structure of the high heat input weld based on nominal composition of 2.5 weight percent nickel and 1.25 weight percent manganese, as revealed by etching in 2% nital. The nital etch clearly delineates the ferrite grain boundaries; however, due to the lack of contrast difference and fine size, the M-A microphase cannot be reliably identified, even when examined at magnifications up to 2000x. Figure 1(b) shows the structure from the same region of the weld after etching with LePera's Reagent. With LePera's Reagent, the ferrite grain boundaries are not strongly etched but the M-A constituent is readily identified as "white" in the structure.

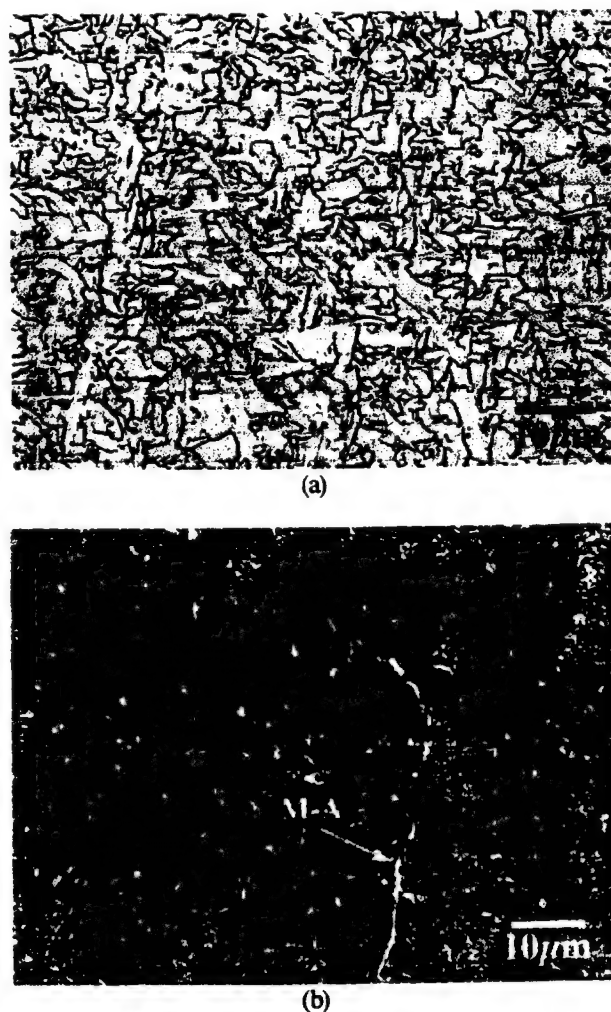


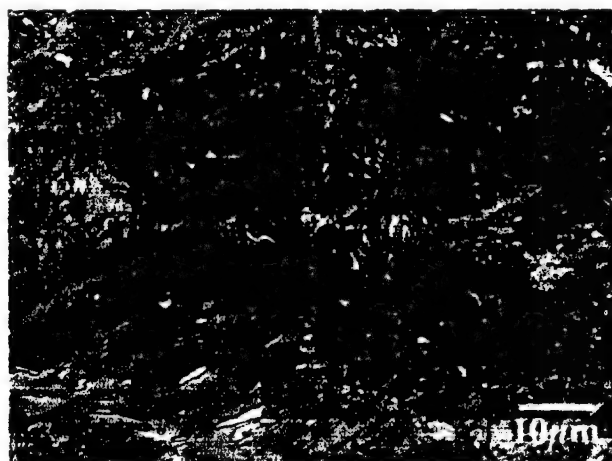
Figure 1. (a) Light micrograph showing weld metal microstructure as revealed by 2% nital and (b) as revealed by LePera's Reagent.

The results of image analysis and XRD are given in Table 1 for four samples representing the range of alloys and heat inputs considered in the welding program. A comparison of results shows reasonable agreement. All of the samples contained less than two percent retained austenite. With one exception, the optical image analysis resulted in lower quantities of retained austenite than XRD due to the inability to optically resolve very fine grains or very thin films of M-A.

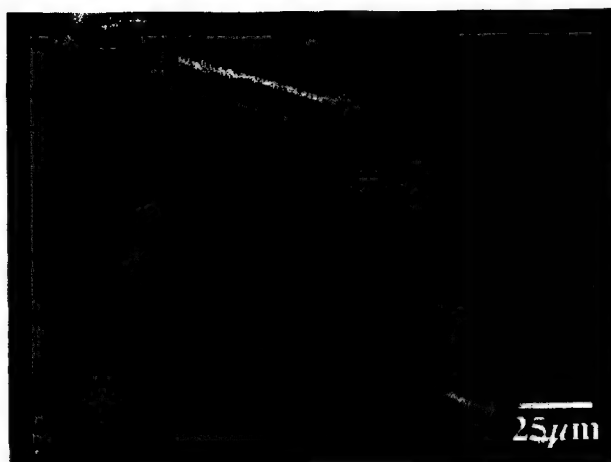
Table 1. Comparison of percentage retained austenite measured by XRD to percentage M-A determined by optical image analysis.

Nom. Comp.	Heat Input	XRD (%)	Optical (%)
2%Ni-1%Mn	2.2 kJ/mm	1.8 to 2.1	1.2
3%Ni-1.5%Mn	2.2 kJ/mm	0.5 to 0.6	0.7
2%Ni-1%Mn	1 kJ/mm	1.7 to 2.0	0.8
3%Ni-1.5%Mn	1 kJ/mm	1.7 to 2.0	0.7

Using LePera's Reagent, even sub-micron sized retained austenite particles could be identified. However there was no reliable distinction in the shade of tinting between primary ferrite (PF), ferrite with second phase (FS), or acicular ferrite (AF) as observed by investigators using this reagent on dual- and triple-phase steels. Similarly, with SEM, retained austenite is observed as smooth, featureless particles leading to easy distinction from PF, FS and AF. Figure 2(a) shows a region of weld metal consisting of acicular ferrite, ferrite with second phase (both Widmanstattan ferrite and bainite) and primary ferrite. The retained austenite exists as both micron to sub-micron sized blocky particles and as elongated particles between the plates of the Widmanstattan ferrite. The scanning electron photomicrograph in Figure 2(b) shows a region of Widmanstattan ferrite, etched in 2% nital, taken from the same region as viewed optically in Figure 2(a). The elongated particles of retained austenite are easily distinguished from the ferritic matrix. Figure 2(c) shows similar elongated particles as viewed



(a)



(b)



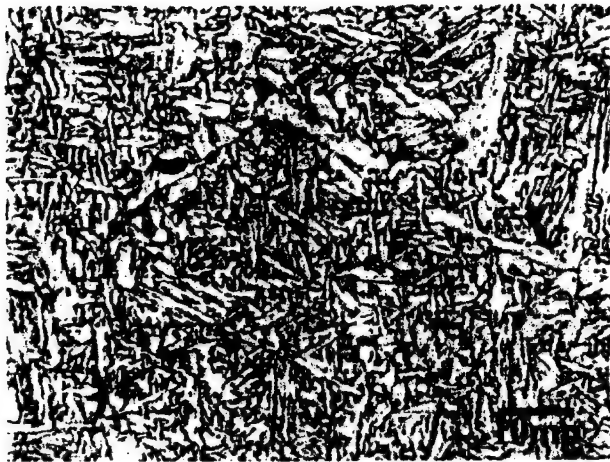
(c)

Figure 2. (a) Light micrograph showing retained austenite as blocky particles throughout the matrix and as elongated particles between plates of Widmanstattan ferrite as revealed by LePera's Reagent. (b) Scanning electron micrograph showing elongated particles of retained austenite between plates of ferrite as revealed by 2% nital. (c) Scanning transmission electron micrograph showing elongated particles of retained austenite between ferrite plates.

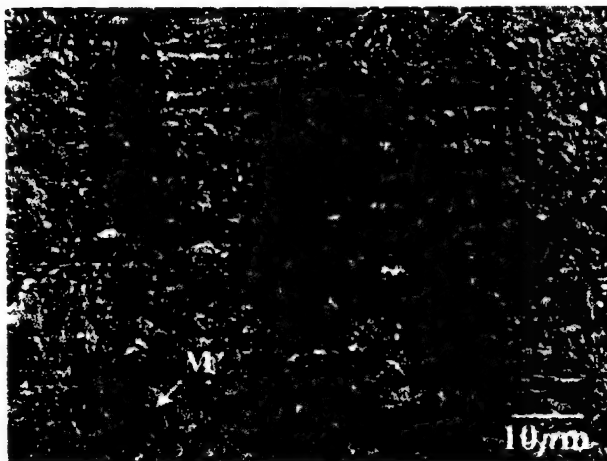
with STEM. Confirmation that these particles are retained austenite by analysis of the X-ray diffraction pattern has not been completed; however, X-ray analysis has qualitatively shown these particles to be significantly higher in nickel than the surrounding matrix.

The effect of LePera's Reagent on tempered martensite is similar to that of nital. Figure 3(a) shows the microstructure of the weld metal intercritical heat affected zone (ICHAZ) etched with 2% nital. Particles of tempered martensite along the prior austenitic grain boundaries appear "black" in the photomicrograph. Figure 3(b) shows a similar structure etched with LePera's Reagent. In LePera's Reagent the tempered martensite also appears "black". With SEM, Figure 3(c) the evidence of substructure and carbide precipitation in the tempered martensite is apparent.

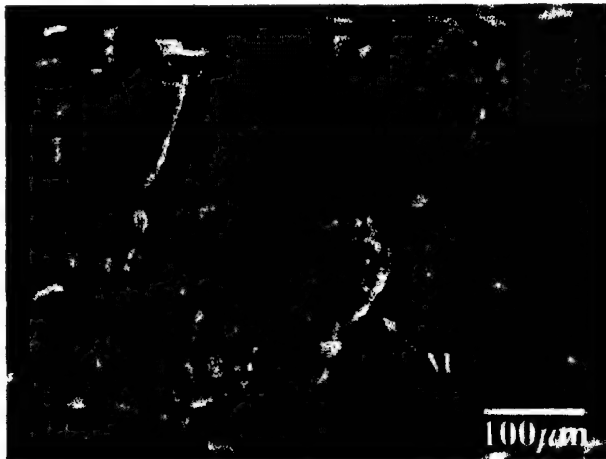




(a)



(b)

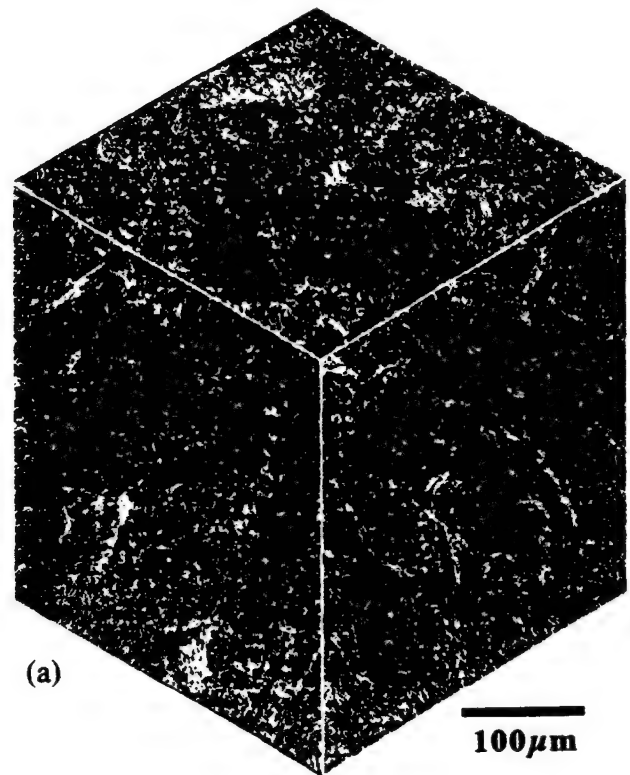
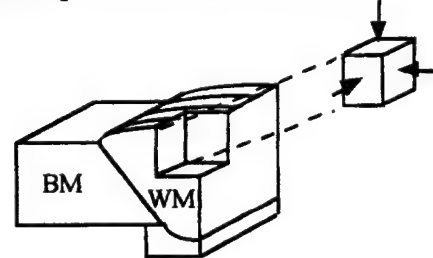


(c)

Figure 3. (a,b) Light and (c) scanning electron micrographs showing tempered martensite along prior austenitic grain boundaries in the ICHAZ. (a,c) 2% nital and (b) LePera's Reagent.

In an effort to minimize the quantities of picric acid waste, alternate combinations and etching sequences with sodium metabisulfite were investigated. One of these combinations

using an etch in 4% picral, followed by a rinse, then tinting in 1% sodium metabisulfite revealed the cellular solidification structure of the weld. Figure 4(a) is a three-dimensional, composite micrograph showing the longitudinal, long-transverse, and short-transverse structures of a top bead as revealed by etching in 2% nital. Little evidence of the cellular solidification structure is apparent. Figure 4(b) shows a three-dimensional composite photomicrograph of the same structure after etching in 4% picral, rinsing, and staining in 1% sodium metabisulfite. In Figure 4(b), the cellular solidification structure of the weld is clearly evident. A WDX trace, analyzing for manganese, nickel, molybdenum and iron was performed to identify the nature of the observed segregation. Figure 5(a) shows the region of the microstructure which was analyzed by WDX, with the resulting plot for nickel composition. Similarly, Figure 5(b) shows the structure along with the resulting plot for manganese. Both manganese and nickel contents are lower in the dark-stained regions and higher in the light, unstained regions. As apparent in the three-dimensional cube shown in Figure 4(b), the white, unstained regions correspond to the inter-cellular regions. As solidification takes place manganese and nickel (both austenite stabilizers) are rejected from the initial ferrite to solidify, enriching the inter-cellular regions in these elements.



(a)

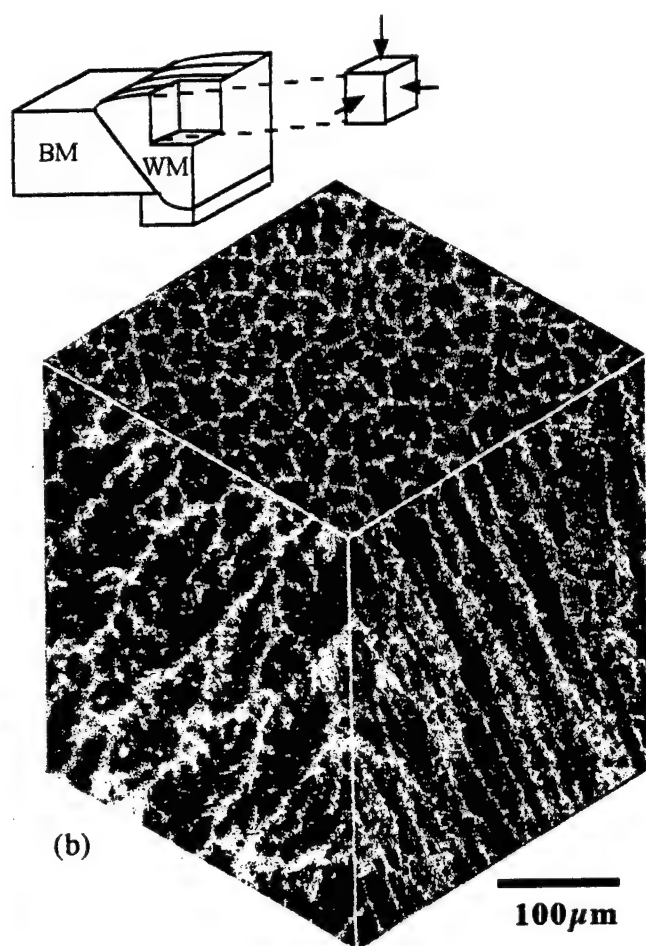


Figure 4. Three-dimensional light micrograph showing as-deposited microstructure as revealed by 2% nital (a), and solidification segregation (b), as revealed by modified LePera's Reagent.

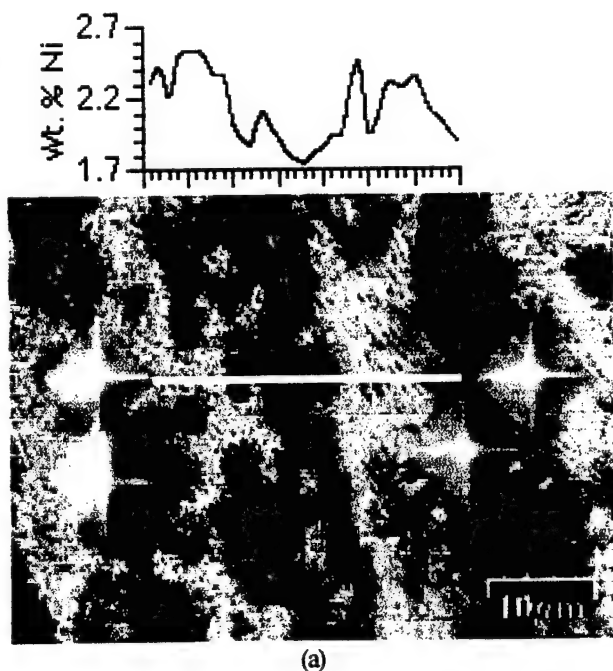


Figure 5. WDX analysis of segregation structure showing variation in nickel (a), and manganese (b) composition along the indicated trace.

## Summary and Conclusions

1) A method has been established to identify M-A constituent using light optical microscopy in multi-pass SMA HSLA weld metals with nominal compositions ranging from 2.0 to 3.0 weight percent nickel and 1.0 to 1.5 weight percent manganese.

2) Submicron-sized particles of M-A could be easily distinguished from primary ferrite, ferrite with second phase, acicular ferrite and tempered martensite in light microscopy when etched with a fresh solution of 4% picric acid in ethanol mixed with a 1% solution of sodium metabisulfite in distilled water in a 1:2 volume ratio.

3) The cellular solidification structure resulting from the enrichment of the inter-cellular region with nickel and manganese was evident in light microscopy when the samples were etched in 4% picral, rinsed, and then tinted in 1% sodium metabisulfite.

## Acknowledgments

The authors acknowledge the research support offered by the Office of Naval Research. The assistance of the Lincoln Electric Company in preparing the welding consumables and test weldments is greatly appreciated, as is the assistance of Mr. Yosi Saryel of the Department of Materials Engineering, Ben Gurion University of the Negev for performing the XRD for retained austenite.

## References

1. IIW Doc. No. IX-1533-88, IXJ-123-87, Revision 2, June 1988, "Guide to the Light Microscope Examination of Ferritic Steel Weld Metals."
2. Q.Y. Long, D. Tseng and K. Tangri, *Metallography*, 20, 61-73 (1987)
3. W.C. Jeong, D.K. Matlock and G. Krauss, *Materials Science and Engineering*, A165, 1-8 (1993)
4. J.R. Kilpatrick, A.O. Benscoter and A.R. Marder, *Metal Progress*, 100, 79-81 (1971)
5. F.S. LePera, *JOM*, 38-39 (1980)
6. F.S. LePera, *Metallography*, 12, 263-268 (1979)
7. K.L. Kenney: MS Thesis: Colorado School of Mines, Golden, Colorado (1996)
8. P.T. Oldland, C.W. Ramsay, D.K. Matlock and D.L. Olson, *Welding Journal*, 158-s to 168-2 (April 1989)
9. ISO 2560 - 1973, "Covered Electrodes for Manual Arc Welding of Mild and Low Alloy Steel."

**B. Dual-Precipitation Agent Selection for Minimizing Mechanical Property Fluctuations in the Reheated Weld Metal in Multipass High Strength Steel Welds, by J. E. Ramirez, S. Liu, and D. L. Olson, Colorado School of Mines**

Based on a dual-precipitation scheme,  $\epsilon$ -Cu and niobium carbide, an alloy weld metal was designed to: first, provide high heat input welds (with a ferritic matrix) with additional strength required to match a specified set of properties; and second, minimize the undesirable property fluctuations observed in the heat-affected zone of the weld metal during multipass welding required in heavy section fabrication. The design of weld metal properties using second-phase precipitates was based on simple metallurgical principles such as precipitation reaction and adequate control of grain growth.

The selection procedure was demonstrated by screening several potential precipitation agents. Initially, the solid solution behavior of different elements in  $\alpha$ -iron was analyzed. The iron-copper system offers several important advantages for designing an alloy that develops its strength by precipitation. This system has an extended  $\gamma$ -field, and the copper atoms are about the same size as the iron atoms (ratio of radii Cu:Fe = 1.003). The degree of supercooling and supersaturation that can be achieved result in higher nucleation rate and promote homogeneous nucleation.

Copper additions were found to precipitation-strengthen the high-strength steel weld metals. Welds of higher heat input, 3.6 kJ/mm, were observed to benefit more from copper precipitation strengthening. An estimated yield strength of 900 MPa (130 ksi) can be achieved, during single-pass welding, with approximately 2.8 wt.% of copper addition. Nevertheless, multipass welding over copper-enhanced weld metal resulted in non-uniform weld metal properties in the reheated zone of the underbead weldments.

It was appropriate to select niobium carbide precipitates, with a high equilibrium solubility temperature, to control the onset and extent of the grain growth. Besides, the higher thermal stability of niobium carbide as compare to  $\epsilon$ -Cu precipitates provides a complementary and more stable precipitation-strengthening effect to the weld metal. Therefore, to overcome the undesirable property variations of  $\epsilon$ -Cu-strengthened, high-strength steel weld metal, observed during multipass welding, the use of two different precipitates in the weld metal, a combination of both  $\epsilon$ -copper and niobium carbide, was used in this research work.

Dual precipitation of  $\epsilon$ -copper and niobium carbides was observed to provide the needed strength throughout the multiple thermal cycles. At approximately 3.2 wt.% copper and 0.05 wt.% niobium in the weld deposits, the two elements provided the strengthening effect and stable precipitates to obtain high-strength steel weld metal with acceptable properties in a wide range of heat input welding conditions, during single- and multipass welding.

The synergistic effect of copper and niobium in high-strength steel weld metal derives from, first, the combination of two kinds of precipitates with distinct precipitation reaction kinetics; second, the combination of two kinds of precipitates

with different thermal stability; and third, the effect of niobium on the segregation pattern of copper in the weld metal. The dual precipitation scheme controls the precipitation coarsening and grain-growth reactions to result in acceptable and more uniform mechanical properties of high-strength steel weld metals, during single- and multipass welding conditions in a broad range of heat inputs.

C. **Some New Ideas about the Nonmetallic Inclusions Present in the Fusion Zones of Steel Arc Weldments**, by A. G. Fox, Naval Postgraduate School; M. G. Vassilaros, G. L. Franke, and R. J. Wong, Naval Surface Warfare Center

It is well known that nonmetallic inclusions can have profound effects on the mechanical properties of both wrought steels and their weld metals. For example, modern weldable steels for high-strength applications are usually desulfurized and calcium- or rare earth-treated to ensure any residual nonmetallic inclusions are strong and nondeformable so that mechanical properties are close-to-isotropic and resistance to lamellar tearing is improved. In submerged arc weld (SAW) metal in steels, attempts are usually made to control the number, size, distribution, and chemical composition of the nonmetallic inclusions so that the amount of intragranular acicular ferrite is maximized. This, in turn, improves both the strength and toughness of the weld metal.

In the present work, many multirun gas tungsten arc welds (GTAW), gas metal arc welds (GMAW) and submerged arc welds (SAW) welds were made on ULCB-100, HSLA-100 and HY-100 steels. For the GTAW, the cover gas used was pure argon and for the GMAW, a series of argon-based cover gases containing different amounts of O<sub>2</sub> and/or CO<sub>2</sub> were used. For the SAW welds, the effect of varying the oxygen activity through flux basicity on the weld metal was investigated. Samples from each weld metal were cut and polished and the inclusion size distribution determined by back-scattered imaging in the scanning electron microscope (SEM). These samples were then etched to see if the inclusion content had had any effect on the microstructure. Carbon extraction replicas were taken from each sample and the average inclusion composition determined by energy dispersive x-ray analysis in the transmission electron microscope (TEM). This inclusion data was then correlated with the overall chemical composition and microstructure of the weld metals.

As expected, the volume fraction of inclusions increased as the oxygen content of the welds increased. This ranged from 0.00037 for a GTAW weld metal containing 70 ppm oxygen to as high as 0.00966 for a SAW weld metal containing 320 ppm O. The inclusion size distribution for each welding process was quite different. For the GTAW weld metal where the total oxygen content was found to be low (between 60 and 130 ppm), the average inclusion diameter was 0.434  $\mu\text{m}$  with almost all the inclusions being less than 1.0  $\mu\text{m}$  in size with a close-to-symmetrical distribution about the mean. For the GMAW weld metal, the total oxygen content varied between 180 and 280 ppm with an average inclusion diameter of 0.310  $\mu\text{m}$  and most inclusion diameters were than less than 1.5  $\mu\text{m}$ .

Reprinted from

# **MATERIALS SCIENCE & ENGINEERING**

## **A**

---

Materials Science and Engineering A216 (1996) 91-103

Dual precipitation strengthening effect of copper and niobium in  
high strength steel weld metal

J.E. Ramirez<sup>a</sup>, S. Liu<sup>b</sup>, D.L. Olson<sup>b</sup>

<sup>a</sup>*Instituto Colombiano del Petroleo, Bucaramanga, Colombia*

<sup>b</sup>*Center for Welding, Joining and Coatings Research Department of Metallurgical and Materials Engineering, Colorado School of Mines, Golden,  
Colorado 80401, USA*



# MATERIALS SCIENCE AND ENGINEERING A

The journal provides an international medium for the publication of theoretical and experimental studies and reviews of the properties and behavior of a wide range of materials, related both to their structure and to their engineering application. The varied topics comprising materials science and engineering are viewed as appropriate for publication: these include, but are not limited to, the properties and structure of crystalline and non-crystalline metals and ceramics, polymers and composite materials.

---

## Editor-in-Chief

Professor H. Herman

## Associate Editors

M. Koiwa (*Japan*)

G. Kostorz (*Switzerland*)

## Editorial Board (MSE A)

J. Ågren (*Sweden*)

G. Ananthakrishna (*India*)

R. J. Arsenault (*USA*)

D. Brandon (*Israel*)

H. K. D. H. Bhadeshia (*UK*)

J. Cadek (*Czech Republic*)

J. B. Cohen (*USA*)

J. Driver (*France*)

J. D. Embury (*Canada*)

Y. Estrin (*Australia*)

H. Fischmeister (*Germany*)

C. Garcia de Andrés (*Spain*)

H. Gleiter (*Germany*)

M. W. Grabski (*Poland*)

M. Kato (*Japan*)

Y. G. Kim (*Korea*)

C. Laird (*USA*)

J. Lendvai (*Hungary*)

W. Mader (*Germany*)

M. McLean (*UK*)

L. Priester (*France*)

S. Sampath (*USA*)

V. K. Sarin (*USA*)

P. Shen (*Taiwan*)

M. Suery (*France*)

S. Suresh (*USA*)

N. S. Stoloff (*USA*)

M. Taya (*USA*)

A. K. Vasudévan (*USA*)

A. Vevecka (*Albania*)

B. Wilshire (*UK*)

M. Yamaguchi (*Japan*)

T. S. Yen (*China*)

## Print and Electronic Media Review Editor

A. H. King (*USA*)

## Administrative Editor

Barbara Herman

## Advisory Board (MSE A and B)

H. Herman, Chairman (*USA*)

H. Curien (*France*)

M. E. Fine (*USA*)

A. Kelly, FRS (*UK*)

R. Lang (*Japan*)

H. Mughrabi (*Germany*)

P. Rama Rao (*India*)

---

## Types of contributions

Original research work not already published; plenary lectures and/or individual papers given at conferences; reviews of specialized topics within the scope of the journal; engineering studies; letters to the editor.

## Subscription Information 1996

Volumes 205–221, each volume containing 2 issues, are scheduled for publication. Prices are available from the publishers upon request. Subscriptions are accepted on a pre-paid basis only. Issues are sent by SAL (Surface Air Lifted) mail wherever this service is available. Airmail rates are available upon request. Please address all requests regarding orders and subscription queries to

## ELSEVIER SCIENCE SA

P.O. Box 564, 1001 Lausanne, Switzerland

Telephone: (21) 3 20 73 81

Telex: 450620 ELSA CH    Telefax: (21) 3 235 444; E-mail: [essa-o@elsevier.ch](mailto:essa-o@elsevier.ch)

Issues are sent by surface mail after air delivery to Argentina, Australia, Brazil, Canada, China, Hong Kong, India, Israel, Japan, Malaysia, Mexico, New Zealand, Pakistan, Singapore, South Africa, South Korea, Taiwan, Thailand and the USA. Airmail rates for other countries are available on request.

For advertising rates apply to the publishers. A specimen copy will be sent on request.

US and Canadian customers may obtain information from the following.

## ELSEVIER SCIENCE INC.

Attn.: Journal Information Center, 655 Avenue of the Americas  
New York, NY 10010, USA.

Telephone: (212) 633 3750    Telex: 420 643 AEP UI

Telefax: (212) 633 3764.

## Abstracting and/or Indexing Services

American Ceramic Society; Cambridge Scientific Abstracts; Chemical Abstracts; Current Contents; Engineering Index; FIZ Karlsruhe; Fluid Abstracts; Fluidex; Glass Technology Abstracts; Inspec/Physics Abstracts; Metals Abstracts; Pascal (Centre National de la Recherche Scientifique); Physikalische Berichte; Research Alert™; Science Citation Index.

## Advertising Information

Advertising orders and enquiries may be sent to: **International:** Elsevier Science, Advertising Department, The Boulevard, Langford Lane, Kidlington, Oxford OX5 1GB, UK. Tel.: +44 (1865) 843 565. Fax: +44 (1865) 843 952. **USA and Canada:** Weston Media Associates, Dan Lipner, P.O. Box 1110, Greens Farms, CT 06436-1110, USA. Tel.: +1 (203) 261 2500. Fax: +1 (203) 261 0101. **Japan:** Elsevier Science Japan, Advertising Department, 1-9-15 Higashi-Azabu, Minato-ku, Tokyo 106; Tel: +81-3-5561-5033; Fax: +81-3-5561-5047. E-mail: [KYFO4035@niftyserve.or.jp](mailto:KYFO4035@niftyserve.or.jp).



# Dual precipitation strengthening effect of copper and niobium in high strength steel weld metal

J.E. Ramirez<sup>a</sup>, S. Liu<sup>b</sup>, D.L. Olson<sup>b</sup>

<sup>a</sup>*Instituto Colombiano del Petroleo, Bucaramanga, Colombia*

<sup>b</sup>*Center for Welding, Joining and Coatings Research Department of Metallurgical and Materials Engineering, Colorado School of Mines, Golden, Colorado 80401, USA*

## Abstract

Experimental work to produce high strength steel welds with systematic additions of copper (up to 3.5 wt.pct.) and niobium (up to 0.45 wt.pct.) at  $3.6 \text{ kJ mm}^{-1}$  ( $90 \text{ kJ in}^{-1}$ ) heat input was carried out. Copper additions were found to precipitation strengthen the high strength steel weld metals. An estimated yield strength of 900 MPa (130 ksi) can be achieved in single-pass welds with approximately 2.8 wt.pct. of copper addition. Nevertheless, multipass welding over the copper-enhanced weld deposit resulted in nonuniform weld metal properties across the weld beads. Niobium additions did not provide as powerful a strengthening effect in the single-pass high heat input welds as the copper additions.

At approximately 3.2 wt.pct. copper and 0.06 wt.pct. niobium in the weld deposits, the two elements provided the required strengthening effect with thermally stable precipitates to produce high strength steel weld metals that exhibited acceptable properties in high heat input, single- and multi-pass conditions. The combined effect of copper and niobium in high strength steel weld metal derives from the combination of two kinds of precipitates with distinct precipitation reaction kinetics and thermal stability.

**Keywords:** Precipitation strengthening; High strength steel welds; Copper; Niobium

## 1. Introduction

The economical utilization of high strength steels with yield strengths greater than 690 MPa (100 ksi) in fabricated structures depends on the development of adequate welding consumables for high heat input processing. To expand the usable heat input range for high production welding of high strength steels, this research work considered filler metals that contain alloying elements that promote precipitation hardening.

### 1.1. Weld metal strengthening mechanisms

The overall effect of alloying elements on the weld metal strength can be divided into the following main groups: (a) Influence of the elements (in solid solution) on the ferrite strength and toughness; (b) Influence of the elements on austenite/ferrite stability and on the refinement of the austenite decomposition products; and (c) Influence of the elements in the form of precipitates on ferrite strength. Assuming an additive effect, the total yield strength of the weld metal,  $\sigma_t$ , can be expressed as:

$$\sigma_t = \sigma_i + \Delta\sigma_d + \Delta\sigma_{ss} + \Delta\sigma_{ppt} \quad (1)$$

where  $\sigma_i$  is the strength component for the alloy-free ferrite matrix.  $\Delta\sigma_d$  is the strength increment due to grain refinement and best expressed by the Hall-Petch relationship.  $\Delta\sigma_{ss}$  is the strength increment by the solid solution of alloying elements in iron and  $\Delta\sigma_{ppt}$  is the strengthening effect caused by the second phase precipitates during the cooling of the weld metal.

### 1.2. Selection of second phase precipitates

In the selection of alloy systems that will result in the effective second phase precipitation, the following characteristics must be considered: (a) A system based on substitutional solid solutions — the lower diffusivity of substitutional elements, as compared to that of interstitial elements, has a strong influence on the size and stability of the precipitates; (b) A system which has decreasing solubility with decreasing temperature; (c) A system with a low maximum solid solubility — a low maximum solid solubility provides conditions for the



Table 1  
Chemical composition (in wt.pct). of the HY-130 steel base metal and welding wires

	C	Mn	Si	P	S	Ni	Mo	Cr	Cu
Base Metal	0.090	0.72	0.28	0.007	0.003	4.85	0.41	0.55	0.150
LINDE-TEC 140	0.076	1.55	0.39	0.004	0.002	2.47	0.80	0.73	0.031
AIRCO AX-140	0.093	1.71	0.24	0.006	0.004	2.10	0.63	1.02	0.047

formation of a supersaturated solid solution, even with only small amounts of alloying addition; and (d) A crystal structure and lattice parameter that favor a coherent precipitate/matrix interface — the crystal structure of the precipitate and the strain associated with its formation may affect the nucleation rate.

A survey of the iron-base substitutional binary systems identified copper, niobium, vanadium, and titanium as the most desirable elements to precipitation strengthen high strength steel weld metals [1]. However, the iron-copper system offers several important advantages. It has an extended  $\gamma$ -field which results in a high copper supersaturation and a high degree of undercooling. This condition also provides a high driving force to result in a large number of small  $\epsilon$ -copper nuclei, a high nucleation rate, and the possibility of having homogeneous nucleation at a higher temperature [2,3]. Besides, copper atoms and iron atoms have similar radii (ratio of Cu:Fe radii = 1.003). Therefore, the presence of copper atoms in the iron matrix will only result in a minimum strain energy, leaving interfacial energy to determine the nucleation energy barrier. As a result, the critical degree of undercooling,  $\Delta T_c$ , is expected to decrease and promote preferential nucleation in the matrix [2]. Finally, the solubility of copper in ferrite is very limited at room temperature. These factors support the selection of copper as the precipitation agent for high strength steel welds.

### 1.2.1. Multipass welding

The multiple thermal cycles associated with successive passes in multipass welds generate volumes of weld metal known as reheated zones [4,5]. These zones can be divided into a number of subzones according to the different microstructures and mechanical properties. Thus, the reheated zone of an  $\epsilon$ -copper precipitation-strengthened weld metal may experience localized property fluctuations due to grain growth, dissolution or overaging of  $\epsilon$ -Cu precipitates during multipass welding. Therefore, the design of welding consumables using second phase precipitates demands proper control of the stability of the matrix and the degree of grain growth, and of the precipitation reactions to obtain uniform weld metal properties during multipass welding.

The onset and extent of grain growth are known to be influenced by the presence of precipitates. Experi-

mental observations have indicated that grain growth in many steels occurs predominantly at temperatures above the equilibrium solubility temperatures of carbides and nitrides [3]. On this basis, it seems appropriate to select a carbide precipitate with a high equilibrium solubility temperature to control the degree of grain growth. From equilibrium solubility data for carbides in steels [6], niobium carbide is reported to have a higher solution temperature compared with titanium carbide and vanadium carbide, if the same concentration of the carbide forming elements is considered. Additionally, niobium minimizes the formation of other carbides such as chromium and molybdenum commonly found in high strength steel weld metals. Both chromium and molybdenum carbide form at lower temperatures than niobium carbide.

Besides controlling grain growth, NbC has a greater thermal stability than the  $\epsilon$ -Cu precipitates which will provide a complementary and more stable precipitation strengthening effect to the weld metal.

Hence, to overcome the undesirable property variations of  $\epsilon$ -Cu strengthened high strength steel weld during multipass welding, the use of niobium carbide in the weld metal is proposed in this research work. Even though the use of niobium and copper for optimizing properties in HSLA steel base plate (wrought condition) is well known, few studies have been conducted to evaluate the combined effect of copper and niobium in as-welded high strength steel weld metals. HY-130 steel, with approximately 900 MPa (130 ksi) yield strength, was used as a prototype in this research work. However, the study developed and the results obtained are applicable to other high strength steels.

## 2. Materials and experimental procedure

A 51 mm thick HY-130 steel plate was used as the base material. Welds were prepared using two different commercially available gas metal arc welding wires: LITEC-140 (Linde) and AX-140 (Airco). The 1.6 mm (1/16 in) diameter wires were produced to meet the MIL-1403-1 specification. The chemical analyses for the plate and the wires are given in Table 1. Different levels of copper and niobium additions were carried out using the procedures described in the following.

Table 2  
Welding parameters used in the experimental work

Weld (Wire) ID	Welding Current (A)	Welding Voltage (V)	Welding Speed (mm s <sup>-1</sup> )	Heat Input (kJ mm <sup>-1</sup> )	Wire Diameter (mm)
C(1)	410	29.7	3.4	3.6	1.6
D(1)	300	30.0	2.5	3.6	1.2
E(2)	410	29.7	3.4	3.6	1.6

Wire 1: Linde 140. Wire 2: Airco AX-140.

### 2.1. Copper additions

Copper additions were made systematically with a sequence of welds. First, the 6 mm deep, 80° V-grooves were buttered with copper using gas tungsten arc welding (190 A, 15 V, 1.7 mm s<sup>-1</sup> [4 ipm], and argon gas shielding). Depending on the desired copper content in the weld metal, layers of copper of different thicknesses were deposited using a variable-speed copper wire feeder. Then, a gas metal arc weld was deposited. The remelting and mixing of the copper and the steel deposit occurred during the final pass.

### 2.2. Niobium additions

An Ar–25%CO<sub>2</sub> shielding gas and high purity (99.8 pct.) niobium powder of particle size between 1–5 microns were used in the experiments. A suspension of niobium powder in acetone was prepared and brushed on to the V-grooves. Depending on the desired niobium content in the weld metal, layers of niobium of different thicknesses were deposited. The melting and mixing of the niobium and the steel deposit occurred during gas metal arc welding.

To characterize the combined effect of copper and niobium in multipass welding, additions of about 3.0 wt.pct. copper and about 0.06 wt.pct. niobium were made to the weld metal via experimental metal cored welding wires supplied by ESAB-Alloy Rods Corporation.

### 2.3. Welding conditions

Coupons of 150 × 50 × 25 mm (approximately 6 × 2 × 1 in.) with V-grooves were used for welding. A small number of welds were also deposited on 19 and 50 mm thick coupons. The surfaces of the weld coupons were grit-blasted to remove any paint or oxide scale and degreased prior to welding. The welding conditions were set to result in nominal heat input of 1.2, 2.4 and 3.6 kJ mm<sup>-1</sup> (approximately 30, 60 and 90 kJ in<sup>-1</sup>). The 3.6 kJ mm<sup>-1</sup> welding parameters are given in Table 2. The reported weld metal hardness values correspond to the average of at least six hardness readings, which show a standard deviation of about one percent.

### 2.4. Multipass welding simulation

The aging behavior of the weld metal precipitates during multipass welding was simulated using isothermal heat treatments. The temperature ranged from 475–1300 °C and the holding times varied from 30 s to 120 min. All specimens were first air cooled to 700 °C and then water quenched to avoid the formation of martensite.

To determine the prior austenite grain size, 3 mm thick specimens of 12 × 6 mm (0.125 × 0.5 × 0.25 in.) were heated in a Lindberg box furnace at 900, 1200 and 1300 °C for 1 and 3 min in an argon shielded atmosphere. Each specimen was water quenched, from its specific time and temperature to room temperature, to preserve the prior austenite grain size and the state of the precipitation present at the elevated temperature.

## 3. Results and discussions

The experimental work was carried out in four segments, each leading to decisions regarding weld metal composition and the parameters for the following phase.

### 3.1. Reference weld metal evaluation

This segment of work allowed for proper comparison and correlation of unalloyed reference weld metals with copper and/or niobium-enhanced weld metals. To establish a 'baseline', reference weld metal deposits using available commercial welding wires (without any intentional alloying additions) were made at 1.2, 2.4, and 3.6 kJ mm<sup>-1</sup> and evaluated for chemical composition, microstructure and hardness. The chemical analyses of the 3.6 kJ mm<sup>-1</sup> heat input welds are shown in Table 3. Despite the changing heat input, the weld metal composition remained relatively constant, which suggests that variations in the cooling rates (changes in heat input) are mainly responsible for the observed microstructural changes.

Table 3  
Chemical composition (in wt. pct.) of the reference weld deposits

Weld ID	Heat Input ( $\text{kJ mm}^{-1}$ )	Weld Metal Composition (wt. pct.)								
		C	Mn	Si	P	S	Ni	Mo	Cr	Cu
C	3.6	0.07	1.1	0.30	0.010	0.017	3.0	0.6	0.7	0.08
D	3.6	0.07	1.1	0.28	0.010	0.018	3.1	0.5	0.7	0.09

### 3.1.1. Microstructure and mechanical properties

With an increasing heat input, the weld metal microstructure changed from primarily martensitic to mainly ferritic. Fig. 1(a), (b) and (c), resulting in changes of hardness and tensile properties of the weld metal.

In Fig. 2, the hardness values of these reference weld metals are plotted as a function of the cooling rate, which is determined by heat input ( $1.2, 2.4$  and  $3.6 \text{ kJ mm}^{-1}$ ), plate thickness ( $19, 25$  and  $50 \text{ mm}$ ) and joint geometry (V-groove). As the cooling rate decreased with increasing heat input, the hardness of the reference

welds decreased from 400 to around 300 HVN. The decrease in hardness agreed with the corresponding microstructural changes observed, from martensite to ferrite. Fig. 3 shows the room temperature tensile properties of these weld metals as a function of the heat input [7]. Both the yield and tensile strengths decreased and the elongation at failure increased with an increasing heat input.

Based on the tensile and hardness data obtained, a correlation between the yield strength and hardness was established and a reference weld metal hardness of 360 HVN was determined to correspond to the minimum yield strength of 900 MPa specified for the HY-130 high strength steel. Thus, the higher heat input ( $3.6 \text{ kJ mm}^{-1}$ ) reference welds with hardness below 360 HVN did not meet the strength requirement. The weld metal hardness of 360 HVN is used throughout this article as a reference to evaluate the effect of copper and niobium in the weld metal.

### 3.2. Weld metal copper investigation

Single-pass HY-130 steel welds were produced with systematic additions of copper, from 0–2.85 wt.pct, at  $3.6 \text{ kJ mm}^{-1}$  heat input. The behavior of the copper-enhanced weld metals during multipass welding thermal conditions was also investigated.

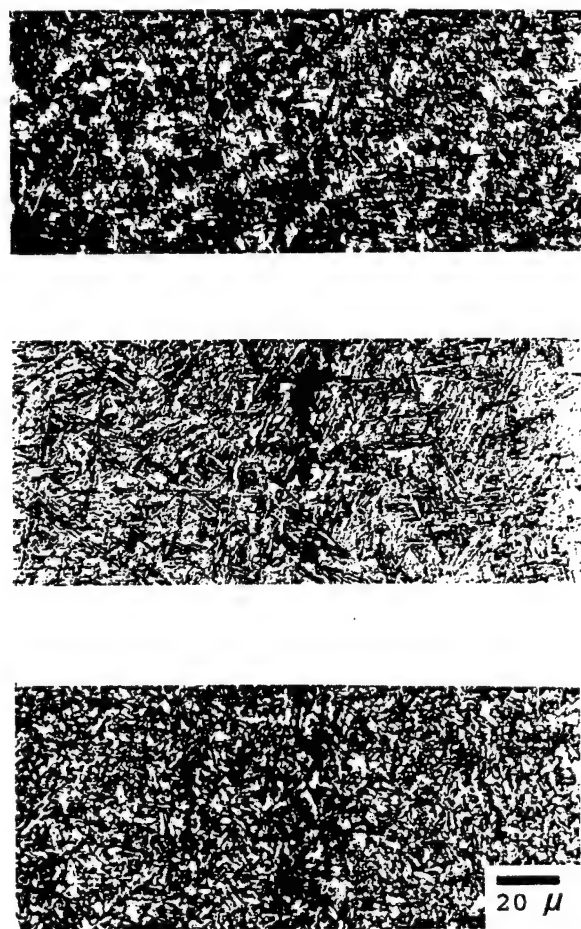


Fig. 1. Microstructure of the reference weld metals without copper additions. (a) Martensitic:  $1.2 \text{ kJ mm}^{-1}$  heat input. (b) Martensitic-Bainitic:  $2.4 \text{ kJ mm}^{-1}$  heat input. (c) Predominately Ferritic:  $3.6 \text{ kJ mm}^{-1}$  heat input.

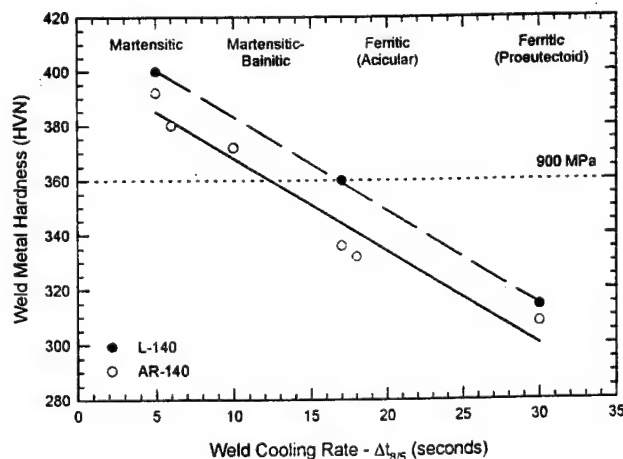


Fig. 2. Hardness and microstructure of the reference weld metals, prepared using commercial welding wires without alloying additions, as a function of cooling rate.

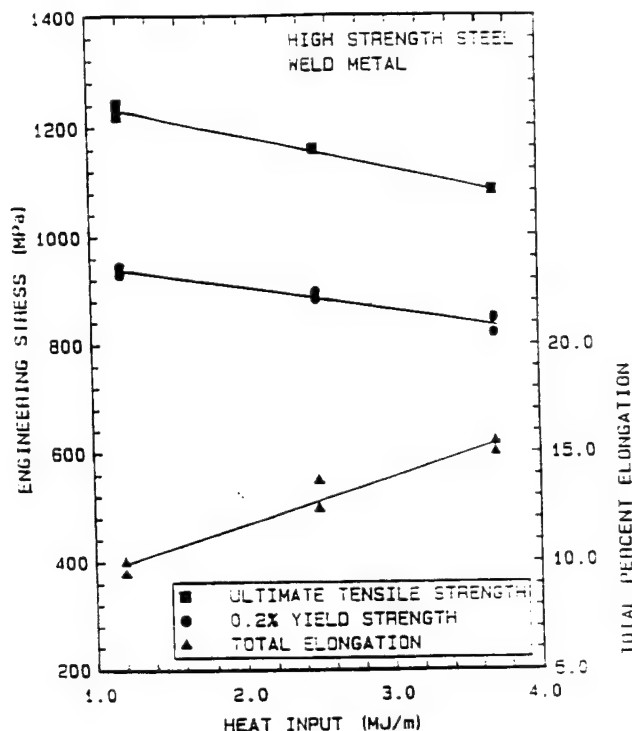


Fig. 3. Room temperature tensile properties of the reference weld metals as a function of heat input. Welds made on 50 mm thick plate (2).

### 3.2.1. Mechanical properties

Fig. 4 shows the single-pass weld metal hardness as a function of the weld metal copper content. The hardness was observed to increase only slightly with low copper additions (below 1.0 wt.pct.). The slight hardness increase can be interpreted as a strengthening of the ferrite matrix by copper in the solid solution. The strengthening effect became more effective when copper additions were higher than 1.0 wt.pct. and can be

attributed to copper precipitation in the weld metal. With 2.8 wt.pct. copper in the weld metal, the estimated yield strength in the weld metal was already equal to that of the base metal, approximately 900 MPa (130 ksi) as shown in Fig. 4.

### 3.2.2. Multipass welding

Multipass welding using copper-strengthened weld deposits has shown a tendency to exhibit localized hardness fluctuations in the heat affected zone of the underbead weld deposits, from 280–385 HVN [8]. The heating of weld beads by a later deposit promotes grain growth and precipitation or aging of  $\epsilon$ -copper, leading to hardening/softening of the heat affected zone. This observation suggests that with copper additions as the sole precipitation strengthener, only the last bead will have consistent hardness across the weld metal. All prior reheated beads are subjected to significant hardness variations. To overcome these undesirable property variations, a second precipitation agent (niobium) in the weld metal was needed.

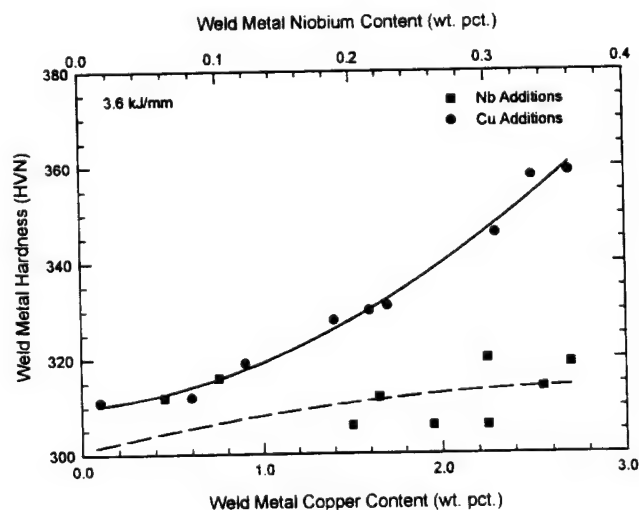


Fig. 4. Hardness of the weld metal as a function of the weld metal copper and niobium content.

### 3.3. Weld metal niobium investigation

Systematic niobium additions from 0–0.4 wt.pct. were made to HY-130 steel single-pass weld deposits at  $3.6 \text{ kJ mm}^{-1}$  heat input.

### 3.3.1. Mechanical properties

Fig. 4 also shows the weld metal hardness as a function of the weld metal niobium content. The hardness was observed to increase only slightly with niobium additions. This slight hardening effect can be interpreted as a weak strengthening effect of the ferritic matrix by niobium in solid-solution.

The effect of copper and niobium, when added individually, on the single-pass weld metal hardness can be summarized as follows. At high heat input,  $3.6 \text{ kJ mm}^{-1}$ , a copper addition of 2.8 wt.pct. is required to obtain 360 HVN in the weld metal, which corresponds to a yield strength of 900 MPa. Niobium does not produce a significant strengthening in high heat input weld metal.

### 3.4. Dual precipitation effect of copper and niobium

The two purposes of the third segment of the experimental work were to prove the effectiveness of dual precipitation ( $\epsilon$ -copper and niobium carbide) in reducing weld metal hardness fluctuations during multipass welding and to determine the levels of copper and niobium content that would produce precipitates that were aging resistant to produce uniform mechanical properties during multipass welding.

Based on the findings in the experiments with individual copper and niobium additions, controlled co-additions of up to 3.5 wt.pct. copper and up to 0.45 wt.pct. niobium were made.

#### 3.4.1. Microstructure

The microstructure of the high heat input weld metals was mainly ferritic and did not experience any significant changes with copper-niobium additions. Fig. 5 shows the microstructure of a  $3.6 \text{ kJ mm}^{-1}$  weld metal that contains 3.0 wt.pct. copper and 0.06 wt.pct. niobium.

#### 3.4.2. Mechanical properties

Fig. 6(a) shows the hardness of high heat input single-pass welds as a function of the copper and niobium content in the weld metal. The solid curve in Fig. 6(a), which represents the change in the weld metal hardness with copper as a single alloying addition, has been included as a reference to evaluate the dual precipitation effect of copper and niobium on weld metal hardness. In general, the hardness increase with copper-niobium additions was comparable to that observed in the welds with copper additions, which indicates that copper precipitation is the main strengthening mechanism. Niobium exerts only secondary influence in a high heat input single-pass weld metal.

However, an interesting behavior of the weld metal hardness as a function of copper and niobium con-

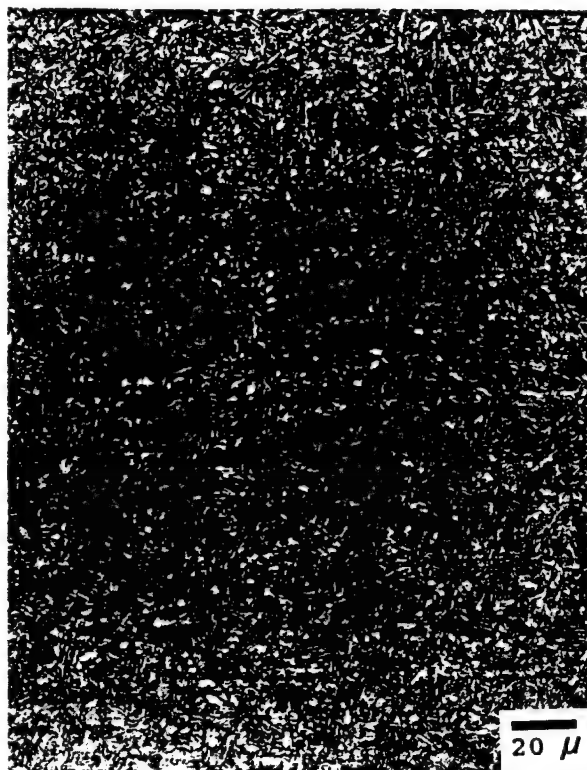


Fig. 5. Ferritic microstructure of weld metal containing 3.0 wt.pct. Copper and 0.06 wt.pct. Niobium, prepared at  $3.6 \text{ kJ mm}^{-1}$  heat input.

tent was observed as shown in Fig. 6(b). For the sake of clarity of illustration, only three ranges of niobium content in the weld metal have been included in this figure. When the weld metal copper content exceeded 2.5 wt.pct., higher levels of niobium additions (0.2–0.35 wt.pct.) led to lower and more irregular hardnesses when compared with those of the copper-enhanced weld metal. At lower levels of niobium additions (approximately 0.1 wt.pct.), the hardness readings were uniform and indicated an acceptable strength. Therefore, niobium levels lower than 0.1 wt.pct. are considered as appropriate for high copper additions to avoid the irregular hardness of the copper-niobium-enhanced weld metal observed.

#### 3.4.3. Multipass welding

To evaluate the dual precipitation effect of copper and niobium in the weld metal during multipass welding, the reheated zones of the welds were characterized by microanalytical (copper and niobium) and microhardness profiling, starting from the fusion line of a weld into the reheated weld metal.

Fig. 7 shows the microhardness and composition profiles of copper and niobium along the reheated zones of a copper-niobium-enhanced weld deposit.

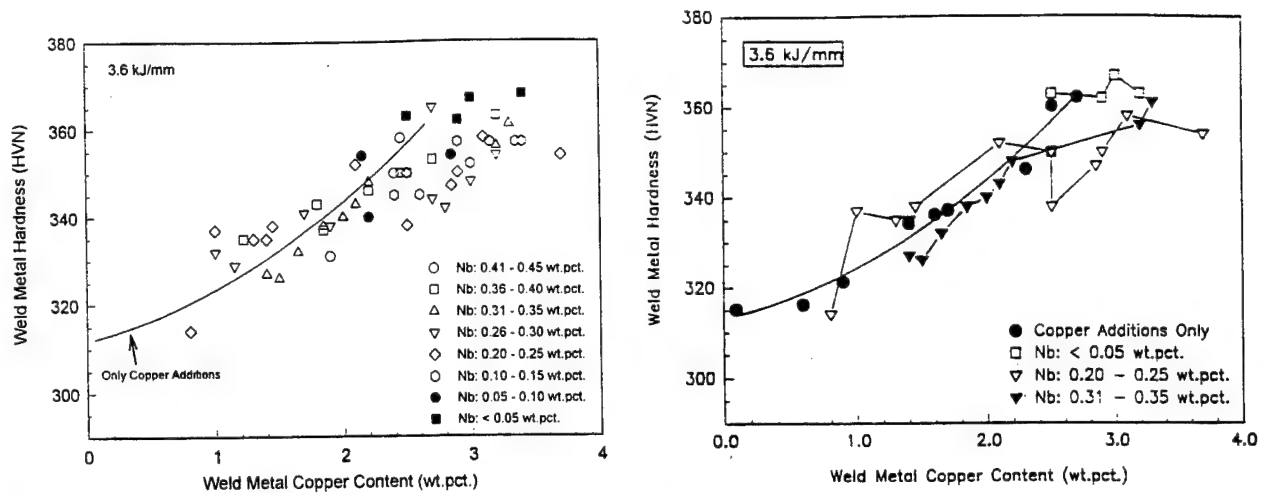


Fig. 6. High heat input ( $3.6 \text{ kJ mm}^{-1}$ ) weld metal hardness as a function of copper and niobium content in the weld metal. (a) With all niobium additions. (b) Selected niobium additions.

The hardness of the reheated zone was generally higher or equal to the reference weld metal hardness of 360 HVN (estimated yield strength of 900 MPa), and did not experience the drastic changes observed in the copper-enhanced multipass weld metals [8]. These results are a manifestation of the dual precipitation effect of copper and niobium in the high strength steel weld metal during multipass welding.

In summary, the dual precipitation of  $\epsilon$ -copper and niobium carbides is effective in providing the required hardness/strength and reduced hardness fluctuations. Additions of approximately 3.2 wt.pct. copper and up to 0.1 wt.pct. niobium in the weld metal provided the strengthening effect in high heat input single- and multi-pass welds.

### 3.5. Multipass welding simulation

To determine the fundamental phenomena responsible for the dual precipitation strengthening effect of copper and niobium in high strength steel weld metals, multipass welding conditions were simulated using isothermal heat treatments to promote precipitate aging and to develop prior austenite grain boundaries for evaluation.

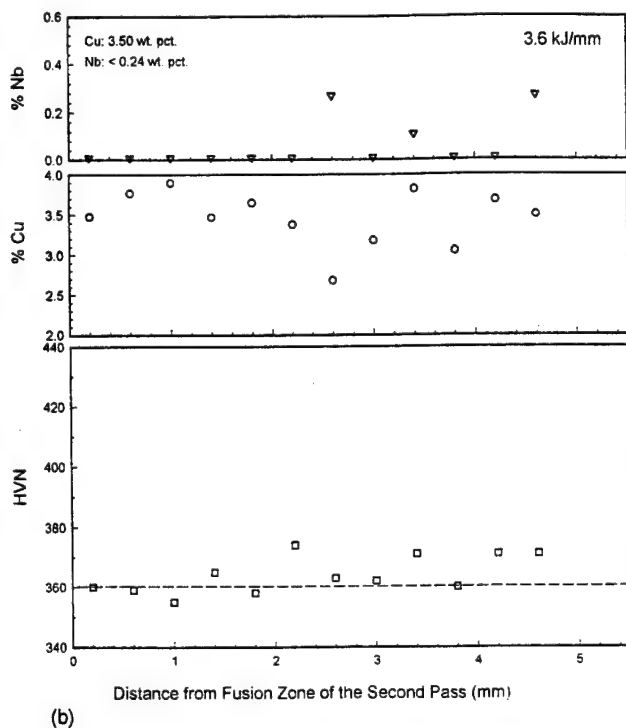


Fig. 7. Weld metal microhardness, copper and niobium (concentration) profiles across the reheated weld metal during multipass welding. (3.5 wt.pct. Cu and < 0.24 wt.pct. Nb.)

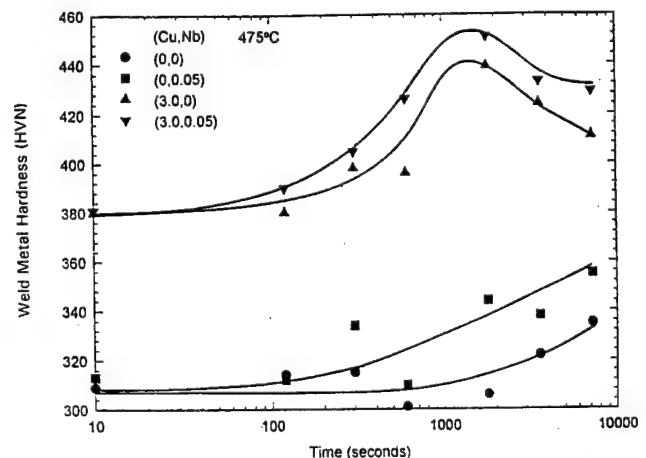


Fig. 8. Precipitation aging behavior of the experimental weld metal systems at  $475^\circ\text{C}$ .



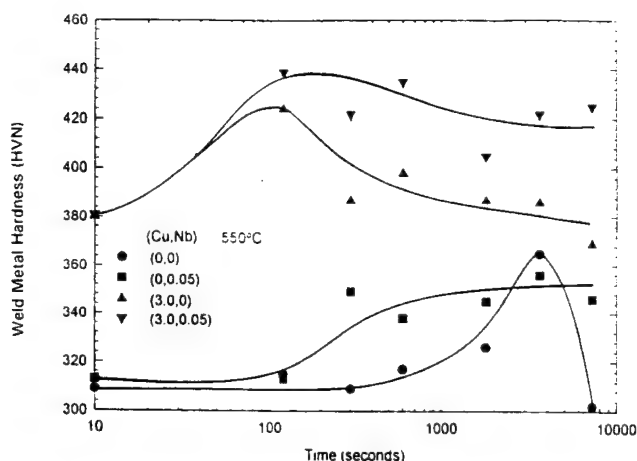


Fig. 9. Precipitation aging behavior of the experimental weld metal systems at 550 °C.

### 3.5.1. Isothermal precipitation aging

The isothermal precipitation aging behavior of the reference weld, niobium-enhanced weld metals, copper-enhanced weld metals, and copper-niobium-enhanced weld metals, at temperatures from 475–675 °C, is shown in Figs. 8–11.

The aging curve of the reference weld metal displayed a hardness peak for the holding times of 1 h (3600 s) and 5 min (300 s) at 550 and 625 °C, respectively (See Figs. 9 and 10). However, no correlation could be observed between these hardness peaks and the precipitation aging behaviors of the copper-niobium-enhanced weld metal (See Figs. 9–11).

From 475–675 °C, both the copper-enhanced and the copper-niobium-enhanced weld metal showed the expected precipitation aging behavior. Both the hardness peak and the time to reach it decreased with increasing aging temperature. At 475, 550 and 625 °C the precipitation reaction kinetics of the niobium-enhanced weld metal were observed to be more slug-

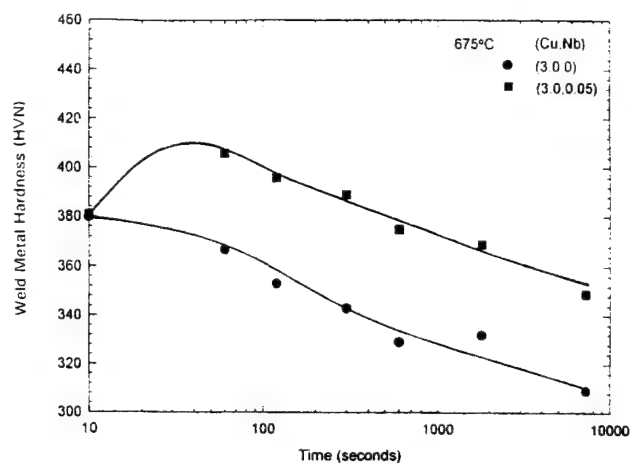


Fig. 11. Precipitation aging behavior of the experimental weld metal systems at 675 °C.

gish than that of the copper-enhanced weld metal, requiring a longer time for the hardness peaks to develop.

The dual precipitation effect of copper and niobium in the weld metal heat treated at 475 °C, Fig. 8, is not very strong, with only a small increase in hardness (approximately 12 HVN), when compared with that of the copper-enhanced weld metal. However, as the aging temperature is increased to 550, 625 and 675 °C, the copper-niobium enhance system shows significantly stronger weld metal and better thermal stability. A longer hardness plateau and/or a longer time taken to reach maximum hardness conditions were observed (See Figs. 9–11).

The behavior of the weld metal during multipass welding, as characterized by using isothermal heat treatment simulation, can be best understood in Figs.

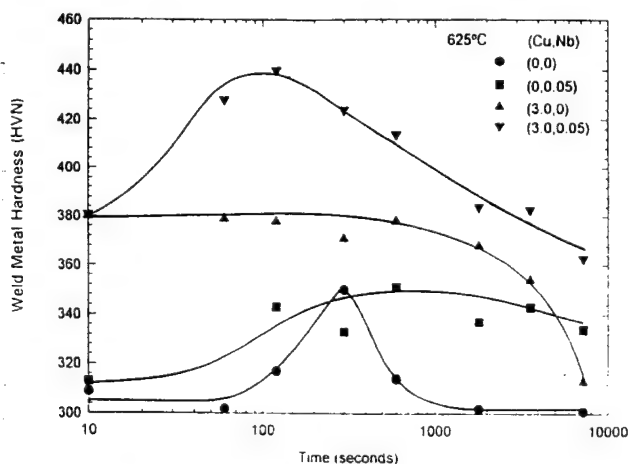


Fig. 10. Precipitation aging behavior of the experimental weld metal systems at 625 °C.

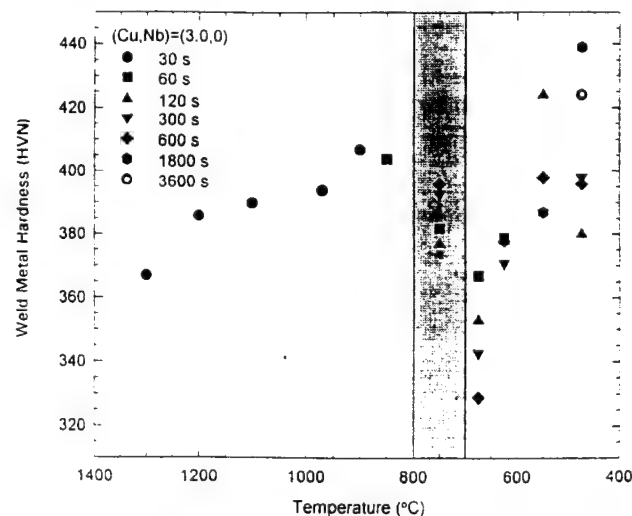


Fig. 12. Weld metal hardness as a function of heat treating temperature simulating the reheated zone of the copper-enhanced weld metal during multipass welding.

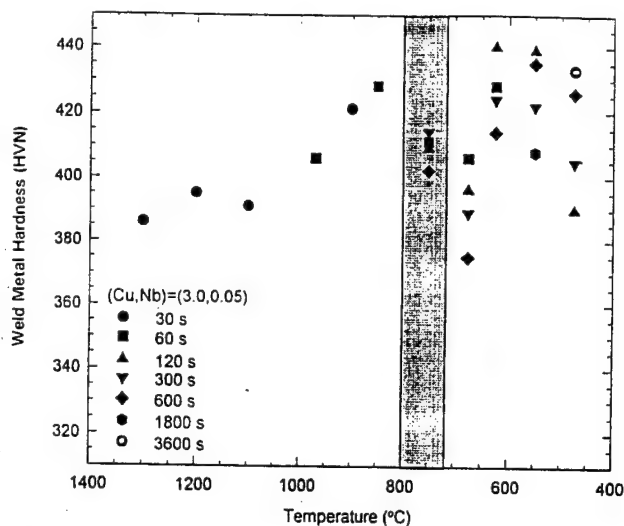


Fig. 13. Weld metal hardness as a function of heat treating temperature simulating the reheated zone of the copper–niobium enhanced weld metal during multipass welding.

12 and 13, when hardness for the copper-enhanced weld metal and the copper–niobium-enhanced weld metal are plotted as a function of the holding temperature and the holding time. The shaded region corresponds to the intercritical (ferrite plus austenite phase field) reheated region of the weld metal. The temperature scale in Figs. 12 and 13 can also be used to represent the distance from the fusion zone in the reheated zone of the weld metal during multipass welding.

As shown in these two figures, maximum softening in the reheated zone was observed to take place at 675 °C (subcritical reheated zone). The increases in diffusivity, interfacial mobility and solubility of cop-

per and niobium in the ferritic matrix with increasing temperature are responsible for the precipitate growth and substantial softening observed at 675 °C.

Despite that both the copper-enhanced and the copper–niobium-enhanced weld metal exhibited softening in the subcritical region, the copper-enhanced weld metal showed a higher susceptibility to weld metal softening than the copper–niobium-enhanced weld metal (Compare Figs. 12 and 13.) The hardness of the copper-enhanced weld metal decreased below 360 HVN with holding time at 675 °C as short as 1 min (60 s). However, the hardness of the copper–niobium-enhanced weld metal remained higher than the hardness of the weld metal in the as-welded condition for holding times at 675 °C of almost 10 min (600 s). Notice that this holding time is much longer than the normal time experienced during welding which indicates that significant hardness fluctuations in the subcritical zone are not expected in the copper–niobium-enhanced weld metals during welding. The greater and more stable strengthening effect results from the dual precipitation effect of copper and niobium, each with a different precipitation reaction kinetics.

By increasing the holding temperature to 750 °C, within the intercritical region of the weld metal system, the hardness of the reheated weld metal increased with the holding time. This observation is attributed to the transformation of an increasing fraction of ferrite into austenite with an increasing holding time at the holding temperature. During cooling, the austenite retransforms to a finer grain size ferrite which produces an increase in the strength of the weld metal.

At reheating temperatures above the intercritical region and up to 900 °C, the hardness of the weld metal increased due to ferrite grain size refinement during austenite decomposition on cooling. However, the hardness of the weld metal decreased when the reheating temperature was greater than 900 °C. The coarsening of the austenite grains is considered as responsible for the softening. Weld metal hardness below that of the weld metal in the as-welded condition (360 HVN) was reached at reheating temperatures above 1200 °C and above 1300 °C for the copper-enhanced and the copper–niobium-enhanced weld metal, respectively.

Both copper-enhanced weld metal and copper–niobium-enhanced weld metal experienced softening more strongly at temperatures well above the temperatures of complete dissolution of the  $\epsilon$ -copper and niobium carbide precipitates, as determined by their solubility product. During welding, since thermal equilibrium is not reached due to the rapid thermal cycle, the particles experience some superheating [2,3,9–11] resulting

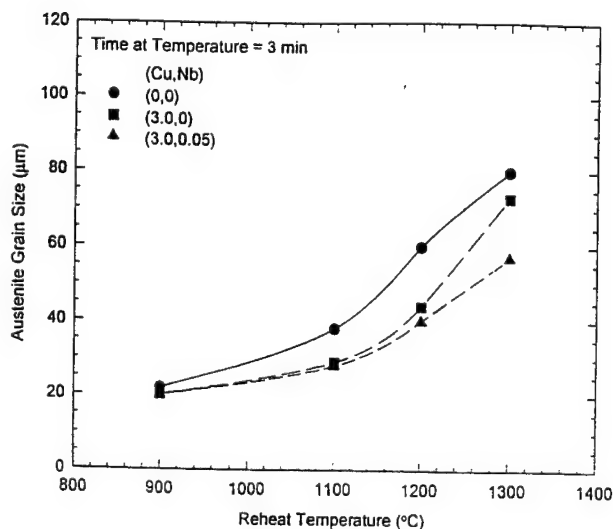


Fig. 14. Prior austenite grain size of the weld metals as a function of reheating temperature for three minutes holding time.



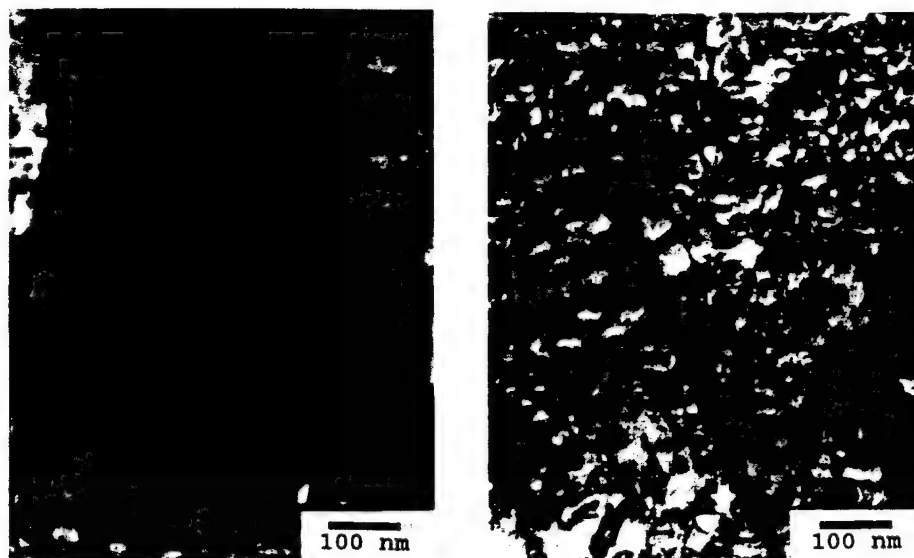


Fig. 15. TEM micrograph of single-pass weld metals prepared at  $3.6 \text{ kJ mm}^{-1}$  heat input. (a) as-welded reference weld metal (115kX). (b) as-welded niobium-enhanced weld metal (115kX).

in a higher temperature of complete dissolution of the precipitates.

To evaluate the dual precipitation effect of copper and niobium on prior austenite grain growth control, the prior austenite grain size of these welds was determined.

### 3.5.2. Prior austenite grain size

The prior austenite grain coarsening behavior for the copper-enhanced and the copper-niobium-enhanced weld metals are presented in Fig. 14. At temperatures of up to  $1150^\circ\text{C}$ , changes in the austenite grain coarsening rate were small. When the temperature was above  $1150^\circ\text{C}$ , the austenite grain growth rate was observed to change drastically with increasing temperature. It is clear from Fig. 14 that the copper-niobium-enhanced weld metal (average grain diameters  $< 60 \mu\text{m}$ ) showed better prior austenite grain growth control than the copper-enhanced weld metal (average grain diameter  $\sim 80 \mu\text{m}$ ). This effect can be attributed to the dual precipitation of  $\epsilon$ -copper and niobium carbide, with a greater ability to control grain size over an extended temperature range.

### 3.5.3. Transmission electron microscopy

To further characterize the dual precipitation phenomena, TEM work was performed using a Phillips EM400 transmission electron microscope. Electron micrographs of the  $3.6 \text{ kJ mm}^{-1}$  reference weld metal (without copper and/or niobium additions) indicated that the weld metal was, in general, composed of a ferritic microstructure with moderate dislocation den-

sity, Fig. 15(a). Fig. 15(b) shows that with 0.06 wt.pct. niobium addition, the microstructure remained the same as the reference welds, only with a higher dislocation density.

Extensive precipitation, however, was observed in the single-pass copper-enhanced weld metal, Fig. 16(a). The precipitates were small, less than  $40 \text{ nm}$  diameter, and randomly distributed. These small  $\epsilon$ -copper precipitates dispersed in the weld metal were responsible for the pronounced strengthening effect observed in the  $3.6 \text{ kJ mm}^{-1}$  copper-enhanced weld metal. After aging for 2 h at  $675^\circ\text{C}$ , however, the copper-enhanced weld metal revealed a microstructure composed of  $\epsilon$ -copper-rich areas and  $\epsilon$ -copper-free areas, as shown in Fig. 16(b). This separation can be explained as a result of copper segregation during solidification. The segregation of copper may also have caused a partitioning of carbon between the regions of copper-poor austenite and copper-rich austenite, because of the high repulsive interaction between carbon and copper in austenite [12]. This alternated distribution of  $\epsilon$ -copper rich and  $\epsilon$ -copper free areas is considered to be responsible for the broad range of copper distribution and nonuniform mechanical properties observed in the reheated zone of the weld metal during multipass welding condition. The precipitates also coarsened with aging.

Finally, Fig. 17(a) shows a TEM micrograph of a single-pass copper-niobium-enhanced weld metal (3.0 wt.pct. copper, 0.06 wt.pct. niobium) with a uniform distribution of fine precipitates. These precipitates were also found to resist aging. Fig. 17(b) shows a TEM micrograph of a copper-niobium-enhanced weld

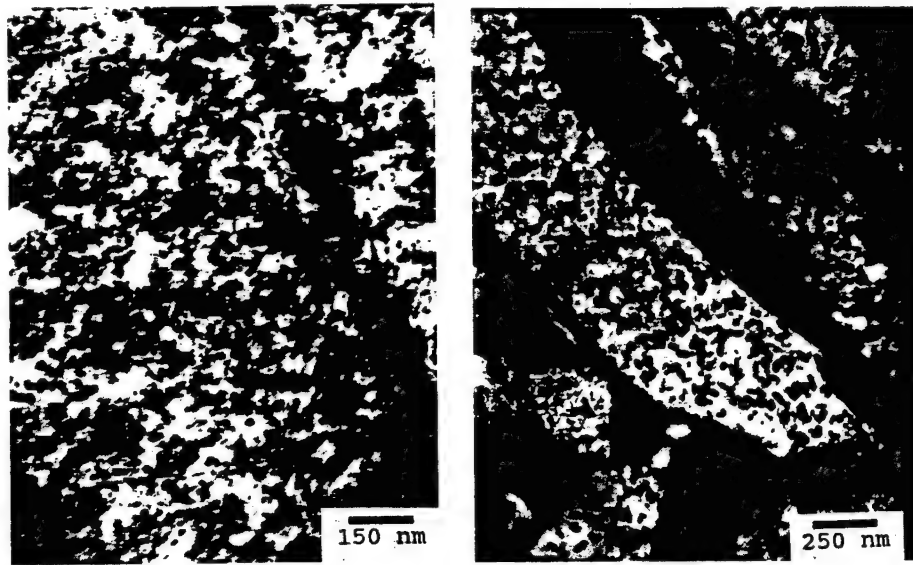


Fig. 16. TEM micrograph of single-pass copper-enhanced weld metals prepared at  $3.6 \text{ kJ mm}^{-1}$  heat input. (a) As-welded condition (70kX). (b) Aged for 2 h at  $675^\circ\text{C}$  (115kX).

metal aged at  $675^\circ\text{C}$  for 2 h. The thermal stability of the fine and uniform precipitate distribution is considered to be responsible for the more uniform mechanical properties observed in the reheated zone of the weld metal during multipass welding.

The lack of contrast of the precipitates in the electron micrographs is due to the similarity of the scattering factor of iron and copper and the negligible strain produced by the precipitates because of the small difference in the atomic radii of the two elements. Additionally, identification of the precipitates by indexing diffraction pattern was impossible, even with the SAD (selected area diffraction) technique, because the precipitates are very small at this early stage of the precipitation.

In summary, the dual precipitation effect of copper and niobium in the high strength steel weld metal is two-fold. First, the formation of niobium carbide precipitates reduces the amount of free carbon in the matrix and affects the distribution pattern of copper and niobium in the weld metal. Therefore, the normal pattern of alternating high and low carbon regions due to the poor chemical affinity between carbon and copper [12], decreases. As a result, a better spatial distribution of the precipitates (both  $\epsilon$ -copper and niobium carbide) in the matrix and more uniform mechanical properties are obtained. Second, the combination of two kinds of precipitates with different thermal stability and distinct precipitation reaction kinetics provide a better overall strengthening effect to the weld metal. Niobium carbides are more stable at

high temperatures and provide a better control to prior austenite grain growth. Additionally, Niobium carbides precipitate slower in iron alloys than the  $\epsilon$ -copper precipitates [13–15]. While the  $\epsilon$ -copper precipitates coarsen and lose part of their strengthening effect as a result of the thermal cycle, the niobium precipitates nucleate and age to provide the additional strengthening effect.

Therefore, the dual precipitation mechanism reduces the hardness fluctuations and produces high strength steel weld metal with acceptable properties (hardness and strength) at high heat input welding conditions during single — and multipass welding. In fact, tensile testing of multipass welds with 3.2 wt.pct. copper and 0.06 wt.pct. niobium additions showed yield strengths between 124–130 ksi, tensile strengths between 154–164 ksi, and elongations between 16–25%. Hardness fluctuation in the reheated zones of these welds was successfully controlled to around 20 HVN, a three to four fold decrease from the copper-enhanced welds.

#### 4. Conclusions

1. To strengthen  $3.6 \text{ kJ mm}^{-1}$  heat input HY-130 steel weld metals with copper precipitation, a minimum of 1.0 wt.pct. of copper is required.

2. Copper precipitation is very effective in strengthening HY-130 steel weld metal at high heat input ( $3.6 \text{ kJ mm}^{-1}$ ). An addition of 2.8 wt.pct. copper in the

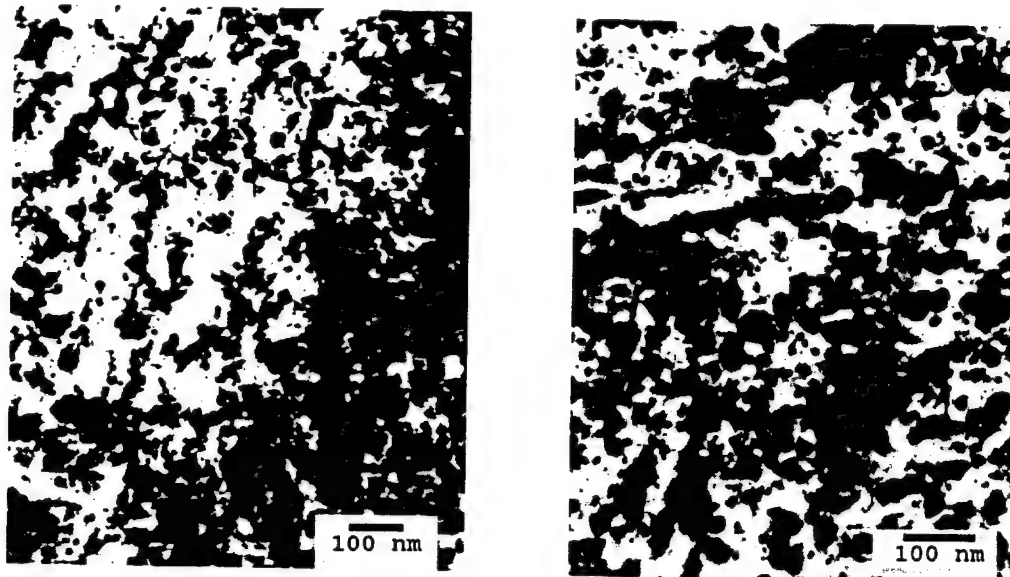


Fig. 17. TEM micrograph of single-pass copper–niobium enhanced weld metals prepared at  $3.6 \text{ kJ mm}^{-1}$  heat input. (a) As-welded condition (90kX). (b) Aged for 2 h at  $675^\circ\text{C}$  (115kX).

weld metal produced a 360 HVN weld metal hardness, which corresponds to a yield strength of 900 MPa. Niobium, in contrast, does not produce significant strengthening in the high heat input weld metal.

3. Reheated weld deposits that contain copper are subject to hardness variations across multipass welds due to the overaging of  $\epsilon$ -copper precipitates. Precipitation agents other than copper, such as niobium, are needed to interact with copper to minimize such nonuniform weld properties.

4. Reheated weld deposits that contain approximately 3.2 wt.pct. of copper and up to 0.1 wt.pct. niobium exhibited adequate weld metal hardness, equal to or higher than 360 HVN which corresponds to a yield strength of 900 MPa, at  $3.6 \text{ kJ mm}^{-1}$ . The dual precipitation scheme controls precipitation coarsening and grain growth, which results in acceptable and more uniform mechanical properties of high strength steel weld metals, during single — and multipass welding conditions.

5. The combined effect of copper and niobium in high strength steel weld metal derives from:

- the combination of two kinds of precipitates with distinct precipitation reaction kinetics,
- the combination of two kinds of precipitates with different thermal stability, and
- the effect of niobium on the distribution pattern of copper in the weld metal.

#### Acknowledgements

The authors acknowledge and appreciate the support of NSWC-CD and ONR.

#### References

- [1] E. Hornbogen, Precipitation from Binary Substitutional Solid Solution of Alpha Iron, *Symposium on Precipitation from Iron-Base Alloys*, AIME, 1965, pp. 1–67.
- [2] D.A. Porter and K.E. Easterling, *Phase Transformation in Metals and Alloys*, Van Nostrand Reinhold, Berkshire, 1981, pp. 265–278, 426.
- [3] K. Easterling, *Introduction to the Physical Metallurgy of Welding*, Butterworths, London, 1st edn., 1983, pp. 126.
- [4] L.P. Conner (ed.), *Welding Handbook*, V1, 8th edn., American Welding Society, Miami, 1987, pp. 108–111.
- [5] G.S. Huppi, Reheat Zone Microstructural Development and Toughness in Selected HSLA Steel Weld Metals, *Ph.D. Thesis T-3175*, Colorado School of Mines, May 1986.
- [6] R.W.K. Honeycombe, *Structure and Strength of Alloy Steels*, Climax Molybdenum, London, 1973.
- [7] P.T. Oldland, The Effect of Heat Input and Molybdenum on the Microstructure and Mechanical Properties of High Strength Steel Weld Metal, *Thesis T-3599*, Colorado School of Mines, Golden, Colorado, 1989.
- [8] E. West, Colorado School of Mines, Golden, CO, unpublished Research, 1990.
- [9] M.F. Ashby, and K.E. Easterling, A First Report on Diagrams for Grain Growth in Welds, *Acta Metall.*, 30 (1982) 1969–1978.
- [10] B. Lehtinen, and P. Hansson, Characterization of Microalloy Precipitation in HSLA Steel Subjected to Different Weld Thermal Cycles, *Scand. J. Metall.*, 18 (1989) 295–300.

# Instructions for Authors

## SUBMISSION OF PAPERS

Manuscripts for the main part of the journal and for the Letters Section should be submitted as follows:

### *For authors in Europe*

Editor-in-Chief  
Professor Herbert Herman  
Department of Materials Science and Engineering  
State University of New York at Stony Brook  
Long Island, NY 11794-2275, USA  
Fax: +1 (516) 632 8052

or

Professor Gernot Kosterz  
ETH Zurich  
Institut für Angewandte Physik  
CH-8093 Zurich, Switzerland  
Fax: +41 (1633) 1105

### *For authors in Japan*

Professor Masahiro Koiwa  
Department of Materials Science and Engineering  
Faculty of Engineering  
Kyoto University  
Yoshida-Honmachi, Sakyo-ku  
Kyoto 606-01, Japan  
Fax: +81 (75) 751 7844

### *For authors in North and South America and the rest of the world*

Professor Herbert Herman  
USA

## Manuscripts

Three copies should be submitted to the Editor, in double-spaced typing on pages of A4 size and with wide margins (Letters should not exceed 2000 words and a maximum of 5 figures). All tables and illustrations should bear a title or legend.

An *abstract* should accompany reviews, original papers and Letters. It should present (preferably in 100–150 words; 50 words or less for Letters) a brief and factual account of the contents and conclusions of the paper, and an indication of the relevance of new material.

*References* should be indicated by numerals in square brackets, introduced consecutively and appropriately in the text.

References must be listed on separate sheet(s) at the end of the paper. Every reference appearing in the text should be quoted in the reference list, and *vice versa*. When reference is made to a publication written by more than two authors it is preferable to give only the first author's name in the text followed by "*et al.*". However, in the list of references the names and initials of all authors must be given.

Three sets of figures should be submitted. One set of line drawings should be in a form suitable for reproduction, drawn in Indian ink on drawing or tracing paper (letter height, 3–5 mm). Alternatively, such illustrations may be supplied as high contrast, black-and-white glossy prints. Duplicate original micrographs should be provided wherever possible to facilitate the refereeing process. Magnifications should be indicated by a ruled scale bar on the micrograph. Captions to illustrations should be typed in sequence on a separate page.

All abbreviated terms must be defined when first used (both in the abstract and in the text) and authors must express all quantities in SI units, with other units in parentheses if desired. Authors in Japan please note that information about how to have the English of your paper checked, corrected and improved (before submission) is available from: Elsevier Science Japan, 1-9-15 Higashi-Azabu, Minato-ku, Tokyo 106, Japan; Tel: +81-3-5561-5032; Fax: +81-3-5561-5045; e-mail: KYFO4037@niftyserve.or.jp.

## Further information

All questions arising after the acceptance of manuscripts, especially those relating to proofs, should be directed to: Elsevier Editorial Services, Mayfield House, 256 Banbury Road, Oxford OX2 7DH, UK (tel: +44 1865 314900; fax: +44 1865 314990).

## Submission of electronic text

The final text may be submitted on a 3.5 in or 5.25 in diskette (in addition to a hard copy with original figures). Double density (DD) or high density (HD) diskettes are acceptable, but must be formatted to their capacity before the files are copied on to them. The main text, list of references, tables and figure legends should be stored in separate text files with clearly identifiable file names. The format of these files depends on the word processor used. WordPerfect 5.1 is the most preferable but for other formats please refer to the Instructions to Authors booklet. It is *essential* that the name and version of the wordprocessing program, type of computer on which the text was prepared, and format of the text files are clearly indicated.

The final manuscript may contain last minute corrections which are not included in the electronic text but such corrections must be clearly marked on the hard copy.

© 1996—Elsevier Science. All rights reserved

0921-5093/96/\$15.00

This journal and the individual contributions contained in it are protected by the copyright of Elsevier Science S.A., and the following terms and conditions apply to their use:

### Photocopying

Single photocopies of single articles may be made for personal use as allowed by national copyright laws. Permission of the publisher and payment of a fee is required for all other photocopying, including multiple or systematic copying, copying for advertising or promotional purposes, resale, and all forms of document delivery. Special rates are available for educational institutions that wish to make photocopies for non-profit educational classroom use.

In the USA, users may clear permissions and make payment through the Copyright Clearance Center, Inc., 222 Rosewood Drive, Danvers, MA 01923, USA. In the UK, users may clear permissions and make payment through the Copyright Licensing Agency Rapid Clearance Service (CLARCS), 90 Tottenham Court Road, London W1P 0LP, UK. In other countries where a local copyright clearance centre exists, please contact it for information on required permissions and payments.

### Derivative works

Subscribers may reproduce tables of contents or prepare lists of articles including abstracts for internal circulation within their institutions.

Permission of the publisher is required for resale or distribution outside the institution.

Permission of the publisher is required for all other derivative works, including compilations and translations.

### Electronic storage

Permission of the publisher is required to store electronically any material contained in this journal, including any article or part of an article, contact the publisher at the address indicated.

*Except as outlined above, no part of this publication may be reproduced, stored in a retrieval system or transmitted in any form or by any means, electronic, mechanical, photocopying, recording or otherwise, without prior written permission of the publisher.*

### Disclaimers

No responsibility is assumed by the publisher for any injury and/damage to persons or property as a matter of products liability, negligence or otherwise, or from any use or operation of any methods, products, instructions or ideas contained in the material herein.

Although all advertising material is expected to conform to ethical (medical) standards, inclusion in this publication does not constitute a guarantee or endorsement of the quality or value of such product or of the claims made of it by its manufacturer.

No responsibility is assumed by the Publisher for any injury and/or damage to persons or property as a matter of products liability, negligence or otherwise, or from any use or operation of any methods, products, instructions or ideas contained in the material herein.

© The paper used in this publication meets the requirements of ANSI/NISO Z39.48-1992 (Permanence of Paper).

Printed in The Netherlands

- [11] J. Agren. Kinetics of Carbides Dissolution. *Scand. J. Metall.*, 19 (1990) 2–8.
- [12] G.K. Sigworth, and J.F. Elliot, The Thermodynamics of Liquid Dilute Iron Alloys, *Met. Sci.*, 8(9) (1974) 298–302.
- [13] M.R. Krishnaved, and A. Galibois. Some Aspects of Precipitation of Copper and Columbium (Nb) Carbide in an Experimental High Strength Steel. *Met. Trans.*, 6A (1975) 222–224.
- [14] E. Hornbogen. Precipitation and Mechanical Properties of Iron Alloys, *Colloq. Metall.*, 16 (1975) 431–452.
- [15] R. Simoneau, G. Begin, and A.H. Marquis, Progress of NbCN Precipitates in HSLA Steel as Determined by Electrical Resistivity Measurements, *Met. Sci.*, August (1978) 381–386.

1.25% Mn-2% Ni, was only slightly above (116,700 psi) the specified strength range. Charpy V-notch toughness substantially exceeded the project goals of 60 ft-lbs at 0°F and 35 ft-lbs at -60°F.

A high level of toughness and insensitivity of mechanical properties to variations in heat input was observed in spite of high levels of primary ferrite in the microstructures. Correlation of transition region Charpy fracture characteristics with reheat and top bead microstructures, and oxide size and distribution, revealed those parameters which promoted microvoid nucleation and suppressed the initiation of cleavage fracture. The Charpy energy absorbed was compared to the length of the fibrous regions at the notch (the stretch zone width (SZW) and stable crack length (SCL)) and the brittle fracture zone. The absorbed energy was shown to correlate with the length of the fibrous region. The microstructural constituents associated with the initiation of brittle fracture were identified.

### Conclusion

A robust, moderate strength, high CVN toughness filler metal has been developed based on a nominal 1% Mn-2% Ni-0.5% Mo composition with 240 to 400 ppm titanium. Good impact toughness has been obtained in spite of relatively large fractions of both primary ferrite and ferrite with second phase observed in the microstructure. Microstructural characteristics which promote microvoid nucleation and correlate with the length of the Charpy V-notch fibrous zone have been identified.

### References

1. Johnson, M. Q., "Microstructure-Property Relationships in Titanium-Bearing High Strength Multipass Shielded Metal Arc Weldments," Ph.D. Thesis No. T-4769, Colorado School of Mines, Aug. 1996.

**D. Effect of Cu Content on Mechanical Properties in Multipass Cu-V Enriched High Strength Steel Weld Metal,**  
*by T. Yamaura, Kawasaki Steel Corporation, Japan; and S. Liu, Colorado School of Mines*

### Introduction

Development of welding consumables for steels of 130 ksi strength level has been conducted to extend the usable heat input range, in particular, the higher heat input welding conditions. The dual precipitation mechanism for HY-130 steel weld metal with Cu and Nb addition have been proposed by Ramirez, Olson and Liu. In multipass welding, since weld metals are reheated to various temperatures



by subsequent passes, the mechanical properties of weld metals containing precipitation agents such as Cu, Nb and V may show very complicated changes. In this study, the effects of Cu content on the mechanical properties of multipass Cu-V enriched weld metals for HY-130 steel are investigated.

## Procedure

Systems of multi- and single-pass weld metals prepared with six experimental metal cored wires to result in 3 wt.% Cu-0 wt.% V and 0.9, 1.2, 1.6, 2.1, and 3 wt.% Cu-0.1 wt.% V, respectively. Other elements ranged from: 0.04-0.09 wt.% C, 1.3-1.7 wt.% Mn, 2.2-3.2 wt.% Ni, 0.4-0.7 wt.% Cr, 0.4-0.6 wt.% Mo.

For multipass welding, two different heat inputs were applied, *i.e.*, 2.4 kJ/mm and 3.6 kJ/mm, with no preheat and interpass temperatures less than 150°C. Tensile tests of longitudinal weld metals, Vickers hardness test and Charpy impact tests at -18°C and -51°C were performed.

To better clarify mechanical properties changes observed in the multipass weld metals, simulated single peak welding thermal cycles, *i.e.*, six different peak temperatures from 475°C to 1350°C and ( $\Delta t$  800-500: 16 sec), were applied to 5 mm thick specimens extracted from singlepass weld metals prepared at 3.0 kJ/mm. Half-size Charpy impact tests at -18°C and -51°C and Vickers hardness test of the weld metals were performed.

## Results and Discussion

The average hardness of multipass weld metals increased with increasing Cu content in the weld metals. The yield strengths of all six weld metals with 2.4 kJ/mm and 3.6 kJ/mm were higher than 690 MPa (100 ksi). To obtain yield strengths higher than 900 MPa (130 ksi), a minimum of 2.0 wt. % Cu addition was needed. As expected, Charpy impact toughness decreased with increasing Cu content in the weld metals. The level of impact toughness obtained was, nevertheless, respectable for higher strength steels. For example, it was possible to obtain 81 J (60 ft lb) at -18°C with around 1.2 wt.% Cu addition.

The half-size Charpy impact values (CIV) at -51°C of singlepass weld metals also decreased with increasing Cu content at all peak temperatures ( $T_p$ ) including the as welded weld metals. Each weld metal system showed toughness deterioration with  $T_p$  between 475°C and 700°C, in particular at  $T_p$  600°C and with more than 1.6 wt.% Cu. The lowest CIV of each simulated weld metal system corresponded to the CIV in the multipass weld metal of the same system. The average hardness values of the weld metals showed hardening or retardation of softening with  $T_p$  between 475°C and 700°C. These results suggested that precipitation hardening of ( $\epsilon$ -Cu and/or VC or V(CN) deteriorated the toughness of weld metals reheated with  $T_p$  above mentioned. The balance between Cu and V is critical to the development of mechanical properties of reheated weld metals in high strength steels.

## HYDROGEN CONTENT OF UNDERWATER WET WELDS DEPOSITED BY RUTILE AND OXIDIZING ELECTRODES

Alexandre M. Pope  
PETROBRAS Research and Development Center  
Rio de Janeiro  
Brazil

Stephen Liu  
Center for Welding, Joining and Coatings Research  
Colorado School of Mines  
Golden, Colorado

### ABSTRACT

Shielded metal arc wet welding, due to its flexibility and ease of mobilization, is one of the most attractive methods for repair of underwater structures. However, the quality of the weld metals deposited by this process is detrimentally affected by the direct contact of the welding arc with the aqueous environment. Oxygen and hydrogen generated by the decomposition of water in the arc are responsible for the main problems related to this specific process: loss of deoxidizers, oxygen pickup, increase in oxide inclusions content, hydrogen-induced cracking, and porosity. Rutile electrodes are recognized in the literature as being able to deposit welds with adequate mechanical properties but with high hydrogen content. Oxidizing electrodes, on the other hand, are able to deposit welds with lower hydrogen content but higher oxygen content.

The hydrogen contents of underwater wet welds deposited by electrodes with flux coatings of different oxidizing character were determined at a constant water depth (0.5 m). The electrode formulations used in this research ranged from one typically rutile to one totally oxidizing. The changes were made through hematite additions to the flux covering. Using this approach it was possible to vary the weld metal oxygen content from 0.07 to the saturation value, 0.22 wt. pct.

Welds deposited by rutile electrodes presented approximately 90 ml/100g of diffusible hydrogen while oxidizing electrodes produced welds with diffusible hydrogen contents varying from 40 to 50 ml/100g. It was found that the measured diffusible hydrogen contents of underwater wet welds are more dependent on the type of electrode covering than on the weld metal oxygen content. The residual hydrogen content of underwater welds showed a tendency to increase to a constant level of approximately 5 ml/100g as the oxygen content of the weld increased to the saturation value (0.22 wt. pct.). It seems, therefore, that the diffusible hydrogen content of underwater wet welds is more influenced by the amount of total hydrogen absorbed by the liquid metal before solidification than by the

amount of inclusions, acting as hydrogen traps, in the weld metal.

### INTRODUCTION

Hydrogen-induced cracking is one of the problems associated with underwater wet welding. This problem is caused by the combination of hydrogen in the arc with high cooling rates imposed on the welded joint by the aqueous environment. More specifically, hydrogen-induced cracking is caused by the simultaneous occurrence of the following factors (Yurioka and Suzuki, 1990): critical concentration of diffusible hydrogen at the crack tip, a microstructure susceptible to hydrogen, applied tensile stress of sufficient magnitude, and temperature lower than about 200°C.

These conditions are easily met in underwater wet welding particularly in the base metal heat affected zone (HAZ). At this location, cooling times between 800 and 500°C, ( $D_{t_{1-5}}$ ), are short enough to generate a susceptible microstructure (martensite) if the hardenability of the steel is sufficiently high. Several researchers (Stalker, 1977; Hasui and Suga, 1980; and Suga, 1992) reported for underwater wet welding that for welds deposited on plates thicker than 19 mm and heat inputs in the range of 0.8 to 2.0 kJ/mm,  $D_{t_{1-5}}$  lies between 2 and 3 seconds. For this reason the use of wet welding has been suggested only for low strength (Ozaki, Naiman and Masubuchi, 1977) or low carbon equivalent ( $CE < 0.40$  wt.pct.) steels (Grubbs and Seth, 1977). However the interest in applying wet welding in offshore structural steels has led to the research of welding procedures and consumables to minimize the HAZ cracking problem.

The cracking problem can be avoided if at least one of its controlling factors can be minimized. Several investigators (Stalker, 1977; Nóbrega, 1981; and Gooch, 1983) found that hydrogen cracking in underwater welds could be avoided by the use of oxidizing electrodes. It was shown that these type of electrodes are able to deposit underwater wet welds with



diffusible hydrogen of approximately 20 ml/100g of weld thus presenting a lower risk of HAZ cracking. Basic and rutile electrodes generally result in higher levels of diffusible hydrogen and consequently can cause HAZ cracking more easily in underwater wet welding. The lower diffusible hydrogen measured in the welds deposited by the oxidizing electrodes has been attributed to their higher inclusion content (Stalker, 1977).

A better understanding of the oxygen-hydrogen relationship in underwater wet welds is necessary not only to guide the development of consumables that are able to deposit welds with lower oxygen and diffusible hydrogen levels, but also to provide an insight about the limitations of the underwater wet welding process. The experimental work in this research was oriented to investigate the influence of the oxidizing character of the electrode covering on the hydrogen contents of underwater wet welds. Electrode formulations investigated in this work ranged from one typically rutile to one totally oxidizing, by adding hematite ( $\text{Fe}_2\text{O}_3$ ) to the flux covering.

## EXPERIMENTAL PROCEDURE

### Materials

The chemical compositions of the batches of electrodes specially manufactured for this research are shown in Table 1. It should be observed in this Table that electrodes A, B, C, and D have the same base composition, and only the hematite/rutile ratio vary, increasing from batch A to D. Electrodes from batch D are fully oxidizing electrodes, with 50 wt.pct. of  $\text{Fe}_2\text{O}_3$ . Electrodes from batch E are similar to the electrodes from batch B, except for the 10 wt. pct. magnesium oxide which substituted part of the rutile. It should also be noticed that these electrodes do not contain any addition of deoxidizers such as Fe-Mn or Fe-Si. Ingredients such as feldspar, mica, and silica are necessary in the flux composition as slag formers and to control the viscosity of the slag (Jackson, 1973). Potassium titanate is mainly used as an arc stabilizer. Potassium silicate was used as the binder. In order to keep constant any second order interaction among the flux ingredients that could affect the experimental results the amounts of these elements were maintained unchanged in the five electrode formulations.

The flux ingredients were extruded on 3.2 mm diameter low carbon steel rods. The electrodes were dried at 350 °C for 1 hour. To waterproof the flux coating three coats of vinyl varnish were applied to each electrode after they cooled to room temperature. The chemical compositions of the base metal and electrode core rod are shown in Table 2.

In addition to the electrodes described above two additional commercial electrodes included in this study. They were:

- Electrode F - an oxidizing electrode able to deposit underwater wet welds containing around 2.0 wt.pct of nickel with improved impact resistance (Pope et al., 1995)
- Electrode G - a commercial rutile electrode classified as AWS E6013 type.

The exact flux composition of the electrodes F and G are not known. It is known, however, that commercial rutile electrodes usually contain some amounts of deoxidizers, usually ferro-silicon or ferro-manganese. Qualitative energy dispersive analyses carried out on the coating of electrode F revealed the presence of Fe-Mn and titanium-rich particles.

Welds were deposited manually, in the flat position, under 0.5 m of fresh water. A constant current welding power source was used with the electrode connected to the negative pole. The welding current used was in the 120-130 A range. The welding speed varied between 100 and 140 mm/min, approximately.

The welding procedure described above was used to deposit single bead-on-plate welds for hydrogen determinations and multiple bead-on-plate welds for chemical analyses.

Weld droplets were collected for metallographic analysis. In this case an electric arc was established underwater between the testing electrode and a copper plate. The electrode was held vertically, with the arc directed downwards, and forming approximately 30° with the copper plate. The droplets, not sticking on the copper surface, were collected in a tray placed below. They were dried and stored for later metallographic analysis.

### Weld Metal Chemical Analysis

The weld metal oxygen contents were determined using a Leco oxygen analyzer. For each electrode batch a minimum of five samples were collected along the weld length avoiding the start and the end of the bead. The chemical compositions of the deposited welds were determined by optical spectroscopy.

### Weld Metal Hydrogen Determinations

The total amount of hydrogen absorbed by the weld metal can be divided in two fractions: the diffusible and the residual hydrogen contents. The methods used to determine these two weld hydrogen contents are described in the following subsections.

**Diffusible Hydrogen Determination.** Weld metal diffusible hydrogen were determined for each electrode batch according to the AWS A4.3-93, Standard Mercury Displacement Method (American Welding Society, 1993), modified to account for the higher diffusible hydrogen contents normally found in wet welds. The implemented modification was to reduce the length of the test specimen from 80 to 40 mm.

Following the AWS A4.3-93 specification, single stringer weld beads were deposited underwater over a test assembly consisting of three steel pieces: the starting weld tab, the test specimen, and the run-off tab, all held in a proper clamping fixture. The dimensions of each steel piece were 40 mm x 25 mm x 12 mm. The water temperature at the time when the tests were performed was approximately 6 °C. After the arc extinction the test assembly was removed from the fixture and transferred to an acetone-dry ice liquid bath, at less than -60 °C, in less than 5 seconds. After cooling to the bath temperature the test

TABLE 1. CHEMICAL COMPOSITIONS OF THE ELECTRODE FLUX COATINGS (IN WEIGHT PERCENT)

INGREDIENT ↓ ELECTRODE CODE →	A	B	C	D	E
Alumina ( $\text{Al}_2\text{O}_3$ )	2.3	2.3	2.3	2.3	2.3
Feldspar ( $\text{K}_2\text{O} \cdot \text{Al}_2\text{O}_3 \cdot 6 \text{SiO}_2$ )	5.6	5.6	5.6	5.6	5.6
Potassium Titanate ( $\text{K}_2\text{TiO}_3$ )	9.3	9.3	9.3	9.3	9.3
Silica ( $\text{SiO}_2$ )	10.4	10.4	10.4	10.4	10.4
Mica ( $\text{K}_2\text{O} \cdot \text{Al}_2\text{O}_3 \cdot 6 \text{SiO}_2 \cdot 2\text{H}_2\text{O}$ )	2.3	2.3	2.3	2.3	2.3
Kaolin ( $\text{Al}_2\text{O}_3 \cdot 2 \text{SiO}_2 \cdot 2 \text{H}_2\text{O}$ )	2.6	2.6	2.6	2.6	2.6
Hematite ( $\text{Fe}_2\text{O}_3$ )	0	20	30	50	20
Rutile ( $\text{TiO}_2$ )	50	30	20	0	20
Magnesia ( $\text{MgO}$ )	0	0	0	0	10
Potassium Silicate ( $\text{K}_2\text{O} \cdot \text{SiO}_2$ )	17	17	17	17	17

TABLE 2. CHEMICAL COMPOSITIONS (IN WT.PCT.) OF BASE METAL AND ELECTRODE CORE ROD

	C	Mn	Si	S	P
Base Metal	0.12	0.81	0.26	0.03	0.03
Core Rod	0.03	0.31	nd	0.02	0.01

nd = not detected

specimens were separated from their two adjacent tabs and all the slag was removed. During this cleaning operation the temperature of test specimen was not allowed to exceed  $0^\circ\text{C}$ .

After cleaning the test specimens were inserted in eudiometer tubes containing mercury at  $45^\circ\text{C} \pm 3^\circ\text{C}$ . The amount of hydrogen diffused out of the specimen was collected in the tube displacing a certain volume of mercury. The volume of hydrogen collected in the eudiometer was converted to the Standard Temperature and Pressure ( $V_H$ ) according to the procedure described in the AWS Standard (American Welding Society, 1993). At the time the diffusible hydrogen measurements were made the barometric pressure was approximately 615 mm Hg. For each batch of electrode at least three hydrogen measurements were made.

**Residual Hydrogen Determination.** Samples of the weld metal, with approximately 0.3 g, were taken from each diffusible hydrogen test specimen and analyzed in a Leco hydrogen determinator. In this equipment the samples were heated up to  $1100^\circ\text{C}$  in a nitrogen flow. The amount of hydrogen extracted from the sample at this temperature, the residual hydrogen, was determined in a thermal conductivity cell. Three measurements were made for each electrode batch.

### Metallographic Analysis

Light and scanning electron microscopy were used to observe metallographic sections of the weld metals, electrode tips and weld droplets. These techniques were used to identify the slags formed at the tip of the electrodes and around the metal droplets.

Due to a possible interference of superficial FeO films or FeO-rich slags on the hydrogen absorption process, metallographic work was directed to identify the presence of wüstite in slags generated by the electrode tested. Wingrove's results (1970) on identification of iron oxides under the reflected light microscope were used to interpret the present results.

Samples from weld metals, electrode tips and droplets were mounted in metallographic resin for metallographic observations using light and scanning electron microscopes.

### RESULTS AND DISCUSSION

The chemical analyses of multilayer welds deposited by the tested electrodes are shown in Table 3. In these analyses samples were taken from regions where the welding process was under quasi-steady state regime, i.e., samples from the starting point and from the crater were not analyzed. The diffusible and residual hydrogen contents of the underwater wet welds deposited by electrodes A to G are summarized in Table 4.

TABLE 3. CHEMICAL COMPOSITION OF WELDS ( IN WEIGHT PERCENT)

ELECTRODE	C	Mn	Si	P	S	Ni	O <sup>(*)</sup>
A (50% TiO <sub>2</sub> )	0.53	0.02	0.16	0.017	0.01	nd	0.1717 ± 0.0261
B (20% Fe <sub>2</sub> O <sub>3</sub> )	0.07	0.1	0.08			nd	0.2219 ± 0.0068
C (30% Fe <sub>2</sub> O <sub>3</sub> )	0.08	0.03	0.04			nd	0.2051 ± 0.0020
D (50% Fe <sub>2</sub> O <sub>3</sub> )	0.042	0.02	0.02	0.014	0.008	nd	0.2117 ± 0.0035
E (20% Fe <sub>2</sub> O <sub>3</sub> + 10% MgO)	0.073	0.08	0.04			nd	0.1747 ± 0.0147
F (oxid., 2%Ni)	0.05	0.02	0.012	0.018	0.015	1.96	0.2221 ± 0.0065
G (E6013)	0.11	0.44	0.23	0.011	0.018	nd	0.0734 ± 0.0046

nd: not detected

(\*): average of three measurements

TABLE 4. HYDROGEN CONTENTS OF UNDERWATER WET WELDS AND RESPECTIVE STANDARD DEVIATION (IN ml/100g OF DEPOSITED METAL)

ELECTRODE	DIFFUSIBLE HYDROGEN	RESIDUAL HYDROGEN
A (50% TiO <sub>2</sub> )	92.3 ± 8.6	4.1 ± 1.9
B (20% Fe <sub>2</sub> O <sub>3</sub> )	43.9 ± 9.8	2.9 ± 0.7
C (30% Fe <sub>2</sub> O <sub>3</sub> )	42.4 ± 3.6	4.9 ± 0.4
D (50% Fe <sub>2</sub> O <sub>3</sub> )	39.8 ± 1.8	4.2 ± 1.9
E (20% Fe <sub>2</sub> O <sub>3</sub> + 10% MgO)	51.3 ± 15.5	4.3 ± 0.4
F (oxidizing, 2%Ni)	44.9 ± 5.1	4.4 ± 1.5
G (E6013)	99.5 ± 2.5	2.8 ± 1.2

In order to examine the effect of oxygen on the weld metal hydrogen content, hydrogen data (from Table 4) were plotted against the weld metal oxygen content (from Table 3). Residual and diffusible hydrogen contents of the welds are shown in Figures 1 and 2, respectively.

The residual hydrogen contents showed a slight tendency to increase as the weld metal oxygen content increased. Although the scatter in the residual hydrogen data is appreciable it can be suggested that a saturation value is achieved for welds with oxygen contents above 0.17 wt.pct. This result is in agreement with the fact that the iron matrix-inclusion interfaces act as

trapping sites for hydrogen. It has been demonstrated that the oxygen content of welds is limited to approximately 0.20 wt.pct. independent of how and how much oxygen is introduced in the liquid metal (Kuwana and Sato, 1986; Ibarra, Grubbs and Olson, 1987; Pope, Liu and Olson, 1994). Accordingly the amount of oxide inclusions also reaches a constant value (Kuwana and Sato, 1986) limiting the matrix-inclusion interfacial area, acting as hydrogen trapping sites, to a constant value. It is then reasonable to expect that high oxygen welds should present approximately the same residual hydrogen content (at some saturation value).

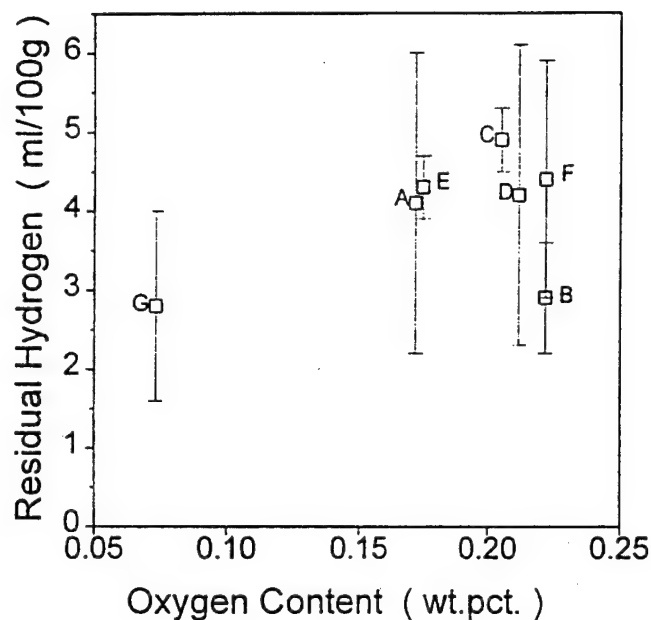


FIGURE 1. WELD METAL RESIDUAL HYDROGEN AS A FUNCTION OF THE OXYGEN CONTENT OF UNDERWATER WET WELDS.

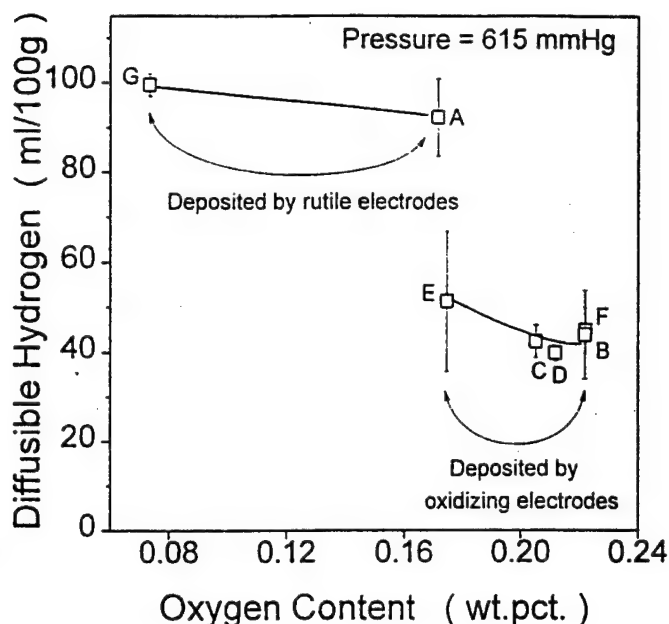


FIGURE 2. WELD METAL DIFFUSIBLE HYDROGEN CONTENT AS A FUNCTION OF THE OXYGEN CONTENT OF UNDERWATER WET WELDS.

It can be observed in Figure 2 that the diffusible hydrogen contents of welds deposited by the oxidizing electrodes (B, C, D, E, and F) are situated in a level lower than that of welds deposited by the rutile electrodes (A and G). Although the weld metal oxygen content varied from 0.07 to 0.17 wt.pct., for the rutile electrodes, and from 0.17 to 0.22 wt.pct., for the oxidizing electrodes, oxygen had a small influence on the diffusible hydrogen content of welds made by electrodes of the same type of flux covering. On the other hand, as shown in Figure 2, there is a significant difference (approximately 50 ml/100g) between the diffusible hydrogen contents of welds deposited by rutile and oxidizing electrodes. Hence, weld metal diffusible hydrogen content seems to be more related to the electrode covering type than the oxygen (or inclusion) content in the weld metal. This fact is particularly well illustrated by the welds deposited by electrodes A (rutile type) and E (oxidizing type), with almost the same oxygen (0.17 wt.pct.) and residual hydrogen contents but quite different average diffusible hydrogen levels (92 and 51 ml/100g respectively). This behavior seems to indicate that the oxygen weld metal (or inclusions) content alone does not explain satisfactorily the lower hydrogen contents of welds deposited by oxidizing electrodes.

It is important to observe in the results shown in Table 4 that the oxidizing electrodes have the lowest total hydrogen content (diffusible + residual). This measured total hydrogen represents the amount of hydrogen present in the weld metal just after cooling to room temperature. Therefore, it seems logical to assume that the lower total (or diffusible) hydrogen associated

with the oxidizing electrodes is most probably due to some process occurring during or before the weld solidification. This fact could be explained by a higher amount of oxygen in the arc atmosphere of oxidizing electrodes promoting the oxidation of some hydrogen to steam, thereby reducing the absorption of this element in the liquid weld (Stalker, 1977).

Other possible explanations for this phenomenon are based on the presence of: (1) surface active solutes, and/or (2) interfacial phases, acting to reduce hydrogen absorption by the liquid metal.

A solute poisoning mechanism was suggested to explain the effect of surface active solutes, such as oxygen, in reducing absorption of nitrogen in iron (Kozakevitch and Urbain, 1963). According to this model, oxygen atoms concentrated at the gas-liquid metal interface form a surface ionic monolayer of  $\text{Fe}^{+2}\text{O}^{2-}$ . Kozakevitch and Urbain (1963) determined that the liquid iron surface becomes saturated with oxygen at a level around 0.02 wt.pct. This surface layer is considered responsible for retarding the absorption of nitrogen in liquid iron. Small, Radzilowski and Pehlke (1973) found a five-fold decrease in the solution rate of hydrogen in iron at 1600 °C when 500 ppm of oxygen was initially present in the melt. Similar effect was found when sulfur, another surface active element, was added to the molten iron. The same solute poisoning model used for nitrogen was used to explain the effect of surface active elements on the absorption of hydrogen by liquid iron. An interfacial reaction of hydrogen with oxygen, from the ionic monolayer, to form water

molecules could be one of the steps responsible for the reduction of hydrogen absorption.

At first sight, the results of diffusible and residual hydrogen for welds deposited by electrodes A and E seem to indicate that the solute poisoning model is not applicable in the case of hydrogen absorption in underwater wet welds. As the welds made by these two electrodes presented approximately the same final weld metal oxygen contents it is reasonable to assume that their kinetics of oxygen absorption were similar. That is, from the electrode tip until the final solidification of the pool, these two welds had approximately the same amount of dissolved oxygen. Therefore, according to the solute poisoning model these two welds should have presented the same level of total hydrogen unless, in the case of the rutile electrode, the iron oxide film did not form or was too thin to prevent the absorption of hydrogen under the turbulent conditions prevailing at the electrode tip and weld pool.

Inouye and Choh (1972) suggested, in the case of nitrogen absorption, that additions of elements (such as C, Mn, and Si) forming oxides more stable than FeO could have an anti-poisoning effect, disrupting or preventing the formation of the FeO monolayer. Also, experiments performed by Nagasaka and Fruehan (1994), studying the kinetics of the reaction of water with liquid iron, demonstrated that FeO did not form on the surface if the carbon content of the melt was above a certain value. The critical carbon level, for the conditions tested, was estimated between 0.08 and 0.2 wt.pct. In the present study the effects of carbon, silicon, and manganese, as measured in the weld metal, on the diffusible hydrogen contents are displayed in Figure 3. The results indicate that the welds presenting higher amounts of deoxidizers were those showing higher diffusible hydrogen contents supporting the anti-poisoning abilities of carbon, manganese, and silicon. Hence, the higher hydrogen content presented by the rutile electrode A could be attributed to the fact that the FeO monolayer was not allowed to form due to the presence of deoxidizers, above a certain critical level, in the liquid metal.

The type of slag that envelopes the electrode tip and weld droplets could also have an influence in preventing or assisting the formation of a protective FeO layer depending whether the electrode covering is based on rutile or hematite (oxidizing), respectively. In both cases it is assumed that a similar high amount of oxygen is absorbed by the liquid iron at the electrode tip. Being surface active, oxygen atoms concentrate at the surface creating conditions for the formation of a protective iron oxide layer. In the case of rutile electrodes, the iron oxide surface layer is probably destroyed by dissolving in the TiO<sub>2</sub> rich liquid slag. In the case of oxidizing electrodes, contrarily, hematite decomposes in FeO and oxygen. Part of the iron oxide reacts with silica forming fayalite. The final result is an iron oxide-rich fayalite slag that, instead of being aggressive to the surface iron oxide protective layer, may help to stabilize it. Although it is difficult to prove the existence of the ionic Fe<sup>+2</sup> O<sup>-2</sup> monolayer in microscopic examinations, EDS analyses revealed the presence of wüstite (light colored dendritic structure) only on

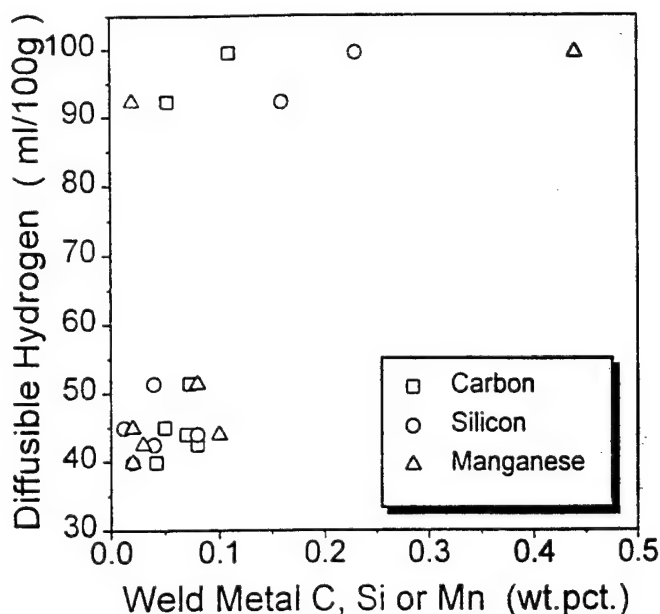


FIGURE 3. WELD METAL DIFFUSIBLE HYDROGEN CONTENT OF UNDERWATER WET WELDS AS A FUNCTION OF WELD CARBON, SILICON OR MANGANESE CONTENT.

electrode tips of oxidizing electrodes (Figure 4) and on droplets collected from these electrodes.

Another explanation for the different weld metal hydrogen absorption patterns, associated with the two different types of electrodes evaluated, is related to the solubility of hydrogen in the slag around the liquid metal. By this mechanism, the higher the hydrogen solubility of the slag, the larger will be the amount of hydrogen absorbed by the liquid metal. Unfortunately a clear view of the effect of the slag on the absorption of hydrogen by underwater wet welds is not possible since there are no data about hydrogen solubility in slags for welding.

## CONCLUSIONS

The following conclusions resulted from the present investigation:

1. The measured diffusible hydrogen contents of underwater wet welds deposited by rutile electrodes were approximately 90 ml/100g while oxidizing electrodes produced welds with diffusible hydrogen contents varying from 40 to 50 ml/100g.
2. The residual hydrogen content of underwater welds showed a tendency to increase to a constant level of approximately 5 ml/100g when the weld oxygen content also reaches a constant value, close to the monotectic composition (0.20 wt.pct.). This result is in accordance with the established fact that the iron matrix-inclusion interfaces act as trapping sites for hydrogen and that as

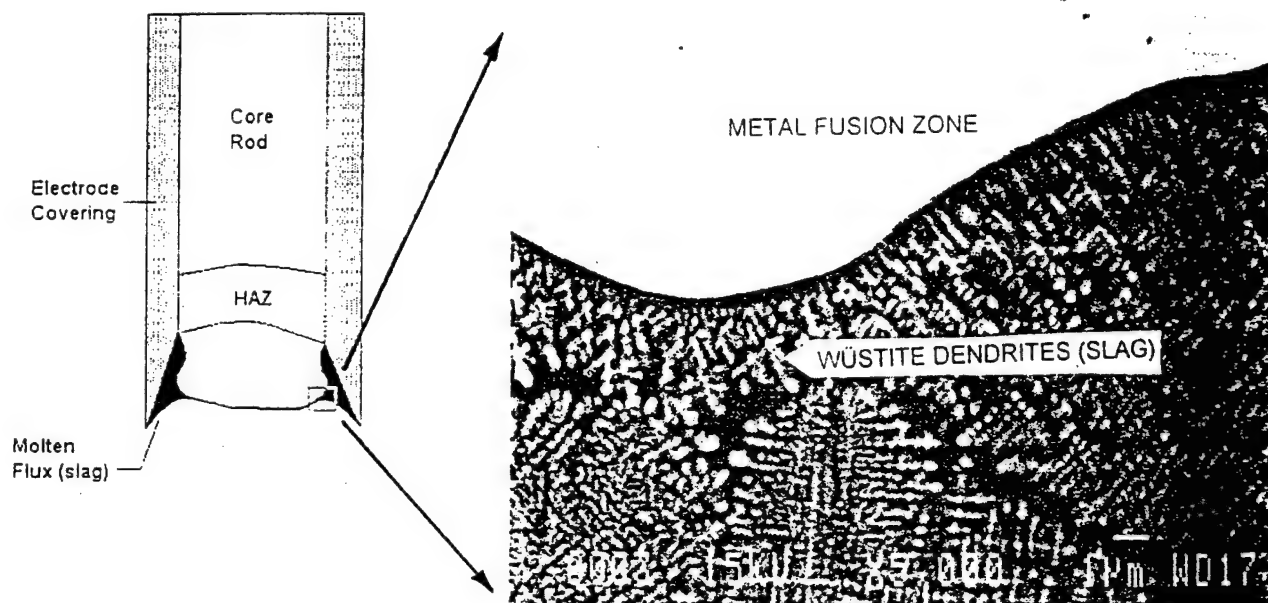


FIGURE 4. BACKSCATTERED ELECTRON MICROGRAPH OF AN AREA, INDICATED BY THE SCHEMATIC DRAWING, AT THE TIP OF AN OXIDIZING ELECTRODE D. THE SOLIDIFIED SLAG CONSISTS OF WÜSTITE DENDRITES IN A SILICATE MATRIX. (SAMPLE NOT ETCHED.)

the metal oxygen content reaches a plateau so does the amount of oxide inclusions and the capacity of the weld to retain hydrogen.

3. The mechanism of hydrogen trapping by oxide inclusions alone, however, cannot explain the difference between the diffusible hydrogen contents measured in welds deposited by rutile and oxidizing electrodes.
4. FeO was detected at the molten tip of the oxidizing electrodes but not the rutile electrodes. The layer of FeO seems to be responsible for the lower weld metal hydrogen content. It is possible that hydrogen reacts with oxygen from the ionic  $\text{Fe}^{2+}\text{O}^{2-}$  monolayer reducing the hydrogen absorption in the weld metal.

#### ACKNOWLEDGMENT

A. M. Pope acknowledges the financial support provided by the Conselho Nacional de Desenvolvimento Científico e Tecnológico (CNPq), and Petrobras, Brazil, and the research support of the Center for Welding, Joining and Coatings Research of the Colorado School of Mines.

#### REFERENCES

- American Welding Society. 1993. Standard methods for determination of the diffusible hydrogen content of martensitic, bainitic, and ferritic steel weld metal produced by arc welding. *ANSI/AWS A4 3-93*. Miami, FL.
- Gooch, T. G. 1983. Properties of underwater welds. Part 1. Procedural trials. *Metal Construction*, 164-167 (March).
- Grubbs, C. E., and O. W. Seth. 1977. Underwater wet welding with manual arc electrodes. In: *Underwater Welding for Offshore Installations*. The Welding Institute, 17-33.
- Hasui, A., and Y. Suga. 1980. On cooling of Underwater Welds. *Trans. of the Japan Welding Society*, 11 (1) (April).
- Ibarra, S., C. E. Grubbs and D. L. Olson. 1987. The nature of reactions in underwater welding. *19th Annual Offshore Technology Conference Paper OTC 5588*. Houston, Texas: 277-281 (April).
- Inouye, M., and T. Choh. 1972. Some considerations on the nitrogen transfer across gas-liquid iron interface. *Trans. ISIJ*, 12: 189-196.
- Jackson, C. E. 1973. Fluxes and slags in welding. *WRC Bulletin 190* (Dec).
- Kozakevitch, P., and G. Urbain. 1963. Influence de certains éléments dissous sur la vitesse de dissolution de l'azote dans le fer liquide. *Mém. Scient. Rev. Métallurg.* 60 (2): 143-156.
- Kuwana, T. and Y. Sato. 1986. Oxygen absorption and oxide inclusion of iron weld metal during arc welding. *III Doc IX-1392-86* (April).
- Nagasaka, T., and R. J. Fruehan. 1994. Kinetics of the Reaction of  $\text{H}_2\text{O}$  Gas with Liquid Iron. *Met. & Mat. Trans.* 25B: 245-253 (April).
- Nóbrega, A. F. 1981. *Study of underwater welding with covered electrodes*. MSc Thesis. Federal University of Rio de Janeiro, Brazil (in Portuguese).



Ozaki, H., J. Naiman, and K. Masubuchi. 1977. A study of hydrogen cracking in underwater steel welds. Welding Journal. : 231s-237s (Aug).

Pope, A. M., S. Liu, D. L. Olson. 1994. Effects of the electrode oxidizing potential on underwater wet welds. Proceedings: 13<sup>th</sup> International Conference on Offshore Mechanics and Arctic Engineering. vol.III : 361-368.

Pope, A. M., J. C. G. Teixeira, V. R. dos Santos, M. P. Paes, and S. Liu. 1995. Use of nickel to improve the mechanical properties of high oxygen underwater wet welds. Proceedings: 14<sup>th</sup> International Conference on Offshore Mechanics and Arctic Engineering. vol.III : 529-535.

Small, W. M., R. H. Radzilowski, and R. D. Pehlke. 1973. Kinetics of Solution of Hydrogen in Liquid Iron, Nickel, and

Copper Containing Dissolved Oxygen and Sulfur. Met. Trans. 4 : 2045-2050 (Sept.)

Stalker, A. W. 1977. Welding Institute Research on Underwater Welding. In: Underwater Welding for Offshore Installations. The Welding Institute. : 63-74.

Suga, Y. 1992. The Effect of Cooling Rate on Mechanical Properties of Underwater Wet Welds in Gravity Arc Welding. Weld. Res. Abroad. XXXVIII (6/7) : 15-20 (June/July)

Wingrove, J. 1970. Identification of iron oxides. J.I.S.I. : 258-264 (March)

Yurioka, N., and H. Suzuki. 1990. Hydrogen assisted cracking in C-Mn and low alloy steel weldments. International Materials Reviews. 35 (4) : 217-249.

## **RECENT DEVELOPMENTS IN THE WELDING OF HIGH STRENGTH AND HIGH TOUGHNESS STEELS**

**Prof. Stephen Liu  
Center for Welding and Joining Research  
Colorado School of Mines  
Golden, Colorado 80401  
U.S.A.**

### **ABSTRACT**

The application of high strength low alloy steels in structural fabrications, such as naval and marine construction, since the 1960s have accelerated the development of new welding consumables to produce weld deposits of mechanical properties comparable to those of the base metal. In these steels, elements such as manganese, nickel, chromium, molybdenum, and copper play important roles in providing strength above 690 MPa (100 ksi). Other elements such as niobium, vanadium and titanium are added in micro-quantities for the control of austenitic and ferritic grain size, thus improving the toughness of the weld metal. The base metal microstructure of these steels can vary from almost exclusively acicular ferrite, in the case of steels with strengths around 500 and 600 MPa (72 and 81 ksi), to a mixed martensite/bainite matrix, in the case of steels of strength above 690 MPa (100 ksi).

When heat is applied to a high strength base metal during welding, the microstructure is modified in two ways: the development of a heat-affected zone and a weld zone. In the heat-affected zone, the thermal stability of the base metal microstructure and the susceptibility of the heat-affected zone to hydrogen cracking are of great concern. Developments in new steels that are thermally insensitive and in hydrogen management will be discussed. Different from the base metal, the weld metal undergoes both solidification and lower temperature, solid-state phase transformations. The resulting microstructure is generally composed of bainite and martensite, surrounded by a network of grain boundary ferrite. This microstructure is characterized by its reduced toughness and high hardness. Nevertheless, studies have demonstrated that by introducing acicular ferrite in this microstructure through ferrite nucleation control, the weld metal hardness is reduced and toughness can be restored to an acceptable level. Microalloying additions such as boron, titanium, aluminum, and zirconium were shown to be efficient in promoting the formation of acicular ferrite. Developments in welding consumables design to disperse acicular ferrite in a bainite/martensite matrix for higher toughness will be discussed. The importance of non-metallic inclusions, especially their bimodal size distribution, in determining the dispersion of acicular ferrite particles in a high strength steel weld metal matrix will be considered. High strength steels and their weld metals also rely heavily on precipitation



*Keynote Presentation*

*Israeli National Welding Conference – Tel Aviv, Israel, October 22, 1996*

(for example,  $\epsilon$ -Cu precipitation) to obtain their final properties. Depending on their thermal stability, these precipitates can age with thermal cycles resulting in fluctuations in mechanical properties in a multipass weld metal. This presentation will discuss the synergistic effect of co-precipitation in promoting uniform mechanical properties in the weld metals. The prediction of weld metal microstructure and cracking susceptibility of steels has been made using carbon equivalent type predictors for decades. The concept of carbon equivalent type predictors and alloy hardenability and phase transformations will be discussed. Expressions that include the inclusion (ferrite nucleation site) formers and predictive diagrams such as the Equal Properties Diagrams will also be discussed,

**E. Effect of Oxidizing Electrodes and Polarity on Hydrogen Mitigation in Underwater Wet Welding,**

*by R. C. de Medeiros and S. Liu, Colorado School of Mines*

Weld metal hydrogen pick-up in underwater wet welding is unavoidable due to the dissociation of water vapor surrounding the welding arc. In conjunction with the fast-quenching nature of the water environment, the high hydrogen content in the weldment leads to hydrogen cracking in the heat-affected zone (HAZ). This undesirable occurrence has been successfully overcome with the use of oxidizing-type electrodes with which low diffusible hydrogen content can be achieved in underwater wet welds. Despite their unique behavior in terms of both low diffusible and low total hydrogen content, there seems to be very little research work undertaken to identify the influence of the slag and the effect of polarity on hydrogen absorption during underwater wet welding.

The aim of this investigation is to understand thoroughly the hydrogen pick-up by the slag as well as the effect of welding current and polarity (direct current straight polarity, DCSP, and direct current reversed polarity, DCRP) on weld metal diffusible hydrogen. To accomplish this purpose, five experimental oxidizing electrodes with systematic ferric oxide ( $\text{Fe}_2\text{O}_3$ ) additions, from 0 to 70 wt.%, to the flux system were investigated. The mole fraction ratio of  $\text{CaO}:\text{SiO}_2$  in the flux system was kept constant, and independent of ferric oxide additions.

Underwater gravity welds were deposited on ASTM A36 steel coupons at 0.27 m city water depth. All welds used similar conditions. Weld metal diffusible hydrogen content was determined using the mercury displacement method according to ANSI/AWS A4.3 (1993).

The measured diffusible hydrogen contents showed that the DCSP produced welds with lower diffusible hydrogen contents than ones produced using DCRP. As an example, with 36 wt.%  $\text{Fe}_2\text{O}_3$  addition in the flux, the diffusible hydrogen were 23.2 ml/100 g of deposited metal (DCSP) and 30.5 ml/100 g of deposited metal (DCRP). Additionally, higher hydrogen values were always related to lower ferric oxide contents initially present in the flux, for example, 70.8 ml/100 g of deposited metal (DCRP - 0 wt.%  $\text{Fe}_2\text{O}_3$ ) and 30.5 ml/100 g of deposited metal (DCRP - 36 wt.%  $\text{Fe}_2\text{O}_3$ ). The program results also reaffirmed the effectiveness of oxidizing electrodes in controlling hydrogen pick-up in underwater wet welds. Mossbauer tests carried out on different slags showed that a large amount of the ferric oxide initially present in the slag had transformed to iron oxide ( $\text{FeO}$ ).

The presence of  $\text{FeO}$  in the welding slag complemented the results of Pope and Liu (1995 and 1996) that  $\text{FeO}$  was found at the molten tip of the electrode. These researches proposed that the  $\text{FeO}$  layer surrounding each metal droplet act as a barrier to hydrogen pick-up by the metal droplet.

Finally, the variations in the weld metal total hydrogen with both polarity and iron oxide content in the slag were successfully predicted by using an electrochemical model for the slag/metal interface equilibrium. The slag/metal interface has been identified as responsible for controlling the hydrogen pick-up. The model assumed that hydrogen is present in the slag as  $\text{OH}^-$  ions and that  $\text{FeO}$  displays ideal solution behavior.

**B. Arc Welding Over Paint Primer,**

*by K. S. Johnson, S. Liu, and D. L. Olson, Colorado School of Mines; and R. W. McClellan, Ingalls Shipbuilding*

When welding is performed over a primer coating, significant amounts of gases are generated. If entrapped in the weld pool, these gases will produce porosity and may result in weld cracking. If the partial pressures of these gases are decreased in the welding arc, porosity can be minimized. Since hydrogen usually presents the most problems associated with porosity and cracking, any decrease in hydrogen generation in the welding environment would lead to better quality welds. According to the *hydrogen-oxygen* equilibrium considerations, an increase in the partial pressure of oxygen would lead to a decrease in the partial pressure of hydrogen. Therefore, a welding consumable that contains chemical ingredients of high oxidizing potential would minimize hydrogen pick-up.

Flux cored arc welding (FCAW) experiments were performed on steel coupons without primer coating using a 4% $H_2$ -96% $CO_2$  shielding gas. Various oxidizing ingredients ( $FeO$ ,  $Fe_2O_3$ ,  $SiO_2$  and  $CaCO_3$  mixed in Fe powder) were deposited on top of the weld coupons for these experiments. The shielding gas was enriched with hydrogen to ensure pick-up in the weld pool, and the fluxes were used to modify the oxygen potential in the weld pool. Welds were also done with no flux and 100%  $CO_2$  shielding gas as a baseline. These different combinations of fluxes and gases were used to help verify the hydrogen-oxygen equilibrium relationship and determine if high oxidizing potential fluxes could control hydrogen production in welds.

The results showed that as the level of oxygen was increased in the weld pool, the level of diffusible hydrogen produced decreased, which proves the inverse relationship between hydrogen and oxygen. Since an inorganic zinc silicate primer (Interplate NQA238) was used to coat the weld coupons, the level of diffusible hydrogen jumped from around 8.0 ml/100g for a sample with no flux, no primer, and 100%  $CO_2$  to around 12.5 ml/100g for a sample with 1.25 mils of primer, and to 18.5 ml/100g for a sample with 2.5 mils of the primer. The increase in diffusible hydrogen was due to the decomposition of the primer. From experiments done with binary and ternary mixtures of the oxidizing ingredients, it was determined that the oxidizing potential effect of the fluxes was not additive, and a ternary mixture of  $CaCO_3$ ,  $SiO_2$ , and  $Fe_2O_3$  gave the best oxidizing potential while maintaining good overall bead appearance. Several welds were made with different combinations of fluxes at different levels of addition to determine an optimal composition to use for further testing, and to eventually be added to the core of a commercial FCAW electrode.

It has been clearly shown that the level of hydrogen production can be controlled through use of the hydrogen-oxygen equilibrium relationship and high oxidizing potential fluxes. As the level of weld metal oxygen is increased, the amount of hydrogen produced decreases. This is important because as the amount of primer on a steel plate is increased, the level of hydrogen produced will also increase substantially requiring tighter control to minimize porosity and cracking.

A. **Effective Hydrogen Control by Means of Fluoride Additions in Flux Cored Arc Welding,**  
by M. Matsushita, S. Liu, and D. L. Olson, Colorado School of Mines

As higher strength steels are developed for structural fabrication, more stringent requirements on weld metal diffusible hydrogen content are also imposed. The value of 5 ml/100g weld metal diffusible hydrogen content, recognized for many years as the upper limit for admissible hydrogen content, is no longer acceptable in many critical applications. It is well known that process control (welding parameters, electrode baking, part surface cleanliness, etc.) can decrease the amount of hydrogen pickup in the weld metal, but the reduction is generally limited. Consumables with ingredients capable of minimizing hydrogen in the arc plasma and in the molten weld pool must be designed to successfully manage hydrogen in high strength steel weldments.

Ingredients that contain fluorine radicals ( $F^{-1}$ ), such as fluorspar ( $CaF_2$ ) and Cryolite ( $K_3AlF_6$ ), have been reported to reduce the amount of diffusible hydrogen in steel welds. In this research, experimental FCAW consumables that contained various complex fluoride compounds were designed and manufactured at CSM. The base formulation was basic in nature, with  $CaF_2$  as one of the main flux ingredients. Welds were performed on both HSLA and low carbon steel plates. Heat input was kept at 1.7 kJ/mm for all welds. Three shielding gases were used in the experiments: 100%  $CO_2$ , 99%  $CO_2$ -1%  $H_2$  and 96%  $CO_2$ -4%  $H_2$ . The two hydrogen-containing gases were used to deliberately promote weld metal hydrogen pickup for comparison with the  $CO_2$  shielding gas. Welding was performed in a globe box with flowing argon gas to avoid the influence of moisture in the air. Three fluorides ( $MnF_3$ ,  $K_3AlF_6$ , and  $KAlF_4$ ) were added in the base fluxes in the range of 0 to 10 weight percent, alternating the  $CaF_2$  content. The amounts of diffusible hydrogen were measured using a gas chromatograph. During the course of research, thermodynamic calculations were performed which indicated the effectiveness of these fluoride compounds in reducing the partial pressure of hydrogen in the arc stream. Gas chromatographic measurements confirmed the calculations.

The experiments proved that the fluorides were effective in reducing the hydrogen content in the weld metal. For example, a reduction of almost 30% was achieved with the addition of 5 weight percent of  $K_3AlF_6$  (10.77 to 6.56ml/100g). The shielding gas was 100%  $CO_2$ . The reduction was even more impressive when hydrogen content in the arc stream was deliberately increased by using the  $CO_2$ - $H_2$  shielding gas. Without the fluoride/complex fluoride, the diffusible hydrogen content was approximately 35ml/100g weld metal. With five weight percent  $AlF_6^{-3}$  addition, the diffusible hydrogen content was reduced to 14.77ml/100g, a reduction of almost 60%.  $MnF_3$  additions showed similar effectiveness in reducing hydrogen pickup. In  $CO_2$ -4%  $H_2$  shielding gas, manganese fluoride was able to lower the hydrogen content to around 10ml/100g.

The effectiveness of the complex fluorides is attributed to its relative high temperature instability and lower melting temperature (when compared with  $CaF_2$ ). As such, more  $F^{-1}$  ions are available for reaction with hydrogen to form HF, which has extremely low solubility in molten iron. Based on thermodynamic

calculation, the  $P_{HF}^2/P_F$  ratio was shown to be useful in estimating the relative effect of the fluorides on diffusible hydrogen control.

**B. Effect of Slag Chemistry on Hydrogen Pickup in Underwater Wet Welds,**  
*by R. C. Medeiros and S. Liu, Colorado School of Mines*

Weld metal hydrogen pickup in underwater wet welding is severe due to the presence and dissociation of water vapor surrounding the welding arc. This undesirable behavior can be minimized, however, with the use of oxidizing-type electrodes. The aim of this investigation has been placed on the thorough understanding of hydrogen pickup by the slag on weld metal diffusible hydrogen. To accomplish this purpose, twenty experimental oxidizing electrodes with systematic ferric oxide ( $Fe_2O_3$ ) additions, ranging from 0 to 70 wt. pct., to the flux system were investigated. The mole fraction ratio of  $CaO/SiO_2$  in the flux ranged from 0.05 to 0.35, independently of ferric oxide additions. Underwater gravity welds were deposited on ASTM A36 steel coupons at 0.27 m (city) water depth using a gravity feed system and similar welding parameters. Weld metal diffusible hydrogen content was determined using the mercury displacement method according to current AWS standard. To correlate weld metal hydrogen content with slag chemistry, the slag hydrogen contents were also determined.

The measured diffusible hydrogen contents showed that  $Fe_2O_3$  was effective in reducing weld metal hydrogen content. Higher hydrogen values were always related to lower ferric oxide contents initially present in the flux, for example, 70.8 ml/100g of deposited metal (DCEP - 0 wt. pct.  $Fe_2O_3$ ) and 30.5 ml/100g of deposited metal (DCEP - 36 wt. pct.  $Fe_2O_3$ ). Amazingly, diffusible hydrogen as low as 13.2 ml/100g was obtained with the B3 electrode (53 wt. pct. of  $Fe_2O_3$  and  $CaO:SiO_2$  equal to 0.15). X-ray diffraction analysis (XRD) conducted on different slags showed that the minimum diffusible hydrogen values were always associated with the presence of fayalite ( $2FeO \cdot SiO_2$ ). Complementing XRD analysis, Mössbauer spectroscopy tests carried out on different slags showed that all ferric ( $Fe^{+3}$ ) oxide initially present in the slag had transformed to ferrous ( $Fe^{+2}$ ) oxide ( $FeO$ ), free or combined.

Chemical analyses showed that weld metal hydrogen pickup was strongly dependent on the water solubility in slags. The total hydrogen content in the weld metal increases monotonically with increasing slag hydrogen content. However, a slag that has high water solubility will, in general, retain more hydrogen in the slag resulting in lower diffusible hydrogen in the weld metal.

Finally, variations in weld metal hydrogen as well as slag hydrogen content with both polarity mode and iron oxide content in the slag were successfully predicted using an electrochemical model for the slag/metal interface equilibrium. In this investigation, the slag/metal interface has been identified as responsible in controlling the hydrogen pickup. The model assumed that hydrogen is present in the slag as (OH) ions and that  $FeO$  displays ideal solution behavior.

## HYDROGEN CONTROL AND MICROSTRUCTURAL REFINEMENT OF STRUCTURAL STEEL WELDS USING FLUORIDE-CONTAINING FCAW ELECTRODES

Kevin S. Johnson, Stephen Liu and David L. Olson  
Center for Welding, Joining and Coatings Research  
Colorado School of Mines  
Golden, CO

### Abstract

When welding is performed over primer-coated steels such as in the shipbuilding and offshore structures fabrication industry, significant amounts of hydrogen and other gases, e.g., CO and  $Zn_{(v)}$ , are generated as the welding arc causes the primer to decompose. If entrapped in the weld pool, the hydrogen and other gases will produce porosity. Since hydrogen has been shown to compose most of the gas generated in a FCA weld over primer-coated steel, it is also the most detrimental. According to the hydrogen-oxygen and hydrogen-fluorine equilibrium considerations, an increase in the partial pressure of oxygen or fluorine could decrease the partial pressure of hydrogen within the welding arc. Consequently, a welding consumable that contains chemical ingredients of high oxygen and fluorine potential would be capable of minimizing hydrogen pick-up in the weld pool. Welds made using a commercially available rutile-based E71T-1 flux-cored consumable produced about 74.3 ml/100g of diffusible hydrogen on a steel sample coated with 5.0 mils of an inorganic, zinc-ethyl silicate primer. The oxygen content for this weld was about 600 ppm. Welds made on a sample coated with 4.0 mils of the same primer, but using an experimental electrode with the addition of oxidizing ingredients and  $MnF_3$ , produced only 15.8 ml/100g of diffusible hydrogen with an oxygen content of about 660 ppm. The decrease in diffusible hydrogen content from the experimental electrodes is due to the effectiveness of the oxide and fluoride flux additions. The results of these experiments prove that a FCAW consumable capable of direct welding over primer-coated steels could be developed using basic pyrometallurgical principles.

### Introduction

Pre-construction primers are used regularly by the shipbuilding and offshore structures fabrication industries to protect steel plates from corrosion during storage and construction. Just prior to the plates being welded, the primers are removed from the weld joint by blasting

or grinding because weld quality is often unsatisfactory when welding directly over a primer-coated surface. The presence of a primer generally leads to arc instability, excessive porosity, carbon pick-up, alloying element loss, and hydrogen damage. Elimination of these welding problems would allow for arc welding directly over primers, decrease the costs associated with primer removal operations, and minimize rework because of defective weld joints. The success of welding over primer would clearly result in significant increases in the productivity of shipbuilding and fabrication of offshore structures.

Under most normal welding conditions, moisture, cutting fluids, and organic solvents are the major sources of hydrogen in the arc environment. In the case of a primer-coated steel, however, the acrylic-based or epoxy-based resins in the primer pyrolyze in the welding arc and provides large amounts of carbon monoxide and hydrogen, among others, to the weld pool. As the weld pool solidifies, these gases are rejected continuously into the remaining liquid, which quickly reaches supersaturation. Gas pores begin to nucleate and grow. Some of the gas bubbles will be eliminated from the weld pool due to turbulence and convective flow of the molten metal, while others are trapped within the solidifying weld pool. Suga et. al. (1) showed that when an inorganic-zinc, primer-coated steel was subjected to flux-cored arc welding, the resultant gas found in the blowholes was about 95% hydrogen. For primers that contain zinc as the active ingredient for corrosion protection, both the organic materials and the zinc contribute to the generation of weld discontinuities. In the case of zinc, it easily vaporizes in the welding arc and may also be trapped in the weld pool as pores.

Porosity in the weld metal that originates from hydrogen and carbon monoxide can be minimized by decreasing the partial pressures of these gases in the weld environment. A welding consumable that contains ingredients with high oxidizing potential is desirable for this purpose. This proposed mechanism could be understood by examining the decomposition reaction for water:





The oxygen in the weld metal is expected to react with hydrogen to form  $\text{H}_2\text{O}$  vapor. Increasing oxygen will shift the equilibrium to the left-hand side of the reaction and decrease the hydrogen concentration in the weld metal. Since the convective flow in the weld pool is believed to remove the water vapor, it is the dissolved hydrogen in the molten weld pool that once becoming supersaturated during solidification nucleates as pores. As a result of increased oxygen content in the weld pool, the amount of porosity is expected to decrease. Fluxes that contain ingredients, such as  $\text{SiO}_2$ ,  $\text{Fe}_2\text{O}_3$ , and  $\text{FeO}$ , that generate high oxygen potential when they dissociate can be added to the core of a flux-cored arc welding consumable to control the diffusible hydrogen, and thus, porosity produced when using zinc-rich primers.

### Zinc-Rich Primers

Zinc-rich primers are a unique class of cross-linked coatings that provide galvanic protection to a ferrous substrate. These types of coatings harden or cure, and attain their final resistant properties by virtue of a chemical reaction either with a copolymer or with moisture (chemically cured) (2). Having excellent resistance to moisture, and the fact that they can be made resistant to abrasion, ultraviolet and thermal degradation, these coatings are extremely useful for protection of structural steels. If the zinc content is about 95% in the dry primer film and it is in contact with the steel surface at a sufficient number of points, the zinc becomes the sacrificial anode and protects the underlying cathodic steel.

The biggest advantage in using zinc-rich coatings is the thorough protection against pitting and subfilm corrosion, even at voids, pinholes, scratches, and abrasions in the coating system. The only requirement to make the primer coating effective is that the underlying substrate must be cleaned of all rust, old paint, and any other contaminants that may interfere with the metal-to-metal contact. The Steel Structures Painting Council (SSPC) specifies that for blast cleaning, the surface produced should conform to a White or Near-White surface (3). The surface can also be cleaned with power tools or by pickling.

Since the protection provided by the paint is directly related to its thickness, the necessary protection cannot be guaranteed unless the dry film thickness is enough for the environment. However, obtaining a uniform thickness can be quite difficult in an industrial environment.

Organic coatings, such as the epoxy zinc primers, are more tolerant of surface preparation conditions because they wet more readily and seal the rust or old paint that remains on the surface. There is no reaction with the underlying surface other than for the organic vehicle to wet the steel substrate and develop adhesion. However, these primers exhibit several disadvantages that include flammability, blistering, harmful solvent effects, sensitivity to atmospheric influences, and relatively low heat resistance.

Zinc, ethyl-silicate (inorganic) primers are more popular than the epoxy zinc primers because they provide longer galvanic protection.

but are less tolerant of poor surface preparation. The inorganic coatings exhibit better temperature resistance than the organic ones, and they are able to withstand dry heat to over  $370^\circ\text{C}$  ( $700^\circ\text{F}$ ) (4). The inorganic primers also possess superior abrasion and impact resistance, and provide the best overall protection in an industrial environment in which the flux-cored arc welding process is being used.

### Flux-Cored Arc Welding Fluxes

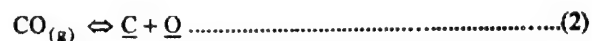
The fluxes in a flux-cored arc welding consumable very often serve several functions. These include control of arc stability and resistivity, slag melting temperature, slag viscosity and detachability, weld bead contour, spatter and fume generation, along with weld pool refinement and alloying. The chemical ingredients used in manufacturing FCAW electrodes can be grouped into five main functional categories: 1) arc stabilizers, 2) deoxidizers, 3) gas formers, 4) slag formers, and 5) alloying elements.

Flux ingredients such as  $\text{SiO}_2$  and  $\text{TiO}_2$  are slag-formers, which form long chains of silicates and titanates.  $\text{FeO}$ ,  $\text{Fe}_3\text{O}_4$ ,  $\text{Fe}_2\text{O}_3$ , and  $\text{CaO}$  (from the decomposition of  $\text{CaCO}_3$ ) tend to break down the anion chains and regulate the slag viscosity. These ingredients are also able to release their oxygen into the arc plasma or into the weld pool affecting the oxygen balance of the weld environment. Their addition can be a means of introducing controlled amounts of oxygen into the weld pool (5) and minimizing the amount of hydrogen pick-up in the weld metal.

When  $\text{CaCO}_3$  is added into the flux, it decomposes in the welding arc to release  $\text{CO}_2$ . At high temperatures,  $\text{CO}_2$  and C react to form CO. Considering the C-O equilibrium,  $p_{\text{CO}_2} / p_{\text{CO}}$  also expresses the

$p_{\text{O}_2}$ . Increasing  $\text{CO}_2$ , i.e., increasing  $p_{\text{O}_2}$ , will decrease the partial pressure of hydrogen in the arc environment and reduce hydrogen pick-up in the weld pool. This relationship can be seen in the Richardson-Ellingham Diagram (6) in Figure 1. The ratio of  $\text{CO}_2$  to CO also determines the recovery of alloying elements. Earlier work done by Sorokin and Sidlin in 1974, shown in Figure 2, proved that increasing oxygen in the weld would result in lower hydrogen (7). By working with alloying elements and marble ( $\text{CaCO}_3$ ) to affect the oxygen potential in the electrode flux coatings, they were successful in decreasing hydrogen levels through increased oxygen levels. Their findings agree with the predictions of Equation 1.

In the case of investigating carbon monoxide formation in the arc and subsequent entrapment in the weld metal as porosity, the carbon-oxygen equilibrium can be examined. The decomposition reaction for CO is as follows:



If oxygen is increased in this reaction, carbon is removed from the weld pool and carbon monoxide is produced. However, if the concentration of carbon is kept low, the amount of CO will also be low leaving hydrogen as the main source of porosity.

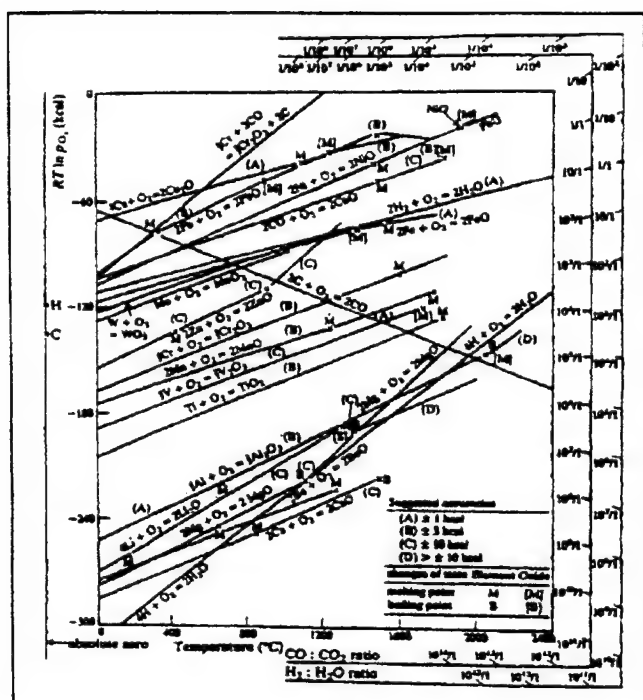


Figure 1. Richardson-Ellingham Diagram of Free Energy versus Temperature for the Oxidation of Metals (6).

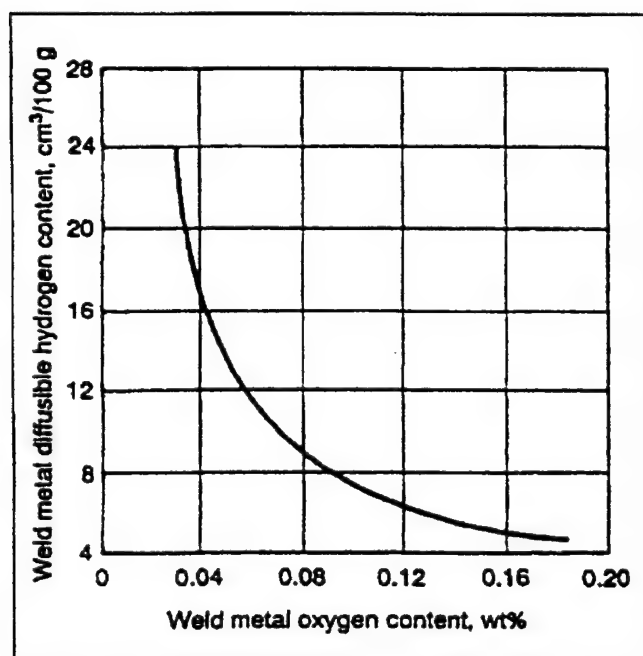


Figure 2. Plot of Weld Metal Diffusible Hydrogen Content versus Weld Metal Oxygen Content (7).

In addition to the chemical properties discussed above, the viscosity

of the slag generated by the flux ingredients must be adequate to protect the weld from contamination, but yet sufficiently permeable to allow gases evolved from the molten metal to escape. If the slag is too viscous for the gases to pass through, surface pockmarks may result. Finally, the fluxes used to control the properties of the arc and weld metal can also greatly affect the microstructure obtained.

### Weld Metal Microstructural Development

The change of oxygen content in the weld metal as a result of flux additions and primer coatings is expected to affect the weld metal microstructure and mechanical properties. As indicated earlier, oxygen is introduced into the weld pool at high temperatures by flux dissociation, slag-metal reactions in the weld pool, aspiration of air into the arc, and residual oxygen in the shielding gas. Oxygen reacts with alloying elements to form inclusions. Because there are multiple reactions taking place within the weld pool, different oxides can appear in the same weld. In addition to the presence of inclusions in the weld metal, which can act as crack nucleation sites, the hardenability of the weld metal is also decreased because of loss of alloying content. In both of these cases, toughness and impact energy absorbed are low at the extremes of oxygen content which can be seen in work done by Terashima and Tsuboi (8) in Figure 3.

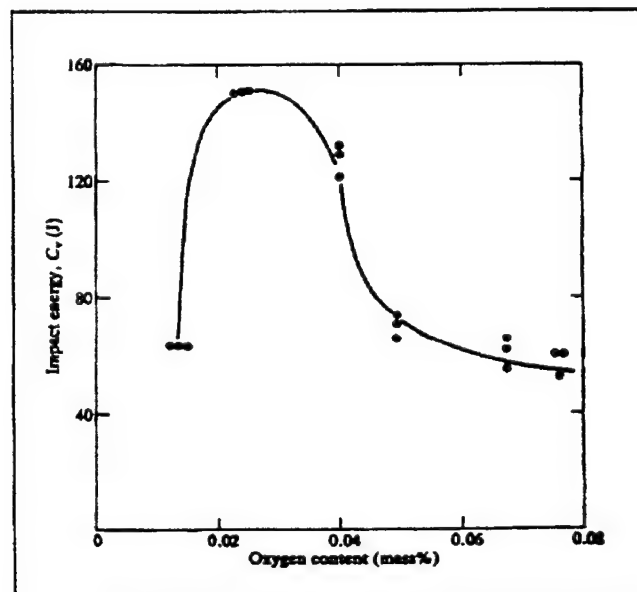


Figure 3. Impact Strength at -15°C of Submerged Arc Weld Metal as a Function of Weld Metal Oxygen Content (8).

Besides the oxygen content of the weld metal, alloy content and cooling rates also affect the microstructure (9). The microstructure desired can be obtained through fine-tuning of the selected flux systems and through alloy additions. Increasing hardenability agents such as Mn promote growth of acicular ferrite, which is characterized by its fine grain size and high impact toughness. Most key microstructural changes in low carbon steel welds take place between



800°C and 500°C, and the time to cool between 800°C and 500°C is denoted as the cooling rate parameter,  $\Delta t_{8-5}$ . A long  $\Delta t_{8-5}$  will generally promote the formation of grain boundary ferrite that is blocky and exhibits low impact toughness. Fine austenite grain size can be obtained with microalloying additions (ex. Nb, V, Ti, and Al) because the precipitates that form "pin" the grain boundaries and inhibit grain growth (10,11,12). If the alloying additions and grain sizes are kept to an optimum, both strength and toughness can be increased.

Microstructural products such as martensite and bainite contain high dislocation densities, and along with solution hardening, contribute to the high hardness and strength in weld metals. However, the toughness and impact properties of these phases are generally not as desirable, and they are susceptible to hydrogen-induced cracking. These types of microstructures are produced in underwater wet welds where there is an abundance of hydrogen. Oxidizing electrodes used in underwater wet welding are capable of controlling the production of diffusible hydrogen.

#### Effect of Oxygen on Hydrogen Control

Research has been conducted by Pope (13) at the Colorado School of Mines examining the effects of oxidizing electrodes on control of diffusible hydrogen contents in underwater wet welds. Weld metal hydrogen pick-up in underwater wet welds is inevitable because of the presence of water vapor surrounding the welding arc, and its dissociation. The increased cooling rates of welds in an aqueous environment, along with the high hydrogen levels in the weld metal, may lead to hydrogen cracking in the heat-affected zone and hydrogen microfissuring in the weld metal. This undesirable result has been lessened to a great extent by the use of oxidizing-type SMAW electrodes. These electrodes lower both the diffusible hydrogen and total hydrogen contents of the welds.

It is well accepted that ferritic, oxidizing-type electrodes perform the best in terms of low weld metal diffusible hydrogen content, despite their poor arc and running characteristics, and poor weld mechanical properties. The most recent investigation on the effects of oxygen on diffusible hydrogen have been conducted by Medeiros (14). His results indicated that depending on the type and proper balance among flux constituents, the hydrogen solubility in the slag could be drastically reduced. If equilibrium is assumed to exist at the slag-metal interface, hydrogen solubility will be lower in the slag, and the amount of hydrogen that will be absorbed by the molten weld pool will be lower.

Using experimental electrodes that contained  $\text{Fe}_2\text{O}_3$ ,  $\text{SiO}_2$ , and  $\text{CaCO}_3$ , Pope (13) obtained wet welds with very low hydrogen contents. The results from the diffusible hydrogen tests in Figure 4 clearly show that diffusible hydrogen contents can be lowered by almost 50% when using an oxidizing electrode instead of a rutile electrode.

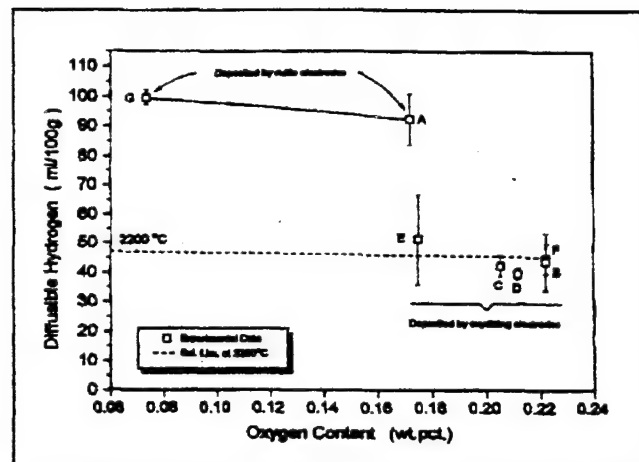


Figure 4. Weld Metal Diffusible Hydrogen Content as a Function of the Weld Metal Oxygen Content of Underwater Wet Welds (13).

#### Effect of Fluorine on Hydrogen Control

Since increasing oxygen also increases the amount of grain boundary ferrite, which lowers the weld metal impact toughness, oxygen cannot be increased indefinitely for the sake of diffusible hydrogen reduction. As a result, another mechanism such as the hydrogen-fluorine equilibrium must be used to assist in lowering diffusible and creating a balance between oxygen, hydrogen, and microstructure. It was thought that if oxidizing fluxes worked based on the hydrogen-oxygen equilibrium, then fluorine-containing fluxes should also work on basically the same chemical equilibrium principle. The principle of the hydrogen-fluorine equilibrium can be seen in the following:



The basic premise is that by increasing the fluorine level in the weld pool, the diffusible hydrogen should be lowered the same way as oxygen lowers the hydrogen. The fluorine in the weld metal is expected to react with the hydrogen to form HF vapor. Increasing fluorine will shift the equilibrium to the left-hand side of the reaction and decrease the hydrogen concentration in the weld metal. The convective flow of the weld pool should remove the HF vapor and minimize the porosity generated by the hydrogen.

The experimental program conducted in this research involved the verification of the hydrogen-oxygen relationship, determination of the oxidizing potential of flux additions, determination of the effects of primer thickness on diffusible hydrogen, verification of the hydrogen-fluorine relationship, and the development of several experimental flux-cored arc welding consumables. These different tasks were accomplished through diffusible hydrogen measurement (collection over mercury), interstitial analysis for oxygen, weld metal chemical analysis, metallography, and mechanical testing, such as tensile tests, Charpy impact tests, and fillet weld break tests.

## [H]-[O] Relationship Verification

The overall goal of this investigation was to prove that high oxidizing potential flux ingredients could be added to a FCAW consumable that would minimize diffusible hydrogen produced when welding over primer-coated structural steels. Initially, several oxidizing fluxes were chosen for examination to verify the hydrogen-oxygen relationship. These included  $\text{Fe}_2\text{O}_3$  and  $\text{SiO}_2$  mixed in with Fe powder. The DH-36 steel (modified A36 steel) coupons used in the experiments were cut to size according to AWS A4.3 Specification (Standard Methods for Determination of the Diffusible Hydrogen Content of Martensitic, Bainitic, and Ferritic Weld Metal Produced by Arc Welding) to allow for diffusible hydrogen testing over mercury. The welding electrode was an E71T-1 type, rutile-based ESAB Dual Shield II71 Ultra (0.052" diameter). These welding experiments involved no primer coatings.

Several test welds were made with the Fe powder,  $\text{Fe}_2\text{O}_3$ , and  $\text{SiO}_2$  mixed in various mole fractions to determine the optimal combinations to give satisfactory weldability. All the flux mixes were baked at 400°C overnight to remove all possible moisture. The  $\text{CO}_2$  shielding gas was doped with 4 volume percent hydrogen to ensure hydrogen pick-up. The fluxes were placed on the weld coupons prior to welding, as shown in Figure 5, which allowed for control of the flux thickness with a copper foil. The particular fixture used is described in the AWS A4.3 specification. The welding parameters used in these experiments were 25V, 230 ipm wire feed speed, and 14 ipm travel speed. The molar combination of the fluxes tested were ( $\text{Fe}_2\text{O}_3/\text{Fe}/\text{SiO}_2$ ): 0/1/3, 0.5/1/3, 1/1/3, 1.5/1/3, 2/1/3, and 0/1/4. Reference welds were also made with no fluxes, a 96/4  $\text{CO}_2/\text{H}_2$  gas mixture and 100%  $\text{CO}_2$  to give reference oxygen levels.

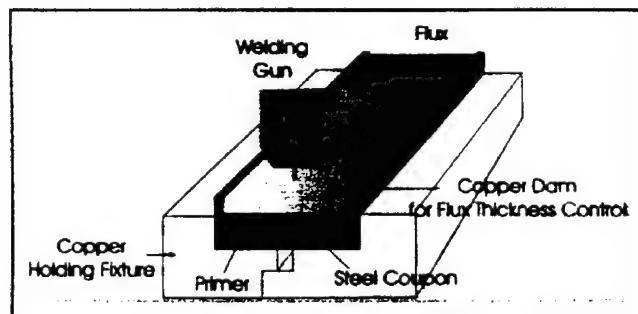


Figure 5. Schematic of Set-up Used for Welding Experiments.

The results of the diffusible hydrogen and interstitial analysis for oxygen, as seen in Figure 6, substantiated the chosen premise. The oxygen content of the reference weld, which was prepared using a commercial E71T-1 electrode and following typical industrial practice, procedure and parameters, was 586 ppm. The 4% hydrogen added to the shielding gas was effective in providing hydrogen to the weld pool. The weld made using 100%  $\text{CO}_2$  had a diffusible hydrogen value of 7.97 ml/100g, while the 96/4  $\text{CO}_2/\text{H}_2$  mixture gave a value of 18.3 ml/100g. When oxide fluxes were used, the lowest diffusible hydrogen value of 10.4 ml/100g was obtained with an oxygen value of 1055 ppm. It is clear to see that by adding high oxidizing potential

fluxes into the weld pool, the diffusible hydrogen content can be lowered.

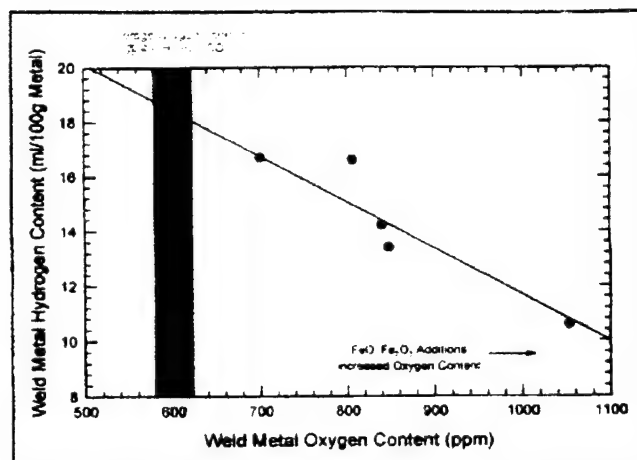


Figure 6. Weld Metal Diffusible Hydrogen Content Illustrating the Inverse Relationship of the Hydrogen-Oxygen Equilibrium.

## Oxidizing Potential of the Flux Additions

To determine the optimal flux oxidizing potential to be included in the experimental tubular wires for hydrogen control, flux mixtures of  $\text{CaCO}_3$ ,  $\text{SiO}_2$ ,  $\text{Fe}_2\text{O}_3$ , and FeO were examined. Since flux thickness and the type of primer used may also affect the oxidizing potential, their effects must also be determined. In this specific group of experiments, the weld coupons were coated using an inorganic, zinc-ethyl silicate primer (Interplate NQA238) to 0, 1.0 and 4.0 mils thickness. The thickness of the flux layers tested were 1/16, 1/8, and 1/4 inch. The flux thickness was controlled by cutting the copper strips used on the copper mold (Figure 5) to specific widths to accommodate the proper flux depth. Again, the commercial E71T-1 electrode was used with the 100%  $\text{CO}_2$  shielding gas, but at different welding parameters, 27V and 290 ipm WFS.

In terms of the individual flux ingredients,  $\text{CaCO}_3$  proved to be the flux addition that provided good welding performance, with oxygen levels around 550 ppm. It was followed by  $\text{SiO}_2$  with about 1000 ppm. Only  $\text{Fe}_2\text{O}_3$  appeared to increase the oxygen content with increasing primer thickness from 1000 to 1500 ppm. FeO appeared not to be greatly affected by the flux and primer thickness with an average weld metal oxygen content around 1800 ppm. Its weldability, however, was poor, and the slag was extremely viscous as indicated by very large pores within the thick slag.

Flux mixtures were also examined using the following combinations: 1)  $\text{FeO-SiO}_2$ ; 2)  $\text{Fe}_2\text{O}_3\text{-SiO}_2$ ; 3)  $\text{CaCO}_3\text{-SiO}_2$ ; 4)  $\text{CaCO}_3\text{-FeO-SiO}_2$ ; and 5)  $\text{CaCO}_3\text{-Fe}_2\text{O}_3\text{-SiO}_2$ . All the combinations welded well. The oxygen analysis provided the following results for each combination: 1) 1106 ppm; 2) 1143 ppm; 3) 593 ppm; 4) 719 ppm; and 5) 935 ppm. These results show that  $\text{CaCO}_3$  additions decrease oxygen content in the weld pool. The  $\text{CO}_2$  that comes from the dissociation of  $\text{CaCO}_3$  provided some shielding gas, but also limited the amount of oxygen in

the weld pool. CaO provided slag viscosity control and improved wetability. A schematic representation of the results can be seen in Figure 7, indicating that the best combination of weld metal oxygen content and weldability occurs with a combination of  $\text{CaCO}_3\text{-Fe}_2\text{O}_3\text{-SiO}_2$ .

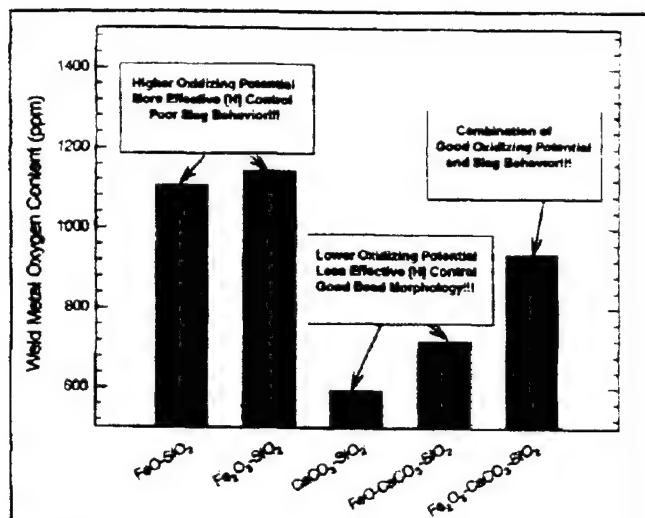


Figure 7. Effect of Flux Composition on Oxidizing Potential, Slag Behavior and Weld Bead Morphology Control.

Metallographic examination of the welds confirmed a well-established trend that increasing oxygen in the weld metal increases grain boundary ferrite and decreases acicular ferrite. There were also minor variations in the amount of FS phase.

### Effect of Primer Thickness

Several welds were made on samples with no primer, 1.25, 2.5, and 5.0 mils of the Interplate primer to determine the effect of primer thickness. One sample with 5.0 mils of the Interplate was placed in an oven at  $300^\circ\text{C}$  to determine what effect the heat of plate baking (required procedure for hydrogen testing) would have on primer stability and diffusible hydrogen. The results of the oxygen analysis showed that the primer had no substantial effect on the oxygen level of about 600 ppm, which is the value of the reference weld metal oxygen. The diffusible hydrogen results can be seen in Figure 8 for increases in primer thickness. It clearly shows that as the primer thickness increases, weld metal diffusible hydrogen also increases. At 5.0 mils primer thickness, the level of diffusible hydrogen produced increased by a factor of seven from a sample with no primer. The baking temperature did not affect the level of diffusible hydrogen produced very much.

It should be pointed out that the shipbuilding industry rarely uses a primer thickness greater than 1.0 mil. However, due to the lack of primer thickness control within the normal yard practices, minor variations in primer thickness can increase the diffusible hydrogen levels substantially. Several welds were also made using an organic,

epoxy-based primer (Valspar V13F40) at the thickness of 4.0 mils. Coupons with higher primer thicknesses were used to prepare a few additional welds. This type of primer did not produce the high levels of diffusible hydrogen that the Interplate did (Epoxy-based primer: 40 ml/100g and Ethyl-silicate based primer: 70 ml/100g). The organic-based primer also caused more spatter and fume generation with thicker primer layers. The results can also be seen in Figure 8.

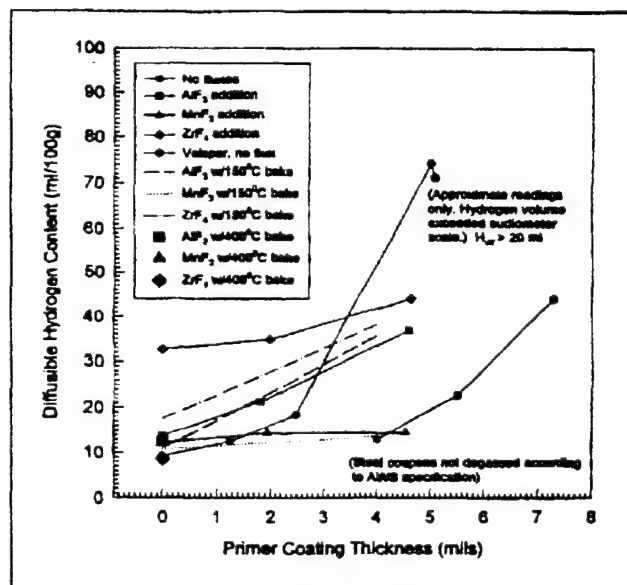


Figure 8. Effect of Primer Coating Thickness and Fluoride Additions on Diffusible Hydrogen Content.

### [H]-[F] Relationship Verification

The second major goal of this investigation was to prove that fluoride fluxes could also be added to a FCAW consumable to help minimize the amount of weld metal diffusible hydrogen.  $\text{AlF}_3$ ,  $\text{MnF}_3$  and  $\text{ZrF}_4$  were the three fluorides tested in this research. Test welds were made on available steel coupons coated with 0, 2.0 and 4.6 mils Interplate primer, and with 100%  $\text{CO}_2$  as shielding gas. The welds made with no primer exhibited good stability and very little spatter. As the primer thickness increased, spatter and fume generation increased significantly. The results of the diffusible hydrogen tests are also plotted in Figure 8.  $\text{MnF}_3$  was most effective in hydrogen control with diffusible hydrogen content around 13 ml/100g, which represented a four-fold reduction from samples with 4.0 mils of the Interplate primer.  $\text{AlF}_3$  was not as effective, especially for thicker primer layers. The diffusible hydrogen content was around 30 ml/100g for 4.0 mils primer layers. Of the three,  $\text{ZrF}_4$  was the least effective in controlling diffusible hydrogen, only able to reduce its content by about 50%. The fluorides in these first sets of welds were not baked due to health concerns and concerns about the stability of the fluorides.

Since most of the fluorides are known to be hygroscopic, it was decided to bake them at  $400^\circ\text{C}$  to remove any trapped moisture. Of the three fluorides,  $\text{ZrF}_4$  was the only one that showed hygroscopicity

as the diffusible hydrogen levels dropped by a factor of four from 32.7 ml/100g to only 8.6 ml/100g. The other two fluorides exhibited signs of breakdown at 400°C and, therefore, were not effective in hydrogen control after the baking experiments.

Thus, a baking schedule of 150°C for 1 hour was tested. The baked fluorides were once again welded over on samples with no primer and 4.0 mils of primer. The  $\text{AlF}_3$  produced 11.0 and 35.6 ml/100g, the  $\text{MnF}_3$  produced 10.6 and 13.8 ml/100g, and the  $\text{ZrF}_4$  produced 17.6 and 38.1 ml/100g. The lower baking temperature appeared to help to maintain the integrity of the  $\text{AlF}_3$  and  $\text{MnF}_3$ , while still producing lower amounts of diffusible hydrogen. The lower baking temperature did not appear to improve the effectiveness of the  $\text{ZrF}_4$  in controlling hydrogen. The diffusible hydrogen values produced by  $\text{MnF}_3$  appeared not to be affected by increases in the primer thickness, which would prove beneficial to fluctuations in primer coating thickness.

Metallographic examination of the samples welded with the fluorides revealed that there was substantial ferrite grain refinement weld metal oxygen. This aspect was not anticipated, but would be extremely beneficial to help control the increased grain size expected with increases in weld metal oxygen.

#### Experimental FCAW Formulation

The results from the flux combination and fluoride tests provided the basis for developing four experimental FCAW consumables for testing. Because the base weld produced an oxygen level around 600 ppm oxygen, and the fact that limiting the oxygen level was desired, it was decided to aim for two oxygen levels: 650 ppm and 750 ppm. To each of these flux combinations,  $\text{MnF}_3$  was added since it was the most tolerant of higher primer thickness without producing excessive hydrogen.

Electrode A, containing a flux combination with molar ratios of 0.5  $\text{CaCO}_3$ /3.0  $\text{SiO}_2$ /1.5  $\text{Fe}_2\text{O}_3$ , was designed to target the oxygen level of 650 ppm. Electrode B contained a flux combination with molar ratios of 0.5  $\text{CaCO}_3$ /1.0  $\text{SiO}_2$ /1.0  $\text{Fe}_2\text{O}_3$  to result in 750 ppm oxygen. To each of these two formulations, 0.5 moles of  $\text{MnF}_3$  was added to result in Electrodes C and D. The four electrodes were used to make multi-pass welds in both the flat and vertical positions. From each of the welds, all-weld-metal tensile specimens, transverse (reduced-section) tensile specimens, and Charpy V-notch specimens were machined and tested according to the AWS B4.0 Specification (Standard Methods for Mechanical Testing of Welds). Weld fillet break tests were also conducted according to the AWS B4.0 Specification. Bead-on-plate welds were made from which diffusible hydrogen testing, oxygen analysis and chemical analysis of the weld metal could be performed. The welds were made on samples with no primer, and 1.5 and 4.0 mils of both the Interplate and Valspar primers.

The results of the diffusible hydrogen and oxygen analysis can be seen in Figure 9. It should be noted that the diffusible hydrogen tests did not exactly conform to the AWS 4.3 Specification for cleanliness because the primer-coated specimens were not baked prior to welding. As such, the diffusible hydrogen levels might be higher than expected. The goal is to show a decreasing trend of diffusible hydrogen with increased oxygen and fluorine values. Despite the large scatter of the

data, Figure 9 shows an overall decreasing trend in diffusible hydrogen for increased oxygen values. Electrode C produced the lowest diffusible hydrogen value for the "no primer" welds at 9.23 ml/100g, followed by Electrode D, at 9.64 ml/100g. The lowest diffusible hydrogen values produced for the 1.5 mil and 4.0 mil Interplate coated samples were 10.87 and 15.77 ml/100g, respectively. For the 1.5 mil Valspar coated samples, it was 10.97 ml/100g. These were produced by Electrode D. Overall, Electrode D had an average diffusible hydrogen content of 13.33 ml/100g, followed by the commercial E71T-1 electrode, 14.95 ml/100g.

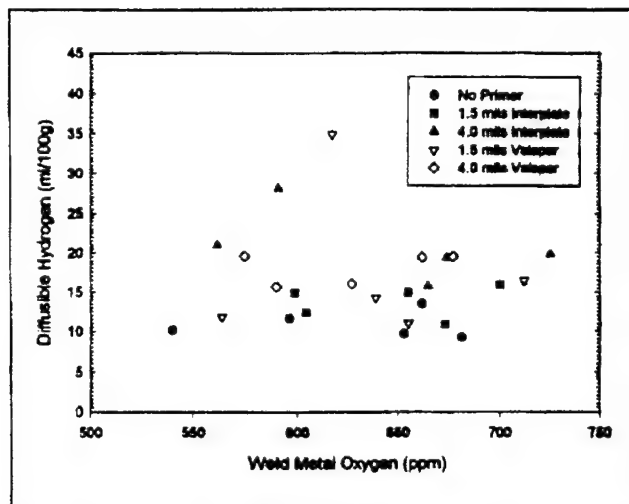


Figure 9. Weld Metal Diffusible Hydrogen Content as a Function of Weld Metal Oxygen Content and Primer Coating for the Experimental Flux-Cored Arc Welding Consumables.

When  $\text{MnF}_3$  was added, the oxygen levels increased by about 70 ppm. This observation was not expected since the total percentage of oxidizing components added in the flux additions actually dropped. However, after examining the free energy of formation ( $\Delta G_f^\circ$ ) data for the formation of  $\text{H}_2\text{O}_{(g)}$  and  $\text{HF}_{(g)}$ , it was found that  $\text{HF}_{(g)}$  is more likely to form than  $\text{H}_2\text{O}_{(g)}$ . With the formation of  $\text{HF}_{(g)}$ , oxygen is freed up to form inclusions, which in turn increases the weld metal oxygen level.

The results of the mechanical test can be seen in Table 1, along with the acceptance criteria based on AWS A5.20 (Specification for Carbon Steel Electrodes for FCAW) and Mil-E-24403/1D (Electrodes - Welding, Flux-Cored, Ordinary Strength and Low Alloy) Specifications. For the all-weld-metal samples in the flat position, only the samples from the commercial E71T-1 electrode, Electrode B and Electrode D passed both standards. The best performing electrode was Electrode D with 66.3 ksi YS, 71.7 ksi UTS and 29.4% elongation. For samples welded in the vertical position, only the commercial electrode, Electrode A and Electrode D passed according to the specifications. Electrode A performed the best (65.2 ksi YS, 72.2 ksi UTS, 28.9% elongation) followed closely by Electrode D (61.6 ksi YS, 70.3 ksi UTS, 29.5% elongation).

Properties	E71T-1	E71T-1	"A"	"A"	"C"	"C"	"B"	"B"	"D"	"D"	Acceptance Standards	
	AVMM	TT	AVMM	TT	AVMM	TT	AVMM	TT	AVMM	TT	AWS A5.20	MIL-E-24403/1D
Yield Strength (ksi; flat)	68.3	61.6	42.7	57.1	62.6	57.2	64.7	59.4	66.3	59.8	58	60 AW / 55 SR
Yield Strength (ksi; vertical)	70.4	57.1	65.2	52.4	58.8	51.8	60.4	58.3	61.6	59.1	58	60 AW / 55 SR
Ultimate Tensile Strength (ksi; flat)	73.8	77	49	70.7	67.6	74.5	70	76.2	71.7	76.2	70	70
Ultimate Tensile Strength (ksi; vertical)	77.6	80.6	72.2	76.5	66.2	73.5	67.1	74.4	70.3	76	70	70
Elongation (%; flat)	32.7	31	31.3	27.5	32.8	28	31.9	27.5	29.4	28	22	22
Elongation (%; vertical)	32.7	32	28.9	26.5	34.2	30	33	29	29.5	29.5	22	22
Reduction of Area (%; flat)	74.7	62.2	73.5	58.4	72.6	58.9	73.2	56.9	71.8	57.9	***	***
Reduction of Area (%; vertical)	70.9	61.5	71.7	55	71.9	61.1	71.4	57.5	70.2	59	***	***
Charpy V-Notch (ft-lbs; flat)												
*@ 20°C (68°F)	135.5	***	94	***	108	***	128	***	137	***	***	***
*@ 0°C (32°F)	108	***	71	***	83.5	***	97	***	64.5	***	***	30
*@ -20°C (-4°F)	68	***	52.5	***	37	***	32	***	36	***	20	20
*@ -40°C (-40°F)	15	***	30	***	8	***	7	***	17	***	***	***
Charpy V-Notch (ft-lbs; vertical)												
*@ 20°C (68°F)	137.5	***	60.5	***	133.5	***	144	***	152.5	***	***	***
*@ 0°C (32°F)	101	***	60.5	***	110.5	***	125	***	132.5	***	***	30
*@ -20°C (-4°F)	14.5	***	27.5	***	73.5	***	107.6	***	52	***	20	20
*@ -40°C (-40°F)	6.5	***	8	***	22	***	17.8	***	10	***	***	***

Table 1. Results from the Mechanical Testing Performed on the Experimental and Commercial E71T-1 FCAW Electrodes.

All of the electrodes passed the requirements set forth in the specifications for Charpy V-notch specimens at -20°C of 20 ft-lbs. It is interesting to note that all of the electrodes performed better in the vertical position compared to the flat position for the CVN impact toughness tests. Welding in the vertical-up position seemed to allow more time for inclusions to float upward as the weld pool proceeded, which keeps them from being trapped in the solidifying weld pool. The cleaner weld metal would result in higher energy absorbed. The highest energy absorbed was 152.5 ft-lbs at 20°C for Electrode D in the vertical position. At the -20°C temperature set forth in the standards, the highest energy absorbed for the vertical position was by Electrode B (107.6 ft-lbs), followed by Electrode C (73.5 ft-lbs) and Electrode D (52.0 ft-lbs). For the flat position, the highest energies were produced by the commercial electrode (68.0 ft-lbs) and Electrode A (52.5 ft-lbs). Based on CVN energy alone, it is difficult to determine which electrode performed best due to differences from the flat and vertical positions. However, since all exceeded the requirements, any one could be chosen.

The results of the fillet break tests showed that Electrode D performed the best, even at higher primer thicknesses. On samples with 1.5 mils of the Valspar primer, there were no worm tracks or pinholes visible on the weld surface. The samples with 1.5 mils of the Interplate primer had only one pinhole formed in the fillet weld. The 4.0 mil samples had randomly dispersed pinholes and some worm tracks visible, but not as many as in welds made with the other electrodes.

Metallographic examination of the welds indicated that the electrodes with the MnF<sub>3</sub> additions show ferrite grain size refinement, as was indicated earlier from the fluoride/weld experiments. Micrographs can be seen in Figure 10 comparing the weld made with Electrode D with the weld prepared using the commercial E71T-1 electrode. These micrographs show that Electrode D produced a weld with finer grain boundary ferrite and acicular ferrite grains than the commercial

electrode. It can be stated that along with helping to lower diffusible hydrogen content, the MnF<sub>3</sub> also helps to refine the microstructure.

## Conclusions

Several conclusions can be made based upon this research. First, the hydrogen-oxygen equilibrium holds true in weldments despite the faster heating and cooling rates than expected in equilibrium conditions. Adding high oxidizing potential fluxes to a FCAW consumable will help to lower the amount of diffusible hydrogen produced in the weld metal. Fluoride additions to the flux will further lower the diffusible hydrogen, especially at higher primer thickness, and also help to refine the weld metal microstructure. A combination of oxide and fluoride additions seems to produce the most effective hydrogen removal and optimal weld metal mechanical properties.

## Acknowledgments

The authors would like to acknowledge the support of Mr. Tim Warren and Mr. Lee Kvidahl of Ingalls Shipbuilding, Mr. Russ McClellan formerly of Ingalls Shipbuilding, Mr. Stan Ferree of ESAB Welding and Cutting Products, Mr. Ed Bohnart and Mr. Don Brooks of Miller Electric Manufacturing, and the financial support of the National Shipbuilding Research Program, SP-7 Group.





Commercial E71T-1 Wire



Electrode D

Figure 10. Photomicrographs of Weld Metal Produced Using a Commercial E71T-1 Wire and Electrode D (Magnification 200X).

## References

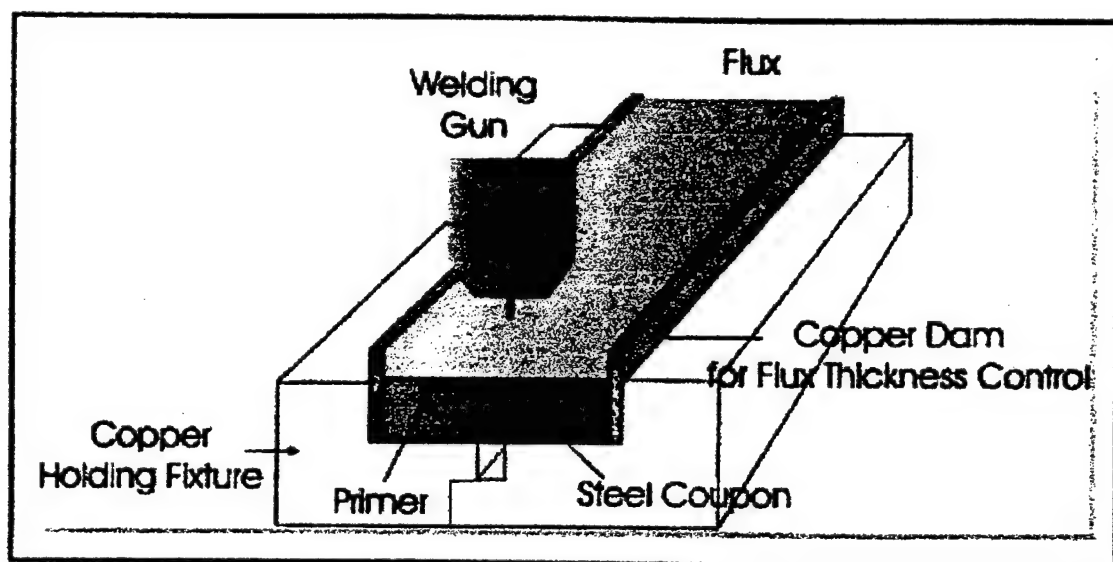
1. Suga, T., Nagakoa, S., Nakano, T. and Suenaga, K., 1996, IIW DOC.XII-1456-96, pg. 275-293.
2. Marriot, A.R., 1994, The Chemistry and Physics of Coatings, The Royal Society of Chemistry.
3. Systems & Specifications, Steel Structures Painting Manual, Volume 2, 7<sup>th</sup> Edition, 1982.
4. Corrosion, Volume 13, ASM Handbook, 9<sup>th</sup> Edition, 1987.
5. Ramsay, C.W., 1989, The Influence of Oxygen and Non-Metallic Inclusions on High-Strength Steel Weld Metal Microstructures and Properties, Colorado School of Mines Thesis Number T-3391.
6. Gaskell, D.R., 1981, Introduction to Metallurgical Thermodynamics, New York: McGraw-Hill, 2<sup>nd</sup> Edition, pg. 287.
7. Sorokin, L.I. and Sidlin, Z.A., Svar. Proizvod., No. 11, 1974, pg. 7-9.
8. Terashima, H. and Tsuboi, J., Metal Construction, Volume 14, 1982, pg. 648-654.
9. Olson, D.L., Liu, S., Frost, R.H., Edwards, G.R. and Fleming, D.A., 1993, Welding, Brazing and Soldering, Vol. 6, ASM Handbook, 9<sup>th</sup> Edition, pg. 55-63.
10. Lancaster, J.F., 1987, Metallurgy of Welding, Allen & Unwin Ltd., 4<sup>th</sup> Edition.
11. Easterling, K., 1992, Introduction to the Physical Metallurgy of Welding, Butterworth-Heinemann Ltd., 2<sup>nd</sup> Edition.
12. Ravi Vishnu, P., 1993, Welding, Brazing and Soldering, Vol. 6, ASM Handbook, 9<sup>th</sup> Edition, pg. 70-87.
13. Pope, A.M., 1995, Oxygen and Hydrogen Control in Shielded Metal Underwater Wet Welding, Colorado School of Mines Thesis Number T-4720.
14. Medeiros, R.C., 1997, Effect of Oxidizing Electrodes and Polarity on Hydrogen Mitigation in Underwater Wet Welding, Colorado School of Mines Thesis Number T-5013.

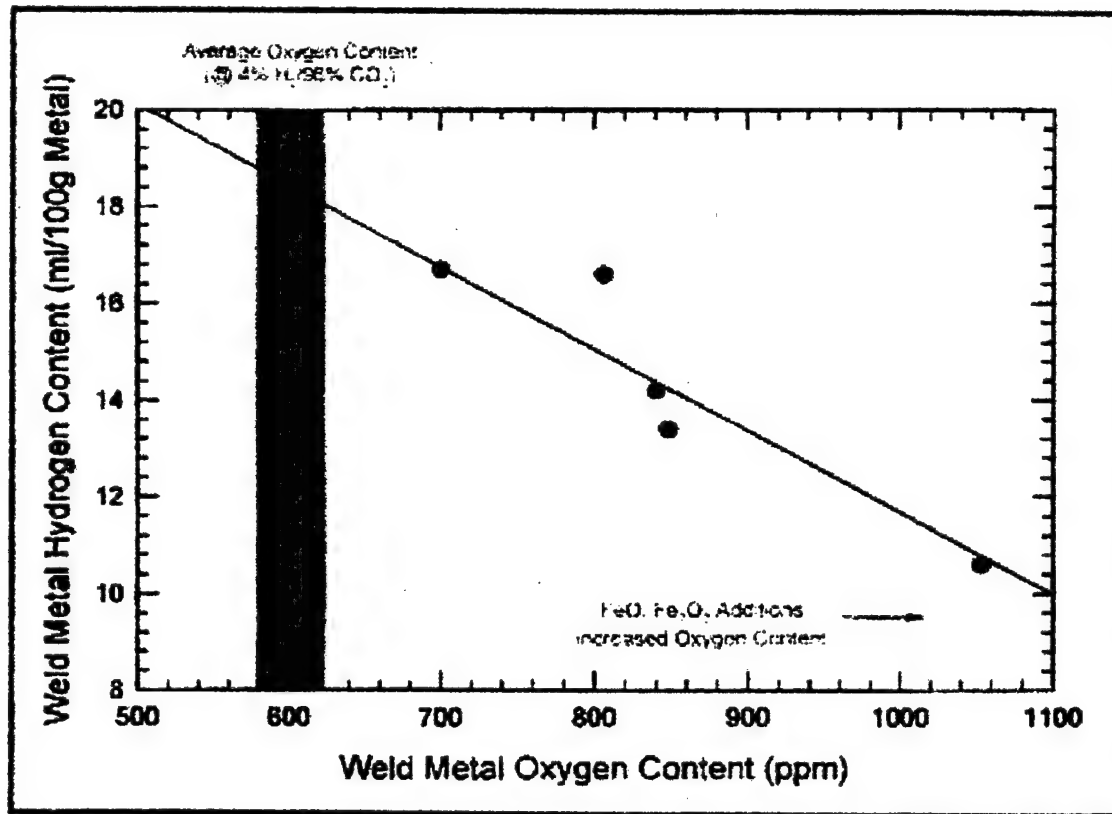


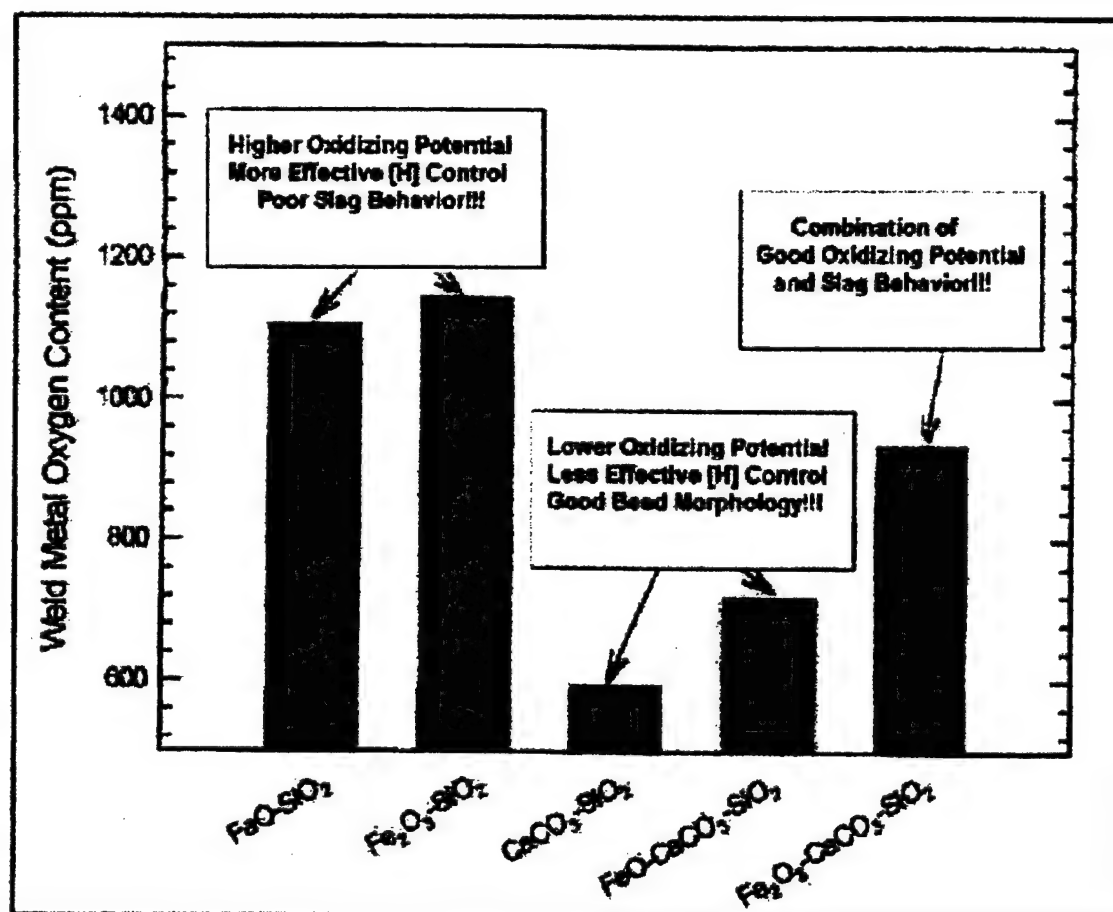
**Commercial E71T-1 Wire**











calculation, the  $P_{HF}^2/P_F$  ratio was shown to be useful in estimating the relative effect of the fluorides on diffusible hydrogen control.

**B. Effect of Slag Chemistry on Hydrogen Pickup in Underwater Wet Welds,**  
*by R. C. Medeiros and S. Liu, Colorado School of Mines*

Weld metal hydrogen pickup in underwater wet welding is severe due to the presence and dissociation of water vapor surrounding the welding arc. This undesirable behavior can be minimized, however, with the use of oxidizing-type electrodes. The aim of this investigation has been placed on the thorough understanding of hydrogen pickup by the slag on weld metal diffusible hydrogen. To accomplish this purpose, twenty experimental oxidizing electrodes with systematic ferric oxide ( $Fe_2O_3$ ) additions, ranging from 0 to 70 wt. pct., to the flux system were investigated. The mole fraction ratio of  $CaO/SiO_2$  in the flux ranged from 0.05 to 0.35, independently of ferric oxide additions. Underwater gravity welds were deposited on ASTM A36 steel coupons at 0.27 m (city) water depth using a gravity feed system and similar welding parameters. Weld metal diffusible hydrogen content was determined using the mercury displacement method according to current AWS standard. To correlate weld metal hydrogen content with slag chemistry, the slag hydrogen contents were also determined.

The measured diffusible hydrogen contents showed that  $Fe_2O_3$  was effective in reducing weld metal hydrogen content. Higher hydrogen values were always related to lower ferric oxide contents initially present in the flux, for example, 70.8 ml/100g of deposited metal (DCEP - 0 wt. pct.  $Fe_2O_3$ ) and 30.5 ml/100g of deposited metal (DCEP - 36 wt. pct.  $Fe_2O_3$ ). Amazingly, diffusible hydrogen as low as 13.2 ml/100g was obtained with the B3 electrode (53 wt. pct. of  $Fe_2O_3$  and  $CaO:SiO_2$  equal to 0.15). X-ray diffraction analysis (XRD) conducted on different slags showed that the minimum diffusible hydrogen values were always associated with the presence of fayalite ( $2FeO \cdot SiO_2$ ). Complementing XRD analysis, Mössbauer spectroscopy tests carried out on different slags showed that all ferric ( $Fe^{+3}$ ) oxide initially present in the slag had transformed to ferrous ( $Fe^{+2}$ ) oxide ( $FeO$ ), free or combined.

Chemical analyses showed that weld metal hydrogen pickup was strongly dependent on the water solubility in slags. The total hydrogen content in the weld metal increases monotonically with increasing slag hydrogen content. However, a slag that has high water solubility will, in general, retain more hydrogen in the slag resulting in lower diffusible hydrogen in the weld metal.

Finally, variations in weld metal hydrogen as well as slag hydrogen content with both polarity mode and iron oxide content in the slag were successfully predicted using an electrochemical model for the slag/metal interface equilibrium. In this investigation, the slag/metal interface has been identified as responsible in controlling the hydrogen pickup. The model assumed that hydrogen is present in the slag as  $(OH)$  ions and that  $FeO$  displays ideal solution behavior.

## A PREDICTIVE ELECTROCHEMICAL MODEL FOR WELD METAL HYDROGEN PICKUP IN UNDERWATER WET WELDS

Raimundo C. de Medeiros

Brazilian Foundation of Welding Technology  
Rio de Janeiro, RJ  
Brazil

Stephen Liu

Center for Welding, Joining and Coatings Research  
Colorado School of Mines  
Golden, Colorado

### ABSTRACT

Weld metal hydrogen pickup in underwater wet welding is severe due to the presence and dissociation of water surrounding the welding arc. This undesirable behavior can be minimized, however, with the use of oxidizing-type electrodes. The purpose of this investigation has been placed on the fundamental understanding of the effect of hydrogen pickup by the slag on the weld metal diffusible hydrogen content in direct current, shielded metal arc welding (SMAW) for both electrode-positive polarity (DCEP) and electrode-negative polarity (DCEN). To accomplish this purpose, twenty experimental oxidizing electrodes containing systematic ferric oxide ( $\text{Fe}_2\text{O}_3$ ) additions, ranging from 0 to 70 wt. pct., to the flux coating were investigated. The mole fraction ratio of  $\text{CaO}/\text{SiO}_2$  in the fluxes ranged from 0.05 to 0.35, independent of the ferric oxide additions. Underwater, bead-on-plate welds were deposited on ASTM A36 steel coupons at 0.27 m (city) water depth using a gravity feed system. Welding parameters were held constant throughout the experiments. Weld metal diffusible hydrogen content was determined using the mercury displacement method according to current AWS standard. To correlate weld metal hydrogen content with slag chemistry, the slag hydrogen contents were also determined.

The measured diffusible hydrogen contents showed that  $\text{Fe}_2\text{O}_3$  was effective in reducing weld metal hydrogen content. Higher hydrogen values were always related to lower  $\text{Fe}_2\text{O}_3$  contents initially present in the flux, for instance, 71 ml/100g (DCEP - 0 wt. pct.  $\text{Fe}_2\text{O}_3$ ) as compared to 31 ml/100g (DCEP - 36 wt. pct.  $\text{Fe}_2\text{O}_3$ ). Amazingly, diffusible hydrogen as low as 13 ml/100g was obtained with the use of DCEN polarity along with 53 wt. pct.  $\text{Fe}_2\text{O}_3$  in the flux coating. X-ray diffraction (XRD) conducted on different slags showed that the lower diffusible hydrogen values were always associated with the presence of fayalite ( $2\text{FeO} \cdot \text{SiO}_2$ ). Complementing XRD analysis,

Mössbauer spectroscopy analyses carried out on different slags showed that all ferric ( $\text{Fe}^{3+}$ ) oxide initially present in the slags had transformed to ferrous oxide ( $\text{FeO}$ ), free or combined. Chemical analyses showed that weld metal hydrogen pickup was strongly dependent on the solubility of water in the slag systems. The total and diffusible hydrogen content in the weld metal increased monotonically with increasing slag hydrogen content.

Finally, variations in weld metal hydrogen as well as slag hydrogen content with both polarity and iron oxide content in the slag were successfully predicted using an electrochemical model that describes the slag/metal interface equilibrium. In this investigation, the slag/metal interface has been identified as responsible in controlling the weld metal hydrogen pickup. The model assumed that hydrogen was present in the slag as  $(\text{OH})^-$  ions and that  $\text{FeO}$  displayed ideal solution behavior.

### INTRODUCTION

Assessment of materials performance in engineering design and manufacturing is a complex process that requires significant knowledge of scientific and engineering principles. An important part of this effort has been dedicated to the aspects of hydrogen mitigation in underwater wet welding (UWW). Hydrogen present as an interstitial impurity has been known for many years to be a factor in delayed cracking of welded joints (Ittrante and Stout, 1964). Weld metal hydrogen pickup in UWW is unavoidable due to the dissociation of water vapor surrounding the welding arc. In conjunction with the fast quenching nature of the water environment, the high hydrogen content in the weldment leads to hydrogen cracking in the heat-affected zone (HAZ).

In a broad consensus, it has been recognized that hydrogen-induced cracking in the HAZ or in the weld metal can be avoided if at least one of its four controlling factors: critical

concentration of diffusible hydrogen, stress intensity of sufficient magnitude, a susceptible microstructure and temperature lower than 200°C, as set for by Easterling (1992), can be minimized. Intuitively, it is quite obvious that these conditions are easily fulfilled in UWW. Thus, weld metal hydrogen pickup in wet welds is expected, leading to increased hydrogen levels in the weld metal and enhanced cracking susceptibility.

In the interest of increased quality and process economics, SMAW has become more common in UWW. In recent years, programs of stick electrode coating development based on the unique behavior of oxidizing-type electrodes on hydrogen mitigation in underwater wet welds, as identified by Stalker (1977), Nóbrega (1981) and Gooch (1983a), have produced new generations of covered electrodes, as reported by Pope et al (1995) and Medeiros (1997), for UWW.

An important characteristic that distinguishes the chemistry in arc welding from the chemistry in steelmaking is that arc welding processes involve low surface areas, direct current and high current densities, while steelmaking practices involve alternating current, high surface areas and low current densities. Under these circumstances it is strongly expected that electrochemical reactions occurring at the slag-environment and slag-metal interfaces will exert a significant influence over the final chemical composition of the weld. An electrochemical approach was used by Forno et al (1971) to explain how the behavior of hydrogen pickup by remelted iron ingots was affected by the mode of current supply - AC, DCEP, and DCEN. Frost, Olson and Edwards (1983), Blander and Olson (1986) and Kim and co-workers (1990), postulated that electrochemical reactions were as important as thermochemical reactions in governing the weld pool chemistry in DC processes. Also, work by Pope, Medeiros and Liu (1995) assessing the solidification mode of UWW, showed that UWW welds solidified at a slower rate than the welds deposited in air. This result indicates that back thermochemical reactions in a slower solidifying weld pool is maximized for UWW, and any deviation in composition can be attributed to electrochemical reactions.

Based on literature that are currently available, no reported experiments could explain satisfactorily the interaction between slag and weld metal hydrogen content. Thus, this program was carried out to examine the effects of slag composition as well as welding current and polarity on hydrogen pickup in underwater wet welds deposited by SMAW.

Quality of underwater wet welds is greatly affected by depth of welding and this can be related to the fact that the arc works inside a steam bubble (Tsai and Masubuchi, 1979). At the high temperatures attained by the arc water vapor decomposes into gaseous oxygen and hydrogen. As pressure increases with the depth of welding the partial pressures of these gases also increase. As a consequence more oxygen and hydrogen are absorbed by the liquid pool. Hydrogen absorption is responsible for porosity (Ando and Asahina, 1983; Suga and Hasui, 1986) while oxygen absorption accounts for the loss of alloying elements (Ibarra, Grubbs, and Olson, 1987) and oxygen (oxide inclusion) pickup (Kuwana and Sato, 1986; Pope, Liu and Olson, 1994). All these phenomena influence weld microstructure that

controls mechanical properties. The objective of this research was to evaluate the changes on weld metal microstructure as a function of depth of welding and how mechanical properties, specifically tensile strength and impact resistance, are affected. The main microstructural features analyzed in this work were porosity, inclusions and amount of weld metal heat affected zone.

## EXPERIMENTAL PROCEDURES

### Materials

Twenty experimental oxidizing electrodes with 3.2 mm diameter and containing systematic ferric oxide ( $\text{Fe}_2\text{O}_3$ ) additions, ranging from 0 to 70 wt. pct., to the flux system were investigated. The mole fraction ratio of  $\text{CaO}/\text{SiO}_2$  in the flux ranged from 0.05 to 0.35, independent of the ferric oxide additions. To avoid any potential secondary effects all other flux ingredients were maintained constant. Figure 1 shows a  $\text{Fe}_2\text{O}_3$ - $\text{CaCO}_3$ - $\text{SiO}_2$  ternary diagram with the compositions of the four series of experimental fluxes, Electrode series A, B, C, and D. All electrodes were waterproofed by the application of three layers of vinyl paint. A 12.7 mm thick ASTM A-36 grade steel plate was used in this research.

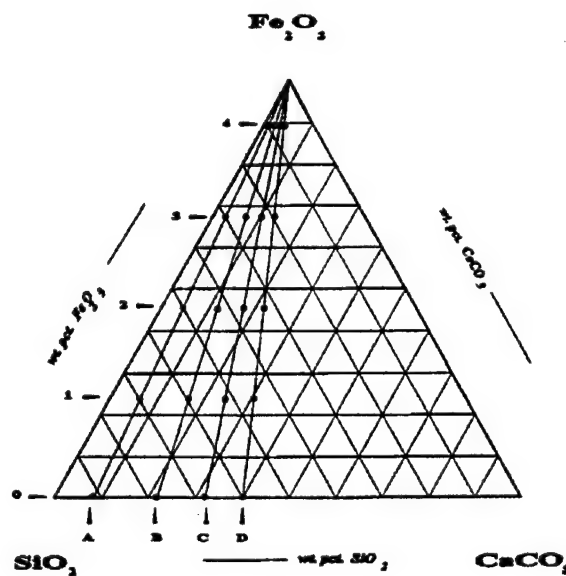


Figure 1. The  $\text{Fe}_2\text{O}_3$  -  $\text{SiO}_2$  -  $\text{CaCO}_3$  hypothetical ternary diagram of flux systems A, B, C, and D showing the compositions of the twenty experimental fluxes from this system.

### Welding Procedure

Direct current, electrode positive (DCEP) and electrode negative (DCEN), single pass bead-on-plate welds were laid

down using a gravity feed unit, as displayed in Figure 2. A typical lead angle of  $60^\circ$  was used throughout the experiments. The welding were done using 125 amperes, 30 to 36 volts and an average travel speed of 3.9 mm/s, under 0.27 m of city water.

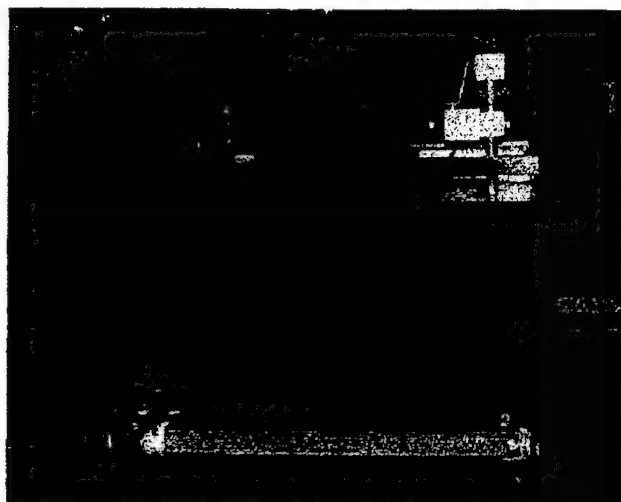


Figure 2. Photograph showing the gravity feeding unit before welding.

#### **Hydrogen Determination**

Weld metal diffusible hydrogen content was assessed for each experimental flux covering using the standard AWS A4.3-93 method. This method received a slight modification to accommodate the higher amount of diffusible hydrogen released during testing. The coupon length was reduced from 80 mm to 30 mm. The weld metal residual hydrogen content was determined in a LECO analyzer equipment.

Analyses of the slags for hydrogen content were carried out on three slag samples collected from the A-series electrodes used in both DCEP and DCEN polarity. Prior to hydrogen determination the slag samples were dried at  $150^\circ\text{C}$  for about 48 hours to remove any physically adsorbed moisture. Subsequently, slag samples weighing 0.4 to 1.0 grams, depending on the expected water content, were crushed down to 325# ( $< 44 \mu\text{m}$  particle size). Then, each slag sample was blended with aluminum powder of 99.9 wt. pct. purity. Aluminum was the selected oxygen-scavenger because it is unstable in the presence of water. After water removal, the powdered samples were carefully vacuum encapsulated in a fused silica tube and baked at  $850^\circ\text{C}$  for approximately 3 hours. The quartz tube was then transferred into a leak-proof aluminum vessel, which was then shook vigorously to break the quartz tube releasing the "unknown" gas mixture. Gas samples of volume equal to 1.0 ml were collected with an analytical syringe and injected into a column of a Perkins Elmer Auto System XL gas chromatography analyzer equipment for hydrogen determination.

#### **X-Ray Diffraction and Mössbauer Spectroscopy Determination**

Slag samples collected from multipass, bead-on-plate welds carried out with the A-series electrodes using DCEN polarity were qualitatively evaluated by x-ray diffraction on a Rigaku rotating anode diffractometer with  $\text{Cu-K}_\alpha$  radiation of 1.54 Å wavelength. Slags samples preparation followed conventional practice.

To evaluate the degree of  $\text{Fe}_2\text{O}_3$  decomposition into FeO in UWW, Mössbauer spectroscopy analyses were performed to characterize the different slags generated with the A-series electrodes, using both polarity modes. Slag samples preparation was similar to those used in x-ray analysis.

### **RESULTS AND DISCUSSION**

#### **Weld Metal Hydrogen Content**

To evaluate the influence of electrochemical reactions on weld metal hydrogen pickup, the hydrogen contents of the welds were first determined. Figure 3 displays graphically the effect of hematite ( $\text{Fe}_2\text{O}_3$ ) additions in electrode coating on weld metal diffusible hydrogen content. The same plot also contains typical values of diffusible hydrogen obtained with commercial rutile grade E6013 electrodes (Pope, 1995) under similar conditions used in this investigation. It is important, however, to first clarify the effect of  $\text{CaCO}_3$  addition before that of  $\text{Fe}_2\text{O}_3$ . Adding approximately 15 wt. pct. of  $\text{CaCO}_3$  to the coating was enough to cause a sharp decrease in the weld metal diffusible hydrogen from 100 ml/100g (E6013 electrodes containing typically 15 wt. pct. of  $\text{CaCO}_3$ ) to a value close to 37 ml/100g (D0 electrodes containing 32 wt. pct. of  $\text{CaCO}_3$ ). This result agreed well with the observations made by Sanchez-Osio, Liu and Olson (1993) and can be attributed to the thermal decomposition of  $\text{CaCO}_3$  with further releasing of various gaseous species able to decrease water vapor partial pressure in the welding arc. An important consequence of the hematite additions was the further decrease in weld metal diffusible hydrogen that resulted. As seen in Figure 3, as the amount of hematite in the electrode coverings increased from 0 to 53 wt. pct., the weld metal hydrogen contents decreased from 50 to 13 ml/100g. In particular, the welds made using the B-series electrodes exhibited the lowest diffusible hydrogen contents of the four electrode series.

The most striking feature in Figure 3, nevertheless, was a sudden inversion on the continuously decreasing diffusible hydrogen content as a result of increasing hematite additions in the coating. Such change in behavior occurred at approximately 53 wt. pct. of hematite. Weld metal diffusible hydrogen increased with furthering hematite addition beyond this value. At a first glance, these results might be interpreted as probable mistakes made during the experiments once an inverse relationship between hydrogen and oxygen should be obtained. To explain the opposite trend of weld metal diffusible hydrogen content at hematite additions greater than 53 wt. pct., slag hydrogen contents were considered. This behavior will be discussed later in the section on phenomenological modeling.



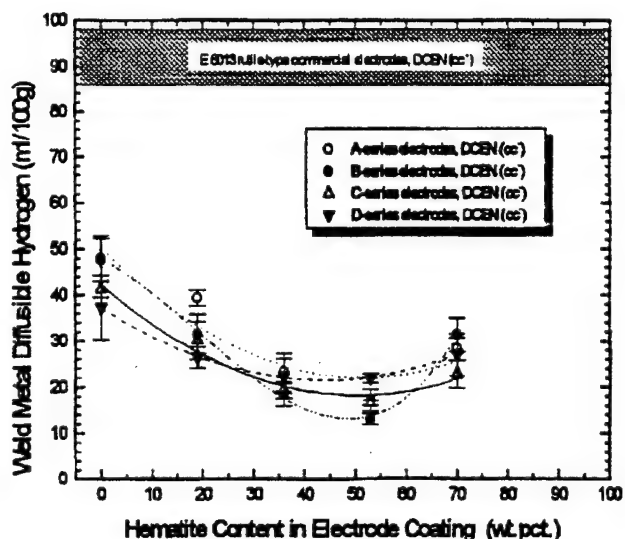


Figure 3. Weld metal diffusible hydrogen dependency on hematite-additions to the electrode coating in underwater wet welding. Mole fraction ratio equals to 0.05, 0.15, 0.25, and 0.35 for A, B, C, and D-series electrodes, respectively.

The influence of polarity (electrochemical effect) on weld metal diffusible hydrogen content was examined for A-series electrodes. The data in Figure 4 show astonishingly similar results as those seen in Figure 3.

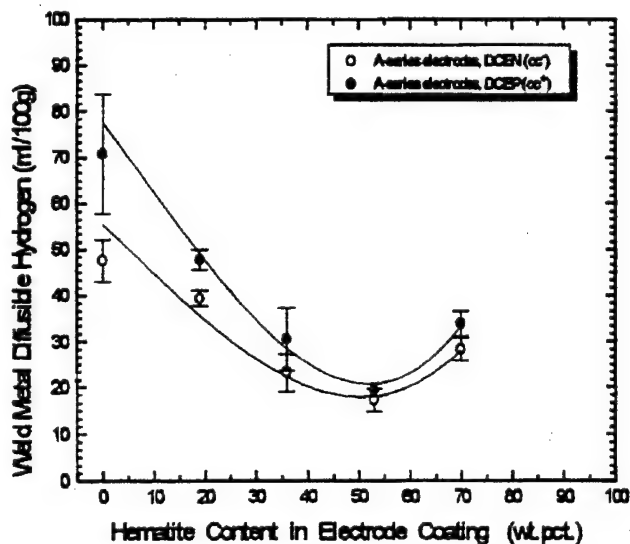


Figure 4. Polarity effect on weld metal diffusible hydrogen for A-series electrodes. Mole fraction ratio  $\text{CaO}:\text{SiO}_2$  equals to 0.05 for A-series electrodes.

The curve associated with DCEP ( $\text{cc}^+$ ) polarity not only presented the same trend as that obtained in DCEN ( $\text{cc}^-$ ); it also shifted to higher values of diffusible hydrogen. This finding, along with the previous discussion, emphasizes the clear importance of water solubility in slags associated with electrochemical half-cell reactions occurring at the electrode tip and at the weld pool surface in controlling weld metal hydrogen pickup.

#### Slag Hydrogen Content

The effect of hematite additions in electrode coating on hydrogen content in slags is graphically represented in Figure 5. Notice that a very good correlation was obtained for all slags. Comparing the results shown in Figure 5 with those displayed in Figure 3, it can be anticipated that the water solubility in slags did affect the weld metal hydrogen pickup.

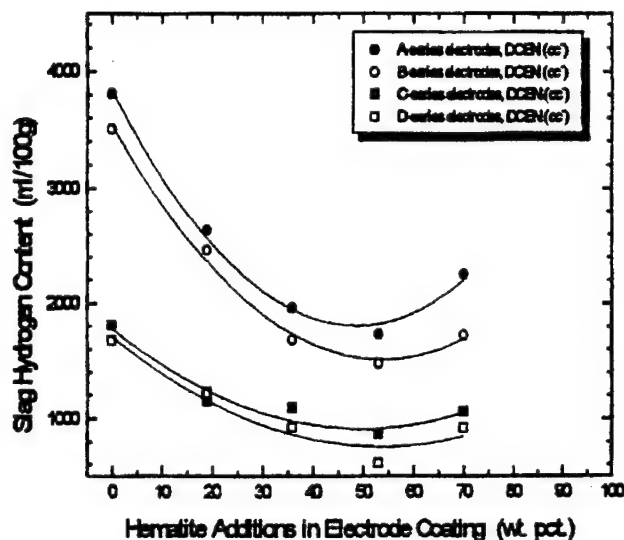


Figure 5. Effect of hematite addition in electrode coating on hydrogen content in slag. Slags generated with A, B, C, and D-series electrodes, presenting mole fraction ratio  $\text{CaO}:\text{SiO}_2$  equals to 0.05, 0.15, 0.25, and 0.35, respectively.

To verify whether polarity influenced slag hydrogen content, the relationship between the amount of hematite added to the electrode coating and slag hydrogen content was plotted for A-series electrodes welded in DCEP ( $\text{cc}^+$ ) and in DCEN ( $\text{cc}^-$ ). As shown in Figure 6, higher slag hydrogen content was always associated with the use of the electrode connected as the positive pole, ( $\text{cc}^+$ ). Moreover, both curves displayed similar inversion in hydrogen content at 53 wt. pct. of hematite. However, the comparison of the results shown in Figure 6 with those obtained for weld metal diffusible hydrogen, Figure 4, indicates an

abnormal behavior, i.e., higher weld metal diffusible (or total) hydrogen content is now associated with lower hydrogen content in slags, and vice-versa.

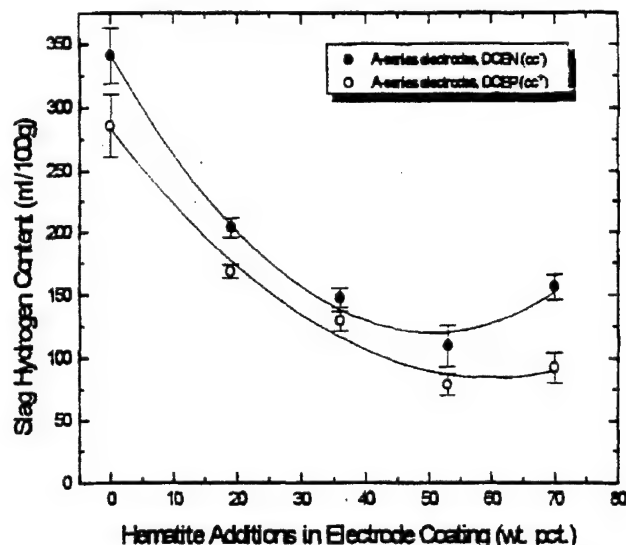


Figure 6. Effect of polarity mode on slag hydrogen content for increasing amount of hematite additions in electrode coating. Mole fraction ratio  $\text{CaO}:\text{SiO}_2$  equals to 0.05 for A-series electrodes.

Nevertheless, this unusual behavior is attributed to the electrochemical reactions taking place at the cathode and anode. Thus, it was crucial to establish a link between total weld metal hydrogen content and slag hydrogen content, for both polarities, as shown in Figure 7. It can be seen that total (or diffusible) weld metal hydrogen content increases monotonically with increasing slag hydrogen content, independent of the polarity, i.e., DCEN ( $\text{cc}^-$ ) or DCEP ( $\text{cc}^+$ ). Unquestionably, these results imply that the ability of the molten slag layer, surrounding the pendant droplet, in acting as a moisture sink during underwater wet welding is important and any factor which promotes moisture retention by the slag layer will enhance future hydrogen cracking problems.

#### Slag Characterization

X-ray diffraction analysis was carried out on slags collected from the welds made with A-series electrodes connected to the negative pole - DCEN ( $\text{cc}^-$ ). The diffraction pattern of these slags are presented in Figure 8. Notice the remarkable increase in crystallinity with increasing hematite additions in the coating, ranging from 0 wt. pct of  $\text{Fe}_2\text{O}_3$  (A0) to 70 wt. pct of  $\text{Fe}_2\text{O}_3$  (A4). It can also be seen that wüstite phase ( $\text{FeO}$ ) started appearing at 53 wt. pct. of  $\text{Fe}_2\text{O}_3$  (A3). It is worthy of mentioning that fayalite ( $2\text{FeO}.\text{SiO}_2$ ) was only found in the slag A3.

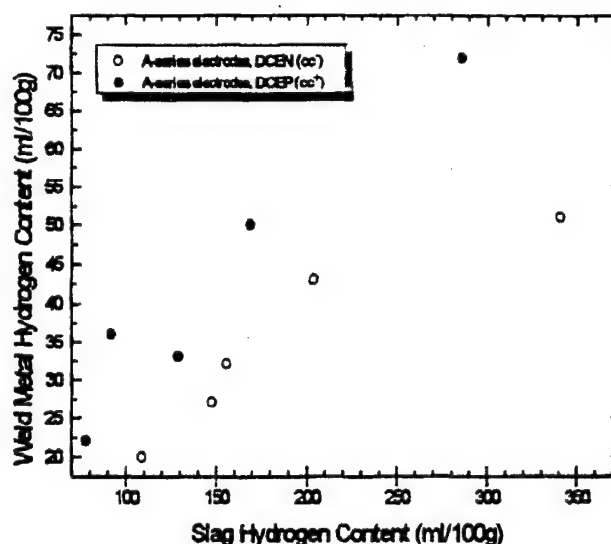


Figure 7. Total weld metal hydrogen content as a function of slag hydrogen content. Mole fraction ratio  $\text{CaO}:\text{SiO}_2$  equals to 0.05 for A-series electrodes.

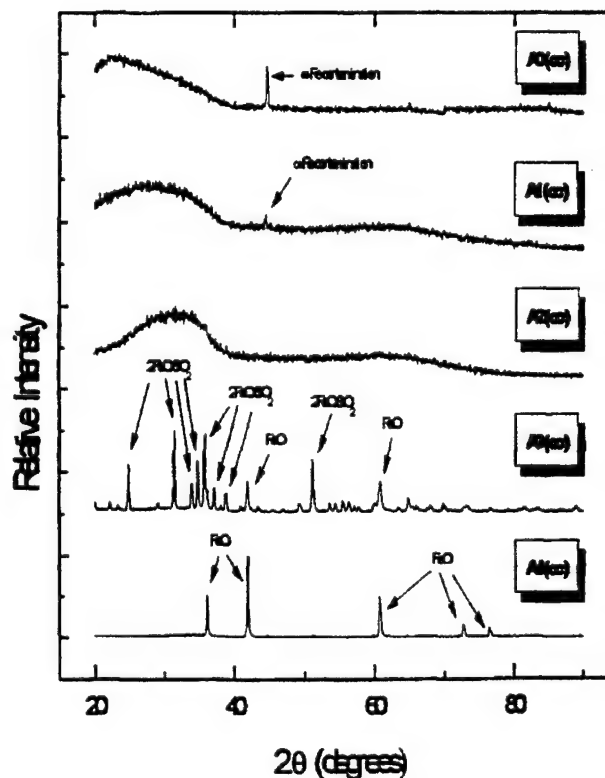


Figure 8. X-ray diffraction analysis for slags generated with A-series electrodes. Mole fraction  $\text{CaO}:\text{SiO}_2$  equals to 0.05 for A-series electrodes.

Coincidentally, the minimum amount of diffusible hydrogen also occurred when this phase was present. This finding is in close agreement with the results obtained by Uys and King (1963). An important consequence of hematite addition above 53 wt. pct. was the suppression of the fayalite phase that resulted. With further addition of hematite in the coating, more FeO (wüstite) was formed and the amount of fayalite was decreased correspondingly. Therefore, one can expect that "free wüstite" may not be the desirable phase controlling weld metal hydrogen pickup.

The Mössbauer spectra of slags collected from the welds made with the A-series electrodes using both polarity is shown in Figure 9. Complementing the x-ray diffraction analysis, the Mössbauer studies carried out on slags provided the substantiation of the presence of  $Fe^{2+}$  ions in all slags analyzed.

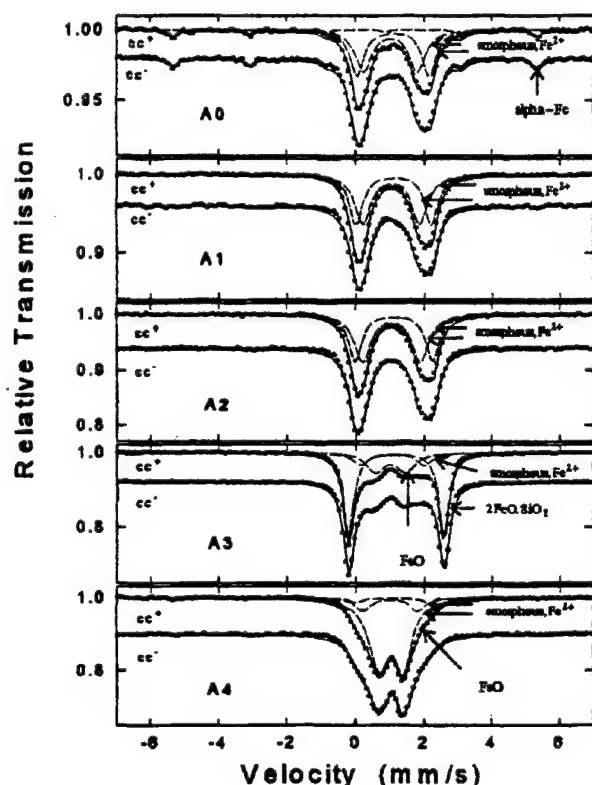


Figure 9. Mössbauer spectra for slag powder absorbers at room temperature. Mole fraction ratio  $CaO:SiO_2$  equals to 0.05 for A-series electrodes.

#### Phenomenological Modeling

Based on the results presented above and on an early pioneering study carried out by Blander and Olson (1986), it was decided that the effect of electrochemical reactions taking place at the atmosphere/slag and slag/metal interfaces on weld metal

hydrogen content must be examined more in detail and modeled. The basic assumption behind the development of the model is that hydrogen is present in slags as  $(OH^-)$  ions (Iwamoto, 1979). Considering the results obtained, it is feasible to assume the following controlling reactions:

#### i - Possible reaction at the slag/environment interface

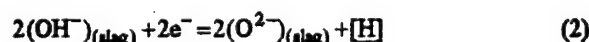
At the slag/environment interface, hydrogen pickup is better described by:



As represented in Equation 1, it is assumed that the water vapor present in the steam bubble surrounding the arc plasma (Pope, Medeiros and Liu, 1995) reacts with the slag to produce  $(OH^-)$  ions. The hydroxyl ions will be transported through the slag to the liquid metal where a further reaction will transfer the hydrogen to the metal.

#### ii - Possible cathodic reactions at the slag/metal interface

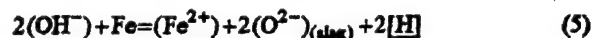
At the slag/metal interface, hydrogen transfer from the liquid slag to the molten metal is better characterized by the following reactions:



Now, equations 2 and 3 may be balanced by anodic reaction such as:



Notice that the reaction described by Equation 4 is in close agreement with the results obtained with Mössbauer spectroscopy. To yield the overall slag-metal reaction that best describes the chemical interaction, Equations 2, 3 and 4 are added together to result in Equation 5:



The behavior of hydrogen with regard to iron oxide present in the slag seems to suggest that the slag/metal droplet interface is the important reaction site for weld metal hydrogen pickup in DCEN ( $cc^-$ ), and the experimental results should be best described by equation (5). This model rests on the simple realization that the lower electrode temperatures encountered in DCEN ( $cc^-$ ) welding would give slower reaction at the environment/slag interface, affecting unfavorably the electrochemical reaction described by equation (2). Conversely, the slag/weld pool interface would be the important reaction site for weld metal hydrogen pickup in DCEP ( $cc^+$ ) welding. A schematic drawing illustrating this model is pictured in Figure 10. It is worth emphasizing here that the work carried out by Becken (1969) provides solid experimental evidence to support

that the electrode tip configuration shown in Figure 10 resembles closely the actual ones.

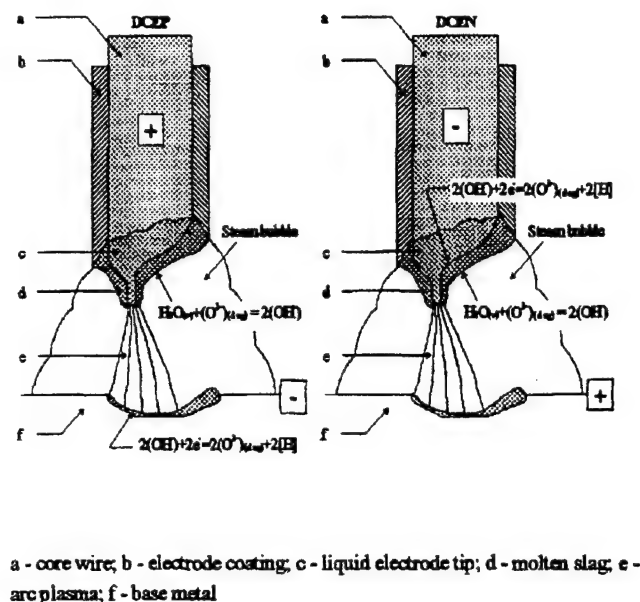


Figure 10. -Schematic drawing of a molten electrode tip and weld pool illustrating the different mechanisms involved in weld metal hydrogen pickup for DCEP (cc<sup>+</sup>) and DCEN (cc<sup>-</sup>). According to the model, weld metal hydrogen pickup occurs at the weld pool surface for (cc<sup>+</sup>) and at the electrode tip for (cc<sup>-</sup>).

Another striking feature of this model is that it can be used to correlate total weld metal hydrogen content with both partial pressure of water vapor and the activity of iron oxide. This task can be accomplished by first calculating the equilibrium constant,  $K$ , of the reactions represented by equations (1) and (5), here designated as  $K_1$  and  $K_2$ , respectively, as follows:

$$K_1 = \frac{(a_{OH^-})^2}{a_{O^{2-}}} \cdot \frac{1}{P_{H_2O}} \quad (6)$$

$$K_2 = \frac{a_{Fe^{2+}} \cdot (a_{O^{2-}})^2 \cdot [H]^2}{(a_{OH^-})^2 \cdot a_{Fe}} \quad (7)$$

In this approach, Turkdogan (1983) pointed out that the activity of an oxide in a polymeric melt is proportional to the product of the activities of the constituent ions. Application of this concept to FeO gives :

$$K_3 = \frac{a_{Fe^{2+}} \cdot a_{O^{2-}}}{a_{FeO}} \quad (8)$$

Finally, substituting equations (7) and (8) into equation (6), and solving for  $[H]$  yields:

$$[H] = K \cdot \sqrt{\frac{P_{H_2O}}{a_{FeO}}} \quad (9)$$

where

$$K = \sqrt{\frac{K_1 \cdot K_2}{K_3}} \quad (10)$$

Equation 9 indicates that weld metal hydrogen pickup can be reduced by increasing the amount of FeO in the slag. It is worth emphasizing here that work carried out by Timucin and Morris (1970) and results reported in the Schlackenatlas (1981) provides solid experimental evidence to support the proposed model.

Finally, in light of the preceding discussion it is worth mentioning that at low pressure values the weld metal hydrogen content is extremely dependent on the activity of FeO. On the other hand, at high pressure values, the effect of the activity is largely overcome by an increase in water vapor pressure surrounding the slag. The net result of these opposing effects is a curve similar to those obtained experimentally (see Figures 3 and 4).

## CONCLUSIONS

Multipass bead-on plate welds were carried out using oxidizing electrodes in fresh water at the depth of 0.27 m using set welding conditions. The effect of the slag composition on hydrogen absorption and on hydrogen transport to the weld metal was assessed. On the basis of the experimental results obtained, the following conclusions can be drawn:

- 1- The results reaffirmed the effectiveness of oxidizing electrodes in controlling hydrogen pickup in underwater wet welds. Weld metal diffusible hydrogen as low as 13.2 ml/100g was obtained with oxidizing electrode coating, as compared with the 90-100ml/100g obtained with rutile type electrodes.
- 2- Lower weld metal hydrogen content values were obtained using DCEN (cc<sup>-</sup>) welding.
- 3- The results indicated that both weld metal hydrogen content and slag hydrogen content were dependent on the phase present in the slag. Invariably, the lowest hydrogen content was associated with the presence of fayalite -  $2FeO \cdot SiO_2$  - independent of the welding polarity used.
- 4- Mössbauer spectroscopy indicated that the only valence state present was  $Fe^{2+}$  for the entire range of hematite additions in the electrode coating.

5- An electrochemical model able to characterize the variations in both weld metal hydrogen content and slag hydrogen content, with polarity and iron oxide present in the slags was proposed. It incorporates the novelty that hydrogen is present in slag as (OH) ions.

6- The reaction responsible for hydrogen transfer from the slag to the weld metal was demonstrated to be controlled by the amount of (OH) ions absorbed in the slag.

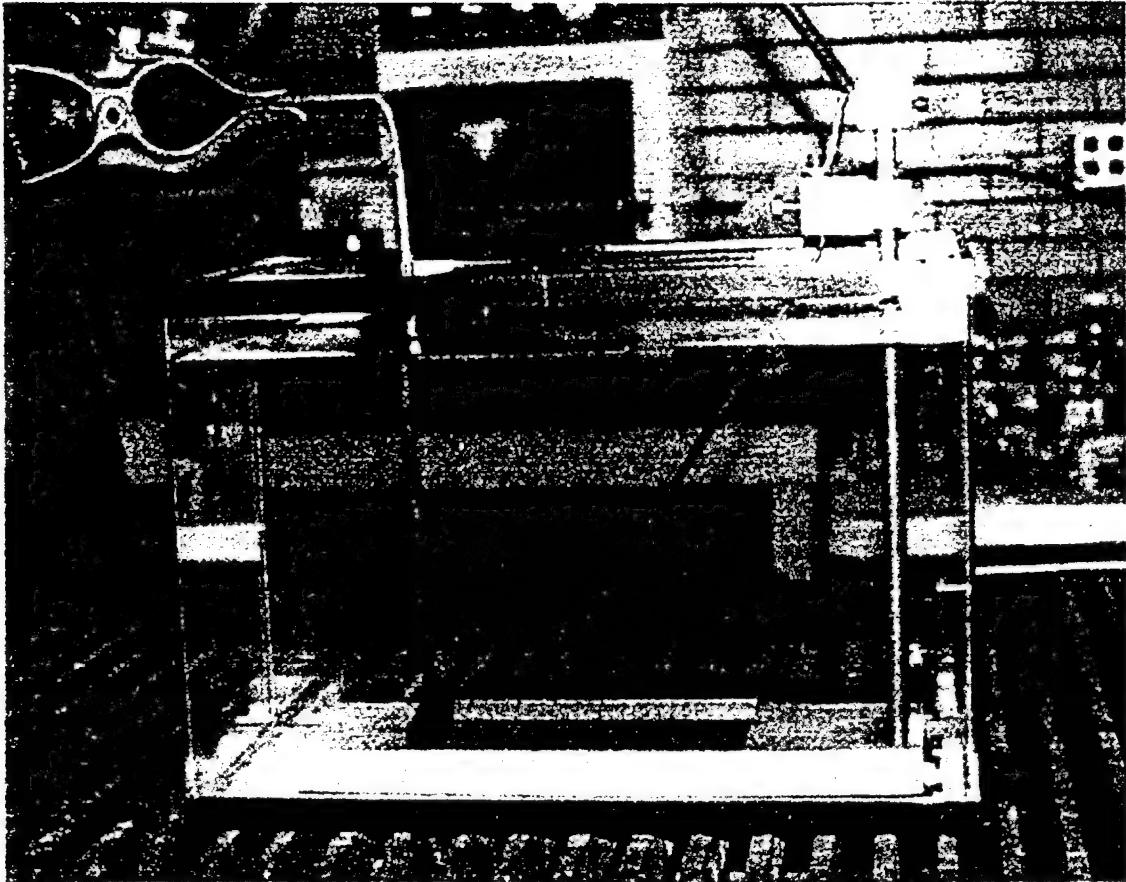
7- The model predicts that weld metal hydrogen pickup occurs at the weld pool for DCEP ( $cc^+$ ) polarity. Conversely, in DCEN ( $cc^-$ ) polarity, hydrogen is transferred to the metal at the pendent droplet.

#### ACKNOWLEDGMENT

The authors wish to acknowledge the support of the Office of Naval Research. Raimundo C. de Medeiros also gratefully acknowledges the Brazilian Council for Scientific and Technological Development-CNPq for the financial assistance received.

#### REFERENCES

- American Welding Society, 1993. Standard methods for determination of the diffusible hydrogen content of martensitic, bainitic and ferritic steel weld metal produced by arc welding. ANSI/AWS A4.3-93. Miami, Florida.
- Blander, M. and Olson, D. L. 1986. Electrochemical effects on weld pool chemistry in submerged arc and D.C. electroslag welding. Proc. International Conference on Trends in Welding Research. 363-366.
- Easterling, K. 1992. Introduction to the physical metallurgy of welding. 2nd. edition. Butterworth-Heinemann.
- Fomo, A. E. J., Peover, M. E., and Powell, J. S. 1971. Control of hydrogen in electroslag remelting of iron. Journal of the Iron and Steel Institute. 209: 966-968. (December).
- Frost, R. H., Olson, D. L., and Edwards, G. R. 1983. The influence of electrochemical reactions on the chemistry of the electroslag welding process. Modeling of Casting and Welding Processes II. The Met. Society of AIME 279-294.
- Gooch, T. G. 1983a. Properties of underwater welds. Part 1. Procedural trials. Metal Construction. 164-167. (March).
- Itterante, C. G. and Stout, R. H. 1964. Delayed cracking in steel weldments. Welding Journal Research Supplement. 43 (4): 145s - 160s.
- Kim, J. H., Frost, R. F., Olson, D. L., and Blander, M. 1990. Effect of electrochemical reactions on submerged arc weld metal compositions. Welding Journal. 446s-453s. (December).
- Nóbrega, A. F. 1981. Study of underwater wet welding with covered electrodes. MSc. Thesis. Federal University of Rio de Janeiro. (in Portuguese).
- Pope, A. M., Teixeira, J. C. G., Santos, V. R., Paes, M. T. P. and Liu, S., 1995. Use of nickel to improve the mechanical properties of high oxygen underwater wet welds. Proceedings of the 14th. International Conference on Offshore Mechanics and Arctic Engineering. American Society of Mechanical Engineers. 529-535.
- Pope, A. M., Medeiros, R. C., and Liu, S., 1995. Solidification of underwater wet welds. Proceedings of the 14th International Conference on Offshore Mechanics and Arctic Engineering. vol. III. Materials Engineering. 517-521.
- Pope, A. M. 1995. Oxygen and hydrogen control in shielded metal underwater welding. Ph.D. Thesis. Colorado School of Mines. Golden, CO, USA.
- Sanchez-Osio, A., Liu, S., and Olson, D. L. 1993. Underwater wet welding consumables for offshore application. Proceedings of 12th. International Conference on Offshore Mechanics and Arctic Engineering. III-A. 119-128.
- Schlackenatlas. 1981. Dusseldorf, Verlag Stahleisen M. B. H.
- Stalker, G. R. 1963. Hydrogen absorption in arc welding. British Welding Journal. 79-88. (August-September).
- Timucin, M. and Morris, A. E. 1970. Phase equilibrium and thermodynamic studies in the system  $CaO-FeO-Fe_2O_3-SiO_2$ . Metallurgical Transactions. vol. I: 3193-3201.
- Turkdogan, E. T. 1983. Physicochemical Properties of Molten Slags and Glasses. The Metals Society. London.
- Uys, J. M. and King, T. B. 1963. The effect of basicity on the solubility of water in silicate melts. Transactions of the Metallurgical Society of AIME. 227: 492-500. (April).





A. **Steel Weld Metal Composition Estimation Including Diffusible and Residual Hydrogen Content**, by D. L. Olson and S. Liu, Colorado School of Mines

Diffusible and residual weld metal hydrogen are major concerns in high strength steel welding, especially when the weld is performed under high cooling rate conditions. Current understanding of the process and modeling does not allow for the prediction of the amount of hydrogen present in the weld metal. Adopted practices in hydrogen investigation include the analytical determination of diffusible and residual hydrogen content in the weld metal. This procedure is extremely useful in ranking consumables, but is cumbersome at times since hydrogen testing is costly and time consuming. There is also concern in the international community of the variation of results obtained from laboratory to laboratory, and the validity of these results.

In the particular case of underwater welding, pores have been reported to contain large amounts of hydrogen (over 90%) with minimum carbon monoxide and carbon dioxide. Despite the difficult experimental determination of gas pore composition, this information is vital to the understanding of the chemical evolution of the weld metal. Quantitative methodologies must be developed for the prediction of the amounts of hydrogen and other gaseous species in the pores.

The pyrometallurgical reactions in a low carbon steel weld pool have been examined using thermodynamic calculations. In this modeling, initial electrode tip-plasma and weld pool-plasma reactions were assumed to saturate the molten droplet with oxygen and hydrogen. Subsequent deoxidation reactions with aluminum, silicon, manganese, carbon, iron, and hydrogen would then occur sequentially according to their thermodynamic stability. Only simple oxides were allowed to form in this calculation. Despite the simplistic model, it was possible to determine the residual amounts of the alloying elements such as manganese, silicon and aluminum. It was also possible to determine the quantity of primary inclusions that form in the weld pool. The amounts of carbon monoxide and hydrogen generated in the weld pool were also determined. The ratio of CO to H<sub>2</sub> was found to vary around 3.5, indicating a much greater contribution of CO than that reported in the welding literature. Finally, the hydrogen trapping model has been used to distinguish the residual hydrogen from the diffusible hydrogen in the weld pool. Again, only simple inclusions were considered as trapping sites.

In spite of the simplistic model, the methodology developed in this research was capable of examining the weld pool and the multiple deoxidation reactions in sequence, and predict the chemical composition of the weld pool. The approach is also capable of predicting, as a first approximation, the weld pore composition and hydrogen (residual and diffusible) content. The proposed procedure is capable of ranking base metal-electrode combinations in terms of hydrogen concentration and cold cracking susceptibility.



## **The Effect of Altitude on Welding**

S. Liu, D.L. Olson  
Colorado School of Mines  
Golden, Colorado

Reprinted from  
**TRENDS IN WELDING RESEARCH**  
*Proceedings of the*  
4th International Conference  
5-8 June, 1995  
Gatlinburg, Tennessee

# **REPRINT**



**The Materials  
Information Society**

Copyright© 1996  
by  
**ASM International®**  
All rights reserved

No part of this book may be reproduced, stored in a retrieval system, or transmitted, in any form or by any means, electronic, mechanical, photocopying, recording, or otherwise, without the written permission of the copyright owner.

First printing, June 1996

Great care is taken in the compilation and production of this Volume, but it should be made clear that NO WARRANTIES, EXPRESS OR IMPLIED, INCLUDING, WITHOUT LIMITATION, WARRANTIES OF MERCHANTABILITY OR FITNESS FOR A PARTICULAR PURPOSE, ARE GIVEN IN CONNECTION WITH THIS PUBLICATION. Although this information is believed to be accurate by ASM, ASM cannot guarantee that favorable results will be obtained from the use of this publication alone. This publication is intended for use by persons having technical skill, at their sole discretion and risk. Since the conditions of product or material use are outside of ASM's control, ASM assumes no liability or obligation in connection with any use of this information. No claim of any kind, whether as to products or information in this publication, and whether or not based on negligence, shall be greater in amount than the purchase price of this product or publication in respect of which damages are claimed. THE REMEDY HEREBY PROVIDED SHALL BE THE EXCLUSIVE AND SOLE REMEDY OF BUYER, AND IN NO EVENT SHALL EITHER PARTY BE LIABLE FOR SPECIAL, INDIRECT OR CONSEQUENTIAL DAMAGES WHETHER OR NOT CAUSED BY OR RESULTING FROM THE NEGLIGENCE OF SUCH PARTY. As with any material, evaluation of the material under enduse conditions prior to specification is essential. Therefore, specific testing under actual conditions is recommended.

Nothing contained in this book shall be construed as a grant of any right of manufacture, sale, use, or reproduction, in connection with any method, process, apparatus, product, composition, or system, whether or not covered by letters patent, copyright, or trademark, and nothing contained in this book shall be construed as a defense against any alleged infringement of letters patent, copyright, or trademark, or as a defense against liability for such infringement.

Comments, criticisms, and suggestions are invited, and should be forwarded to ASM International.

**ASM International®**

Library of Congress Catalog Card Number: 96-84776  
ISBN: 0-87170-567-2  
SAN: 204-7586

**ASM International®**  
Materials Park, OH 44073-0002

Printed in the United States of America

## The Effect of Altitude on Welding

S. Liu, D.L. Olson

Colorado School of Mines, Golden, Colorado

### Abstract

Welding at high altitude has typically been reported as more difficult, particularly in the aspect of porosity control. As a consequence, welding of a similar assembly in cities of high elevation such as Denver, Colorado (U.S.A.) and Mexico City (Mexico) may require different parameters from those selected for welding in Houston, Texas (U.S.A.), Kobe (Japan), and Hamburg (Germany). The atmospheric pressures in these locations are different and the solubilities of gases such as hydrogen in the weld metal are also expected to be different.

The presence of porosity in a weld metal depends on two factors: a) the solubility of gaseous elements in the liquid metal, and b) the ambient pressure. A higher atmospheric pressure implies in a larger amount of gas dissolved in the molten weld pool and probably a larger amount of gas porosity. However, the morphology of the pores and the ease of porosity release from the weld pool into the ambient will also depend on the ambient pressure. Higher pressures will generally result in higher supersaturation of the gaseous species in the matrix and more difficult porosity nucleation and removal. In addition, there is also a tendency of obtaining finely distributed pores, often below the resolution of X-ray radiography and ultrasonic detection. Lower ambient pressures generally facilitate porosity removal because larger and more visible pores will form in the weld pool, even though the total gas content in the weld metal may not be very high.

In this work, the formation of hydrogen and carbon monoxide porosity in low carbon steel weld metals was investigated. The thermodynamic conditions of the chemical reactions that occur in the weld pool were examined. The effects of ambient pressure on the H-O and C-O reactions were estimated for a range of pressures that varied from sea level to approximately 10,000 feet elevation. It was determined that the amounts of carbon monoxide and water in the pores varied measurably with altitude. Since the water vapor molecules that are entrapped in a pore react favorably with the iron atoms on the surface of the pore to form hydrogen and iron oxide, the

amount of retained carbon monoxide and hydrogen would also vary with altitude. Finally, welds performed at lower ambient pressure (in locations of higher elevation) are expected to exhibit a larger amount of porosity because of reaction thermodynamics and nucleation kinetics.

IT IS KNOWN THAT ATMOSPHERIC PRESSURE decreases exponentially with increasing elevation (altitude), reaching zero pressure in space. At sea level, atmospheric pressure is approximately 760 mm Hg (1 atm.); and on top of Mount Everest, at 29,000 ft., the pressure is only about 225 mm Hg, or 0.3 atm. Even though the unit "atmosphere - atm." is commonly used to characterize ambient pressure, the standard unit of pressure is millibars (mb) and the pressure at sea level is around 1013 mb.

Figure 1 shows atmospheric pressure as a function of altitude. Also illustrated in this figure are the ambient pressures of three metropolitan cities, Houston, Denver, and Bogotá (Colombia). Houston is a major U.S. industrial park situated at sea level and is, therefore, expected to have ambient pressure close to 1013 mb. Denver, the Mile-High City at an elevation of 5280 ft., is expected to have ambient pressure of approximately 850 mb (610 mm Hg). Bogotá, at 8,500 ft. altitude and a pressure of around 720 mb, is one of the most elevated cities in the world with fabrication and manufacturing activities. The pressure reduction from Houston to Denver is around 16 percent, and from Houston to Bogotá, approximately 29 percent. It is believed that the pressure reduction will produce noticeable changes in the weld pool with respect to chemical composition, defect formation and mechanical properties.

To a certain extent, the effect of pressure change (as a result of altitude change) on welding can be related to that of underwater welding. Traveling from the depth of 600 ft. to the surface, a decrease in pressure of approximately  $17 \times 10^3$  mb is observed. The major difference between the two cases (elevation change and water depth change) lies entirely on the water head, which exerts a much greater pressure than the at-

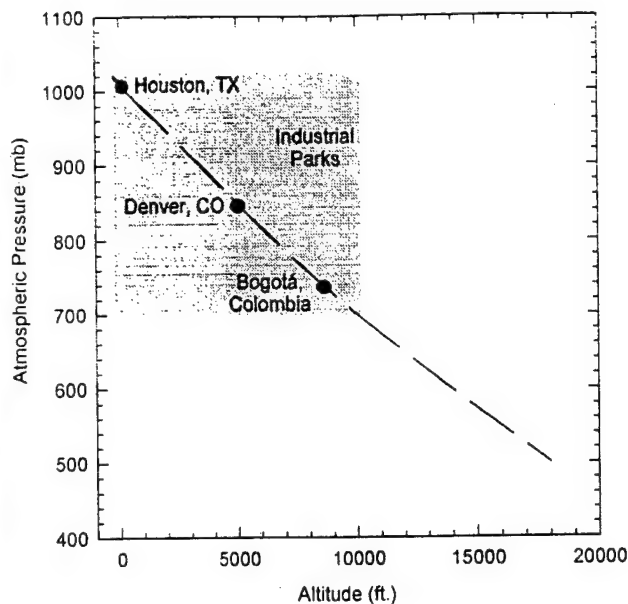


Figure 1. Atmospheric Pressure as a Function of Altitude.

mosphere. Figure 2 demonstrates the decrease in pressure with decreasing water depth.

Hyperbaric habitat welding studies (1,2) indicated that the chemical composition of a low carbon steel weld varied with increasing water depth (pressure). Underwater wet welds showed oxygen contents increasing linearly with increasing depth to around 2000 ppm at saturation, depicted in Figure 3 (3). It is believed that water dissociation in the arc contributed significantly to the high oxygen content in the weld pool. However, the concentrations of alloying elements such as manganese and silicon decreased with increasing depth (1,3), as il-

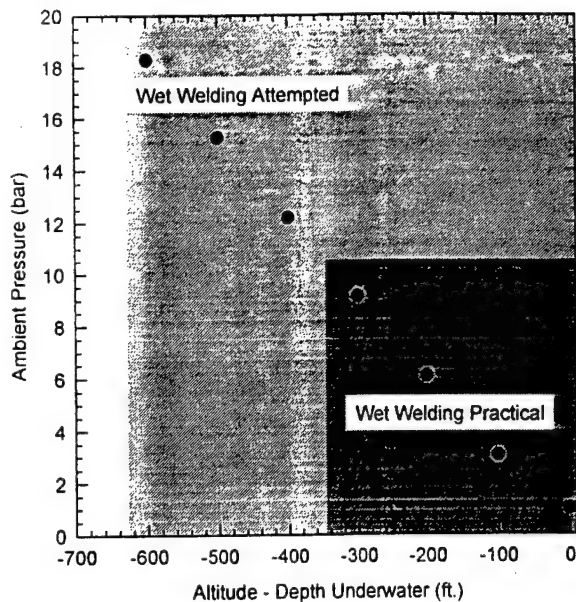


Figure 2. Ambient Pressure as a Function of Water Depth.

lustrated in Figure 3. Their decrease can be attributed to the oxidation reactions that occur in the weld pool. Along with the changes in chemical composition, weld metal porosity was also observed to increase with pressure, Figure 4 (4).

Compared to underwater welding, the changes observed in surface welds with pressure are not expected to be that significant. The changes in pressure (altitude) in surface welding is less than five percent of those experienced in underwater welding. Nevertheless, at different elevations, the changes in weld pool chemistry and porosity are expected to be noticeable.

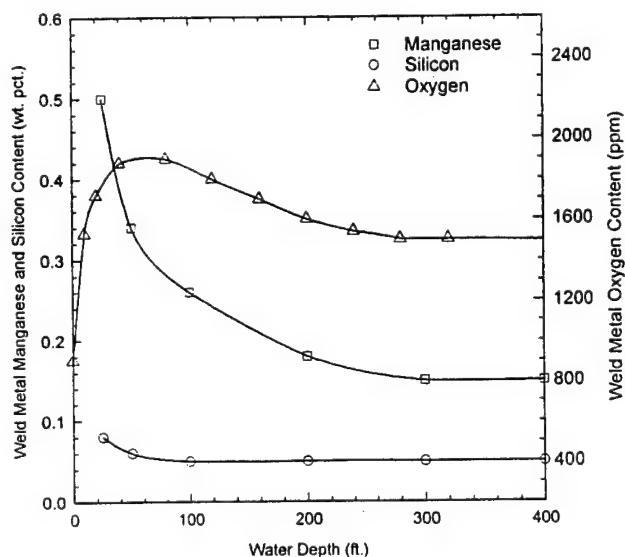


Figure 3. Underwater Wet Weld Metal Alloying Elements and Oxygen Contents as a Function of Water Depth (1-3).

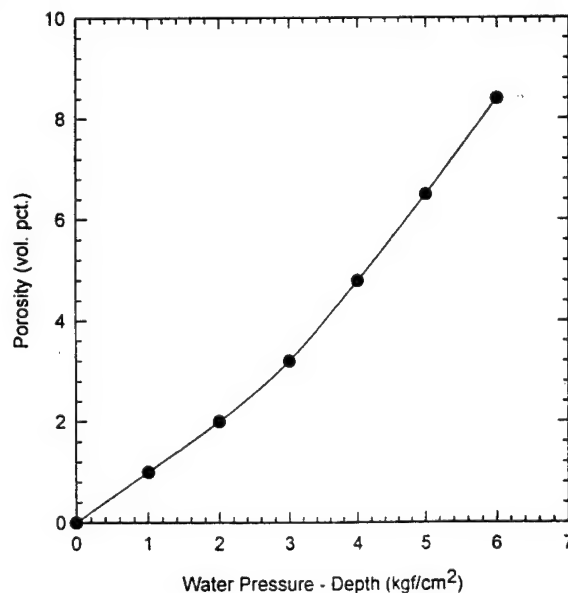


Figure 4. Underwater Wet Weld Metal Porosity as a Function of Water Depth (4).

## Weld Metal Porosity

Several researchers (4,5) have investigated the chemical composition of underwater wet weld metal porosity and determined that they contain mostly H<sub>2</sub>, with only a small amount of CO and CO<sub>2</sub>. Table I reports some of these analyses.

Table I. Weld Metal Porosity Composition (in vol. pct.) (4,5).

	H <sub>2</sub>	CO	CO <sub>2</sub>	Others
<b>Suga &amp; Hasui</b>	96.0	0.4	0.06	—
<b>Silva</b>	62/82	11/24	4	4

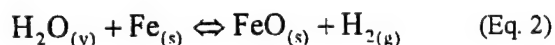
In the case of underwater wet welding, the water surrounding the arc is the major source of hydrogen and porosity. Assuming that only simple chemical reactions occur in the arc and weld pool, water can be considered as dissociating into hydrogen and oxygen, which subsequently dissolve in the molten weld pool according to Equation 1.



The oxygen pickup explains the increased oxygen concentration in the weld metal. With excellent mobility, atomic hydrogen often recombine in the weld pool to form diatomic hydrogen molecules, responsible for pore formation in the solidifying weld metal. Hence, changes in the partial pressure of H<sub>2</sub>O<sub>(v)</sub> is expected to affect significantly the amounts of dissolved hydrogen and oxygen, and the amount of porosity in a weld.

Note that hydrogen buildup in a low carbon steel weld pool may also display a strong electrochemical nature that hydrogen ions (H<sup>+</sup>) are actually the active chemical species in the welding arc (6). In the cathode drop region, the hydrogen ions are reduced by the "excess" electron charges and absorbed in the molten weld pool. Likewise, these hydrogen atoms may recombine in the liquid metal to form hydrogen gas molecules and porosity.

Another mechanism of porosity formation is related to the formation of water vapor in the weld pool which is the reverse reaction described by Equation 1. Trapped in a pore and at high temperatures, the H<sub>2</sub>O<sub>(v)</sub> molecules oxidize the surrounding iron atoms to form FeO and H<sub>2</sub> (7).



Whether it is by recombination of hydrogen atoms or by reduction of water vapor, hydrogen is expected to be present in weld metal porosity.

Carbon monoxide\* and carbon dioxide are the other components found in gas pores in structural steel welds. In addition

to being the major alloying element in steels, carbon is also originated from the decomposition of organic materials (cellulose, lubricants, coolants, rust inhibitors, etc.) and inorganic carbonates, is abundant in the arc environment. When dissolved in the molten steel, carbon can, in principle, react with oxygen to form both CO and CO<sub>2</sub>. Entrapment of these gas molecules in the weld pool will result in porosity. However, at temperatures around 1600 to 1800°C (weld pool temperature), CO is more stable than CO<sub>2</sub> and will, thus, predominate in the weld pores.

In surface welds, the partial pressure of water vapor is much lower than that found in the underwater welding conditions. However, parts that have been processed with lubricants and not thoroughly cleaned will release hydrogen, carbon and oxygen into the arc by thermal decomposition. Components that are not properly rinsed and dried after degreasing will also exhibit porosity problems during welding. Surface oxides tend to pick up moisture from the surrounding environment and form hydrates, which decompose readily in the arc and feed hydrogen into the weld pool.

In summary, the presence of hydrogen and carbon monoxide in weld pores is well established and that the relative amount of each of the two gases will depend on the ambient pressure and moisture content.

## H-O Relationship as a Function of Altitude

It has been reported in the steelmaking literature (8) that water vapor is present in the arc furnace atmosphere at levels of less than six percent, and that the partial pressure of moisture in an electric arc furnace is at the order of 0.015 atm. Using 23.3 mb (17.5 mm Hg) (9) as the saturation pressure of water vapor, P<sub>sat</sub>, at 25°C (77°F), and the local atmospheric pressure, the partial pressure of moisture, P<sub>H<sub>2</sub>O</sub>, in Houston, Denver, and Bogotá were determined as: 0.023, 0.019 and 0.016 atm., respectively. These results show that despite the constant saturation vapor pressure consideration, the partial pressure of moisture varied as a function of ambient pressure. Note also that the estimated partial pressures of moisture are comparable to that reported for the electric arc furnaces.

The use of a single saturation vapor pressure (in this case, 23.3 mb at 25°C) for the calculation of partial pressures of water vapor for all three cities was possible because saturation vapor pressure does not change significantly with ambient pressure (altitude) (15). This behavior can be examined in Equation 3, which describes the change in saturation vapor pressure, ΔP<sub>sat</sub>, as a function of ambient pressure, P<sub>Amb</sub>.

$$\Delta P_{\text{sat}} = P_{\text{Amb}} \frac{\rho_v}{\rho_L} \quad (\text{Eq. 3})$$

Since ρ<sub>v</sub> (water vapor density) is approximately 10<sup>3</sup> times smaller than ρ<sub>L</sub> (liquid water density) and P<sub>Amb</sub> is relatively small for surface welding, ΔP<sub>sat</sub> is generally negligible. In underwater welding and hyperbaric welding, however, P<sub>Amb</sub> be-

comes substantial (compare Figure 1 with Figure 2) which will result in more meaningful  $\Delta P_{\text{sat}}$ 's. In those circumstances, different saturation vapor pressures must be used in the computation of local partial pressure of water vapor.

Considering the water decomposition reaction described by Equation 1, the coefficient of equilibrium for the reaction,  $K$ , can be written as:

$$K = C_1 \frac{[H]^2[O]}{P_{H_2O}} \quad (\text{Eq. 4})$$

where  $[H]$  and  $[O]$  represent the concentration of dissolved hydrogen and oxygen,  $P_{H_2O}$  is the partial pressure of moisture in the atmosphere, and  $C_1$  is a constant that includes the activity coefficients of hydrogen and oxygen. Assuming that the temperature of the weld pool is  $1600^\circ\text{C}$ , and using the following standard free energy of dissociation ( $\Delta G^\circ$ ) expression (8) for Reaction 1,

$$\Delta G^\circ = -RT \ln K = 46,180 + 1.57T \quad (\text{Eq. 5})$$

the concentration of hydrogen and oxygen can be evaluated. The results of this calculation are plotted in Figure 5. Since the partial pressure of water vapor is the highest in Houston, the equilibrium concentration of hydrogen and oxygen are also the highest. On the other hand, low carbon steel welds performed in Bogotá, Colombia will have the smallest amounts of hydrogen and oxygen in solution.

### C-O Relationship as a Function of Altitude

The same procedure described for the hydrogen-oxygen relationship can be used for the evaluation of equilibrium carb-

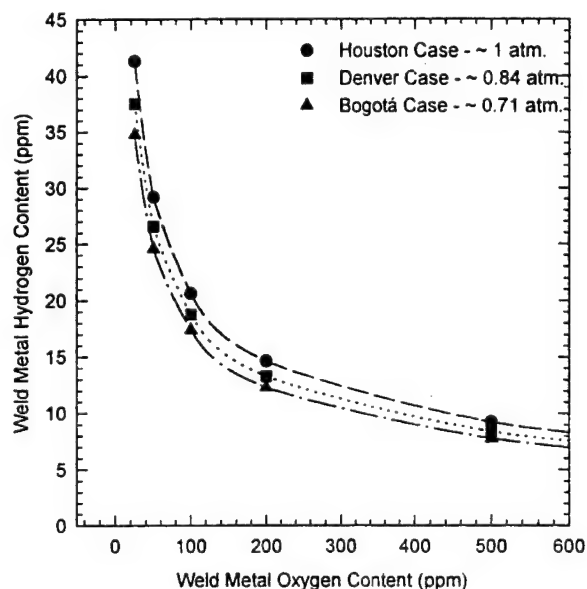


Figure 5. Equilibrium Hydrogen and Oxygen Concentrations at  $1600^\circ\text{C}$  at Three Elevations.

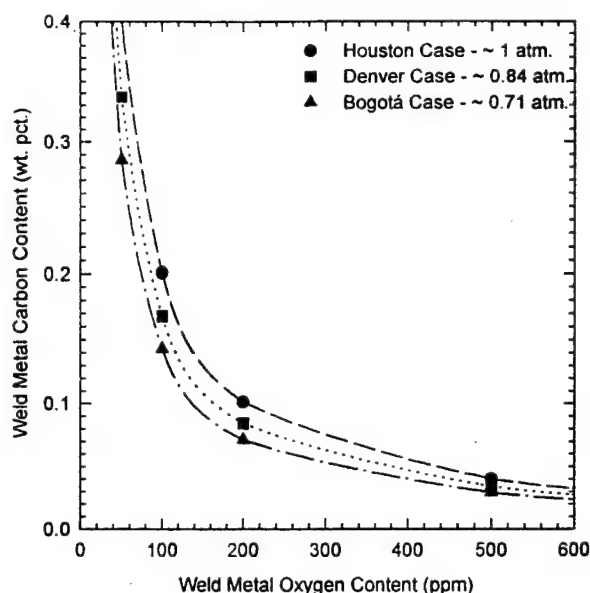


Figure 6. Equilibrium Carbon and Oxygen Concentrations at  $1600^\circ\text{C}$  at Three Elevations.

on and oxygen concentration in the weld pool at  $1600^\circ\text{C}$ . As discussed earlier, both carbon dioxide and carbon monoxide are formed when carbon reacts with oxygen. At temperatures higher than  $700^\circ\text{C}$ , however, carbon dioxide will further decompose into carbon monoxide (8). Therefore, only the CO reaction as described by Equation 6 needs to be considered to determine carbon and oxygen equilibrium in the weld pool.



The standard free energy of CO dissociation is:

$$\Delta G^\circ = 5,350 + 9.48T \quad (\text{Eq. 7})$$

and the reaction constant for the carbon-oxygen reaction, can be written as:

$$K_{\text{CO}} = \frac{[\underline{C}][\underline{O}]}{P_{\text{CO}}} \quad (\text{Eq. 8})$$

In this equation,  $[\underline{C}]$  and  $[\underline{O}]$  are the activity terms of carbon and oxygen in the weld metal which can usually be replaced by their respective concentrations.  $P_{\text{CO}}$  is the partial pressure of carbon monoxide in the welding arc environment. Since the release of  $\text{CO}_{(g)}$  from the weld pool is against the arc pressure,  $P_{\text{CO}}$  can be taken as the local atmospheric pressure which vary with altitude.

Figure 6 plots the results of this calculation. Similar to the hydrogen-oxygen curves, the equilibrium concentrations of carbon and oxygen are the lowest for Bogotá, Colombia. This observation seems to indicate that in comparison with

other cities of lower elevation (Denver and Houston) and for similar amounts of carbon and oxygen pickup from the arc environment, more of the carbon monoxide generated in the welds performed in cities of higher elevation must be eliminated from the molten weld pool for porosity not to occur.

Figures 7 and 8 are combined plots of the hydrogen-oxygen and carbon-oxygen relationship for the three altitudes. In addition, the Mn-O and Al-O equilibrium curves are also included in these figures to illustrate the sequence of deoxidation reactions that occur in the weld pool. Different from the H-O and C-O reactions, the Mn-O and Al-O reactions do not involve gaseous phases and are, therefore, insensitive to ambient pressure changes.

By examining these four reactions, the chemical composition of the porosity can be estimated. Assuming that approximately 1600 ppm of oxygen (maximum oxygen solubility prior to the formation of  $\text{FeO(l)}$  in a liquid steel) and 50 ppm of "hydrogen" are picked up in the droplet in the plasma, much of the oxygen and hydrogen must be released from the

weld pool in the form of oxide inclusions,  $\text{H}_2\text{O(v)}$ ,  $\text{H}_2$  and CO to reach the final weld metal composition.

As a first approach to the analysis of the complex weld pool reactions, the thermodynamic stability of each oxide will be used as an indication of the order according to which a reaction takes place. Being  $\text{Al}_2\text{O}_3$  the most stable oxide in the weld system, the Al-O reaction will be the first to occur following the Al-O path indicated in the two diagrams. The slope of the reaction path is determined by the stoichiometric ratio between aluminum and oxygen. The subsequent reactions will be Mn-O, C-O and H-O, each following their reaction path, also shown in the two figures. The intersection of each of the reaction paths with their respective equilibrium curves will determine the equilibrium concentrations in solution. The procedure described above followed the scheme of estimating deoxidation sequence proposed by Liu and Olson (7).

In the case of Houston, Texas, the presence of 0.03 wt. pct. of aluminum reduced the "free" oxygen from 1600 to 1300 ppm. The Mn-O reaction follows lowering the oxygen

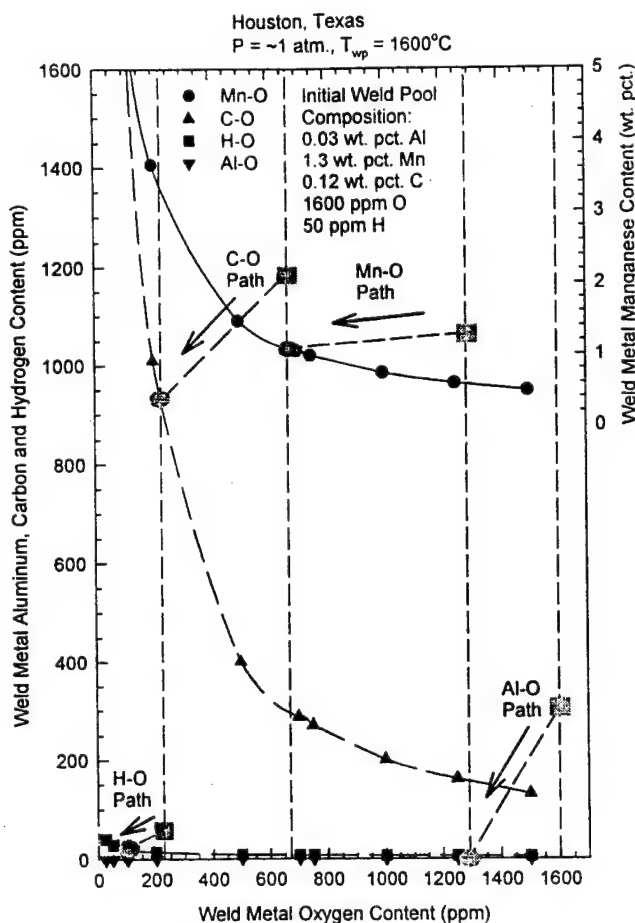


Figure 7. Combined H-O and C-O Curves for the case of a City Located at the Sea Level (Houston, Texas).

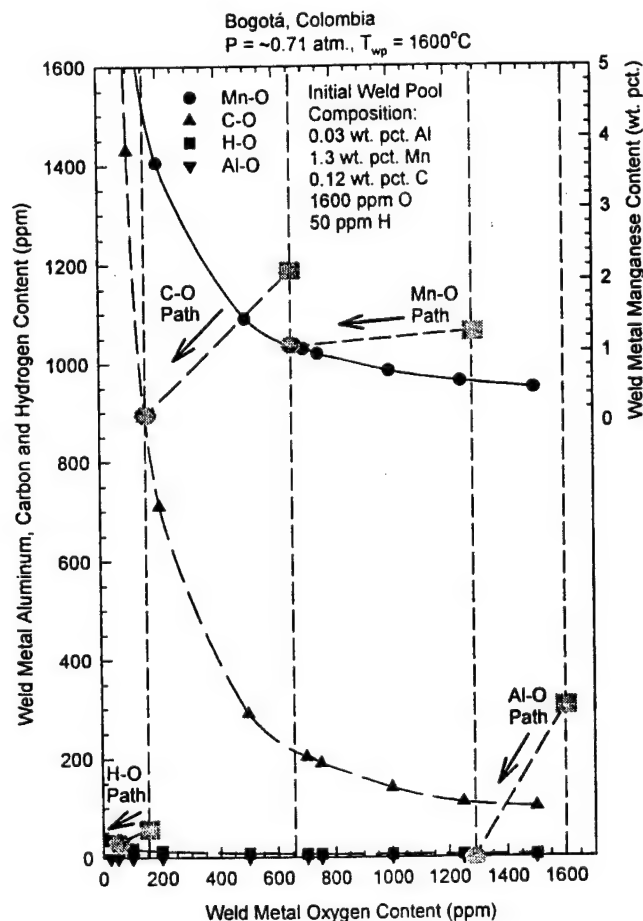


Figure 8. Combined H-O and C-O Curves for the case of a City Located at a Higher Elevation (Bogotá, Colombia).



content to around 680 ppm. The final two reactions are the gas (pore) producing reactions. The C-O reaction will reduce the oxygen level to 220 ppm and the H-O reaction, to approximately 100 ppm. These two reactions will produce around 800 ppm of CO and 150 ppm of H<sub>2</sub>O (H<sub>2</sub>). Assuming that these would be the only gases in the pores, the composition will contain 22 vol. pct. H<sub>2</sub> and 78 vol. pct. CO with the ratio CO/H<sub>2</sub> equal to 3.6. The equilibrium hydrogen content is estimated to be 21 ppm. This value represents the total hydrogen expected (diffusible and residual) in the weldment.

Following the same procedure outlined, the concentration of H<sub>2</sub> and CO in a gas pore in low carbon steel welds produced in Bogotá, Colombia were estimated to be: 884 ppm CO and 110 ppm H<sub>2</sub> which correspond to 16 and 84 vol. pct., respectively. The equilibrium hydrogen content is 35 ppm. Note that these concentrations can only be verified if elimination of the oxide inclusions and gases is complete.

The calculations clearly show the different chemical composition of the pores in welds produced in low and high altitudes. Additionally, an increase of 5.6 pct. of gaseous products (CO + H<sub>2</sub>) was also estimated for the welds performed in Bogotá, Colombia when compared with welds made in Houston. Consequently, welds performed at higher elevations may require more careful control to minimize gas porosity.

### Porosity Nucleation Kinetics

Aside from the thermodynamics of the gas producing reactions, the kinetics of pore nucleation must also be considered to determine the feasibility of CO and H<sub>2</sub> elimination from the weld pool. Nikiforov and Redchits (10) reported an expression for the nucleation rate (I) as a function of the critical pore size (r<sub>c</sub>).

$$I = A \exp\left(-\frac{4\pi r_c^3 \gamma}{3kT}\right) \quad (\text{Eq. 9})$$

In this equation, A is the pre-exponential constant,  $\gamma$  is the surface tension between the molten metal and the gas in the pore. k is the Boltzmann Constant and T is the temperature in degrees Kelvin. The critical pore size, r<sub>c</sub>, can be written as:

$$r_c = \frac{2\gamma V}{kT \ln\left(\frac{P_g}{P_\infty}\right)} \quad (\text{Eq. 10})$$

where V is the atomic volume of the gas phase, P<sub>∞</sub> is the solubility of the metastable gas phase and is a function of the ambient pressure. P<sub>g</sub> is the pore gas pressure which is a sum of the ambient pressure and the pressure increase due to the curvature of the pore. Assuming that P<sub>g</sub> is the amount of hydrogen dissolved in the melt at the highest temperature of the welding process, T<sub>wp</sub>, it is obvious that as solubility drops with temperature, the ratio P<sub>g</sub>/P<sub>∞</sub> gets increasingly larger. Correspondingly the critical pore size and activation energy barrier get

smaller. This equation also shows that as the ambient pressure decreases (i.e., increasing altitude), the critical pore radius decreases facilitating pore nucleation during welding. As a result, there is a greater probability of pore entrapment in the weld metal during solidification for welds produced at higher elevation.

### Conclusions

Based on the discussion and calculations made in this work, the following major conclusions can be reached:

- Altitude affects the chemical composition and amount of porosity in structural steel welds.
- As altitude increases, i.e., decreasing atmospheric pressure, the equilibrium C-O and H-O concentrations decreased.
- Gas porosity contains both carbon monoxide and hydrogen and the amount of carbon monoxide is significantly higher than those reported in the literature.
- The final weld composition is a function of the deoxidation reactions that occur in the weld pool. Local ambient pressure and partial pressure of water vapor affect the extent of the gas forming reactions.

### Acknowledgment

The authors acknowledge the support of the Office of Naval Research (ONR) and the National Shipbuilding Research Program - Welding Panel (NSRP-SP7).

### References

1. Christensen, N. "The Metallurgy of Underwater Welding," Underwater Welding, IIW Conf. Proc., Trondheim, Norway, Pergamon Press, pp. 71-79 (1983)
2. Grong, Ø., D.L. Olson and N. Christensen, Metal Construction, V. 17(12), pp. 810R-814R (1985).
3. Ibarra, S. and D.L. Olson, Key Engineering Materials, Vol. 69-70, pp. 329-378 (1992).
4. Suga, Y. and A. Hasui, IIW DOC IX-1388-86, American Council, AWS, (1986).
5. Silva, E.A., Naval Engineer's Journal, 12 (1971)
6. Ibarra, S. D.L. Olson and S. Liu, Interpretive Report, Welding Research Council (1995).
7. Liu, S., D.L. Olson and S. Ibarra, OMAE Conf. Proc., Vol. 3, pp. 291-298 (1994).
8. L.G. Twidell, "Physical Chemistry of Iron and Steelmaking," Montana College of Mineral Science and Technology (1980).
9. D. Tabor, "Gases, Liquids and Solids, and Other States of Matter," 3rd Ed., Cambridge University press (1991).
10. Nikiforov, G.D. and V.V. Redchits, Svar. Proiz, No. 8, pp. 53 (1977).

## **Martensite Start Temperature as a Weldability Index**

D.L. Olson, S. Liu, W. Wang,  
R.R.G.M. Pieters  
Colorado School of Mines  
Golden, Colorado  
S. Ibarra  
AMOCO Research  
Naperville, Illinois

Reprinted from  
**TRENDS IN WELDING RESEARCH**  
*Proceedings of the*  
4th International Conference  
5-8 June, 1995  
Gatlinburg, Tennessee

# **REPRINT**



**The Materials  
Information Society**

Copyright© 1996  
by  
**ASM International®**  
All rights reserved

No part of this book may be reproduced, stored in a retrieval system, or transmitted, in any form or by any means, electronic, mechanical, photocopying, recording, or otherwise, without the written permission of the copyright owner.

First printing, June 1996

Great care is taken in the compilation and production of this Volume, but it should be made clear that NO WARRANTIES, EXPRESS OR IMPLIED, INCLUDING, WITHOUT LIMITATION, WARRANTIES OF MERCHANTABILITY OR FITNESS FOR A PARTICULAR PURPOSE, ARE GIVEN IN CONNECTION WITH THIS PUBLICATION. Although this information is believed to be accurate by ASM, ASM cannot guarantee that favorable results will be obtained from the use of this publication alone. This publication is intended for use by persons having technical skill, at their sole discretion and risk. Since the conditions of product or material use are outside of ASM's control, ASM assumes no liability or obligation in connection with any use of this information. No claim of any kind, whether as to products or information in this publication, and whether or not based on negligence, shall be greater in amount than the purchase price of this product or publication in respect of which damages are claimed. THE REMEDY HEREBY PROVIDED SHALL BE THE EXCLUSIVE AND SOLE REMEDY OF BUYER, AND IN NO EVENT SHALL EITHER PARTY BE LIABLE FOR SPECIAL, INDIRECT OR CONSEQUENTIAL DAMAGES WHETHER OR NOT CAUSED BY OR RESULTING FROM THE NEGLIGENCE OF SUCH PARTY. As with any material, evaluation of the material under end use conditions prior to specification is essential. Therefore, specific testing under actual conditions is recommended.

Nothing contained in this book shall be construed as a grant of any right of manufacture, sale, use, or reproduction, in connection with any method, process, apparatus, product, composition, or system, whether or not covered by letters patent, copyright, or trademark, and nothing contained in this book shall be construed as a defense against any alleged infringement of letters patent, copyright, or trademark, or as a defense against liability for such infringement.

Comments, criticisms, and suggestions are invited, and should be forwarded to ASM International.

**ASM International®**

Library of Congress Catalog Card Number: 96-84776  
ISBN: 0-87170-567-2  
SAN: 204-7586

**ASM International®**  
Materials Park, OH 44073-0002

Printed in the United States of America

## Martensite Start Temperature as a Weldability Index

D.L. Olson, S. Liu, W. Wang, R.R.G.M. Pieters

Colorado School of Mines, Golden, Colorado

S. Ibarra

AMOCO Research, Naperville, Illinois

### Abstract

Traditionally, welding experts have used carbon equivalent type expressions, which include chemical composition and cooling rates, to determine the susceptibility of a steel and its weldment to hydrogen damage. Experimental diagrams that map cracking versus non-cracking behavior as a function of hydrogen and carbon equivalent have also been proposed for practical applications. More recently, however, there is a growing concern that the hydrogen distribution across the weldment is non-uniform. Depending on the hardenability of the heat affected zone (base metal) and the weld metal, the two regions may undergo austenite decomposition, more specifically, martensite transformation at different times. As a result of the earlier or later transformation of the weld metal (compared with the heat affected zone), hydrogen may accumulate in the weld metal or in the heat affected zone. Selective distribution of hydrogen will lead to decreased or increased hydrogen damage susceptibility of the welded joint. By investigating the martensite start temperature of the weld metal and of the base metal, together with the amount of hydrogen pickup, the hydrogen outgassing behavior and distribution across the weldment can be modeled.

THE DETERMINATION OF HYDROGEN damage susceptibility of steel weldments and the need for supplemental heat treatment prior to and/or after welding has been traditionally resolved by using various empirically determined expressions, such as the carbon equivalent and the  $P_{cm}$ . These expressions (1,2) sum coefficient-weighted compositional terms to produce a hardenability index for correlation. These calculated indices are often compared to previously established critical values. If the calculated value exceeds the critical value, then specific processing requirements for crack minimization are recommended. Figure 1 illustrates one effective use of the  $P_{cm}$  index with

diffusible hydrogen content to distinguish conditions where hydrogen cracking can occur in high strength steel weldments (3). In this particular example, a  $P_{cm}$  of 0.3 or greater is highly susceptible to cracking even at minimum diffusible hydrogen content. Low carbon equivalent alloys will be more tolerant to hydrogen cracking.

Primarily used as indicators of hard phase formation in the heat-affected zone, these hardenability indices come in many mathematical forms. Carbon equivalent type equations have been in use for almost forty years to correlate alloy composition with cracking susceptibility. The IIW carbon equivalent (CE) is given in the following:

$$CE = C + \frac{Mn}{6} + \frac{Cr + Mo + V}{5} + \frac{Ni + Cu}{15} \quad [1]$$

In this equation, the concentrations of the alloying elements are expressed in weight percent. As the carbon equivalent of an alloy increases, the likeliness of martensite and bainite formation will increase, as well as the cracking susceptibility.

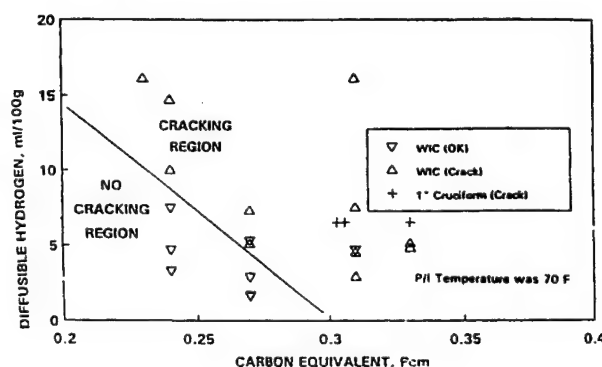


Figure 1. Criteria for hydrogen cracking susceptibility as a function of diffusible hydrogen content and  $P_{cm}$ .

In practice, welding engineers recommend preheat and postheat treatments for alloys according to their carbon equivalent values:

Preheat - 0.60 wt. pct. > CE > 0.45 wt. pct.

Pre-and Postheat - CE > 0.60 wt. pct.

Aside from the carbon equivalent, there are other cracking susceptibility equations developed specifically for particular steel groups such as the microalloyed steels. An example of such expressions for the microalloyed low carbon steel grade is the  $P_{cm}$ , which is given below:

$$P_{cm} = C + \frac{Si}{30} + \frac{Mn}{20} + \frac{Cu}{20} + \frac{Ni}{60} + \frac{Cr}{20} + \frac{Mo}{15} + \frac{V}{10} + 5B \quad [2]$$

Note that the coefficients for the alloying elements in this equation are different from those coefficients found in the CE equation. The fact that the coefficients are different indicates the empiricism of these equations, generally developed for a particular sample population. As a result, the successful application of these equations will also be limited to the particular type of steels from which the coefficients were derived.

Liu et al. (4) have investigated the proper form of these expressions based on thermodynamic and kinetic concepts. For higher alloy contents, interaction effects require the introduction of cross-product terms such as CMn and MnSi for better prediction of carbon equivalent equations. Onsoien et al. (5) have reported a  $P_{cmo}$  index that includes oxygen content for the prediction of microstructure-property relationships in gas metal arc weld metals.

One significant short coming of these traditional expressions is that they do not consider cooling rate which is essential in considering the evolution of steel weld microstructure. As such, these carbon equivalent expressions can only be used in the comparisons involving similar heat inputs and plate thickness. Only recently, comprehensive expressions that incorporate cooling rates have been developed to predict microstructurally sensitive properties such as hardness in the heat affected zone (6,7,8). Among these, the Yurioka equation (7) provided the best correlation between measured and calculated maximum hardness values,  $H_{max}$ , in the coarse grained heat-affected zone.

$$H_{max} = 422C + 99CE_{II} + 206 + (402C - 90CE_{II} + 80) \cdot \arctan(x) \quad [3]$$

where

$$x(rad) = \frac{\log \Delta t_{8/5} - 2.3CE_I - 1.35CE_{III} + 0.882}{1.15CE_I - 0.673CE_{III} - 0.601} \quad [4]$$

In Equations 3 and 4, the  $CE_I$ ,  $CE_{II}$ , and  $CE_{III}$  terms represent the chemical composition effect of the alloy. The

mathematical forms of these carbon equivalents are given in the following:

$$CE_I = C + \frac{Si}{24} + \frac{Mn}{6} + \frac{Cu}{15} + \frac{Ni}{12} + \frac{Cr}{8} + \frac{Mo}{4} + \Delta H \quad [5]$$

$$CE_{II} = C + \frac{Si}{24} + \frac{Mn}{5} + \frac{Cu}{10} + \frac{Ni}{18} + \frac{Cr}{5} + \frac{Mo}{2.5} + \frac{V}{5} + \frac{Nb}{3} \quad [6]$$

$$CE_{III} = C + \frac{Mn}{3.6} + \frac{Cu}{20} + \frac{Ni}{9} + \frac{Mo}{4} \quad [7]$$

$\Delta H$  in Equation 5 is a function of boron and nitrogen content.

Despite the excellent reported predictive capability of these equations, they still suffer from the same restrictions as the simpler, regressionally determined equations in that their application must be limited to a restricted group of steels and environmental conditions (e.g. hydrogen content) and stress state. Since the occurrence of hydrogen cracking requires a susceptible microstructure, sufficient diffusible hydrogen content and sufficient tensile stress, new expressions which are sensitive to factors other than just microstructure must be developed.

Recently, Karppi and Nevasmaa (9) introduced a method (VTT/OU method) that uses specific indices, which include  $\Delta t_{8/5}$ , steel composition, and diffusible hydrogen content to predict the tendency for hydrogen cracking. Their method incorporates this information into an expression whose magnitude is compared to a calculated critical value which included a stress severity parameter dependent on the groove and bead geometry, net stress across the weld throat, the restraint intensity, and a safety factor. They demonstrated the capability of the methodology for specific welding practices and materials.

Even though the predictive approaches are becoming more comprehensive in their efforts to incorporate all variables, these approaches still need to address the fact that the hydrogen content is non uniform across the weldments. This paper will consider the influence of hydrogen transport in the weldment on the resultant non-uniform hydrogen distribution. The effect of hydrogen damage is magnified when the location of the susceptible microstructures (martensite) overlaps the localized high hydrogen content.

### Hydrogen Transport and Distribution

The hydrogen content in a weldment is dependent on both the hydrogen source and the ability of the weldment to transport hydrogen from the weld metal to the heat affected zone. The transport aspect becomes important because of the higher solubility but much lower diffusion rate of hydrogen in austenite (FCC) compared to ferrite and martensite (10). As a result of this differential hydrogen diffusivity, different amounts of hydrogen may be retained in the coarse grained heat-affected zone of a weldment depending on the austenite

decomposition behavior of the alloys. Additionally, because different locations in the heat-affected zone have different thermal experiences, and therefore, exhibit different austenite-to-martensite/ferrite transformation behavior, the hydrogen transport and distribution in the heat affected zone will be non-uniform (11,12).

Christensen et al. (13) were the first to measure the spatial distribution of weld metal hydrogen. Their results, shown in Figure 2, show the non-uniform distribution of hydrogen in a vertical cross-section of the weld deposit and the heat affected zone. Evans et al. (14) also reported on the hydrogen distribution along the length and across the weld deposit, and indicated transient end effects. The non-uniform distribution of weld metal hydrogen becomes even more complex in multiple pass welds because of the overlapping thermal cycles. It becomes apparent that a major difficulty arises in correlating hydrogen cracking to measured diffusible hydrogen content because of current inability to define where the hydrogen is concentrated in the weldment.

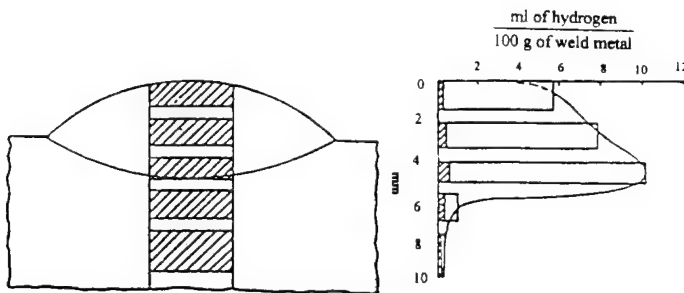


Figure 2. Hydrogen distribution in a vertical cross section of a steel weld deposit and the heat-affected zone.

Kronshtal and Kharin (15) have shown that the heterogeneity of microstructure and the thermal gradient in a hydrogen-saturated steel block strongly influence the diffusion of hydrogen and the resulting hydrogen distribution. They showed that the solubility and transport differences between two regions, such as ferrite and austenite, and the large thermal gradients across these regions can result in localized high concentrations at specific locations.

Musiychenko and Kasatkin (16) compared the hydrogen distribution across the fusion line of a steel weldment. They investigated two cases, considering different initial weld metal hydrogen contents and different degrees of preheating, and found the peak hydrogen content in one case in the heat affected zone but adjacent to the fusion line, and in the other case, in the weld metal, as illustrated in Figure 3. In this figure,  $C_1$  represents the compositional profile for hydrogen when welding without preheat, and  $C_2$  represents the compositional profile under the influence of a typical preheat.

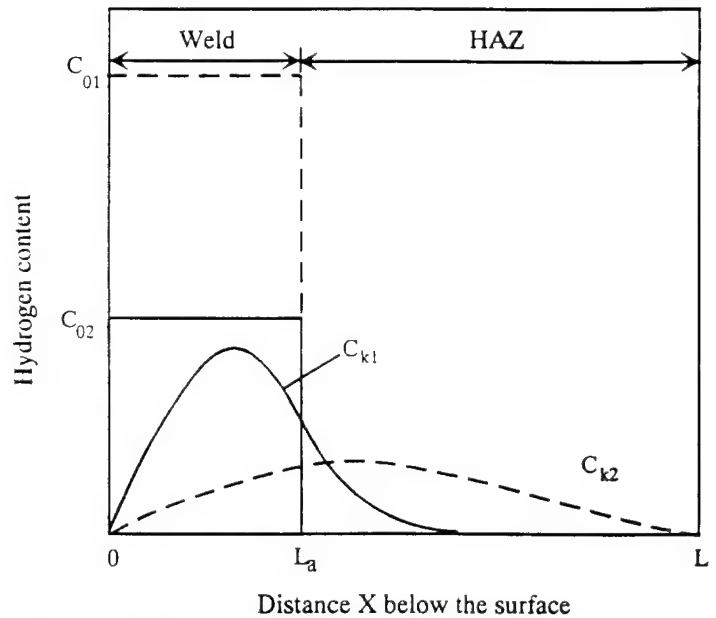


Figure 3. The hydrogen distribution across the fusion line of a weldment for two cases which represent different initial hydrogen content and preheat treatment experience (16).

Using a laser beam spot fusion technique coupled with mass spectrometric analysis of evaporative hydrogen, Tarlinski (17) performed a hydrogen analysis by traversing the weld. Figure 4 illustrates the localized concentration of hydrogen at the fusion line.

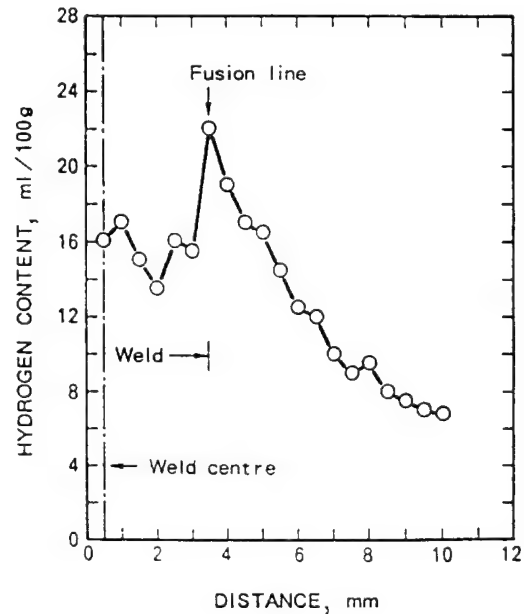


Figure 4. Hydrogen distribution across the weld fusion line (17).

Yurioka and Ohshita (18) used finite difference analysis to evaluate the influence of both stress concentration and preheat treatment on the hydrogen content distribution in steel weldments. Their results, as shown in Figure 5, suggest



a highly localized hydrogen concentration developing in the weld toe area and along the fusion line. This computed result was produced by using a potential which relates to the localized stress state. The weld toe is a common location for the initiation of underbead cracking. They found that the hydrogen concentration at the weld toe increased with time after welding and could potentially reach values susceptible to cracking. This increase in localized hydrogen content was attributed to hydrogen transport due to localized stress gradients. This "up hill" stress-driven transport was very sensitive to the preheat treatment. The calculations suggest that the proper preheat treatment will alleviate such localized buildup of hydrogen.

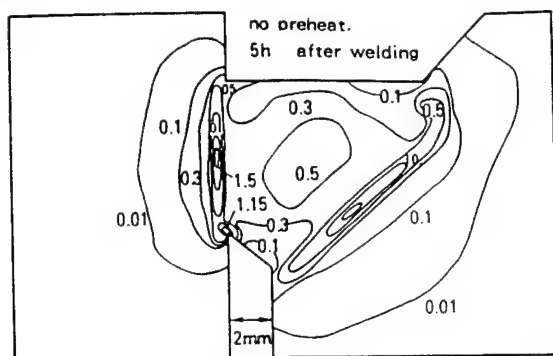


Figure 5. Calculated compositional distribution of hydrogen relative to the various positions of a steel weldment. This distribution was attributed to stress gradient-driven hydrogen transport (18).

A significant factor for the transport of hydrogen is the time that the iron matrix remains at a certain temperature and in a specific phase. For the higher strength steels, the martensite start temperature indicates a transition during cooling between the slow and fast diffusion rates. The higher the martensite start temperature, the larger will be the temperature range available for rapid hydrogen transport in the ferrite (BCC) or martensite (BCT) phase, and more hydrogen will be transported away from the coarse grained heat affected zone to the less hydrogen susceptible fine grained heat affected zone. Thus, the martensite start temperature is both a measure of the microstructure evolution and the ability to have available a phase for rapid hydrogen transport.

#### Martensite Start Temperature Expressions

The effect of specific alloying additions on the martensite start temperature is commonly represented by the formulations of Andrews (19) and shown in Equation 8:

$$M_s = 539 - 423C - 30.4Mn - 17.7Ni - 12.1Cr - 7.5Mo \quad [8]$$

The Andrews equation has been of great use since 1965, and the predictions are quite accurate for alloyed steels with a 6 wt. pct. max. carbon, 4.9 wt. pct. max. manganese, 5.0 wt. pct. max. chromium, 5.0 wt. pct. max. nickel, and 5.4 wt.

pct. max. niobium. Self et al. (20-22) developed more comprehensive expressions for both the HAZ and weld metal which are able to predict the martensite start temperature over a large compositional range. These expressions are given as follows:

#### Plate

$$M_s = 521 - 350C - 14.3Cr - 17.5Ni - 28.9Mn - 37.6Si - 29.5Mo - 1.19CrNi - 23.1(Cr + Mo)C \quad [9]$$

#### Weld Metal

$$M_s = 521 - 350C - 13.6Cr - 16.6Ni - 25.1Mn - 30.1Si - 20.4Mo - 40Al - 1.07CrNi + 21.9(Cr + 0.73Mo)C \quad [10]$$

Since a weldment is a composite of weld metal, heat affected zone and unaffected base metal, the differences in martensite start temperature for the weld deposit and base plate will influence whether the weld deposit or the heat affected zone has the greatest accumulation of hydrogen and resulting cracking susceptibility.

As discussed earlier, a result of the significant difference in the hydrogen diffusion coefficient and solubility in austenite and ferrite, the temperature at which the steel transforms to ferrite or martensite will affect the degree of hydrogen transport. When welding, the temperature and time at which the weld metal and base metal transform are different and therefore, two cases can be considered:

**Case 1: Weld Metal with Lower  $M_s$  Temperature than the HAZ.** This case can be described as a situation where the weld metal is overmatched with respect to the base plate. With higher alloying content, the weld metal exhibits higher strength than the base metal, and the austenite decomposition temperature is depressed to below that of the base metal. While the austenite in the HAZ has begun decomposition, the austenite in the weld metal remains unchanged. For a period of time the HAZ immediately adjacent to the fusion zone will transport hydrogen at a high rate compared to the weld metal. If this HAZ martensite start ( $M_s$ ) temperature is sufficiently high, the hydrogen will be able to diffuse a significant distance into the parent metal. However, the hydrogen transport cannot proceed extensively until the weld metal transforms because austenite has the ability to store high hydrogen contents, but can not move it fast enough to the fusion line. After the weld transforms, especially at a moderately elevated temperature, the localized hydrogen content in the hard microstructure adjacent to the fusion line can potentially be reduced, thus reducing the hydrogen cracking susceptibility.

If the weld metal  $M_s$  temperature is too low, the hydrogen transport from the weld metal will be limited and very little hydrogen can get to the heat affected zone adjacent to the fusion line. Even though hydrogen diffusion will increase with the martensite transformation, the



reduction in content may not be fast enough to avoid weld metal cracking.

To demonstrate the effect of martensite start temperature on hydrogen transport, the diffusion process was modeled considering incremental time and temperature decreases according to the welding heat input and cooling rate. Austenite decomposition was allowed to occur in the HAZ and weld metal, but at different times. Simple but reasonable boundary conditions were established for results in the accumulation of hydrogen in the weld pool and the solution of Fick's 2nd law. Several hydrogen profiles were determined, and it was observed that this situation may promote hydrogen cracking in the weld deposit which has been observed for some high strength weldments. Figure 6 illustrates the diffusible hydrogen distribution for the case where the HAZ  $M_s$  temperature is much greater than the weld metal  $M_s$  temperature, and for a specific location, as indicated at the top of the weld.

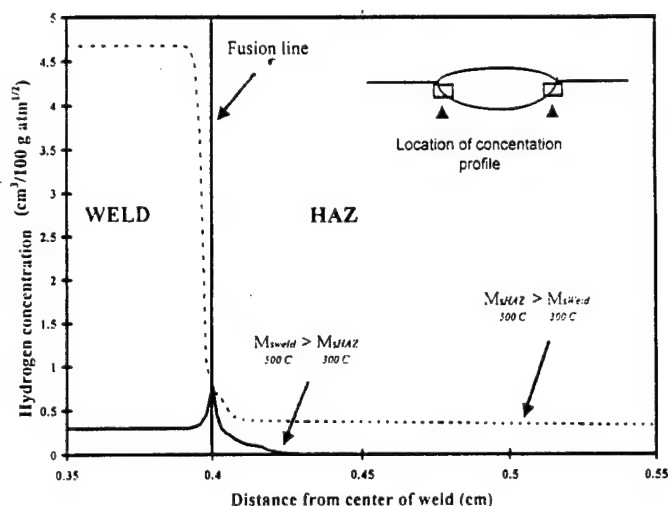


Figure 6. Hydrogen distributions across the fusion line of a steel weldment for  $M_{s, \text{weld}} > M_{s, \text{HAZ}}$  and  $M_{s, \text{weld}} < M_{s, \text{HAZ}}$ .

**Case 2: HAZ with Lower  $M_s$  Temperature Than the Weld Metal.** This case can be described as a situation where the weld metal is undermatched with respect to the base plate. Since the heat affected zone transforms from austenite to ferrite at lower temperatures and at later times than the weld metal, the HAZ then becomes an austenitic diffusion barrier for hydrogen transport resulting in a high hydrogen accumulation in the heat affected zone, adjacent to the fusion line. This situation promotes underbead hydrogen cracking. Figure 6 also plots the hydrogen profile obtained in calculation following the modeling procedure outlined in Case 1. Instead of having high hydrogen concentrations in the weld metal, the hydrogen peak is observed at the fusion line. Hydrogen accumulation in the weld metal also agrees with the typical observation that hydrogen cracking can occur both at a short distance (a few grain diameters) from

the fusion line (austenite), and either at the heat-affected zone or in the weld deposit.

The modeling results clearly demonstrate that hydrogen crack susceptibility and location of cracking depend on:

1. The martensite start temperature ranges
2. Whether the weld metal or HAZ has the lower  $M_s$  temperature
3. The magnitude of  $M_s$  temperature difference for the HAZ and weld metal

Further considering the  $M_s$  temperature equations presented earlier, it is possible to obtain a  $\Delta M_s$  temperature expression, and the sign and magnitude of this  $\Delta$  expression will determine the hydrogen diffusion behavior:

$$\Delta M_{s, \text{HAZ}} = M_{s, \text{HAZ}} - M_{s, \text{WM}}$$

If  $\Delta M_s$  temperature  $> 0$ , hydrogen accumulation will be in the weld metal. If  $\Delta M_s$  temperature  $< 0$ , hydrogen accumulation in the HAZ is possible and underbead cracking may occur.

In summary,  $M_s$  and  $\Delta M_s$  temperatures are extremely useful in the characterization of hydrogen diffusion and distribution in the weld metal. Special experimental set-ups must be developed to precisely determine the location of the hydrogen accumulation and to further refine the coefficients of the  $M_s$  temperature equation for improved correlation ability. Also, a weld metal  $M_s$  temperature expression which incorporates the influence of the weld metal oxygen content needs to be determined to better describe the effect of oxide inclusions on austenite decomposition kinetics. It is anticipated that  $\Delta M_s$  temperature vs.  $(M_{s, \text{HAZ}})(\Delta t_{5/1})$  plots (where  $\Delta t_{5/1}$  is the time to cool from 500 to 100°C) can give significant improvement in predicting the nature and tendency of hydrogen cracking in high strength weldments.

### Acknowledgment

The authors acknowledge and appreciate the research support of the Office of Naval Research.

### References

1. S. Liu, S. Ibarra, and D.L. Olson, Offshore Technology Conference Proceedings, IOTC 7597, pp. 299-306 (1994).
2. C.D. Lundin, T.P.S. Gill, C.Y.P. Gao, Y. Wang, and K.K. Khan, 'Carbon Equivalence and Weldability of Microalloyed Steels', Ship Structure Committee Report SSC-357, U.S. Coast Guard, Washington, DC (1991).
3. R. Wong, U.S. Navy, CDNSWC, Private Communication (1995).

4. S. Liu, D.L. Olson, and D.K. Matlock, *J. Heat Treating* **4** (4), pp. 309-316 (1986).
5. M.I. Onsoien, S. Liu, and D.L. Olson, "Shielding Gas Oxygen Equivalent in Weld Metal Microstructure Optimization", submitted to *Welding Journal* (1995).
6. K. Lorenz and C. Duren, *IIW Doc. IX-B-11-82*, pp. 1-36 (1982).
7. N. Yurioka and H. Suzuki, *International Materials Reviews*, **35** (4), pp. 217-149 (1990).
8. A.O. Kluken, S. Ibarra, S. Liu, and D.L. Olson, *Offshore Mechanics and Arctic Engineering, Materials Engineering*, vol. A, pp. 1-7 (1992).
9. R.A.J. Karpil and P. Nevasmaa, "Contribution to Comparison of Methods for Determining Welding Procedures for the Avoidance of Hydrogen Cracking", *VTT Publ. #107*, Espoo, Finland, *IIW Doc. IX-1673-092* (1992).
10. Th. Bollinghaus, H. Hoffmeister, and A. Dangeleit, "A Scatterband for Hydrogen Diffusion Coefficients in Microalloyed and Low Carbon Structural Steels", *IIW Document IX-1767-94*, AWS, American Council, Miami, FL (1994).
11. H. Granjon, "Cold Cracking in Welding of Steels", *Int. Symposium on Cracking and Fracture in Welds, Conf. Proc., Japan Welding Society IB*, 1.1 (1971).
12. B.A. Graville, "Hydrogen Cracking Sensitivity of HSLA Steels", *The Metallurgy, Welding, and Qualification of Microalloyed (HSLA) Steel Weldments*, *Int. Conf. Houston*, pp. 127 (1990).
13. N. Christensen, I. Gjermundsen, and R. Rose, *Brit. Weld. J.*, pp. 272-281 (1958).
14. G.M. Evans, "Diffusion of Hydrogen in Mild Steel Metal Arc Weldments", *Reprints from Schweiss Mitteilungen, Oerlikon Report* (1977).
15. O.V. Kronshtal and V.S. Kharin, *Soviet Materials Science* **28** (5), pp. 475-586, May (1993).
16. V.F. Musiyachenko and S.B. Kasatkin, *Automatic Welding*, pp. 22-26, September (1985).
17. V.D. Tarlinski, *Avtom. Svarka* **27** [6], 16-20 (1974).
18. N. Yurioka and S. Ohshita, "An Analysis of Effect of Microstructure, Strain, and Stress on the Hydrogen Accumulation in HAZ", *IIW Doc. IX-1161-80* (1980).
19. K. Andrews, *JISI*, **203**, pp. 721-727 (1985).
20. J.A. Self, D.K. Matlock, and D.L. Olson, *Welding Journal* **63** (9), pp. 282s-288s (1984).
21. J.A. Self, D.L. Olson, and G.R. Edwards, "The Stability of Austenitic Weld Metal", *Cryogenic Properties of Metals*, NBS Publication, pp. 181-189, Boulder, Colorado (1987).
22. J.A. Self, B.F. Carpenter, D.L. Olson, and D.K. Matlock, "Phase Transformation and Alloy Stability in Fe-Mn-Ni-Cr-Al Weld Metal", "Alternate Alloying for Environmental Resistance", pp. 37-46 (1987).

## USE OF MARTENSITE START TEMPERATURE FOR HYDROGEN CONTROL

W.W. Wang<sup>1</sup>, R. Wong<sup>2</sup>, S. Liu<sup>1</sup>, and D.L. Olson<sup>1</sup>

<sup>1</sup>Center for Welding, Joining, and Coatings Research  
Colorado School of Mines  
Golden, Colorado

<sup>2</sup>Naval Surface Warfare Center Carderock Division  
Carderock, Maryland

### Abstract

There is a growing concern that the hydrogen distribution across a weldment is non-uniform. Depending on the hardenability of the base metal (heat affected zone) and the weld metal, these two regions may undergo austenite decomposition, more specifically martensite transformation, at different times. As a result of the earlier or later transformation of the weld metal (compared with the heat affected zone), hydrogen may accumulate in the heat affected zone or in the weld metal. This behavior will lead to decreased or increased hydrogen damage susceptibility of the two regions and influence the location of the weldment most susceptible to cracking.

### Introduction

The determination of hydrogen damage susceptibility of steel weldments and the need for supplemental heat treatment prior to and/or after welding has been traditionally resolved by using various empirically determined expressions, such as the IIW carbon equivalent and the  $P_{cm}$  equations. These expressions (1,2) sum coefficient weighted compositional terms to produce a hardenability index for correlation. Figure 1 illustrates one effective use of the  $P_{cm}$  index with diffusible hydrogen content to identify conditions where hydrogen cracking can occur in high strength steel weldments (3). These calculated indices are often compared to some previously determined critical value. If the calculated value exceeds the critical value, then specific processing requirements for crack minimization are recommended.

One significant short coming of the traditionally used expressions is that they do not consider cooling rate which is essential in the consideration of microstructural evolution in steel welds. As such, these carbon equivalent expressions can only be used in the comparisons involving similar heat inputs, plate thickness and joint geometry. Only

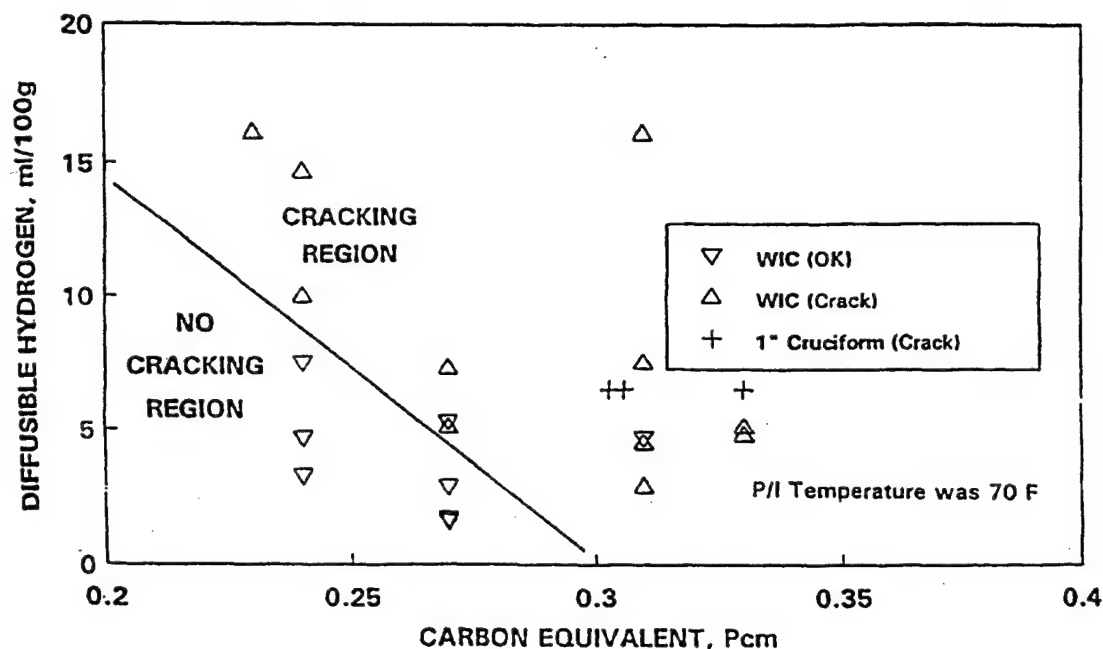


Figure 1. Criteria for hydrogen cracking susceptibility as function of diffusible hydrogen content and  $P_{cm}$  (3).

recently that more comprehensive expressions incorporating cooling rates have been developed to predict microstructural sensitive properties such as hardness in the heat affected zone (6,7,8).

Despite the excellent prediction capability of these improved expressions, they still suffer from the same restrictions as the regressionally-determined equations, in that their application must be limited to a restricted group of steels and environmental conditions (hydrogen content and stress state). Since the occurrence of hydrogen cracking requires a susceptible microstructure, sufficient localized diffusible hydrogen content and sufficient tensile stress, new expressions which are also sensitive to these latter factors must be developed to more reliably predict the cracking behavior.

Recently Karppi and Nevasmaa (9) introduced another method (VTT/OU method) of using specific indices, which include  $\Delta t_{8/5}$ , the composition of steel, and diffusible hydrogen content, to predict the tendency for hydrogen cracking. Their method incorporates this information into an expression whose magnitude is compared to a calculated critical value which included a stress severity parameter dependent on the groove and bead geometry, net stress across the weld throat, the restraint intensity, and a safety factor. They demonstrated how the methodology would work for specific welding practice and materials.

Even though the predictive algorithms are becoming more comprehensive with the incorporation of more process and material variables, these approaches still need to address

the fact that the hydrogen content is non-uniformly distributed across the weldments. This paper will consider the influence of hydrogen transport in the weldment on the resultant non-uniform hydrogen distribution. The effect of hydrogen damage is magnified when the location of the susceptible microstructures (martensite) overlaps the localized, high hydrogen content.

### Hydrogen Transport And Distribution

The hydrogen content in a weldment is dependent on both the hydrogen source and the ability of the weldment to transport hydrogen from the weld metal to the heat affected zone. The transport aspect becomes important because of the higher hydrogen solubility but lower hydrogen diffusion rate in austenite (FCC crystal structure), in contrast to ferrite and martensite which have orders of magnitude higher hydrogen diffusion coefficient than austenite (10). As a result of the differential hydrogen diffusivity in austenite compared to martensite/ferrite, different amounts of hydrogen may be retained in the coarse grained heat affected zone of a weldment according to the austenite decomposition behavior of the alloys. Since different locations in the heat affected zone will experience different thermal experience and, therefore, different austenite-to-martensite/ferrite transformation behavior, the hydrogen transport and distribution in the heat affected zone will be non-uniform (11,12).

Christensen et al. (13) was first to measure the spatial distribution of weld metal hydrogen. Their results, shown in Figure 2, show the non-uniform distribution of hydrogen in a transverse cross-section of the weld deposit and the heat affected zone. Evans et al. (14)

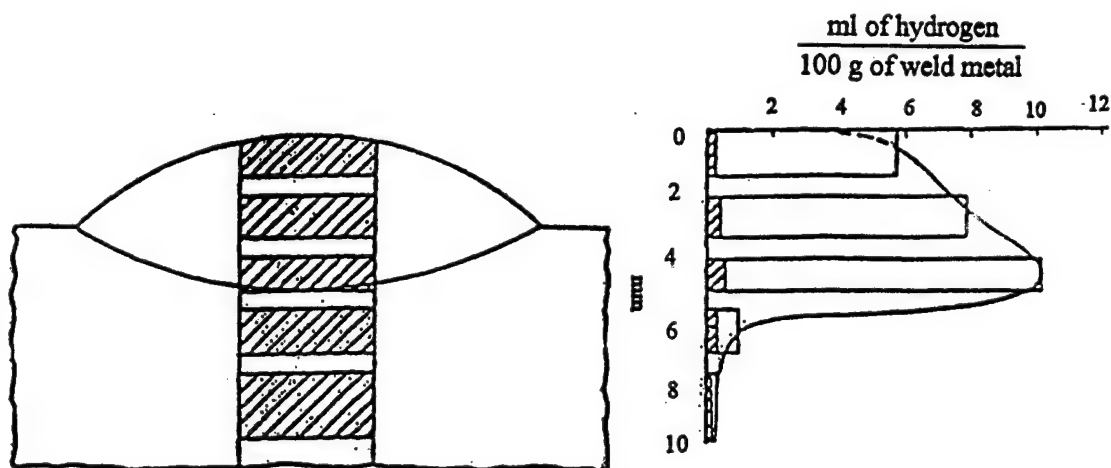


Figure 2. Hydrogen distribution in a vertical cross-section of a steel weld deposit and the heat affected zone (13)

reported the hydrogen distribution along the length of a weld and indicated transient end effects. The non-uniform distribution of weld metal hydrogen became even more complex in multiple pass welds because of the overlapping thermal cycles. The correlation of hydrogen cracking to measured diffusible hydrogen content is extremely difficult because of the inability to define where the hydrogen is concentrated in the weld metal.

Kronshtal and Kharin (15) have shown that the heterogeneity of microstructure and the thermal gradient in a hydrogen-saturated steel block strongly influence the diffusion of hydrogen and the resulting distribution of hydrogen in the steel block. They also showed that the solubility and transport differences between two regions, such as ferrite and austenite, and the large thermal gradients across the two regions can result in localized high hydrogen concentrations.

Musiyachenko and Kasatkin (16) compared the distribution of hydrogen content across the fusion line of a steel weldment. They considered the effects of different initial weld metal hydrogen contents and different degrees of preheating, and found the maximum in hydrogen content, in one case, in the heat affected zone but adjacent to the fusion line; and in the other case, the maximum hydrogen content was located in the weld metal. Figure 3 illustrates the two cases described.  $C_{k1}$  represents the compositional profile for hydrogen when welding without preheat and  $C_{k2}$  represents the hydrogen compositional profile under the influence of a typical preheat. Figure 3 clearly depicts the non-uniform distribution of hydrogen in a weldment and the influence of processing conditions.

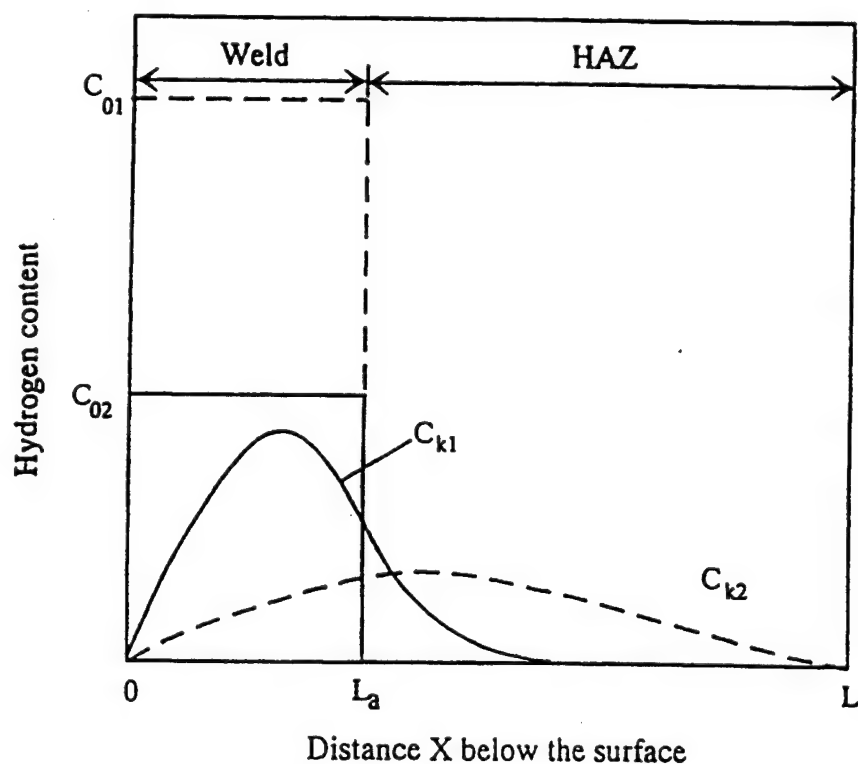


Figure 3. The hydrogen distribution across the fusion line of a weldment for two cases which represent different initial hydrogen content and preheat treatment experience (16).

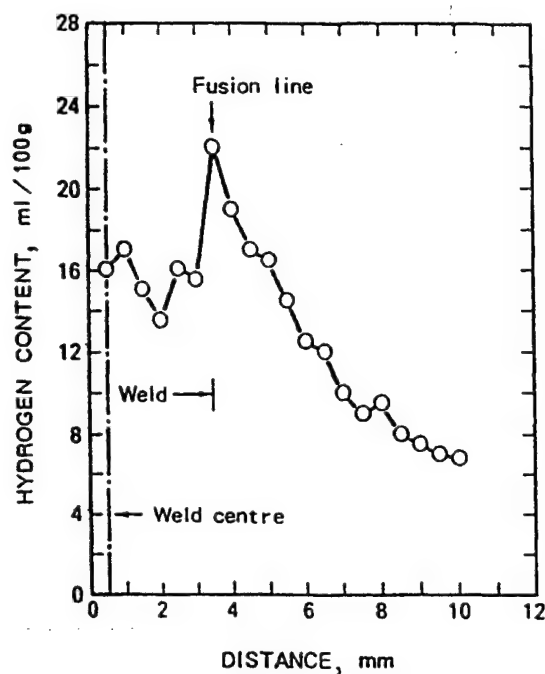


Figure 4. Hydrogen distribution across the weld fusion line (17).

Using a laser beam spot fusion technique coupled with mass spectrometric analysis of evaporative hydrogen, Tarlinski (17) performed a hydrogen analysis by traversing the weld. Figure 4 illustrates the localized concentration of hydrogen at the fusion line.

Yurioka and Ohshita (18) used finite difference analysis to evaluate the influence of both stress concentration and preheat treatment on the hydrogen content distribution in steel weldments. Their results, as shown in Figure 5, suggest a highly localized hydrogen concentration in the weld toe area and along the fusion line, which agrees with the general notion that the weld toe is a common location for the initiation of underbead cracking. They also found that the hydrogen concentration at the weld toe increased with time after welding and could potentially reach values susceptible to cracking. The accumulation of hydrogen in the weld toe region required "up-hill" diffusion of hydrogen assisted by localized stress gradients. This "up-hill" stress-driven transport was very sensitive to the preheat treatment. The calculations suggest that proper preheat treatment will alleviate such localized buildup of hydrogen.

A significant factor for the transport of hydrogen is the time that the iron matrix remains at a certain temperature and as a specific phase. Traditionally, martensite start temperature has been used as indicators of the alloy hardenability and austenite stability. For the higher strength steels, however, the martensite start temperature can also indicate a transition during cooling between the slow and fast diffusion rates of hydrogen. The higher the martensite start temperature, the larger will be the temperature range available for rapid hydrogen transport in the ferrite (BCC) or martensite (BCT) phase, and more hydrogen



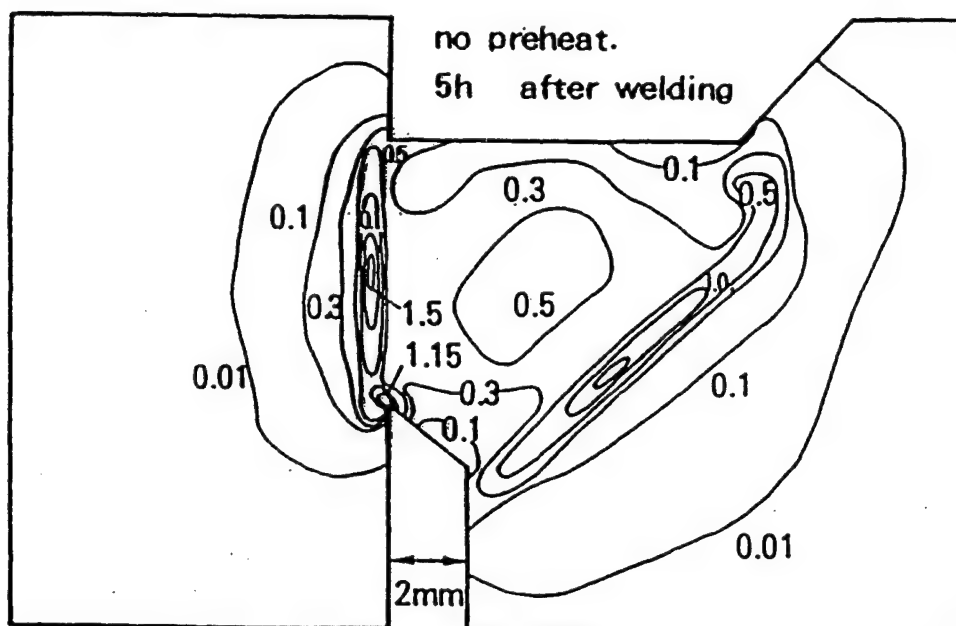


Figure 5. Calculated composition distribution of hydrogen relative to the various positions of a steel weldment. This distribution was attributed to stress gradient-driven hydrogen transport (18).

will be transported away from the coarse grained heat affected zone to the less hydrogen susceptible fine grained heat affected zone. Thus, the martensite start temperature is both a measure of the microstructure evolution and the ability to have available a phase (ferrite/martensite) for rapid hydrogen transport (11,12).

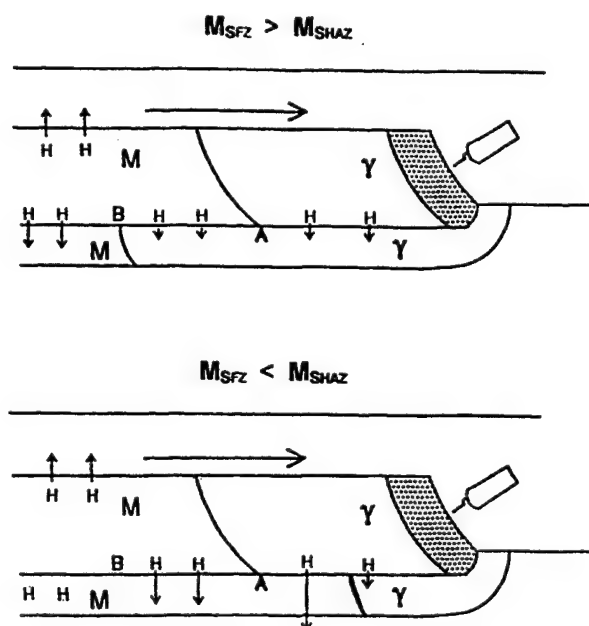


Figure 6. Illustration of hydrogen diffusion at different martensite start temperatures for weldment and base metal (11).

Granjon (11) introduced a conceptual model which describes how the austenite-ferrite (or austenite/martensite) phase transformation in steel weldments affects the resulting hydrogen distribution. Two cases are illustrated in Figure 6. When the austenite-martensite transformation in the fusion zone occurs at a higher temperature than the heat affected zone diffusible hydrogen will segregate in the heat affected zone just under the fusion line. This HAZ region is, oftentimes, the location of underbead cracking in high strength steel weldments. On the other hand, when the martensite transformation in the heat affected zone occurs at a higher temperature than in the fusion zone, it is possible that excess hydrogen contents may result in the weld metal. This situation could promote weld metal hydrogen cracking or micro-fissuring.

Graville (12) has calculated the hydrogen distribution for the situation where the base and weld metal have different transformation temperatures. Figure 7 illustrates his results for one combination of material and three different annealing temperatures. Significant location variations in hydrogen contents are found at the boundary region of the two materials.

#### Martensite Start Temperature Expressions

The effect of specific alloying additions on the martensite start temperature has been investigated by Andrews (19) and one of his formulations is shown in Equation 1:

$$M_{s(\text{Andrews})} (^{\circ}\text{C}) = 539 - 423\text{C} - 30.4\text{Mn} - 17.7\text{Ni} - 12.1\text{Cr} - 7.5\text{Mo} \quad (1)$$

The Andrews equation has been of great use since 1965 and the predictions are quite

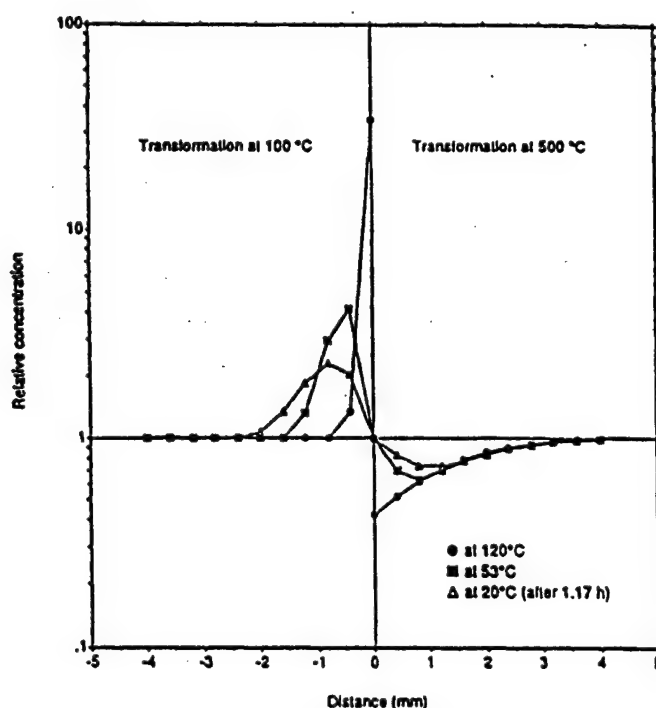


Figure 7. Distribution of hydrogen across a phase boundary at various temperatures (12).

accurate for alloyed steels with a 0.6 wt. pct. max. carbon, 4.9 wt. pct. max. manganese, 5.0 wt. pct. max chromium, 5.0 wt. pct. max. nickel, and up to 5.4 wt. pct. of molybdenum. Self et al. (20-22) developed more comprehensive expressions for both the HAZ and weld metal which are able to predict the martensite start temperature over a large compositional range. These expressions are given as follows:

#### Base Metal-HAZ

$$M_{s(\text{Self})} (^{\circ}\text{C}) = 521 - 350\text{C} - 143\text{Cr} - 17.5\text{Ni} - 28.9\text{Mn} - 37.6\text{Si} - 29.5\text{Mo} \\ - 1.19\text{Cr} \cdot \text{Ni} - 23.1(\text{Cr} + \text{Mo}) \cdot \text{C} \quad (2)$$

#### Weld Metal

$$M_{s(\text{Self})} (^{\circ}\text{C}) = 521 - 350\text{C} - 13.6\text{Cr} - 16.6\text{Ni} - 25.1\text{Mn} - 30.1\text{Si} - 20.4\text{Mo} \\ - 40\text{Al} - 1.07\text{Cr} \cdot \text{Ni} + 21.9(\text{Cr} + 0.73\text{Mo}) \cdot \text{C} \quad (3)$$

Since a weldment is a composite of weld metal, heat affected zone and unaffected base metal, the differences in martensite start temperature between the weld deposit and base metal will influence whether the weld deposit or the heat affected zone has the greatest accumulation of hydrogen and cracking susceptibility.

And as discussed earlier, because of the significant differences in the hydrogen diffusion coefficient and solubility in austenite and ferrite/martensite, the temperature at which the steel transforms to ferrite or martensite will affect the degree of hydrogen transport. During welding the temperature and time at which the weld metal and base metal transform are different and therefore, two cases can be considered.

Case 1: Weld Metal with Lower  $M_s$  Temperature than the HAZ. This case can be described as a situation where the weld metal is overmatching with respect to the base metal. With higher alloying content, the weld metal exhibits higher strength than the base metal and the austenite decomposition temperature is depressed to below that of the base metal. While the austenite in the HAZ has begun decomposition, the austenite in the weld metal remains unchanged. For a period of time the HAZ immediately adjacent to the fusion zone will transport hydrogen at a high rate compared to the weld metal. If HAZ martensite start temperature ( $M_s$ ) is sufficiently high, the hydrogen will be able to transport a significant distance into the parent metal. However, the hydrogen transport cannot proceed extensively until the weld metal transforms because austenite has the ability of storing high hydrogen contents but can not move it fast enough to the fusion line. Especially if the transformation occurs at a moderately elevated temperature, the situation described can potentially reduce the localized hydrogen content in the hard microstructure adjacent to the fusion line, thus reducing the hydrogen cracking susceptibility.

If the weld metal  $M_s$  temperature is too low then the hydrogen transport from the weld metal will be limited and very little hydrogen can reach the heat affected zone adjacent to the fusion line which may eventually lead to weld metal cracking.

To demonstrate the effect of martensite start temperature on hydrogen transport, the diffusion process was modeled considering incremental time periods and temperature decreases according to the welding heat input and cooling rate. Austenite decomposition was allowed to occur in the HAZ and weld metal, but at different times. Simple but reasonable boundary conditions were established for the solution of Fick's 2nd law. Several hydrogen profiles were determined and the traced line in Figure 8 illustrates the diffusible hydrogen distribution for the case where HAZ  $M_s$  temperature is greater than the weld metal  $M_s$  temperature, and for a location at the top of the weld. This situation is prone to promote hydrogen cracking in the weld deposit which has been observed for some high strength weldments.

Case 2: HAZ with Lower  $M_s$  Temperature Than the Weld Metal. This case can be described as a situation where the weld metal is undermatched with respect to the base metal. Since the heat affected zone transforms from austenite to ferrite at lower temperatures and at later times than the weld metal, the HAZ then becomes an austenitic diffusion barrier for hydrogen transport, resulting in a high hydrogen accumulated in the heat affected zone, adjacent to the fusion line. This situation promotes underbead hydrogen cracking. Figure 8 also plots the hydrogen profile (solid line) obtained in calculation following the procedure outlined in Case 1. Instead of having high hydrogen concentration in the weld metal, hydrogen peaks are observed in the heat affected zone. This profile

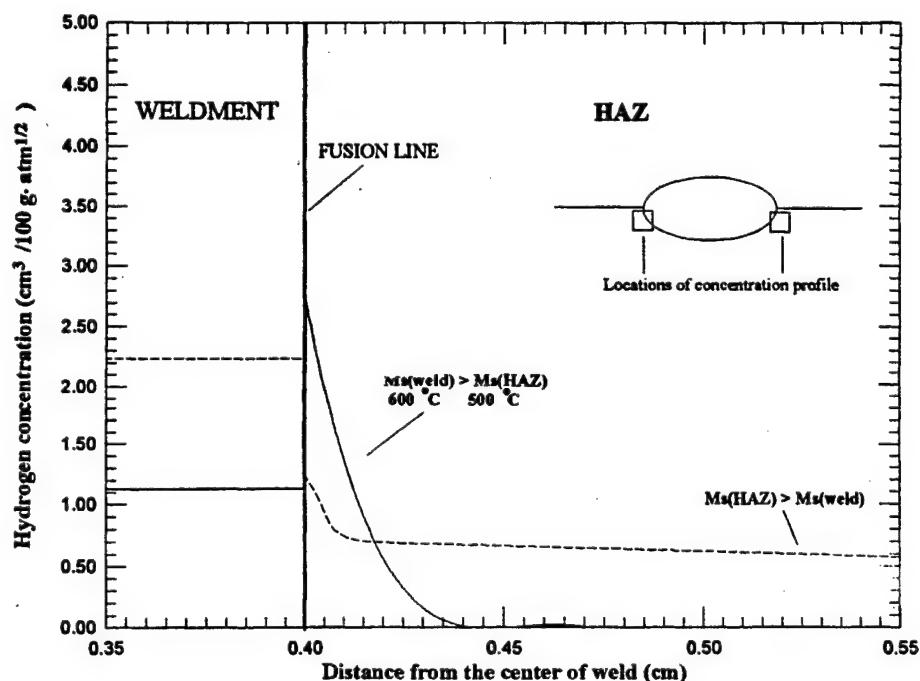


Figure 8. Hydrogen distributions across the fusion line of a steel weldment for  $M_s \text{ weld} > M_s \text{ HAZ}$  and  $M_s \text{ weld} < M_s \text{ HAZ}$ .

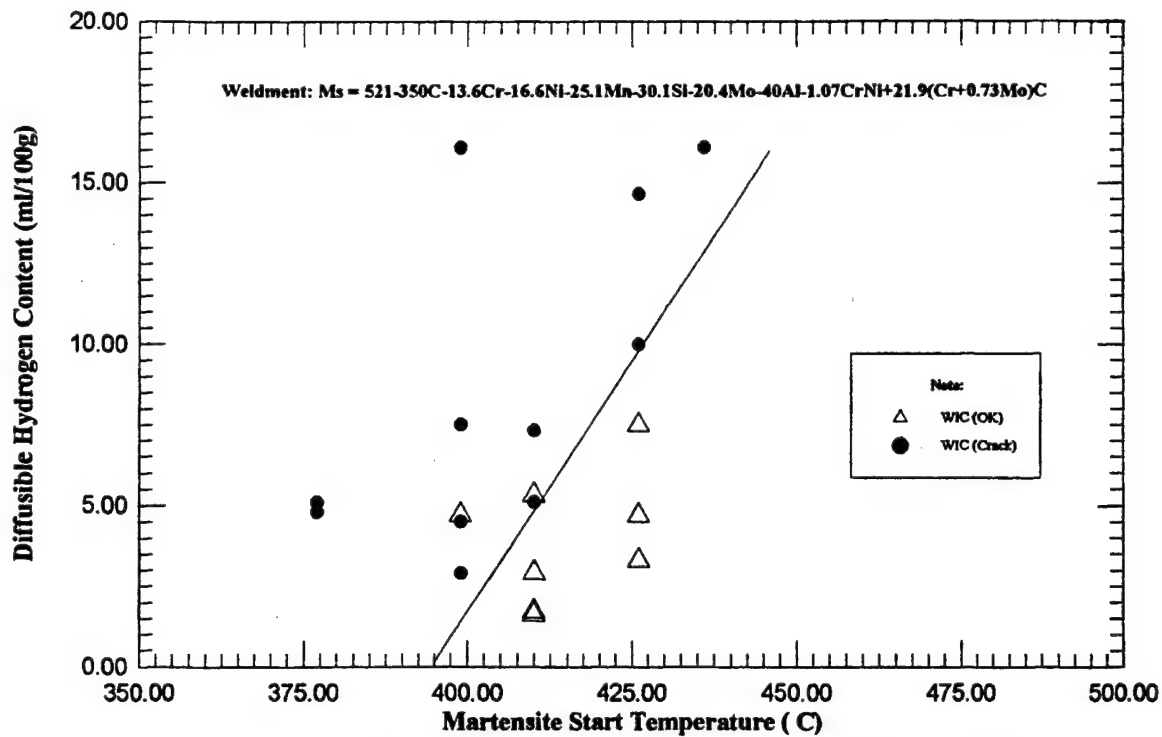


Figure 9. Illustration of hydrogen cracking/uncracking zones by hydrogen content and martensite start temperature.

supports the hydrogen distribution model as proposed. The hydrogen accumulation in the weld metal also agrees with the typical observation of hydrogen cracking being limited to a few grains (austenite) adjacent to the fusion line. Thus, HAZ with lower  $M_s$  temperature may result in underbead hydrogen cracking and localized weld metal cracking along the fusion line.

To evaluate the ability of using the martensite start temperature as a hydrogen cracking index, the diffusible hydrogen content was plotted as a function of weld metal martensite start temperature (calculated using the Self Equation) for welds made on the same base metal. Figure 9 illustrates a demarcation line between the cracked and the uncracked weldments. Comparing Figure 9 with Figure 1 it is apparent that the martensite temperature is as good, and maybe better than the  $P_{cm}$  index in determining cracking susceptibility.

In summary, the modeling results clearly demonstrate that hydrogen crack susceptibility and location of cracking depend on:

1. The martensite start temperature ranges.
2. Whether the weld metal or HAZ has the lower  $M_s$  temperature.
3. The magnitude of  $M_s$  temperature difference for the HAZ and weld metal.

Further considering the  $M_s$  temperature equations presented earlier, it is possible to obtain a  $\Delta M_s$  expression, and the sign and magnitude of this  $\Delta M_s$  expression will determine the hydrogen diffusion behavior:

$$\Delta M_s = M_{s(WM)} - M_{s(BM)} \quad (4)$$

If  $\Delta M_s < 0$ , hydrogen accumulation will be in the weld metal. If  $\Delta M_s > 0$ , hydrogen accumulation in the HAZ is possible and underbead cracking may occur. Plotting weld cracking data on a  $\Delta M_s$  versus diffusible hydrogen content map, Figure 10, shows that  $\Delta M_s$  may suggest some promise as a indicator for hydrogen effects on cracking. A boundary line was drawn to delimit safe (no crack) and unsafe (crack) welding regions for high strength steels.

A conceptual view of the use of  $\Delta M_s$  is shown in Figure 11 where  $\Delta M_s$  is related with the HAZ  $M_s$  and  $\Delta t_{5/1}$ . The term  $\Delta t_{5/1}$  denotes the time that a weld cools from 500 to 100°C which represents the time of fast diffusion of hydrogen in ferrite or martensite. The value of  $\Delta M_s$  would indicate location of cracking, weld metal or HAZ, and the product of  $M_{sHAZ} \Delta t_{5/1}$  is an indication of the ability to transport hydrogen in the weldment. Figure 11 illustrates the predicted tendency for hydrogen cracking by delineating the boundary between cracking and no-cracking for welds of constant hydrogen content. If  $\Delta M_s$  has a large positive value then the weldment is susceptible to HAZ cracking. If  $\Delta M_s$  has a large negative value, then cracking may be expected to occur in the weld deposit. For large  $\Delta M_s$ , whether positive or negative, the cracking region is expanded, with the cracking/no cracking boundary shifted to the right. This observation indicates that for a weldment with a large positive  $\Delta M_s$ , even for an increased  $\Delta t_{5/1}$ , the hydrogen transport in the HAZ would not be sufficient to remove the large amount of hydrogen "released" from the weld metal during austenite decomposition to a safe level for no-cracking. In the case of large negative  $\Delta M_s$ , the high solubility of hydrogen in austenite retains the hydrogen in the weld metal

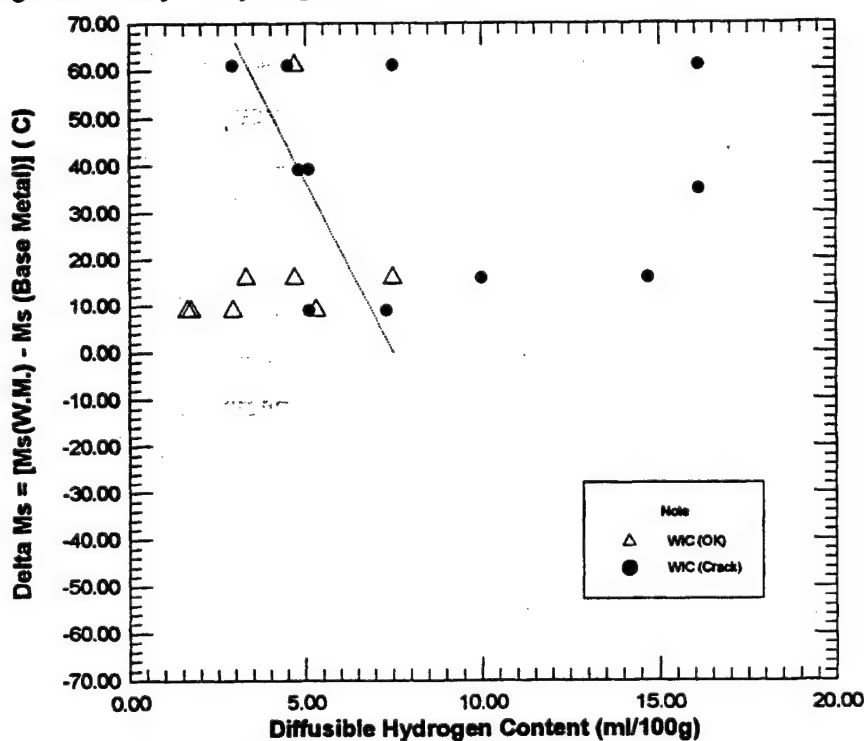


Figure 10. Hydrogen cracking indicated by the martensite start temperature difference between weldment and base metal.

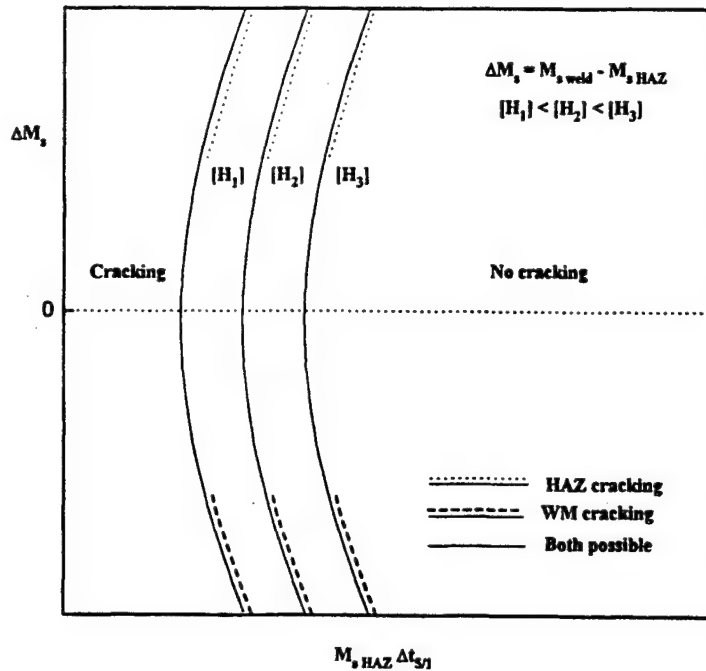


Figure 11. Conceptual illustration of cracking prediction.

that by the time it transforms, the temperature would be too low for massive outgassing, thus, expanding the cracking region. As the hydrogen content increases the demarcation line between cracking and non-cracking is moved to the right with higher and short cooling rates.

Some preliminary hydrogen cracking data is plotted as  $\Delta M_s$  as a function of  $M_s$  HAZ in Figure 12. The  $\Delta t_{5/1}$  is assumed constant for this data since constant welding condition and test specimen dimensions were used. Figure 12 does indicate some ability to establish a demarcation line between cracking and non cracking. Further work is necessary to evaluate the correlation between cracking and  $\Delta M_s$  since the limited data suggests a trend inconsistent with the conceptual diagram (Figure 11).

In summary,  $M_s$  and  $\Delta M_s$  temperatures are potentially useful in the characterization of hydrogen diffusion and accumulation in the weld metal. Special experimental set-ups must be developed to precisely determine the location of the hydrogen accumulation and to further refine the coefficients of the  $M_s$  temperature equation for improved correlation ability. Also, a weld metal  $M_s$  expression which incorporates the influence of the weld metal oxygen content needs to be determined to better describe the effect of oxide inclusions on austenite decomposition kinetics. It is anticipated that  $\Delta M_s$  temperature versus  $(M_s \text{ HAZ}) \cdot (\Delta t_{5/1})$  plots can give significant improvement in predicting the nature and tendency of hydrogen cracking in high strength steel weldments.



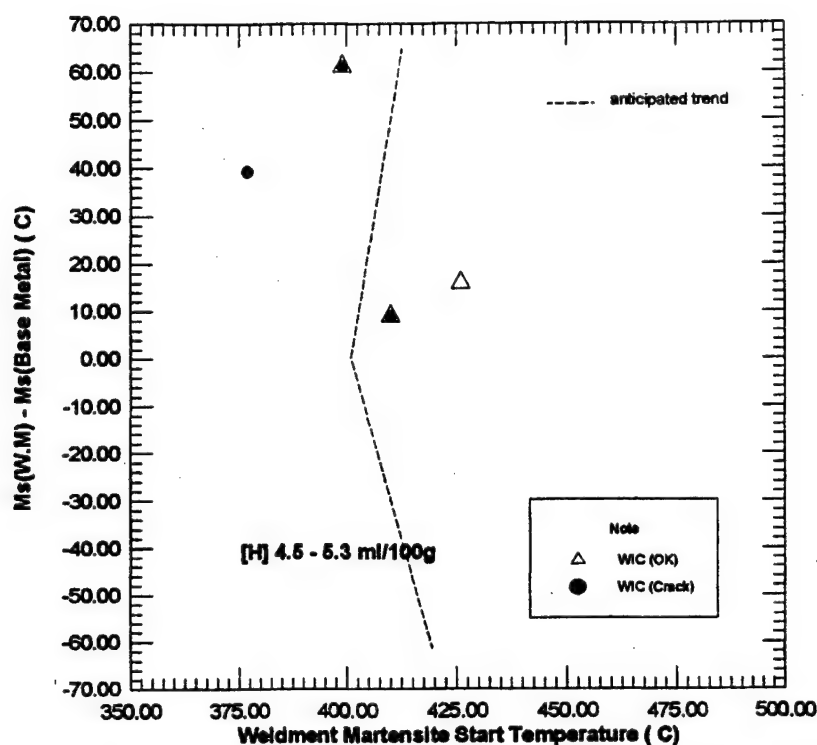


Figure 12. Illustration of anticipated trend and preliminary demarcation by the martensite start temperature difference between weldment and base metal.

### Conclusions

Based on the analysis and discussion presented, three major conclusions are reached and listed in the following.

1. Martensite start temperature can correlate weld metal composition to hydrogen cracking susceptibility.
2. The difference in  $M_s$  between the weld deposit and the base metal influences the final hydrogen distribution in the weldment and affects the location of the hydrogen cracking, whether in the weld metal or in the HAZ.
3. Quantitative models involving  $M_s$  HAZ and  $\Delta M_s$  can be developed to predict hydrogen cracking tendency of a high strength steel plate.

### Acknowledgment

The authors acknowledge and appreciate the research support of the Office of Naval Research.

### References

1. S. Liu, S. Ibarra, and D.L. Olson, "Assessment of Microstructural and Property Prediction Equations in Structural Welding," (Offshore Technology Conference, OTC 7597, 1994), 299-306.

2. C.D. Lundin, T.P.S. Gill, C.Y.P. Giau, and Y. Wang, "Validity of Conventional Carbon Equivalent Formulae to the Weldability of Low Carbon Microalloyed Steels for Marine Structures". (Univ. Tennessee Report to Ship Structure Committee, 1989).
3. R. Wong, private communication with author, U.S. Navy CDNSWC, 1995.
4. S. Liu, D.L. Olson, and D.K. Matlock, *J. Heat. Treating* 4(4) (1986), 309-316.
5. M.I. Onsoien, S. Liu, and D.L. Olson, "Shielding Gas Oxygen Equivalent in Weld Metal Microstructure Optimization", submitted to *Welding Journal* (1995).
6. K. Lorenz and C. Duren, (IIW Doc. IX-B-11-82, 1982).
7. N. Yurioka and H. Suzuki, *International Materials Reviews*, 35 (4) (1990), 217-149.
8. A.O. Kluken, S. Ibarra, S. Liu, and D.L. Olson, *Offshore Mechanics and Arctic Engineering, Materials Engineering*, vol. A, (1992), 1-7.
9. R.A.J. Karpil and P. Nevasmaa, "Contribution to Comparison of Methods for Determining Welding Procedures for the Avoidance of Hydrogen Cracking". (VTT Publ. #107, Espoo, Finland, 1992), (IIW Doc. IX-1673-092, 1992).
10. Th. Bollinghaus, H. Hoffmeister, and A. Dangeleit, "A Scatter band for Hydrogen Diffusion Coefficients in Microalloyed and Low Carbon Structural Steels". (IIW Document IX-1767-94, 1994).
11. H. Granjon, "Cold Cracking in Welding of Steels", Intl. Symposium on Cracking and Fracture in Welds, Conf. Proc. Japan Welding Society, (1971) IB, 1.1.
12. B.A. Graville, "Hydrogen Cracking Sensitivity of HSLA Steels," The Metallurgy, Welding, and Qualification of Microalloyed (HSLA) Steel Weldments, (1990), 127.
13. N. Christensen, I. Gjermundsen, and R. Rose, *Brit. Weld. J.*, (1958), 272-281.
14. G.M. Evans, "Diffusion of Hydrogen in Mild Steel Metal Arc Weldments," (Oerlikon Publication).
15. O.V. Kronshtal and V.S. Kharin, *Soviet Materials Science* 28 (5) (1993), pp. 475-586.
16. V.F. Musiyachenko and S.B. Kasatkin, *Automatic Welding* 9 (1985), pp. 22-26.
17. V.D. Tarlinski, *Avtom. Svarka* 27(6) (1974), 16-20.
18. N. Yurioka and S. Ohshita, "An Analysis of Effect of Microstructure, Strain, and Stress on the Hydrogen Accumulation in HAZ". (IIW Doc. IX-1161-80, 1980).
19. K. Andrews, *JISI*, 203 (1985), 721-727.
20. J.A. Self, D.K. Matlock, and D.L. Olson, *Welding Journal* 63 (9) (1984), 282s-288s.

21. J.A. Self, D.L. Olson, and G.R. Edwards, "The Stability of Austenitic Weld Metal", Cryogenic Properties of Metals. (NBS Publication, 1987), pp. 181-189.

22. J.A. Self, B.F. Carpenter, D.L. Olson, and D.K. Matlock, "Phase Transformation and Alloy Stability in Fe-Mn-Ni-Cr-Al Weld Metal", Alternate Alloying for Environmental Resistance, (1987), 37-46.

## CONSEQUENCES OF WELD UNDERMATCHING AND OVERMATCHING: NON-UNIFORM HYDROGEN DISTRIBUTION

W.W. Wang, S. Liu and D.L. Olson

Center for Welding, Joining and Coatings Research  
Colorado School of Mines  
Golden, Colorado 80401  
U.S.A.

### Abstract

In the past ten years, welding scientists have discussed extensively the concept of overmatching and undermatching of the weld metal with respect to the strength of the base metal. Important knowledge related to the propagation behavior of an existing crack and fracture control in a weld joint has been gained by these studies (1-5). For a given set of base metal and welding consumables, predictive models have been developed to describe the fracture behavior of the weld joint, the effect of applied loading conditions, chemical composition, welding conditions, and hydrogen level (6-13). An aspect that has not been thoroughly investigated is the effect of non-uniform hydrogen distribution in the weld joint. Depending on the hardenability of the base metal (heat affected zone) and the weld metal, these two regions may undergo austenite decomposition, more specifically martensitic transformation, at different temperatures and times during cooling. As a result of the earlier or later transformation of the weld metal (compared with the heat affected zone), hydrogen may accumulate in the heat affected zone or in the weld metal. Therefore, the amount of hydrogen and its distribution in the weld joint can magnify the "mechanical" effects of overmatching and undermatching on weld cracking.

### Hydrogen Transport in Weldments

The hydrogen content in a weldment is dependent on both the hydrogen source and the ability of the weldment in transporting hydrogen from the weld metal to the heat affected zone. The transport aspect is important because of the higher hydrogen solubility but lower hydrogen diffusion rate in austenite - FCC crystal structure. In contrast, ferrite (BCC) and martensite (BCT) have significantly higher hydrogen diffusion coefficient than austenite, but much lower solubility (14). The time and temperature at which austenite begins to decompose into ferrite/martensite will thus control the hydrogen transport in the weldment.

Traditionally, martensite start temperature ( $M_s$ ) has been used as an indicator of the alloy hardenability and austenite stability. In the case of high strength steel welding, however,

the martensite start temperature can also indicate a transition between the slow and fast diffusion rates of hydrogen in the cooling cycle. Depending on the differences in chemical composition and hydrogen diffusivity between the filler metal and base metal, the temperature ranges available for rapid hydrogen transport in the weld metal or heat affected zone will be different. As a result, hydrogen may accumulate preferentially in the weld metal or in the heat affected zone, along the fusion line. Thus, the martensite start temperature can be considered as a measure of both the microstructural evolution and the ability of having available a phase (ferrite/martensite) in which rapid hydrogen transport can occur. The concept of using martensite start temperature as a weldability index was proposed by Olson, Liu and co-workers (15-16).

Since different locations in a weldment experience different thermal cycles and, therefore, exhibit different austenite-to-martensite/ferrite transformation behavior, the hydrogen transport properties and distribution in the weldment will be non-uniform. This characteristics will also lead to a decreased or increased hydrogen damage susceptibility of the weld metal and the heat affected zone. Granjon (17) proposed a qualitative model describing the importance of austenite decomposition and hydrogen transport on the amount of residual hydrogen content in a weldment.

### Non-Uniform Hydrogen Distribution in Weldments

Christensen et al. (18) were first to show the non-uniform distribution of hydrogen in a transverse cross-section of the weld deposit and the heat affected zone. Evans et al. (19) also reported the hydrogen distribution along the length of a weld with significant transient end effects.

Using a hydrogen-saturated steel block, Kronshtal and Kharin (20) showed that the heterogeneity of microstructure and the thermal gradient could strongly influence the diffusion of hydrogen and the resulting distribution of hydrogen in the steel block, with localized high hydrogen concentrations.

Musiyachenko and Kasatkin (21) compared the distribution of hydrogen content across the fusion line of a steel weldment. Considering different initial weld metal hydrogen contents and different degrees of preheating, they determined in one case that the maximum hydrogen concentration peak was located in the heat affected zone, but closely adjacent to the fusion line; and in a second case, the hydrogen peak was located within the weld metal. These observations clearly depict the non-uniform distribution of hydrogen in a weldment and the influence of processing conditions on this distribution.

Using a laser beam spot fusion technique coupled with mass spectrometric analysis of evaporative hydrogen, Tarlinski (22) mapped the hydrogen profile of a weld in the transverse direction. The localized hydrogen peak adjacent to the fusion line is shown in Figure 1.

Yurioka and Ohshita (23) used finite difference analysis to evaluate the influence of both stress concentration and pre-

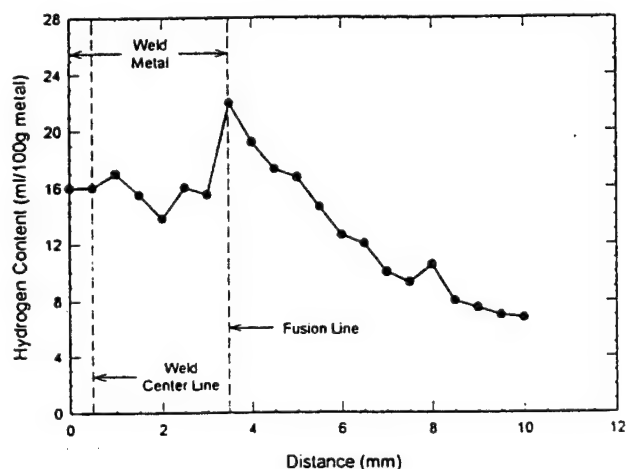


Figure 1. Non-Uniform Hydrogen Distribution in a Weld as determined by Tarlinski (22).

heat treatment on the hydrogen distribution in steel welds. Their results also suggested highly localized hydrogen concentration along the fusion line and in the weld toe area. Their finding agrees with the generally accepted notion that the weld toe is a common location for the initiation of underbead cracking. They also determined that the hydrogen concentration at the weld toe was time dependent and increased with time after welding.

Graville (24) also calculated the hydrogen distribution for the situation where the base and weld metal have different transformation temperatures, and found significant location variations in hydrogen contents at the boundary region between the weld metal and heat affected zone.

Based on the observations described in the previous paragraphs, it may be possible to explain why cracking sometimes occurs in low carbon steel welds that contain low average hydrogen content. The peak hydrogen concentration, together with martensite/ferrite transformation and thermal stress concentration, could increase the susceptibility of the weld to hydrogen cracking.

#### Weld Metal Overmatching and Undermatching

When the weld metal is overmatched with respect to the base metal, the austenite decomposition temperature of the weld metal will be depressed to below that of the base metal. While the austenite in the HAZ has begun decomposition, the austenite in the weld metal remains unchanged. For a certain time, the HAZ immediately adjacent to the fusion zone will transport hydrogen to the fine grained heat affected zone at a high rate compared to the weld metal. If the HAZ martensite start temperature is sufficiently high, the hydrogen will be able to transport a significant distance into the parent metal. However, the hydrogen transport cannot proceed extensively until the weld metal also transforms because despite the higher hydrogen solubility in austenite, hydrogen atoms are not quickly transported to the fusion line due to the lower temperature. Especially if the HAZ transformation occurs at a moderately elevated temperature, the situation described can potentially reduce the localized hydrogen content in the hard microstructure adjacent to the fusion line, thus reducing the hydrogen cracking susceptibility. However, the delayed austenite decomposition in the weld metal and greater hydrogen "retention" in the weld metal may promote hydrogen fissuring in the weld metal.

When the weld metal is undermatched, the heat affected zone will transform from austenite to ferrite/martensite at lower temperatures and at later times than the weld metal. In this case, the HAZ becomes an austenitic diffusion barrier for hydrogen transport, resulting in a high hydrogen accumulated in the heat affected zone, adjacent to the fusion line. This situation may promote underbead hydrogen cracking.

#### Martensite Start Temperature to predict Weld Metal Hydrogen Distribution

To verify the effect of martensite start temperature on hydrogen transport and distribution, the diffusion process was modeled by solving Fick's 2nd law considering incremental time intervals and temperature decreases according to the welding heat input and cooling rate. Austenite decomposition and hydrogen diffusion were allowed to occur in the HAZ and weld metal, but at different temperatures and times. Several diffusible hydrogen profiles were calculated to illus-

trate the non-uniform hydrogen distribution for different HAZ and weld metal  $M_s$  temperatures. The Calculations were based on actual steel base metal and weld compositions shown in Table I.  $\Delta M_s$ , defined as  $M_s(WM) - M_s(BM)$ , were also calculated and correlated with hydrogen distribution in the weldments to illustrate the effect of the different hydrogen transport behavior.

The martensite start temperatures in degrees Celsius were calculated using the equations developed by Self et al. (25-26). In comparison to other  $M_s$  equations, the Self expressions are more applicable over a large compositional range. These expressions are given as follows:

*Base Metal - (Eq. 1)*

$$M_{s_{HAZ}} = 521 - 350C - 14.3Cr - 17.5Ni - 28.9Mn - 37.6Si \\ - 29.5Mo - 1.19Cr \cdot Ni + 23.1(Cr + Mo) \cdot C$$

*Weld Metal - (Eq. 2)*

$$M_{s_{WM}} = 521 - 350C - 13.6Cr - 16.6Ni - 25.1Mo - 30.1Si \\ - 40.4Mo - 40Al - 10.7Cr \cdot Ni + 21.9(Cr + 0.73Mo) \cdot C$$

Of the six sets of weldments selected for calculation, the first represents a case of overmatching and the remaining five

regions. Figure 2 shows the resulting hydrogen profile with a high concentration in the weld metal, 0.88 ml/100g weld metal. The concentration of hydrogen decreases with distance moving away from the fusion line. It is possible that the limited hydrogen transport from the weld metal into the heat affected zone eventually leads to weld metal cracking, known also as hydrogen fissuring. Observed in some high strength steel weldments, these defects will generally have an orientation that is parallel to the solidification substructure, such as dendrites or columnar grains.

*Case 2: Undermatching -  $\Delta M_s > 0$  - Weld Metal with Higher  $M_s$  Temperature than the HAZ (WM-2/BM-2, WM-3/BM-3, WM-4/BM-4, WM-5/BM-5)*

This case can be described as a situation where the weld metal is undermatched with respect to the base metal. Since the heat affected zone transforms from austenite to ferrite at lower temperatures and at later times than the weld metal, the HAZ then becomes an austenitic diffusion barrier for hydrogen transport, resulting in a high hydrogen accumulated in the heat affected zone, adjacent to the fusion line. This situation is prone to promote underbead hydrogen cracking. Figures 3 to 7 plot the non-uniform hydrogen profiles obtained in the modeling work. Opposite from the overmatching case, the hydrogen peaks are all located in the heat

Table I. Chemical Composition (in wt. pct.) and  $M_s$  (in  $^{\circ}C$ ) of Six Sets of Base Metals and Weldments used in the Calculation.

	C	Mn	Si	Ni	Mo	Cr	Nb	V	Al	Ti	Cu	$M_s$
WM-1	0.065	2.39	0.84	—	—	0.06	—	—	—	—	—	411
BM-1	0.090	0.70	0.18	0.06	0.03	0.01	0.006	—	0.007	0.011	0.04	460
WM-2	0.073	1.70	0.39	1.86	0.32	0.42	—	—	—	—	—	398
BM-2	0.170	0.38	0.18	2.58	0.30	1.56	—	0.060	—	—	—	355
WM-3	0.080	1.16	0.25	2.79	0.41	0.57	0.061	—	—	—	2.16	394
BM-3	0.090	0.72	0.28	4.85	0.41	0.55	—	—	—	—	0.15	348
WM-4	0.090	0.66	0.19	7.20	0.96	0.89	—	0.043	—	—	—	312
BM-4	0.160	0.20	0.10	8.50	0.90	0.65	—	0.060	—	—	—	262
WM-5	0.100	0.97	0.47	0.05	0.02	0.06	0.012	—	0.008	—	0.11	446
BM-5	0.140	1.38	0.41	0.14	0.06	0.11	0.042	—	—	—	0.18	410
WM-6	0.069	0.94	0.47	0.89	0.21	0.30	0.016	0.003	0.006	0.001	0.90	436
BM-6	0.060	1.01	0.34	1.78	0.51	0.61	0.037	0.004	0.025	0.003	1.22	401

sets, undermatching. For the illustration of their effect on hydrogen distribution, the weldments also possess different  $\Delta M_s$ , varying from  $-49$  to  $35^{\circ}C$ .

*Case 1: Overmatching -  $\Delta M_s < 0$  - Weld Metal with Lower  $M_s$  Temperature than the HAZ (WM-1/BM-1)*

With higher alloying content, the weld metal exhibits lower martensite start temperature,  $411^{\circ}C$ , than the base metal,  $460^{\circ}C$ . While the austenite in the HAZ has begun decomposition, the austenite in the weld metal remains unchanged, thus affecting the hydrogen transport in the two

affected zone. In fact, the higher hydrogen concentration is situated within approximately 0.4 mm (0.04 cm) from the fusion line. Assuming that the average grain diameter in the coarse grain heat affected zone is between 100 and 150  $\mu m$ , the hydrogen peak is located within a layer of approximately three grains adjacent to the fusion line. Typical experimental observation of hydrogen cracking is also limited to a few grains (austenite) adjacent to the fusion line. Thus, HAZ with lower  $M_s$  temperature may result in underbead hydrogen cracking and localized weld metal cracking along the fusion

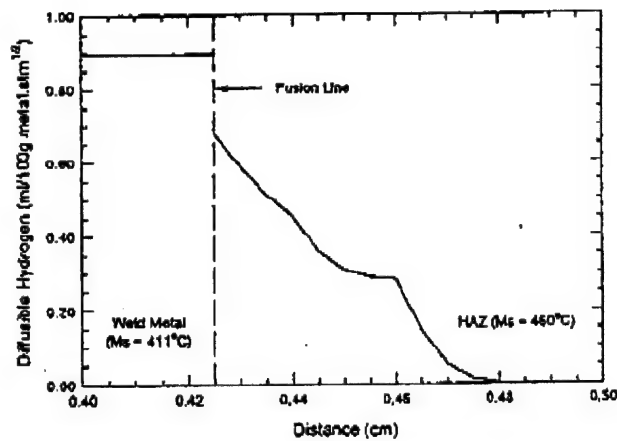


Figure 2. Non-Uniform Hydrogen Distribution with Hydrogen Peak located in the Weld Metal. Overmatching Case.

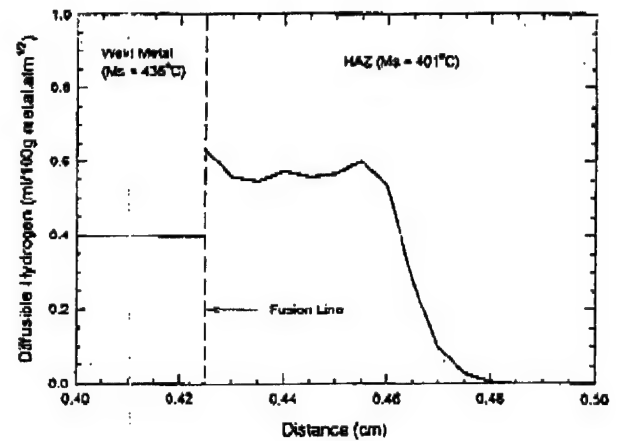


Figure 4. Non-Uniform Hydrogen Distribution with Hydrogen Peak located in the Heat Affected Zone. Undermatching Case.

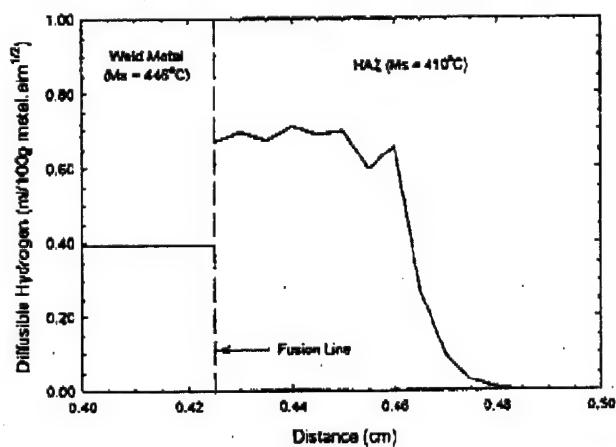


Figure 3. Non-Uniform Hydrogen Distribution with Hydrogen Peak located in the Heat Affected Zone. Undermatching Case.

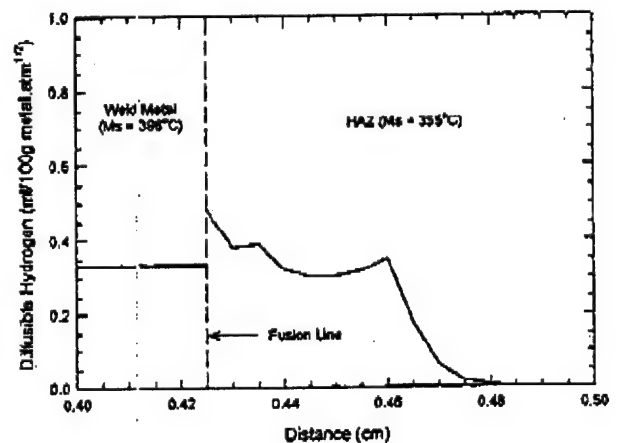


Figure 5. Non-Uniform Hydrogen Distribution with Hydrogen Peak located in the Heat Affected Zone. Undermatching Case.



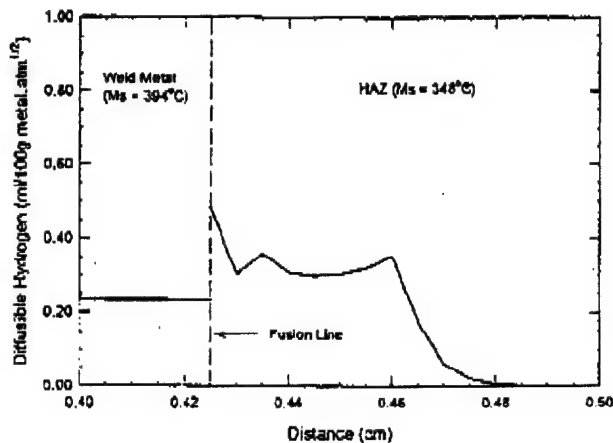


Figure 6. Non-Uniform Hydrogen Distribution with Hydrogen Peak located in the Heat Affected Zone. Undermatching Case.

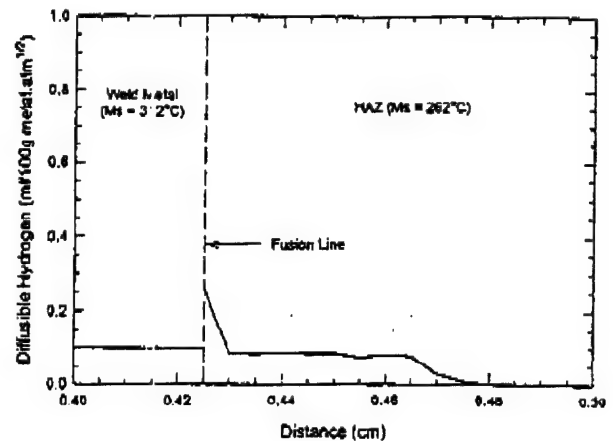


Figure 7. Non-Uniform Hydrogen Distribution with Hydrogen Peak located in the Heat Affected Zone. Undermatching Case.

line. This observation agrees well with the trends reported by other researchers (20-21).

Figures 3 to 7 also demonstrate the non-uniform distribution of diffusible hydrogen in these weldments. It is obvious that average hydrogen content does not necessarily express the real cracking susceptibility of a weldment. Additionally, depending on the relative magnitude of the martensite start temperatures, the hydrogen peak is located at different locations.

To further explore the concept of martensite start temperature and its applicability as an indicator of weld cracking susceptibility, the differences in hydrogen concentration in the weld metal and heat affected zone along the fusion line were determined and correlated with  $\Delta M_s$ . In this analysis, the  $\Delta H_{diff}$  is defined as:

$$\Delta H_{diff} = H_{WM} - H_{HAZ} \quad (\text{Eq. 3})$$

Figure 8 shows the linear relationship between the  $\Delta H_{diff}$  and  $\Delta M_s$ . When the base metal and weld metal have similar composition, such as the case of an autogenous weld, the difference in austenite decomposition behavior of the two regions should be minimal. In this case,  $\Delta M_s$  can be treated as zero. As such, the  $\Delta H_{diff}$  should also be close to zero. With increasing  $\Delta M_s$ , that is, higher martensite transformation

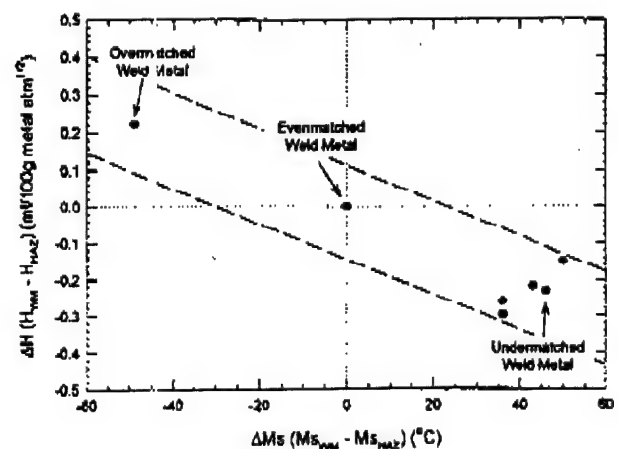


Figure 8.  $\Delta H_{diff}$  plotted as a Function of  $\Delta M_s$  indicating the Weld Cracking Susceptibility.

temperature in the undermatched weld metal, more hydrogen will be able to diffuse across the fusion line into the heat affected zone. That is, hydrogen will accumulate preferentially in the heat affected zone. If the hydrogen peak is located in the coarse grain heat affected zone, this region may be susceptible to cracking in the presence of an applied tensile stress state. However, if the  $\Delta M_s$  is negative, i.e. an overmatched weld metal, hydrogen transport is slower in the weld metal and will accumulate preferentially in the weld metal. In this case, hydrogen fissuring may occur as a result of shrinkage stress. In other words, the  $\Delta H_{dif}$  term can also be treated, along with  $\Delta M_s$ , as a parameter that defines cracking susceptibility of a weldment.

### Summary

Based on the analysis and discussion presented, six major conclusions are reached and listed in the following.

- 1. The diffusion modeling results clearly demonstrate the non-uniform distribution of hydrogen in a weldment.
- 2. As a result of the non-uniform distribution of hydrogen in a weldment, the amount of experimentally determined diffusible hydrogen alone is inadequate to express the cracking susceptibility of the weldment. Instead,  $\Delta M_s$  is a strong indicator of the hydrogen distribution and accumulation in the weld metal and heat affected zone.
- 3. If  $\Delta M_s < 0$ , i.e. weld metal overmatching, hydrogen accumulation will occur in the weld metal, subjecting the weld to greater probability of hydrogen fissuring.
- 4. If  $\Delta M_s > 0$ , i.e. weld metal undermatching, hydrogen accumulation in the HAZ is possible and underbead cracking may occur in the adjacency of the fusion line. Underbead cracking occurs within a distance approximately 0.5 mm from the fusion line which corresponds to a few grain diameters.
- 5.  $\Delta H_{dif}$  and  $\Delta M_s$  are both powerful indicators of weld cracking susceptibility.
- 6. While overmatching and undermatching are being considered, the non-uniform hydrogen accumulation aspect must be considered to ensure weld quality.

### Acknowledgment

The authors acknowledge and appreciate the research support of the Office of Naval Research.

### References

1. F. Minami, M. Toyoda, C. Thaulow, and M. Hauge, "Effect of Strength Mis-match on Fracture Mechanical Behavior of HAZ-Notched Weld Joint," IIW DOC XF-008-94, 1994.
2. M. Toyoda, C. Thaulow and J.G. Blauel, "Strength Mis-matching and Its Influence on the Performance of Welded Structures," Mis-matching of Welds, ESIS 17, pp. 335-350, 1994.
3. M. Koçak and K.-H. Schwalbe, "Effects of Notch Position and Weld Metal Matching on CTOD of HAZ," Proc. Intl. Conf. on Weld Failures, London, 1988.
4. P.L. Harrison and S.E. Webster, "Effect of Mismatch on Significance of Weld Defect Assessment," IIW DOC X-F-014-94, IIW Sub-Commission X-F "Weld Mismatch Effect", Paris, April 1994.
5. M.T. Kirk, "The Influence of Weld Strength Mismatch on Fitness-for-Purpose Assessment of Welded Steel Structures," Workshop on Naval Applications Technology, Halifax, Nova Scotia, April 1993.
6. K. Lorenz and C. Duren, IIW Doc. IX-B-11-82, 1982.
7. N. Yurioka and H. Suzuki, International Materials Reviews, 35 (4), pp. 217-149, 1990.
8. A.O. Kluken, S. Ibarra, S. Liu, and D.L. Olson, Off-shore Mechanics and Arctic Engineering, Materials Engineering, vol. A, pp. 1-7, 1992.
9. R.A.J. Karpil and P. Nevasmaa, "Contribution to Comparison of Methods for Determining Welding Procedures for the Avoidance of Hydrogen Cracking," VTT Publ. #107, Espoo, Finland, 1992, IIW Doc. IX-1673-092, 1992.
10. S. Liu, S. Ibarra, and D.L. Olson, "Assessment of Microstructural and Property Prediction Equations in Structural Welding," Offshore Technology Conference, OTC 7597, pp. 299-306, 1994.
11. C.D. Lundin, T.P.S. Gill, C.Y.P. Giau, and Y. Wang, "Validity of Conventional Carbon Equivalent Formulae to the Weldability of Low Carbon Microalloyed Steels for Marine Structures," Univ. Tennessee Report to Ship Structure Committee, 1989.
12. S. Liu, D.L. Olson, and D.K. Matlock, J. Heat. Treat- ing 4(4), pp. 309-316, 1986.
13. M.I. Onsoien, S. Liu, and D.L. Olson, "Shielding Gas Oxygen Equivalent in Weld Metal Microstructure Optimization", submitted to Welding Journal, 1995.
14. Th. Bollinghaus, H. Hoffmeister, and A. Dangeleit, "A Scatter band for Hydrogen Diffusion Coefficients in Microalloyed and Low Carbon Structural Steels," IIW Document IX-1767-94, 1994.
15. D.L. Olson, S. Liu, W. Wang, R.P.G. Gm. Pieters, and S. Ibarra, "Martensite Start Temperatures as a Weld- ability Index," Proc. Intl. Conf. on Trends in Welding Re- search, Gatlinburg, Tennessee, June 1995.
16. W. Wang, R. Wong, S. Liu, and D.L. Olson, "Use of Martensite Start Temperature for Hydrogen Control," Proc. Intl. Conf. on Welding and Weld Automation in Shipbuild- ing Symposium, Cleveland, Ohio, October 1995.

17. H. Granjon, "Cold Cracking in Welding of Steels", Intl. Symposium on Cracking and Fracture in Welds, Conf. Proc. Japan Welding Society, IB, 1.1, 1971.

18. N. Christensen, I. Gjermundsen, and R. Rose, Brit. Weld. J., pp. 272-281, 1958.

19. G.M. Evans, "Diffusion of Hydrogen in Mild Steel Metal Arc Weldments," (Oerlikon Publication).

20. O.V. Kronshtal and V.S. Kharin, Soviet Materials Science 28 (5) (1993), pp. 475-586.

21. V.F. Musiyachenko and S.B. Kasatkin, Automatic Welding 9 (1985), pp. 22-26.

22. V.D. Tarlinski, Avtom. Svarka 27(6) (1974), 16-20.

23. N. Yurioka and S. Ohshita, "An Analysis of Effect of Microstructure, Strain, and Stress on the Hydrogen Accumulation in HAZ". (IIW Doc. IX-1161-80, 1980).

24. B.A. Graville, "Hydrogen Cracking Sensitivity of HSLA Steels," in The Metallurgy, Welding, and Qualification of Microalloyed (HSLA) Steel Weldments, pp. 127, 1990.

25. J.A. Self, D.K. Matlock, and D.L. Olson, Welding Journal 63 (9), pp. 282s-288s, 1984.

26. J.A. Self, D.L. Olson, and G.R. Edwards, "The Stability of Austenitic Weld Metal," NBS Publication on Cryogenic Properties of Metals, pp. 181-189, 1987.

**Hydrogen Management  
in  
High Strength Steel Weldments**

**D.L. Olson, I. Maroef, C. Lensing, R.D. Smith, W.W. Wang,  
S. Liu, T. Wildeman and M. Eberhart**

**Center for Welding, Joining and Coating Research  
Colorado School of Mines  
Golden, Colorado 80401-1887  
USA**

## 1. INTRODUCTION

Common practice to reduce cold cracking in high strength steel welding is the pre- or post-weld heat treatment. Heat treatment is performed to control the cooling rate and to ensure sufficient removal of hydrogen from the weld metal. Recent scientific approaches supported by FEM calculation have made it possible to determine the heat treatment that provides an appropriate combination of microstructure (hardness), stress intensity factor and diffusible hydrogen content that does not allow susceptibility to hydrogen cracking (1). More often an acceptable selection of welding parameters to avoid hydrogen cracking is achieved by a costly testing program. However, such methodologies that require tight monitoring and control of the temperature as well as welding parameters are frequently found to be impractical and complicated. Therefore, new approaches to hydrogen management in steel welding, based on more fundamental metallurgical understanding and predictions, are being investigated. The CSM approach is to develop consumables based on three independent proposed practices to hydrogen management. They are described here as three steps.

### 2. STEP 1: PROPER SELECTION OF WELD METAL MARTENSITE START TEMPERATURE.

The hydrogen content in a weldment is dependent on both the hydrogen source and the ability of the weldment to transport hydrogen from the weld metal to the heat affected zone. The transport aspect becomes important because of the higher hydrogen solubility but lower hydrogen diffusion rate in austenite (FCC crystal structure), in contrast to ferrite and martensite that have orders of magnitude higher hydrogen diffusion coefficients than austenite (2). As a result of the different hydrogen diffusivity in austenite compared to martensite/ferrite and the different thermal experience, a non-uniform distribution of hydrogen may result across the weldment according to the austenite decomposition behavior of the alloys (3,4). Evidence of this resulting localized hydrogen distribution can be seen in the laser induced breakdown spectroscopy data (5) for hydrogen spectral emission scans across a weldment as shown in Figure 1. The effect of hydrogen damage is magnified when the location of the susceptible microstructures (martensite) overlaps the localized, high hydrogen content.

Proper alloying elements and their contents in the consumable are being determined to insure maximum hydrogen transport away from the weldment (weld metal and HAZ) during the welding thermal cycle. The martensite start temperature is used as an indicator for effective transport of hydrogen. A large difference between the  $M_s$  (weld metal) and  $M_s$  (base metal) will indicate difficulties in hydrogen transport in the weldment and the tendency for high localization in hydrogen contents. Thus the martensite start temperature is a measure of the microstructure evolution and the ability to have a phase (ferrite/martensite) available for rapid hydrogen transport (3,4).

Granjon (3) introduced a conceptual model that describes how the austenite-ferrite (or austenite-martensite) phase transformation in steel weldments affects the resulting hydrogen distribution. Two cases are illustrated in Figure 2. When the austenite-martensite

transformation in the fusion zone (weld metal) occurs at a higher temperature than the heat affected zone diffusible hydrogen will segregate in the heat affected zone just under the fusion line. This HAZ region is often the location of underbead cracking in high strength steel weldments. On the other hand, when the martensite transformation in the heat affected zone occurs at a higher temperature than in the fusion zone, it is possible that excess hydrogen may accumulate in the weld metal. This situation could promote weld metal hydrogen cracking or micro-fissuring.

#### **CASE 1: WELD METAL WITH LOWER $M_s$ TEMPERATURE THAN THE HAZ.**

This case can be described as a situation where the weld metal is overmatched with respect to the base metal with higher alloying content. The weld metal exhibits a higher strength than the base metal and its martensite start temperature is depressed to below that of the base metal. While the austenite in the HAZ has begun transforming, the austenite in the weld metal remains unchanged. After a period of time, the HAZ immediately adjacent to the fusion zone will transport hydrogen at a higher rate than that in the weld metal. If the HAZ martensite start temperature ( $M_s$ ) is sufficiently high, the hydrogen will be able to transport a significant distance into the parent metal. Especially if the transformation occurs at a moderately elevated temperature, the situation described can potentially reduce the localized hydrogen content in the hard microstructure adjacent to the fusion line, thus reducing the hydrogen cracking susceptibility. However, the hydrogen transport cannot proceed extensively until the weld metal transforms because austenite has the ability of storing high hydrogen contents but can not move it fast enough to the fusion line. If the weld metal  $M_s$  temperature is too low, then the hydrogen transport from the weld metal is limited. Very little hydrogen can reach the heat affected zone adjacent to the fusion line that may eventually lead to weld metal cracking.

To demonstrate the effect of martensite start temperature on hydrogen transport, the diffusion process was modeled considering incremental time periods and temperature which decreases according to the welding heat input and cooling rate. The martensite start was allowed to occur in the HAZ and weld metal, but at different times. Simple but reasonable boundary conditions were established for the solution of Fick's 2nd law. Several hydrogen profiles were determined (6) and the dotted traced line in Figure 3 illustrates the diffusible hydrogen distribution. This profile is the case where the HAZ  $M_s$  temperature is greater than the weld metal  $M_s$  temperature, and for a location indicated in Figure 3. This situation is prone to hydrogen cracking in the weld deposit which also has been observed for some high strength weldments.

#### **CASE 2: HAZ WITH LOWER $M_s$ TEMPERATURE THAN THE WELD METAL.**

This case can be described as a situation where the weld metal is undermatched with respect to the base metal. Since the heat affected zone transforms from austenite to ferrite at lower temperatures and at a later time than the weld metal, the HAZ becomes an austenite diffusion barrier for hydrogen transport. A high hydrogen accumulation in the heat affected zone adjacent to the fusion line results. This situation promotes underbead

hydrogen cracking. Figure 3 also plots the hydrogen profile (solid line) obtained in calculations following the procedure outlined in Case 1. Instead of having a high hydrogen concentration in the weld metal, hydrogen peaks are observed in the heat affected zone as shown in Figure 1. This profile supports the hydrogen distribution model as proposed and suggest that the hydrogen cracking being limited to a few grains (austenite) adjacent to the fusion line. Thus, a HAZ with lower  $M_s$  temperature may result in underbead hydrogen cracking and localized weld metal cracking along the fusion line.

To evaluate the ability of using the martensite start temperature as a hydrogen cracking index, the diffusible hydrogen content was plotted as a function of the calculated weld metal martensite start temperature for welds made on the same base metal (7). Figure 4 illustrates a demarcation line between the cracked and the uncracked weldments.

From the application of the  $M_s$  temperature, it is possible to obtain a  $\Delta M_s$  expression, and the sign and magnitude of this  $\Delta M_s$  expression will better describe the hydrogen diffusion behavior:

$$\Delta M_s = M_{s(WM)} - M_{s(BM)}$$

If  $\Delta M_s < 0$ , hydrogen accumulation will be in the weld metal. If  $\Delta M_s > 0$ , hydrogen accumulation in the HAZ is possible and underbead cracking may occur.

Some preliminary hydrogen cracking data is plotted with  $\Delta M_s$  as a function of  $M_s$  HAZ in Figure 5. This data indicates some ability to establish a demarcation line between cracking and non-cracking. Further work is necessary to evaluate the correlation between cracking and  $\Delta M_s$ .

Selection of the alloy additions has to be determined to achieve only a slightly higher martensite start temperature of the weld metal than that of the HAZ, for maximum hydrogen transport to the base metal. In addition, the absolute martensite start temperatures of the weld metal and the HAZ should be high enough to facilitate rapid hydrogen transport in the martensite phase.

### 3. STEP 2: HYDROGEN ABSORPTION CONTROL BY THERMO-CHEMICAL REACTIONS IN ARC PLASMA

Selected oxides or fluorides are being used as the consumable flux ingredient to minimize hydrogen absorption to the weld pool during arc melting. Hydrogen absorption can be minimized through the formation of water vapor or hydrogen fluoride in a thermo-chemical reaction with oxygen or fluorine gas in the welding plasma. Please notice on attached figures (Fig.6 and Fig. 7) that increasing either oxygen or fluorine will decrease the amount of hydrogen available to enter the weld deposit. These gases shall be generated from the selected fluxes that easily decompose during arc heating. The detrimental effects of excessive amounts of oxygen to the weldment toughness and those effects of fluorine to the working



environment will be considered in the determination of the types and amounts of the flux additions.

Increasing the weld pool oxygen content has been found to reduce the resulting weld metal hydrogen content by perturbing the water reaction (8). A thermodynamic analysis that sequentially follows the oxide (inclusions) formation from solidification to room temperature was performed. This methodology allows for the prediction of total weld metal hydrogen content and has been found to correlate reasonably well with experimental data. The major drawback of using oxygen to control weld metal hydrogen is the resulting oxygen pick up, primarily as inclusions. In excessive amounts, these oxides can alter the mechanical properties detrimentally. This concern requires new research into other weld pool reactions that can also significantly alter the weld metal hydrogen content.

The use of fluorine at small concentration levels to alter the HF reaction, associated with the weld pool and thus reduced the weld metal hydrogen content, is being investigated. Preliminary thermochemical calculations were made and the results illustrated that the use of fluorine holds reasonable promise. Figure 8 illustrates some of the preliminary results where fluorides in the welding flux are used to control hydrogen pick-up during welding of steel with a primer coating (9). It is also known that Teflon<sup>®</sup> additions have been made by some SMA electrode manufacturers to assist in hydrogen management.

#### 4. STEP 3: DIFFUSIBLE HYDROGEN CONTROL BY HYDROGEN TRAPS

Final suppression of diffusible hydrogen will be achieved by introduction of selected rare earth metal and transition metal additions to the weld metal to serve as hydrogen traps. These traps, in the form of oxides or carbo-nitrides have high binding energies with hydrogen. They are capable of immobilizing hydrogen at temperature ranges much higher than 100 °C, before the risk of cold cracking emerges. With proper trap morphology, number and distribution, it is possible to have a large portion of hydrogen being trapped uniformly throughout the weld metal and leave the remaining diffusible hydrogen in a much smaller content. In this way, transport to and accumulation of hydrogen at potential cracking initiation sites will be kept below the critical value for cold cracking initiation.

In steel, hydrogen is not homogeneously distributed as it would be in a perfect iron crystal. Hydrogen will be found not only in the host lattice, but also segregated to atomic and microstructural imperfections such as vacancies, solute atoms, dislocations, grain boundaries, voids, and second phase particles. In these localized regions, the mean residence time of hydrogen atoms is considerably longer than in normal interstitial lattice sites. In the extreme case, these regions are sinks into which hydrogen atoms fall and remain even during loading. Therefore, the generic term for this behavior is hydrogen trapping.

A prominent effect of trapping is to decrease the apparent hydrogen diffusivity (10). The ability of a trap site to hold hydrogen atoms is associated with the hydrogen-trap binding energy. Consequently, a trapped hydrogen atom must acquire an energy substantially greater than the lattice migration energy to escape the trap and contribute to the measured diffusivity.

Numerous studies on different traps have been reviewed by several authors (11-14). From various reported data, values of hydrogen-trap binding energies in iron were identified and are listed in Table 1. In addition, an electronic structure calculation was also applied in searching for other forms of potential traps that can be introduced in steel welding (15). Several inclusions in steel were investigated and, among them,  $\text{Ce}_2\text{O}_3$  oxide was found to have the highest binding energy followed by  $\text{TiC}$ ,  $\text{Y}_2\text{O}_3$ ,  $\text{VC}$ ,  $\text{NbC}$  and finally  $\text{Mo}_2\text{C}$ , in the order of decreasing energy. The binding energy of 60 kJ/mol H for a dislocation or a grain boundary is generally regarded as the typical limiting value of a reversible trap. With this energy level, a reversible trap becomes effective in capturing hydrogen around 400 °K but does not reach saturation at room temperature, as shown in Figure 9. A graphical description of this hydrogen distribution was calculated for selected hydrogen traps and is presented in terms of the saturation temperature in Figure 10. The saturation temperature was approximated for 0.9 fraction of trap occupation and was predicted to increase with increasing binding energy. A reversible trap whose binding energy is lower than 60 kJ/mol will not be able to prevent hydrogen cracking. The trapped hydrogen will be picked up by moving dislocations and eventually be delivered to crack initiation sites (16). The preferred traps are then those having binding energies higher than 60 kJ/mol and are termed irreversible traps (17).

A preliminary numerical study of hydrogen trapping during the welding cooling cycle has been conducted as a basis for criteria of trap selection. This study involved the prediction of diffusible hydrogen content, which changes with time due to both the hydrogen removal out of the weld metal and the hydrogen capture by trap sites in the weld metal. A diffusion model of hydrogen in steel containing trap sites, similar to the McNabb and Foster model (18), has been applied. The calculation was done numerically to take account the variation of both the hydrogen diffusion coefficient and the hydrogen capturing rate by trap sites with temperature and the associated microstructure of the diffusing medium. An example of the calculated result is shown in Figure 11a, where the diffusible hydrogen content (HD) of the weld metal containing traps is predicted to be lower than that of the steel without traps. Also shown in Figure 11a is the trapped hydrogen (HT) whose amount increases with time.

An abrupt change of slope can be observed in the diffusible hydrogen content right at the martensite start temperature of the weld metal. Phase transformation from austenite to martensite is accompanied by a large increase in the hydrogen diffusion coefficient which in turn accelerates both the hydrogen capture and the hydrogen removal out of the weld metal. The kinetics of hydrogen capturing can be more clearly explained in Figure 11b which shows the equilibrium trap occupancy ( $n_{eq}$ ), the actual trap occupancy ( $n$ ) and the rate of hydrogen capture ( $dn/dt$ ). The hydrogen capture rate depends both on hydrogen diffusivity and the driving force for hydrogen entrapment ( $n_{eq}-n$ ). It can be seen that a sudden increase in the rate of capture always follows the occurrence of martensite phase formation where both capture determining factors are maximized.

The criteria for the use of traps to reduce the susceptibility of HAC should include a proper combination of several factors. These factors are the hydrogen-trap binding energy, the trap density, the martensite start temperature and the cooling rate ( $\Delta t_{8/5}$ ). In this preliminary

investigation, each of the above mentioned variables was varied independently and the resulting amount of diffusible hydrogen at 100 °C as well as at 300 °C are summarized in Figures 12 to 15. The temperature 100 °C has been considered as the temperature where the potential for HAC starts to become a problem.

The first important parameter of a trap is the hydrogen-trap binding energy. In this calculation, four values of binding energies that correspond to different trap sites were used. They are 60 kJ/mol for dislocations, 80 kJ/mol for  $\text{Al}_2\text{O}_3$  inclusions, 100 kJ/mol for TiC particles, and 120 kJ/mol for rare earth additions. As shown in Figure 12, the amount of diffusible hydrogen content decreases with increasing hydrogen-trap binding energy. The major advantage of traps with high binding energy is that they provide a high driving force for hydrogen capture within high temperature regions. The data at 300 °C shows a better insight to how much faster the hydrogen is captured by high binding energy traps as opposed to those with low binding energy. Should the HAC start to occur at a higher temperature than 100 °C (which may be possible for weld metal with low martensite start temperature) the weld metal containing high binding energy traps may have a better chance to survive.

The diffusivity of hydrogen in the austenite phase is very low, so that the hydrogen cannot be effectively captured or removed out of the weld metal until the martensite temperature is reached. The lower the martensite start temperature is, the longer time hydrogen has to remain in the weld metal lattice sites. It also means that the available temperature range for effective hydrogen diffusivity and trapping in the ferrite phase becomes narrower and the suppression of diffusible hydrogen content by certain traps becomes less effective. The extreme situation is depicted in Figure 13 for the case of weld metal possessing martensite start temperature of 400 °C. The advantage of using a trap with higher binding energy, i.e., higher capture rate, is then obvious in this very narrow temperature range situation. However, the employment of high binding energy traps for a high martensite start temperature weld metal can lead to a situation where the trapping capacity will be wasted at high temperature regions. This behavior can occur even when the hydrogen diffusivity provides a high potential for easy hydrogen removal out of the weld metal. Therefore, the selection of hydrogen traps must consider other factors than just the weld metal or consumable alloying contents.

Conventional hydrogen management usually applies proper heat treatment or sufficiently low cooling rate to provide easy hydrogen removal out of the weld and to form a less susceptible microstructure to HAC. In case of weld metal containing trap sites, a certain rate of cooling is also necessary to allow for enough hydrogen capture time before the temperature reaches 100 °C. In the present calculation, the cooling rate is assumed to occur naturally and relatively fast, so that sufficient hydrogen removal by lattice diffusion alone can not be obtained. The effect of cooling rate, shown in Figure 14, appears to be similar to that of the martensite start temperature. A very fast cooling rate, such as those with  $\Delta t_{8/5}$  equal to one second, does not permit enough time for hydrogen to leave the weld metal or jump into the trap sites. On the other hand, in a slightly slower cooling rate, the presence of traps may yield a low diffusible hydrogen content at 100°C and alleviate the tendency for weld metal HAC. This prediction shows the potential usage of traps to substitute for the tight heat-treatment procedure necessary for high strength steel welding.

The number of trap sites translates into the capacity to hold hydrogen atoms. A higher number of trap sites in the weld metal will produce a lower diffusible hydrogen content, which is in agreement with the calculated result shown in Figure 15. There is also an apparent threshold number of trap sites for optimum hydrogen trapping that can be observed in Figure 15. The number of traps used in the present calculation corresponds to a 100 to 500 ppm range of substitutional atom traps in the weld metal. In the case of inclusion traps, which is the most probable form of traps in weld metal, the trap sites on the surface are of the inclusion - matrix interface. Depending on the cooling rate, the number of trap sites used in this calculation may correspond to a relatively high inclusion volume fraction that yields weld metal with intrinsically low toughness. Obviously, the number of trap sites that can be used is limited to an extent in which the toughness is still maintained at an acceptable level. This issue suggests that the success of using hydrogen traps should not be related to significant diffusible hydrogen suppression in the weld metal. Its main function should be to promote a proper distribution of hydrogen in weld metal so that a high local accumulation of hydrogen at crack initiation sites can be prevented. Furthermore, in high strength steel welding, where hydrogen is highly accumulated at crack initiation sites, the presence of trap sites may give a higher tolerance for diffusible hydrogen content. Normally, a low maximum acceptable level of hydrogen content in the weldment is usually required for conventional welding procedures.

## 5. PROSPECTIVES

Use of these three steps for hydrogen management will reduce susceptibility to hydrogen cracking in welds. With further quantification and correlations, analytical procedures can be developed for designing welding consumables and practices for high strength steel that require a very low diffusible hydrogen content.

## 6. ACKNOWLEDGMENT

The authors acknowledge and appreciate the research support of the US Army Research Office.

## 7. REFERENCES :

1. R.A.J. Karppi, J. Ruusila, M. Toyoda, K. Satoh, and K. Vartiainen, *Scandinavian Journal of Metallurgy*, Vol. 13, (1984), pp. 66-74.
2. Th. Bollinghaus, H. Hoffmeister, and A. Dangeleit, "A scatter Band for Hydrogen Diffusion Coefficients in Microalloyed and Low Carbon Structural Steels". (IIW Document IX-1767-94, 1994).
3. H. Granjon, "Cold Cracking in Welding of Steels", Intl. Symposium on Cracking and Fracture in Welds, Conf. Proc. Japan Welding Society, (1971), IB, 1.1.
4. B. Gravile, "Hydrogen Cracking Sensitivity of HSLA Steels", *The Metallurgy, Welding and Qualification of Microalloyed (HSLA) Steel Weldments*, (1990), 127
5. R.D. Smith, Private Communication, Colorado School of Mines, (1996).
6. W. Wang, S. Liu and D.L. Olson, "Consequences of Weld Undermatching and Overmatching: Non-Uniform Hydrogen Distribution", in Intl. Conf. on Offshore Mechanics and Arctic Engineering - Materials Engineering', ASME, Vol. III, , Florence, Italy, (1996), pp. 403-409
7. D.L. Olson, S. Liu, W. Wang, R. Pieters, and S. Ibarra, "Martensite Start Temperature as a Weldability Index", in Conf. Proc. on 'Research Trends in Welding Science and Technology', pp. 615-620, Gatlinburg, Tennessee, (1995), ASM Intl., 1996.
8. S. Liu, D.L. Olson & S. Ibarra, "Electrode Formulation to Reduce Weld Metal Hydrogen and Porosity", Intl. Conf. on Offshore Mechanics and Arctic Engineering, ASME-OMAE, (1994), pp. 291-298
9. K. Johnson, Private Communication, Colorado School of Mines, (1996).
10. H.H. Johnson, *Metall. Trans.*, Vol. 19B, (1988), pp. 691-707.
11. J.P. Hirth, *Metall. Trans.*, Vol. 11A, (1980), pp. 861-890.
12. I.M. Bernstein and G.M. Pressouyre, in *Hydrogen Degradation of Ferrous Alloys*, ed. by R.A. Oriani, J.P. Hirth and M. Smialowski, Noyes Pub., (1985), pp. 641-685.
13. P. Kedzierzawski, in *Hydrogen Degradation of Ferrous Alloys*, ed. by R.A. Oriani, J.P. Hirth and M. Smialowski, Noyes Pub., (1985), pp. 271 - 288.
14. R. Gibala and A.J. Kummick, in *Hydrogen Embrittlement and Stress Corrosion Cracking*, ed. by R. Gibala and R.F. Hehemann, ASM, Metals Park, Ohio, (1984), pp. 61 - 77.
15. M. Eberhart, Private communication, Colorado School of Mines, (1995).
16. J.K. Tien, A.W. Thompson, I.M. Bernstein, and R.J. Richards, *Metall. Trans.*, Vol. 7A, (1976), pp. 821-829.
17. G.M. Pressouyre and I.M. Bernstein, *Metall. Trans.*, Vol. 12A, 1981, pp. 835-844.
18. A. McNabb and P.K. Foster, *Trans. of the Metall. Soc. of AIME*, Vol. 227, (1963), pp. 618-627.
19. R. Gibala, in *Stress Corrosion Cracking and Hydrogen Embrittlement of Iron Base Alloys*, ed. by R.W. Staehle, J. Hochmann, R.D. McCright, and J.E. Slater, NACE-5, NACE, Houston, TX, (1977), pp. 244-268.
20. W.Y. Choo and J.Y. Lee, *Metall. Trans.*, Vol. 13A, (1982), p. 135.
21. A.J. Kummick and H.H. Johnson, *Acta Metall.*, Vol. 28, (1980), pp. 33-40.
22. K. Ono and M. Meshi, *Acta Metall.*, Vol. 40 (6), (1992), pp. 1357-1364



23. T. Asaoka, C. Dagbert, M. Aucouturier, and J. Galland, *Scripta Metall.*, Vol.11, (1977), pp. 467-472.
24. E. Chornet and R.W. Coughlin, *J. Catal.*, Vol.72, (1972), pp. 246-265.
25. D.O. Hayward and B.M.W. Trapnell, in *Chemisorption*, Butterworths, London, (1964), p.203.
26. J.R. Scully, J.A. Van den Avyle, M.J. Cieslak, A.D. Romig,Jr., and C.R. Hills, *Metall. Trans.*, Vol.22A, (1991), pp. 2429-2445.
27. K.Y. Lee, J.Y. Lee and D.R. Kim, *Mater. Sci. Eng.*, Vol. 67, (1984), p. 213
28. H.H. Podgurski and R.A. Oriani, *Metall. Trans.*, Vol.3, (1972), pp. 2055-2063.
29. J.L. Lee and J.Y. Lee, *Metal Sci.*, Vol. 17, (1983), p. 462.
30. J.L. Lee and J.Y. Lee, *Metall. Trans.*, Vol. 35A, (1987), pp. 2695-2700
31. P. Lacombe, M. Aucouturier, J.P. Laurent, and G. La Passet, in *Stress Corrosion Cracking and Hydrogen Embrittlement of Iron Base Alloys*, ed. by R.W. Staehle, J. Hochmannn, R.D. McCright, and J.E. Slater, NACE-5, NACE, Houston, TX, (1977), pp. 423-430.
32. H.G. Lee and J.Y. Lee, *Acta Metall.*, Vol.32, (1984), p. 131
33. G.M. Pressouyre and I.M. Bernstein, *Metall. Trans.*, Vol. 9A, (1978), pp. 1571-1580.
34. G.M.Pressouyre, *Metall. Trans.*, Vol. 10A, (1979), pp.1571-1573

Table 1. Hydrogen trapping in Iron. Reference state :  $\bar{H}$  in perfect lattice

Trap Site	Binding Energy (kJ/mol)	Matrix	Assessment Method	Ref.
H-dislocation elastic stress field	0 - 20.2	Iron	calculated	19
H-dislocation core (screw)	20 - 30	Iron	calculated	11
H-dislocation	26	Iron	thermal analysis	20
H-dislocation core (mixed)	59	Iron	permeation	21
H-grain boundary	18 - 20	C-Mn Steel	thermal analysis	20
H-grain boundary	60	Iron	thermal analysis	22
H-grain boundary	59	Iron	permeation	21,23
H-Free surface	70	Iron	permeation	24
H-Free surface	95	Iron	permeation	25
$\beta$ -NiAl	27	Steel *	permeation	26
H-PdAl interface	34	Steel *	permeation	25
H-Fe-oxide interface	47	C-Mn Steel	thermal analysis	27
H-AlN interface	65	Iron	permeation	28
H-MnS interface	72	C-Mn Steel	thermal analysis	29
H-Al <sub>2</sub> O <sub>3</sub> interface	79	C-Mn Steel	thermal analysis	30
H-Fe <sub>3</sub> C interface	84	C-Mn Steel	permeation	23,31
H-TiC interface	87	Iron	thermal analysis	32
H-TiC interface	95	C-Mn Steel	permeation	33
H-Nd	129	Iron	calculated	34

\* Matrix element is precipitation hardened martensitic stainless steel.



## Hydrogen Trapping in Ferrous Weldments

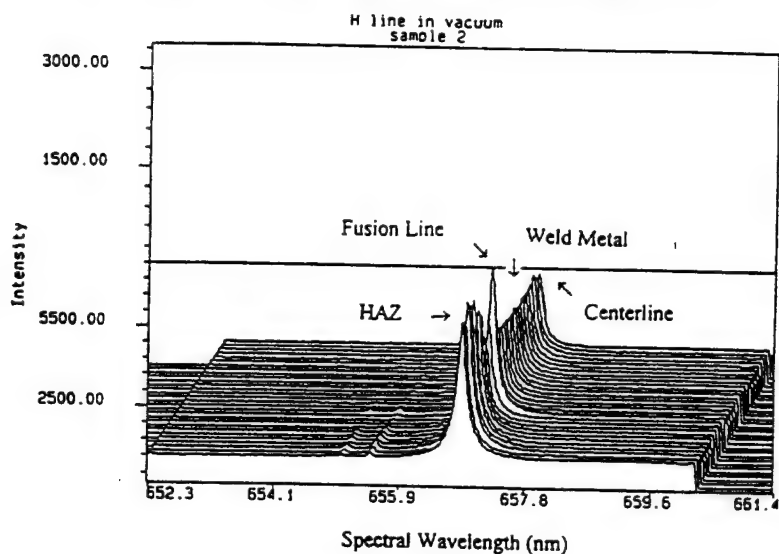


Figure 1. Non-uniform distribution of hydrogen across the center line of a weldment. Intensities of the hydrogen spectral emission are proportional to the hydrogen concentration.

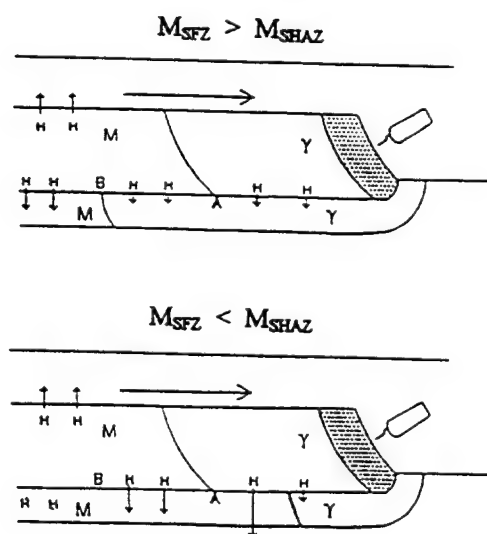


Figure 2. Illustration of hydrogen diffusion at different martensite start temperature for weldment and base metal (3)

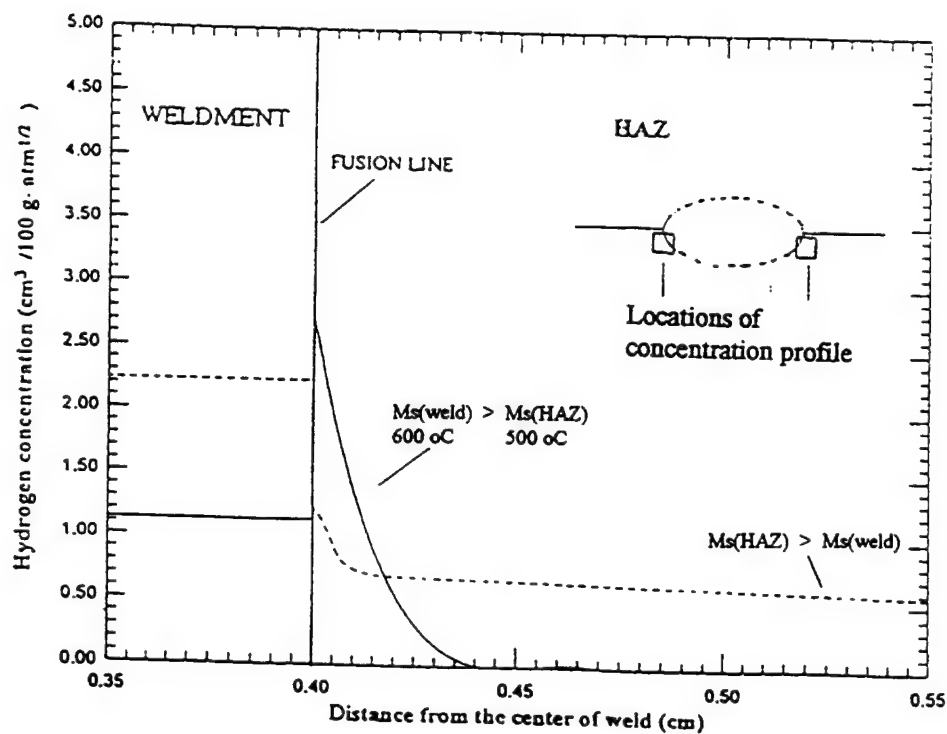


Figure 3. Hydrogen distribution across the fusion line of a steel weldment for  $M_s \text{ weld} > M_s \text{ HAZ}$  and  $M_s \text{ weld} < M_s \text{ HAZ}$ .

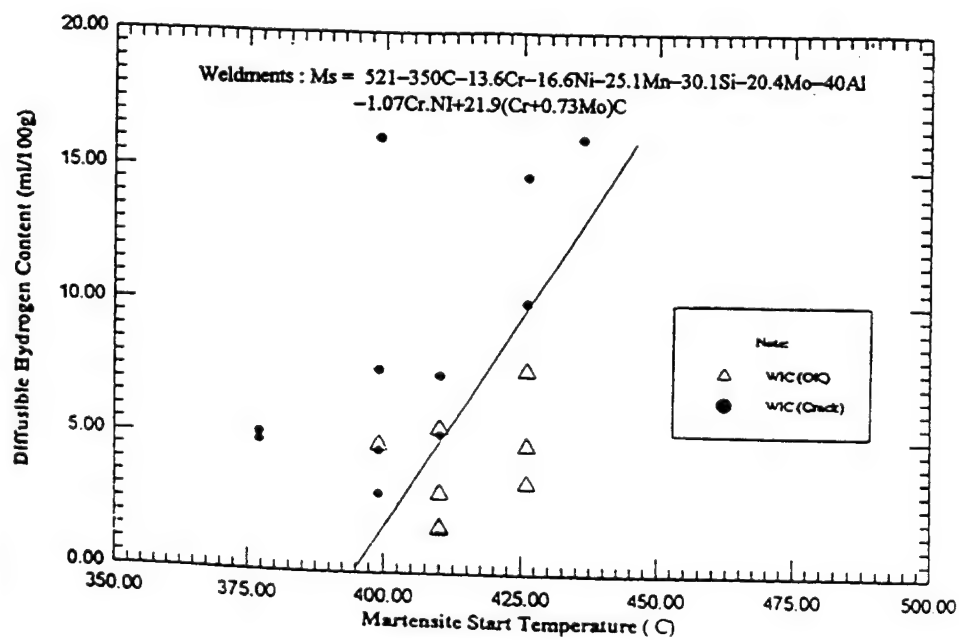


Figure 4. Conceptual illustration of cracking prediction.

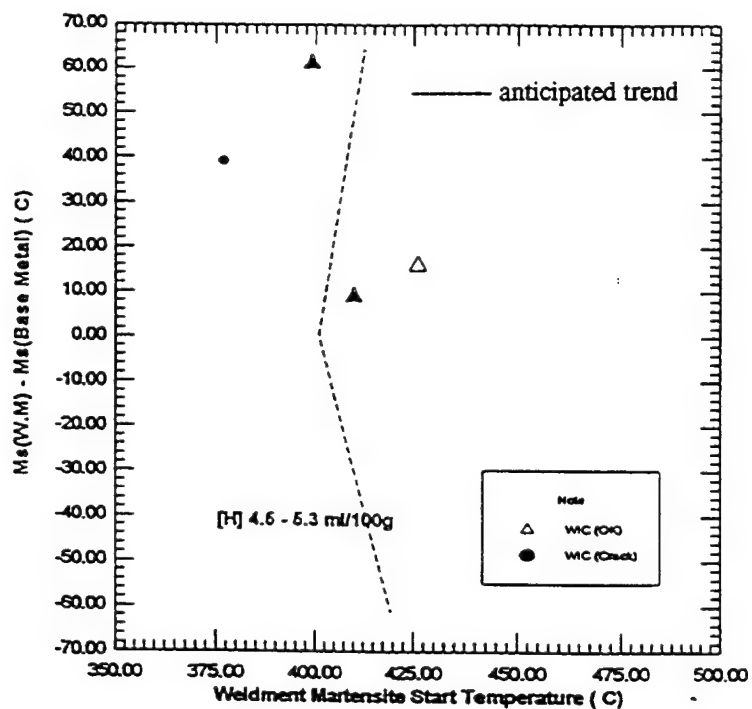


Figure 5. Illustration of hydrogen cracking/uncracking zones by hydrogen content and martensite start temperature.

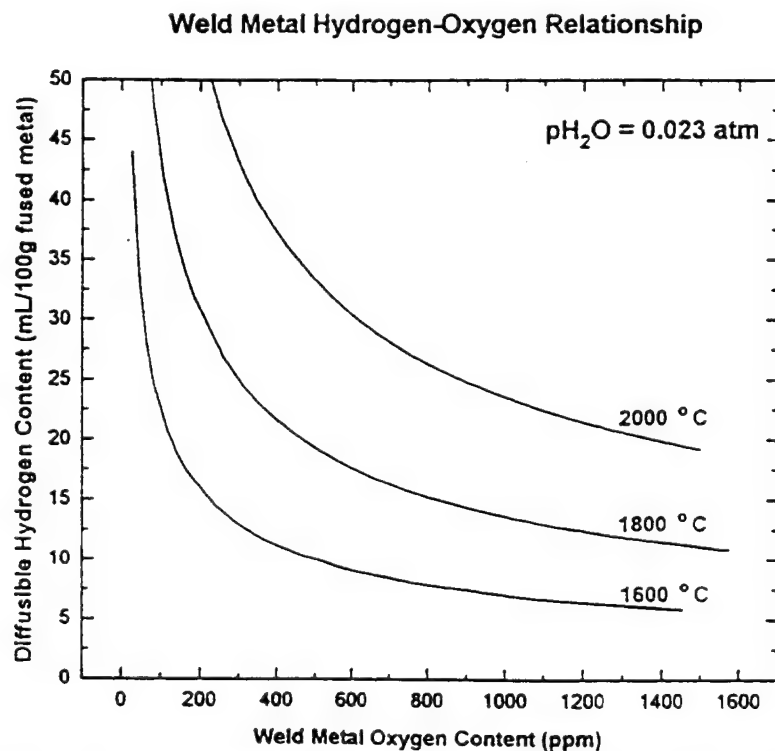


Figure 6. Thermo-chemical reaction between oxygen and hydrogen in the welding plasma.

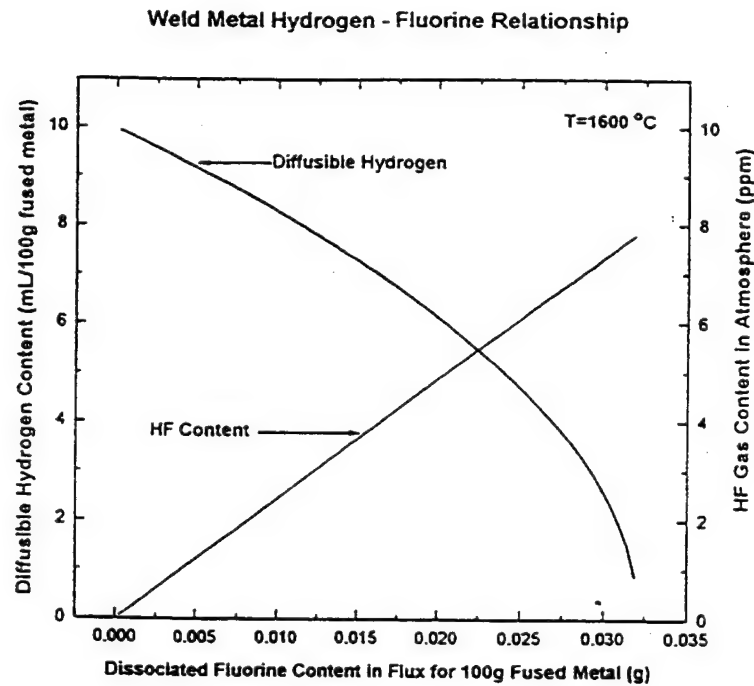


Figure 7. Thermo-chemical reaction between fluorine and hydrogen in the welding plasma.

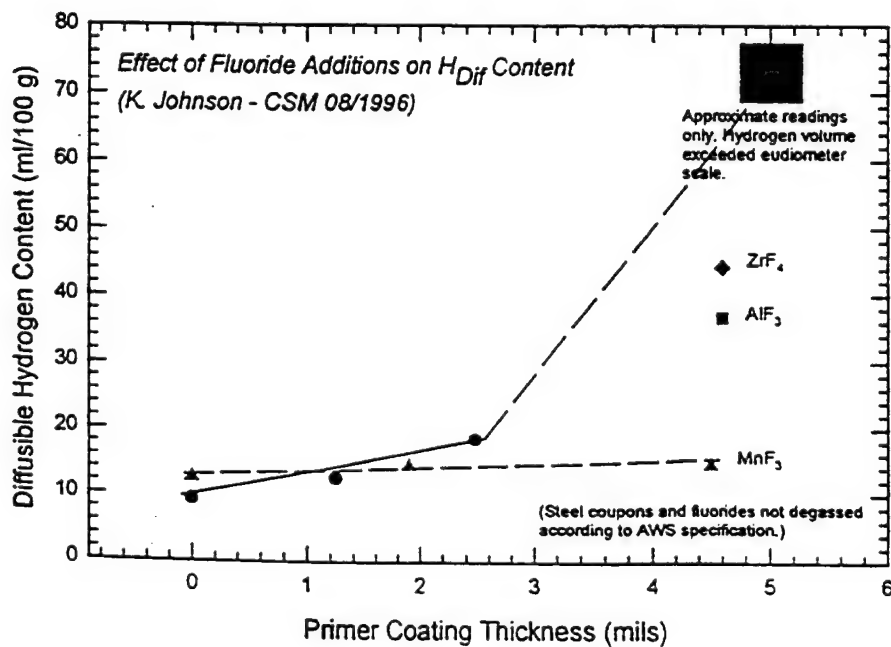


Figure 8. Effect of fluoride additions on  $H_{\text{Diff}}$  content.

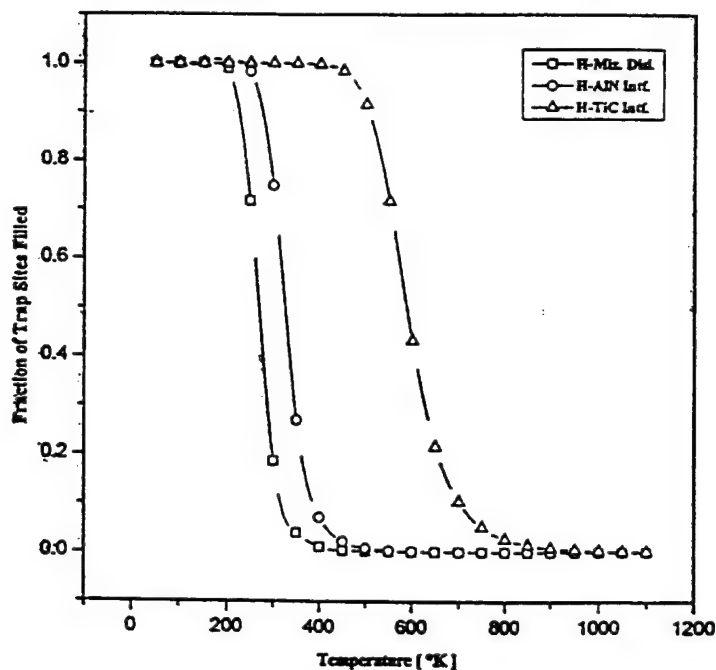


Figure 9. Fraction of trap occupation by hydrogen at trap sites as a function of temperature for various hydrogen-trap binding energies. Partial pressure of hydrogen is 0.0545 Pa.

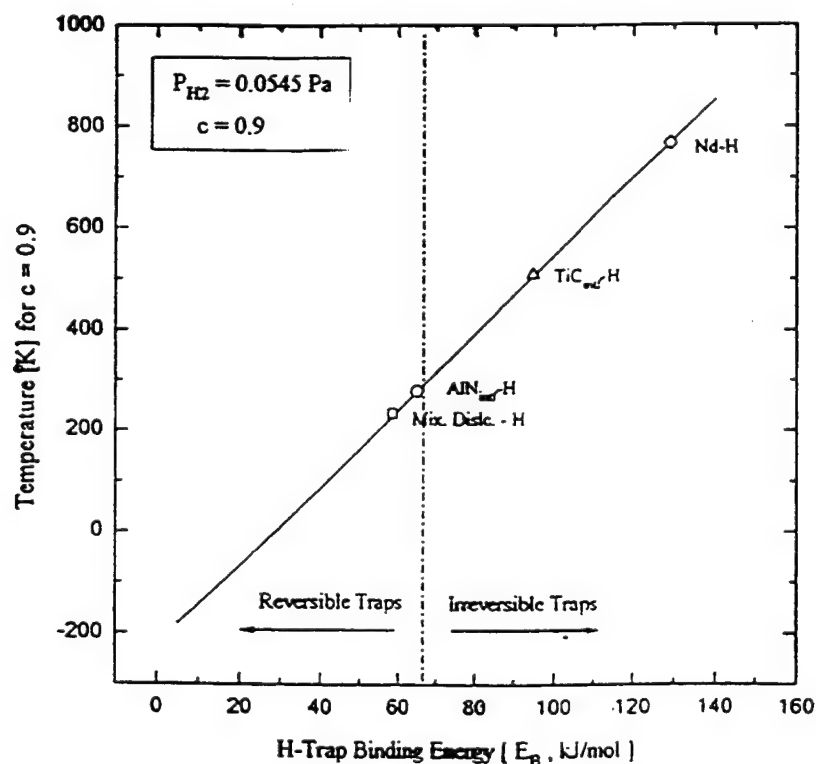
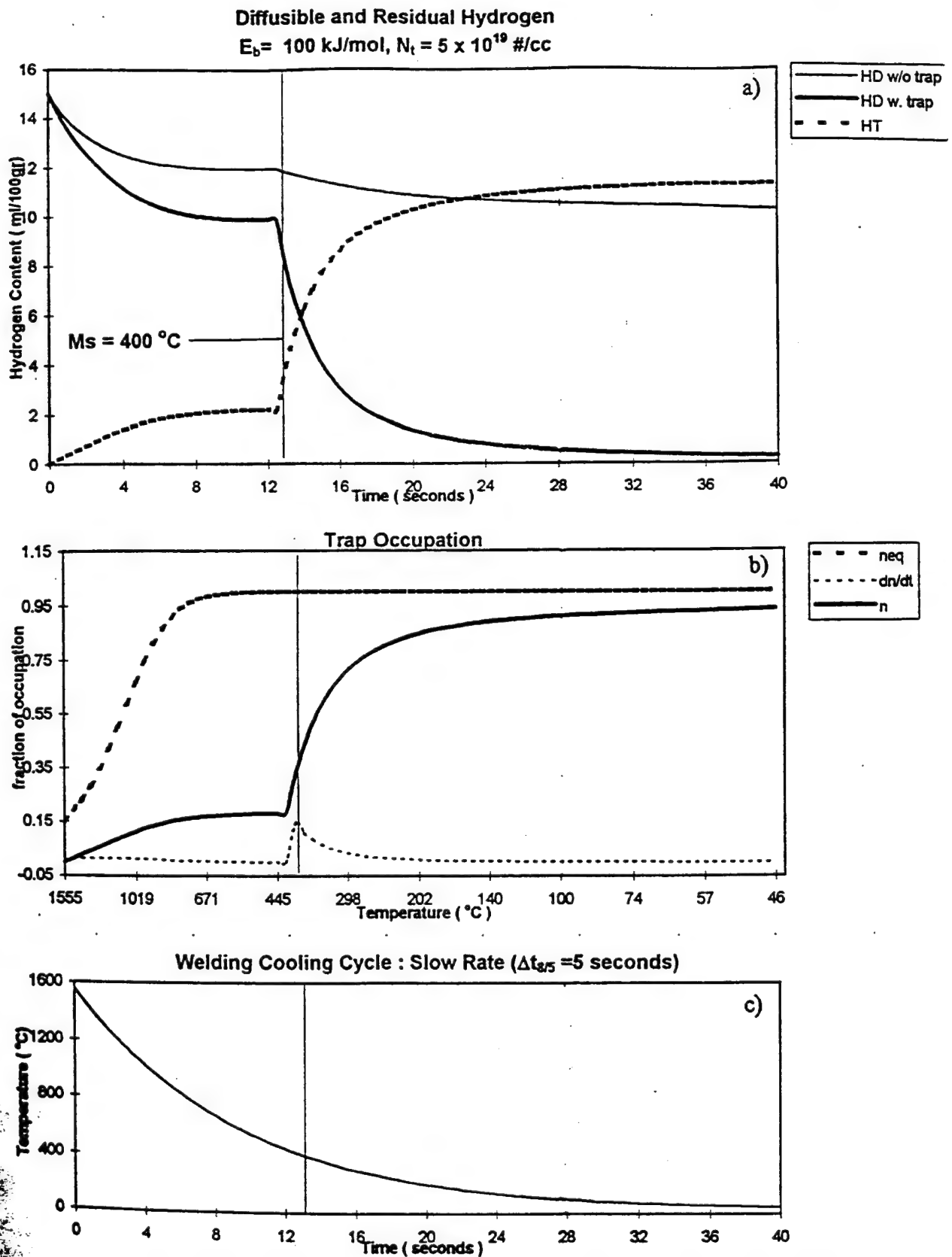


Figure 10. Temperature for ninety percent occupation at various hydrogen trap sites.



**Figure 11.** Hydrogen trapping during welding cooling cycle. Initial diffusible hydrogen in weld metal is 15 ml/100g. In (a), the notation HD stand for diffusible hydrogen, HT is the trapped hydrogen. In (b),  $n$  is the fraction of trap occupation by hydrogen and  $neq$  is the equilibrium fraction of occupation determined by the Fermi-Dirac distribution.

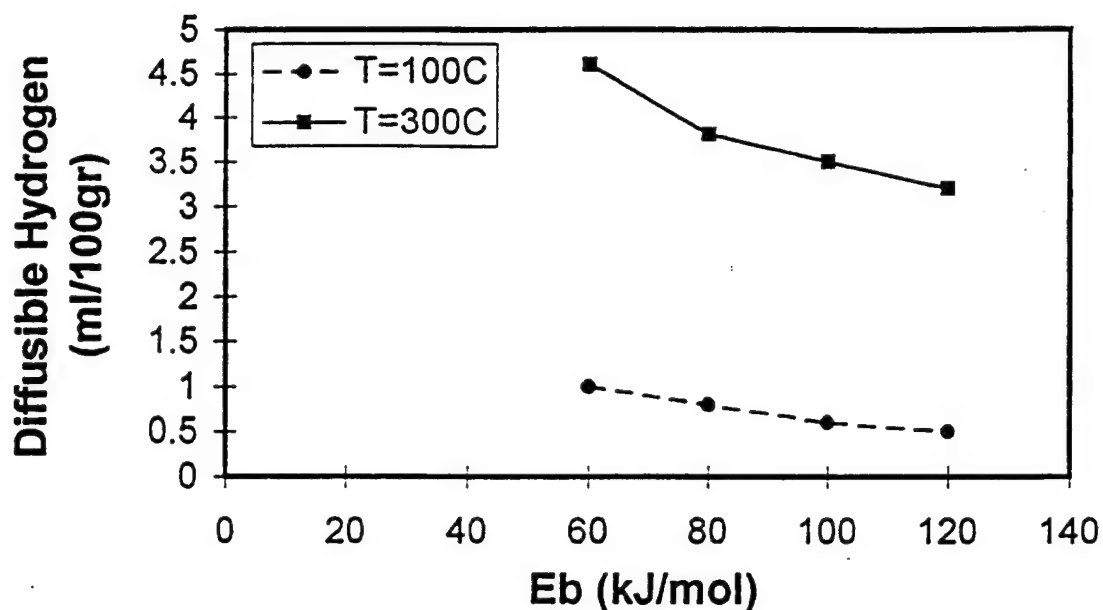


Figure 12. Effect of trap binding energy on the diffusible hydrogen content. Initial diffusible hydrogen content is 15 ml/100g.  $M_s = 400^\circ\text{C}$ ,  $\Delta t_{8/5}$  is 5 seconds, trap density,  $N_t = 5 \times 10^{19} \text{ \#/cc}$ .

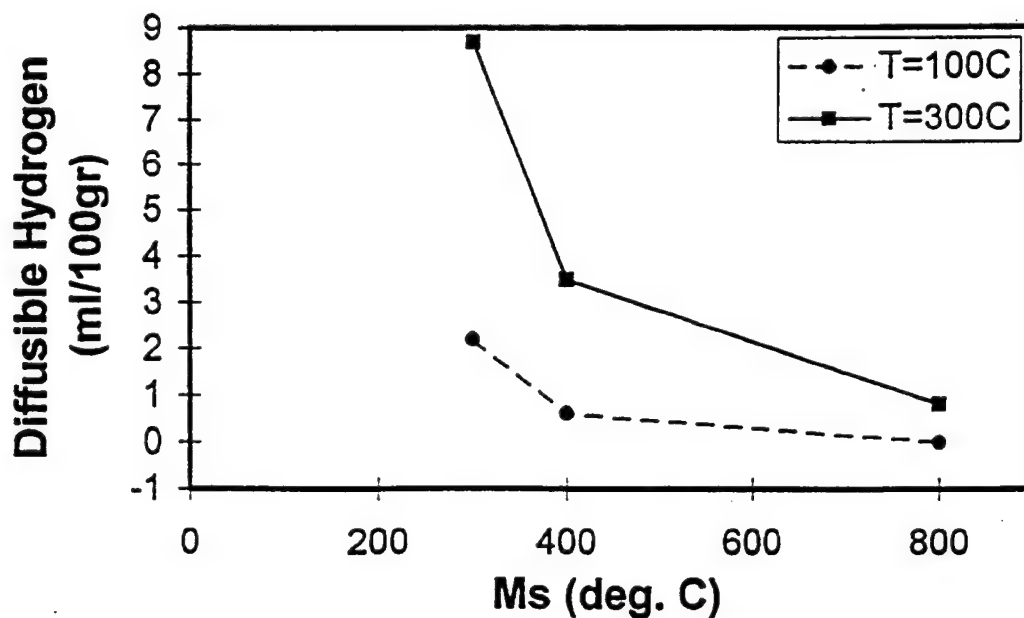


Figure 13. Effect of  $M_s$  temperature on the diffusible hydrogen content. Initial diffusible hydrogen content is 15 ml/100g.  $E_b$  is 100 kJ/mol,  $\Delta t_{8/5}$  is 5 seconds, trap density,  $N_t = 5 \times 10^{19} \text{ \#/cc}$ .



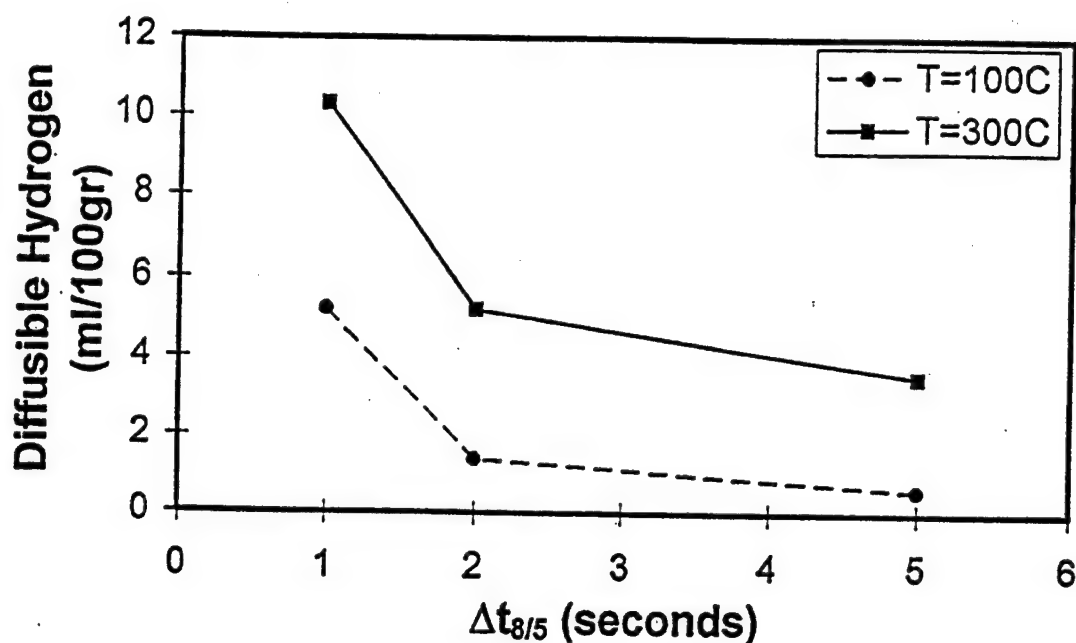


Figure 14. Effect of cooling rate on the diffusible hydrogen content. Initial diffusible hydrogen content is 15 ml/100g.  $M_s = 400^\circ\text{C}$ ,  $E_b$  is 100 kJ/mol, trap density,  $N_t = 5 \times 10^{19} \text{ \#/cc}$ .

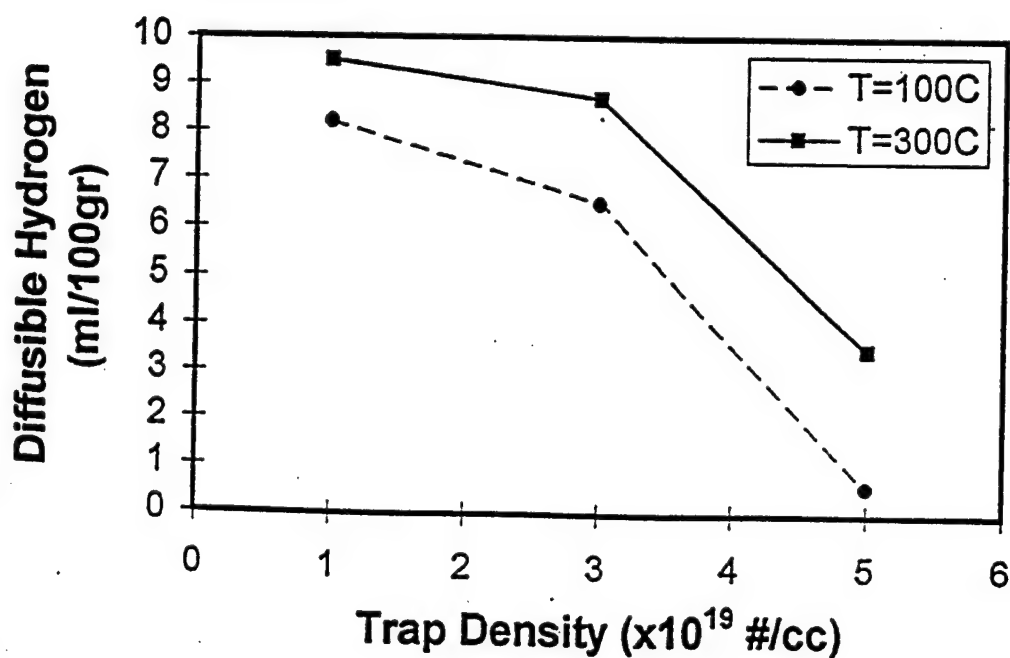


Figure 15. Effect of trap density on the diffusible hydrogen content. Initial diffusible hydrogen content is 15 ml/100g.  $M_s = 400^\circ\text{C}$ ,  $\Delta t_{8/5}$  is 5 seconds,  $E_b$  is 100 kJ/mol.

**B. Weld Metal Hydrogen Trapping, by I. Maroef, D. L. Olson, M. Eberhart, and C. Lensing, Colorado School of Mines**

**Introduction/Background**

Hydrogen management during welding of high strength steels can be improved by the introduction of "traps" that can reduce the amount of diffusible hydrogen at high temperatures. The desired end result is the reduction of diffusible hydrogen to a level that is insufficient to initiate a hydrogen cracking. The hydrogen traps in the form of atomic or microstructural imperfections such as grain boundaries, dislocations, and second-phase particles have higher binding energies with hydrogen than the host lattice does. A prominent effect of this binding energy is to decrease the apparent hydrogen diffusivity relative to that for hydrogen in pure iron. It has long been recognized that when the steel cools to below 200°C, the relationship between this apparent diffusion coefficient,  $D_{Happ}$ , and lattice diffusion coefficient for hydrogen in a pure iron lattice,  $D_{Hpure Fe}$ , is given by:

$$D_{Happ} = \frac{D_{Hpure Fe}}{1 + K \exp\left[\frac{E_b}{RT}\right]}$$

where  $E_b$  is the trap energy which is the difference between hydrogen-trap and hydrogen-Fe lattice binding energies ( $E_b = E_{trap} - E_{Fe}$ ),  $K$  is the density of trap sites and  $RT$  has its usual significance.

A trapped hydrogen atom must acquire an energy substantially greater than the lattice migration energy to escape the trap and contribute to the apparent diffusivity; hence, the effectiveness of a given trap is directly related to the hydrogen-trap energy,  $E_b$ . Trap energies in the range of 20 to 130 kJ/mole have been reported. Calculation using experimentally determined trap formation data shows that certain rare earth and transition metal oxides begin to absorb hydrogen at high temperatures during welding cooling cycle and thus the addition of these rare earth and transition metals to welding consumables holds much promise in significantly reducing the diffusible hydrogen concentration.

The quantity  $E_b$  of a specific trap site can be calculated more directly than it can be measured. The trap energies can be determined using the first principle electronic structure techniques. These techniques were used to quantify the effectiveness of specific potential getter elements, and thus assisted in selection of elemental trap additions. The calculated and experimentally determined trap energy values are reported and compared. Their effect on diffusible hydrogen content and the resulting transport process are reported and discussed. The selection of the type and amount of an effective hydrogen trap elemental addition to the welding consumable is made. The various hindrances of the use of hydrogen trapping are discussed, such as the transferability of the addition across the welding arc and the influence of the multiple thermal cycles resulting from multiple-pass welding.

**Conclusions**

1. Review of the use of hydrogen trapping concept to reduce diffusible hydrogen in weldments is given.
2. Both experimental and theoretical data is used to determined the most effective hydrogen getter addition for welding consumables.
3. Various issues concerning the effective use of hydrogen getters through welding consumable additions are identified.

# A. Hydrogen Trapping in Ferrous Weld Metal,

by C. A. Lensing, I. Maroef, and D. L. Olson, Colorado School of Mines

One method of controlling the content of diffusible hydrogen in ferrous metal welding is through the use of "traps." These traps, in various forms of microstructural defects, can reduce the amount of diffusible hydrogen to a level where susceptibility to delayed cracking is reduced in the weld metal. The effectiveness of a given trap is directly related to the hydrogen-trap binding energy. Certain rare earth and transition metal oxides have been calculated to have high hydrogen-trap binding energies ranging from 100 to 130 kJ/mole, and show promise in trapping hydrogen. A study of one kind of trap has been conducted in pure iron. These results have been used as a basis for the more complex system in high strength low alloy (HSLA) steel where various kinds of traps are working simultaneously.

The amount of diffusible hydrogen content during welding thermal cycle has been predicted based on known hydrogen lattice diffusivity and common trapping kinetic parameters. Combined effects of high binding energy ( $\geq 100$  kJ/mole) and a threshold trap density ( $\cong 5 \times 10^{19}$  #/cc) during a relatively fast cooling rate ( $\Delta t_{8/5} \cong 5$  s) were shown to accelerate the reduction of diffusible hydrogen content. These calculations assumed a high initial value of diffusible hydrogen (15 ml/100 g) at 1600°C and was reduced down to a value less than 4 ml/100 g at 100°C under the above conditions. These predictions are compared to experimental results for further optimization.

Gas metal arc welding (GMAW) was conducted on pure iron and high strength low alloy (HSLA) steel. Controlled level of hydrogen content was introduced through the shielding gas. Gas chromatography (GC) and interstitial analyses were used to analyze the diffusible hydrogen and trapped hydrogen content in the weld metal, respectively. Transmission electron microscopy (TEM) was utilized to characterize the structure and density of traps within the weld metal. In addition, a kinetic method such as thermal analysis was employed to determine the trap binding energy and trapping kinetic parameters. The evolution of hydrogen from trapped sites during constant rate heating results in multiple peaks corresponding to traps with different binding energies. The shape of the individual peak is related to the kinetics of trapping. The nature of hydrogen trapping is discussed in the light of experimental results obtained from pure iron. In turn, a more complex trapping behavior was investigated in HSLA steel weld. The experimental results were compared to the theoretical calculations for verification of the trapping characteristics in the weld metal. Based on these results, the effectiveness of these traps in both pure iron and HSLA steel welds are discussed. Also, an optimum composition has been determined for rare earth and transition metal additions in welding consumables for HSLA welding. Finally, the effects of the trapping additions, the rare earth and transition metals, on the weld metal trapping, on the weldability, and on the weld metal properties are discussed.

## THE ROLE OF HYDROGEN TRAPPING IN HYDROGEN MANAGEMENT OF STEEL WELDING

Olson D.L, Maroef I. and Lensing C.  
Center for Welding, Joining, and Coating Research  
Colorado School of Mines  
Golden, Colorado 80401-1887, USA

### INTRODUCTION

Traditionally, hydrogen assisted cracking in steel welding is considered to occur when the necessary conditions for cracking are fulfilled simultaneously. These conditions encompass the combination of diffusible hydrogen content, restraint stress, hardness, and temperature range between -100 and 100° C [1]. Common practices to prevent hydrogen cracking in high strength steel weldments are the pre- or post-weld heat treatment, the use of non-cellulosic electrodes with proper baking and edge preparation. Heat treatment has been necessary to control the heat affected zone (HAZ) hardness. The higher the strength of the steel, the lower the acceptable weld hydrogen content, even to levels as low as one to two ml H<sub>2</sub>/100 g deposit metal [1,2]. With proper selection and use of welding consumables, a minimal hydrogen content can be introduced to weld pools. However consideration for hydrogen cracking in high strength steel welding involve further aspects. The high strength level of this class of steel yields non-uniform distribution and high levels of restraint stresses in the weld joints. The high levels of restraint stress in the weld joint. Often times, this situation is accompanied by non-uniform hydrogen distribution in then weld joints, requiring very low acceptable hydrogen content [3]. This situation will become a more crucial problem with the welding of ever higher strength steels.

Non-uniform hydrogen distribution across the weldment can result from poorly matched welding consumables and base metal compositions [4]. Stress induced hydrogen diffusion and hydrogen transport by dislocation sweeping are also factors generally considered to be responsible for localized accumulation of hydrogen at stress concentration regions [5,6]. Dislocation sweeping in weld joints will be operative if the hydrogen cracking mechanism is micro-void coalescence, which is a result of localized plasticity, has been shown to occur by Gedeon and Eagar [8].

Recent scientific approaches supported by FEM calculation have made it possible to predict the proper heat treatment that can prevent an undesirable hydrogen distribution in critical weld joints [9]. However, such methodologies require costly testing programs and tight temperature controls as well as controls as well as control of welding parameters. Such controls are frequently found to be impractical and complicated. Therefore, new approaches to hydrogen management in steel welding, based on more fundamental metallurgical understanding and predictions, need to be investigated.

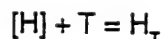
Approaches for mitigating hydrogen cracking by metallurgical modification, including alloy additions has been discussed [10,11]. One of these approaches is to employ hydrogen trap sites in the weld metal. The purpose of introducing hydrogen trap sites is to force a redistribution of absorbed hydrogen, partitioning it between lattices sites and trap sites, so that the critical hydrogen concentration required to induce interfacial decohesion at potential crack initiation sites cannot readily be obtained. In addition, the presence of deep trap sites will minimize the operation of dislocation sweeping by reducing the

probability of hydrogen-dislocation interaction, which is the origin of hydrogen induced micro-plasticity observed in steel. Hydrogen atoms which reside in the lattice sites are generally termed as diffusible hydrogen atoms. They are considered detrimental because they have much more chance to travel and accumulate at any stress concentration regions than those hydrogen atoms trapped in deep trap sites. This paper addresses the feasibility of using weld metal hydrogen trapping as a mean to assist in hydrogen management in high strength steel welds, and thus reduce the susceptibility to hydrogen cracking.

## CHARACTERISTICS OF HYDROGEN TRAPPING IN STEEL.

In steel, hydrogen is not homogeneously distributed. Hydrogen will be found not only in the host lattice, but also segregated to atomic and microstructural imperfections such as: vacancies, solute atoms, dislocations, grain boundaries, voids, and second phase particles. In these localized regions, the mean residence time of a hydrogen atom is considerably longer than in a normal interstitial lattice sites. In the extreme case, these regions are sinks which retain the atom even during mechanical loading. The generic term for this phenomenon is trapping and these localized regions are hydrogen trap sites [12-14].

The strength of trap site, i.e. the fraction of time a hydrogen atom resides in that trap site, depends on the binding energy  $E_b$  of the hydrogen atom to the trap. To qualitatively describe the strength of trap site, a single hydrogen-trap interaction may be written as a first-order reaction:



where  $[H]$  are the diffusible hydrogen atoms,  $T$  is the trap site, and  $H_T$  is the trapped hydrogen. The energy associated with the reaction is the hydrogen - trap binding energy,  $E_b$ . Hydrogen atoms may then be considered as being either released from, or captured by, the trap sites until equilibrium is reached. The kinetics of hydrogen release from and capture by a trap site has been derived by McNabb [15] as follows:

$$\frac{\delta\phi}{\delta t} = kC_L(1-\phi) - p\phi$$

Where  $\phi$  is the fraction of trap occupied at time  $t$ ,  $C_L$  is the diffusible hydrogen concentration, and  $k$  and  $p$  are the rate constants for the capture and release of hydrogen, respectively. The ratio of  $k$  to  $p$  ( $k/p$ ) is proportional to  $\exp(E_b/RT)$ .

Numerous studies on different traps have been reviewed by several authors [16-19]. From various reported data, values of hydrogen-trap binding energies in iron were identified and are listed in Table 1. In addition, an electronic structure calculation was also applied in searching for other forms of potential traps that can be introduced in steel welding [20]. Several inclusions in steel were investigated and, among them,  $Ce_2O_3$  oxide was found to have the highest binding energy followed by  $TiC$ ,  $Y_2O_3$ ,  $VC$ ,  $NbC$  and finally  $Mo_2C$ , in the order of decreasing energy. The binding energy of 60 kJ/mol H for a dislocation or a grain boundary is generally regarded as the typical limiting value of a reversible trap. With this energy level, a reversible trap becomes effective in capturing hydrogen around 400 K but does not reach saturation at room temperature, as shown in Figure 1. A reversible trap with binding energy lower than 60 kJ/mol-H will not be able to prevent hydrogen cracking. The trapped hydrogen will be picked up by moving dislocations and eventually be delivered to crack initiation sites [21]. The preferred traps are then those having binding energies higher than 60 kJ/mol-H and are termed irreversible traps [22].

The microstructure of high strength alloy steel is complex and contains a wide range of trap types, such as dislocations, grain boundaries and inclusions. Observation of specific hydrogen traps in a complex microstructure has been done through the use of hydrogen thermal desorption analysis. This analysis works on the fact that, during constant rate heating, each type of trap site releases hydrogen at a specific temperature range depending on its trapping energy. It enables one to measure the actual amount of hydrogen being trapped at a specific trap site. A typical experimental set-up for this analysis, as shown in Figure 2, includes a temperature controlled furnace for temperature ramping of the hydrogen charged sample and a gas chromatograph for hydrogen gas detection. Hydrogen release from dislocations, grain boundaries, micro-voids and several inclusions; such as TiC particles; have been well documented. Such data, reported by Lee et.al [23, 24] is shown in Figure 3. TiC, which has a higher binding energy than dislocations, releases hydrogen at much higher temperature than does dislocation.

## THE ROLE OF HYDROGEN TRAPS FOR SAFE WELDING CONDITION IN HIGH STRENGTH STEEL WELDING.

Initial hydrogen content which is established upon the completion of welding process will change in a rate that depends on the thermal experience of the weldment. Hydrogen will degas from the weld metal during cooling cycle due to decrease in hydrogen solubility as the temperature drops. In addition, the remaining hydrogen atoms in the weld metal will also redistribute themselves to various microstructural features in the weld metal, to the base plate, and to stress concentration regions in the weld joint as the restraint stress builds up during the cooling cycle. Rather than the initial hydrogen content, Terasaki, Karpi and Satoh [25] showed that it is the remaining diffusible hydrogen at 100° C that correlates to the critical stress required for HAC. Hence, heat treatments of weld joints should be done to minimize the content of diffusible hydrogen that remains at 100° C.

Necessary heat treatments to manage hydrogen content in a complicated weld joint of high strength steel can be suggested through cumbersome finite element analysis. However, in many occasions, these heat treatments require very tight temperature control because it involves a limited window of time and temperature ranges. While an extensive heat treatment is necessary for sufficient degassing of hydrogen, limitations are necessary to maintain mechanical properties and to minimize hydrogen localization. Hydrogen localization at stress concentration regions occurs due to stress assisted hydrogen diffusion and due to the operation of dislocation assisted hydrogen transport (dislocation Sweeping). Localized hydrogen accumulation in high strength steel has been shown to be enhanced after post weld heat treatment is imposed in the weld joint [26]. In Figure 4.b, local accumulation of hydrogen in welded joints is developed after post weld heat treatment. This localized hydrogen accumulation occurred even though the average content of hydrogen is small than that of the weld joint prior to post weld heat treatment, shown in Figure 4a. This result implies that some weld joints may become very critical and highly restrained that there is no acceptable heat treatment that can be easily recommended for its safe welding condition.

Alternative method to prevent HAC in high strength steel requires substitution of heat treatment procedures. The presence of deep hydrogen traps in the weld metal may significantly alter hydrogen content during welding thermal experience. A reduction of the concentration of diffusible hydrogen has been demonstrated in this study, through the introduction of neodymium and yttrium to the weld metal. These additions were introduced as Fe-Nd and Fe-Y powder compounds, which are inserted



into metal cored wire electrodes for gas metal arc welding consumables. The result for low carbon-low alloy steel is shown in Figures 5 which shows significant reduction of diffusible hydrogen (4 to 7 ml  $H_2/100g$ ) when 150 to 600 ppm trapping elements are present in the weld metal. Also in this study, hydrogen evolution of iron weld metal with neodymium additions was contrasted with an iron weld metal free of deep traps. At high temperatures, there is a peak of hydrogen evolution in the trap containing weld sample, indicative of deep traps associated with neodymium. Similar results for yttrium additions to HSLA weld metal is also shown in Figure 7.

Hydrogen trapping has the potential of providing accelerated reduction of diffusible hydrogen; hence, minimizing localization of hydrogen in weldment. Olson et.al [11] investigated the partitioning of hydrogen between lattice sites and trap sites during the welding cooling cycle with diffusion models, similar to that of the McNabb and Foster model [15]. Such a model calculates the variation of diffusible (HD) and trapped (HT) hydrogen content (in Figure 8.a.) as a function of temperature and time during the cooling cycle (in Figure 8.c.) An abrupt change of slope can be observed in the diffusible hydrogen content right after the martensite start temperature,  $M_s$ , of the weld metal. The phase transformation from austenite to martensite is accompanied by a large increase in the hydrogen diffusion coefficient. This model also shows that the diffusible hydrogen content (HD) of the weld metal containing traps is predicted to be lower than that of the steel without traps. The kinetics of hydrogen capture can be more clearly explained from Figure 8.b, which shows the equilibrium trap occupancy ( $\phi_0$ ), the actual trap occupancy ( $\phi$ ), and the rate of hydrogen capture ( $d\phi/dt$ ). the hydrogen capture rate depends both on hydrogen diffusivity and the driving force for hydrogen entrapment ( $\phi_0 - \phi$ ). it can be seen that a sudden increase in the rate of capture always follows the occurrence of martensite phase formation, where both capture rate determining factors are maximized.

This model was developed in order to set criteria for the selection of traps to prevent HAC in high strength steel welding. Proper trap additions should reduce the amount of diffusible hydrogen rapid enough so that, during the cooling cycle, the diffusible hydrogen levels at hydrogen cracking susceptible temperatures (100-300° C) is below the critical limit. The model demonstrates that this requirement can be achieved with proper combination of several factors such as martensite start temperature of the weld metal, trap-binding energy, trap concentration, and welding cooling rate.

The effect of each of these factors to the amount of diffusible hydrogen at 100° C as well as 300° C are summarized and presented in Figure 9 to 12. The first important parameter of a trap is the hydrogen-trap binding energy. In this calculation four values of binding energies that correspond to different trap sites were used. They are 60 kJ/mole-H for dislocations, 80 kJ/mole-H for  $Al_2O_3$  inclusions, 100 kJ/mole-H for TiC particles, and 120 kJ/mole-H for rare earth additions. As shown in Figure 9, the amount of diffusible hydrogen content decreases with increasing hydrogen-trap binding energy. The major advantage of traps with high binding energy is that they provide a high driving force for hydrogen capture in high temperature regions. The data at 300° C provides better insight to how much faster the hydrogen is captured by high binding energy traps as opposed to those traps with low binding energy. Should the HAC start to occur at a higher temperature than 100° C (which may be possible for weld metal with low martensite start temperature) the weld metal containing high binding energy traps will have a better chance to survive.

The diffusivity of hydrogen in the austenite phase is very small, so that the hydrogen cannot be effectively captured or removed from the weld metal until the martensite temperature is reached. The lower the martensite start temperature, the longer time hydrogen has to remain in the weld metal

lattice sites. This behaviour also means that the available temperature range for effective hydrogen diffusivity and trapping in the ferrite phase becomes less effective. The extreme situation is depicted in figure 10 for the case of weld metal possessing martensite start temperature of 400° C. The advantage of using a trap with higher binding energy, i.e., higher capture rate, is then obvious in this very narrow temperature range situation. However, the employment of high binding energy traps for a high martensite start temperature weld metal can lead to a situation where the trapping capacity will be wasted in high temperature regions. This behaviour can occur even when the hydrogen diffusivity provides a high potential for easy hydrogen removal from the weld metal. Therefore, the selection of hydrogen traps must consider other factors than just the weld metal or consumable alloying contents.

Conventional hydrogen management usually applies proper heat treatment or sufficiently low cooling rate to provide easy hydrogen removal from the weld and to form a less susceptible microstructure to HAC. In case of weld metal containing trap sites, a certain rate of cooling is also necessary to allow sufficient hydrogen capture time before the temperature reaches 100° C. In the present calculation, the cooling rate is assumed to occur relatively fast, so that sufficient hydrogen removal by lattice diffusion alone can not be obtained. The effect of cooling rate, shown in Figure 11, appears to be similar to that of the martensite start temperature. A very fast cooling rate, such as a rate with  $\Delta t_5$  equal to one second, does not permit enough time for hydrogen to leave the weld metal or jump to trap sites. On the other hand, at a slightly slower cooling rate, the presence of traps may yield a low diffusible hydrogen content at 100° C and alleviate the tendency for weld metal HAC. This prediction shows the potential use of traps, substituting for the tight heat-treatment procedure necessary for high strength steel welding.

The concentration of trap sites translates into the capacity to hold hydrogen atoms. A higher concentration of trap sites in the weld metal will produce a lower diffusible hydrogen content, which is in agreement with the calculated result shown in Figure 12. There is also an apparent threshold number of trap sites for optimum hydrogen trapping. The concentration of traps used in the present calculation corresponds to a 100 to 500 ppm range of substitutional atom traps in weld metal, the trap sites on the surface are of the inclusion - matrix interface. Depending on the cooling rate the number of trap sites used in this calculation may correspond to a relatively high inclusion volume fraction that yields weld metal with intrinsically low toughness. Obviously, the concentration of trap sites that can be used is limited to an extent in which the toughness is still maintained at an acceptable level. This issue suggests that the success of using hydrogen, so that a high local accumulation of hydrogen at crack initiation sites can be prevented. Furthermore, in high strength steel welding, where hydrogen is highly concentrated at crack initiation sites, the presence of traps may give a higher tolerance for average hydrogen content. Normally, a low maximum acceptable level of hydrogen content in the weldment is required for conventional welding procedures.

The importance of high binding energy in minimizing release of hydrogen during multiple thermal cycles is contrasted in figure 13. A trap site with binding energy of 60 kJ/mol-H would release extensive amount of hydrogen during re-heating, which can easily and contribute to localization of hydrogen at potential crack initiation sites, especially at the weld root. On the other hand a trap with 120 kJ/mol-H binding energy will release very little amount of hydrogen atoms and quickly re-trap them before these hydrogen atoms have the chance to migrate to crack initiation sites.

## SUMMARY AND PROSPECTIVES.

Recent efforts to understand HAC in welding of ever increasing higher strength steels involve investigations on distributions of hydrogen, restraint stress, hardness, and temperature in the weld joint, in addition to the effect of weld thermal history. The high strength level of these steels promotes early restraint stress build up; hence, stress-concentration regions can quickly accumulate hydrogen. It has been proven to cause HAC, even though the nominal diffusible hydrogen concentration is below the critical value.

Introduction of hydrogen traps into the weld metal has two potential advantages which would help reduce the susceptibility of weld joints to hydrogen cracking. The first is the capability to provide accelerated reduction of diffusible hydrogen content. The second is the possibility of these traps to alleviate localization of hydrogen during thermal cycles.

A trap site should have a high binding energy to allow rapid hydrogen capture, especially in cases where the martensite start temperature is low, as well as minimizing release of hydrogen from trap sites during multi-pass welding. In addition, depending on the concentration of trap sites and their binding energies, a minimum cooling rate is still required to achieve diffusible hydrogen content below the critical limit. However, this minimum cooling rate is still predicted to be faster than those of most conventional heat treatments used to prevent HAC in weld joints.

## ACKNOWLEDGMENT

The authors acknowledge and appreciate the research support of the US Office of Naval Research.

## REFERENCES

1. N. Bailey, F.R. Coe, T.G. Gooch, P.M. Hart, N. Jenkins, and R.J. Pargeter, *Welding Steel without Hydrogen Cracking*, 2nd Edition, Abington, 1993.
2. R. Wong, J. Blackburn, J. DeLoach, and R. DeNale, in *Conf. Proc. Hydrogen Management in Steel Weldments*, DSTO and WTIA, Melbourne, Australia, Oct, 23, 1996, 35 - 48.
3. V.F. Musiyachenko and S.B. Kasatkin, *Automatic Welding*, Sept. 1985, 22-26.
4. W. Wang, S. Liu, and D.L. Olson: in *Proc. Intl. Conf. 'Offshore Mechanics and Arctic Engineering - Materials Engineering'*, Vol. III, Florence, Italy, 1996, ASME, 403 -409.
5. N. Yurioka and H. Suzuki: *International Materials Reviews*, 1990, 35(4), 217 - 249.
6. V.F. Musiyachenko and S.B. Kasatkin: *Automatic Welding*, 1985, 22 - 26.
7. C.D. Beachem, *Metal. Trans. A*, Vol. 3, 1972, 437-451.
8. S.A. Gedeib and T. Eagar: *Welding Journal*, 1990, 213 - 220s
9. T. Boellinghaus, H. Hoffmeister, and C. Schubert: in *Proc 4th Intl. Conf. 'Trends in Welding Research'*, Gatlinburg, Tennessee, 5-8 June 1995, 25 - 30.
10. J.R. Scully, J.A. Van Den Avyle, M.J. Cieslak, A.D. Romig, Jr., and C.R. Hills: *Met. Trans. A*, 1991, Vol. 22, 2429-2445.
11. D.L. Olson, I. Maroef, C. Lensing, D. Smith, T. Wildeman, and M. Eberhart: in *Conf. Proc. 'Hydrogen Management in Steel Weldments'*, DSTO AND WTIA, Melbourne, Australia, Oct. 23, 1996, 1 - 19.
12. G.M. Pressouyre and I.M. Bernstein, *Metall. Trans. A*, Vol. 9, 1978, 1571-1580.
13. G.M. Pressouyre and I.M. Bernstein, *Metall. Trans. A*, Vol. 12, 1981, 8835-844.
14. I.M. Bernstein and G.M. Pressouyre, in *Hydrogen Degradation of Ferrous Alloys*, ed. by R.A. Oriani, J.P. Hirth and M. Smialowski, Noyes Pub., 1985, 641-685.

15. A. McNabb and P.K. Foster, *Trans. TMS-AIME*, Vol. 227, 1963, 618-627.
16. J.P. Hirth, *Metall. Trans. A*, Vol. 11, 1980, 861-890.
17. I.M. Bernstein and G.M. Pressouyre, in *Hydrogen Degradation of Ferrous Alloys*, ed. by R.A. Oriani, J.P. Hirth and M. Smialowski, Noyes Pub., 1985, 641-685.
18. P. Kedzierzawski, in *Hydrogen Degradation of Ferrous Alloys*, ed. by R.A. Oriani, J.P. Hirth and M. Smialowski, Noyes Pub., 1985, 271 - 288.
19. R. Gibala and A.J. Kurnick, in *Hydrogen Embrittlement and Stress Corrosion Cracking*, ASM, Metals Park, Ohio, 1984, 61 -77.
20. M. Eberhart, Private communication, Colorado School of Mines, 1995.
21. J.K. Tien, A.W. Thompson, I.M. Bernstein, and R.J. Richards, *Metall. Trans. A*, Vol. 7, 1976, 821 - 829.
22. G.M. Pressouyre and I.M. Bernstein, *Metall. Trans. A*, Vol. 12, 1981, 835-844.
23. W.Y. Choo and J.Y. Lee, *Metall. Trans. A*, Vol. 13, 1982, 135-140.
24. S.M. Lee and J.Y. Lee, *Acta Metall.*, Vol. 35(11), 1987, 2695-2700.
25. T. Terasaki, R. Karppi, and K. Satoh, *Trans. Japan Welding Society*, Vol. 10(1), 1979, 53-57.
26. Grivnyak I, in *Scientific Problems in Welding and Special Electrometallurgy Part 3*, Kiev Naukova dumka, 1970, 38-48.
27. A.J. Kurnick and H.H. Johnson, *Acta Metall.*, Vol. 28, 1980, 33-40.
28. K. Ono and M. Meshi, *Acta Metall.*, Vol. 40 (6), 1992, 1357-1364.
29. T. Asaoka, C. Dagbert, M. Aucouturier, and J. Galland, *Scripta Metall.*, Vol. 11, 1977, 467-472.
30. E. Chornet, and R.W. Coughlin, *J. Catal.*, Vol. 72, 1972, 246-265.
31. D.O. Hayward and B.M.W. Trapnell, in *Chemisorption*, Butterworths, London, 1964, 203.
32. J.R. Scully, J.A. Van den Avyle, M.J. Cieslak, A.D. Romig, JR., and C.R. Hills, *Metall. Trans. A*, Vol. 22, 1991, 2429-2445.
33. K.Y. Lee, J.Y. Lee and D.R. Kim, *Mater. Sci. Eng.*, Vol. 67, 1984, 213.
34. H.H. Podgurski and R.A. Oriani, *Metall. Trans.*, Vol. 3, 1972, 2055-2063.
35. J.L. Lee and J.Y. Lee, *Metal Sci.*, Vol. 17, 1983, 462-432.
36. J.L. Lee and J.Y. Lee, *Metall. Trans. A*, Vol. 17, 1986, 2183-2186.
37. P. Lacombe, M. Aucouturier, J.P. Laurent, and G. La Passet, in *Stress Corrosion Cracking and Hydrogen Embrittlement of Iron Base Alloys*, R.W. Staehle, J. Hochmann, R.D. McCright, and J.E. Slater, eds., NACE-5, Houston, TX, 1977, 423-430.
38. H.G. Lee and J.Y. Lee, *Acta Metall.*, Vol. 32, 1984, 1581-1589.
39. G.M. Pressouyre and I.M. Bernstein, *Metall. Trans. A*, Vol. 9, 1978, 1571-1580.
40. G.M. Pressouyre, *Metall. Trans. A*, Vol. 10, 1979, 1571-1573.

Table 1. Hydrogen trapping in Iron. Reference state: H in perfect lattice.

Trap Site	Binding Energy (kJ/mol)	Matrix	Assessment Method	Ref.
H-Dislocation	26	Iron	Thermal analysis	23
H-Dislocation	59	Iron	permeation	27
Core (mixed)				
H-grain boundary	18-20	C-Mn Steel	thermal analysis	23
H-grain boundary	60	Iron	thermal analysis	28
H-grain boundary	59	Iron	permeation	27,29
H-Free surface	70	Iron	permeation	30
H-Free surface	95	Iron	permeation	31
b-NiAl	27	Steel *	permeation	32
H-PdAl interface	34	Steel *	permeation	31
H-Fe-oxide interface	47	C-Mn Steel	thermal analysis	33
H-AlN interface	65	Iron	permeation	34
H-MnS interface	72	C-Mn Steel	thermal analysis	35
H-Al <sub>2</sub> O <sub>3</sub> interface	79	C-Mn Steel	thermal analysis	36
H-Fe <sub>3</sub> C interface	84	C-Mn Steel	permeation	29,37
H-TiC interface	87	Iron	thermal analysis	38
H-TiC interface	95	C-Mn Steel	permeation	39
H-Nd	129	Iron	calculated	40

\* Matrix element is precipitation hardened martensitic stainless steel.

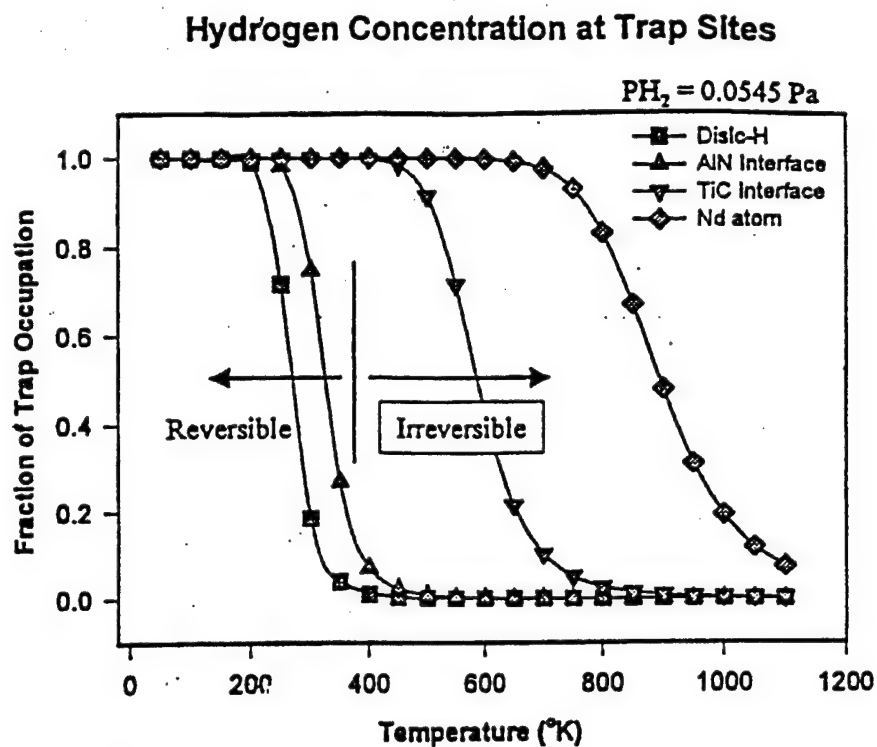


Figure 1. Fraction of filling by hydrogen at trap sites as a function of temperature for various hydrogen-trap binding energies.

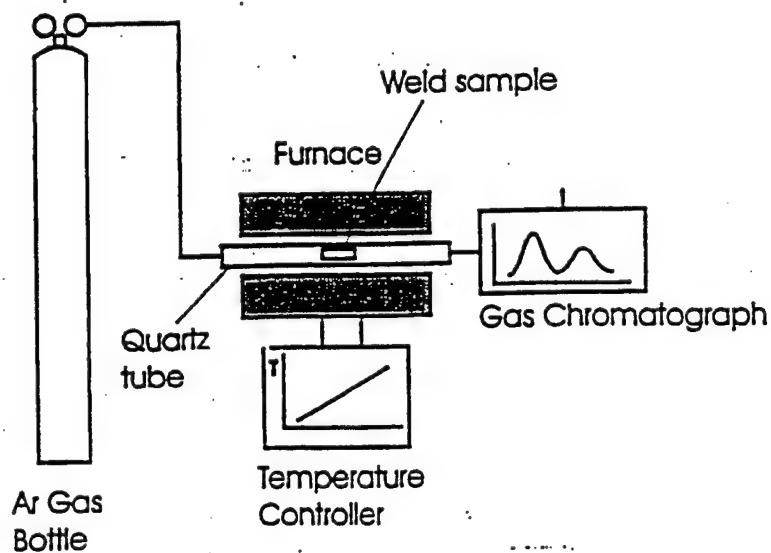


Figure 2. Typical set-up for hydrogen thermal desorption analysis.

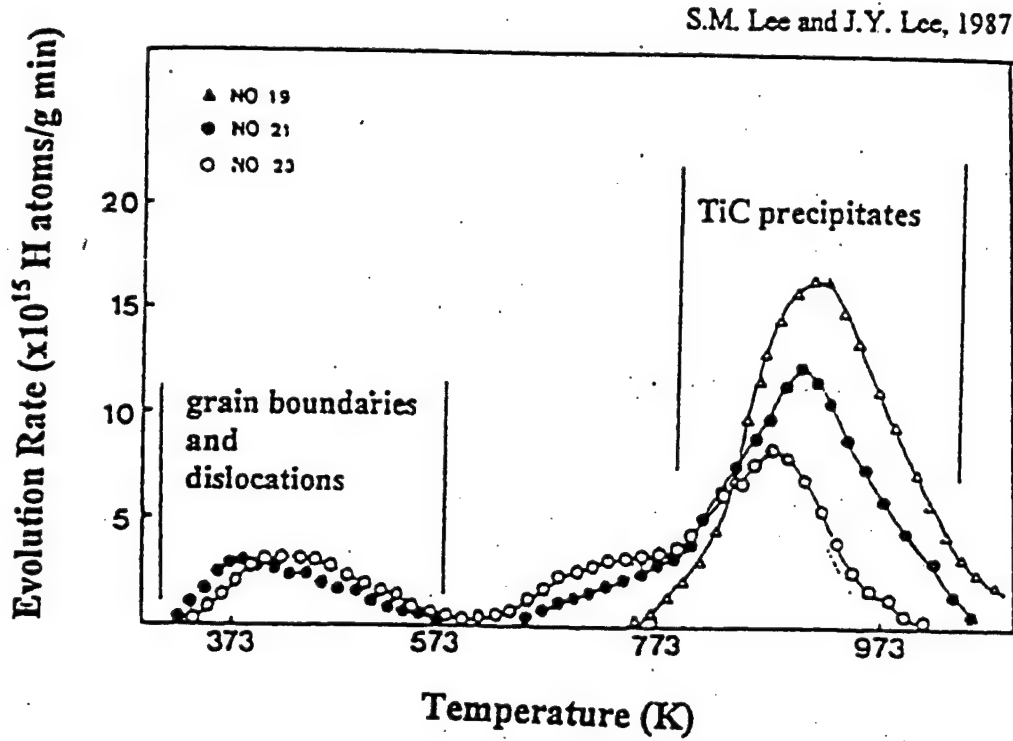


Figure 3. Hydrogen thermal desorption of steel containing TiC particles. Due to variation in annealing, the TiC interface structure changes from coherent at small size to incoherent at larger size. This change of interface structure is accompanied by an increase of hydrogen release temperature [24].



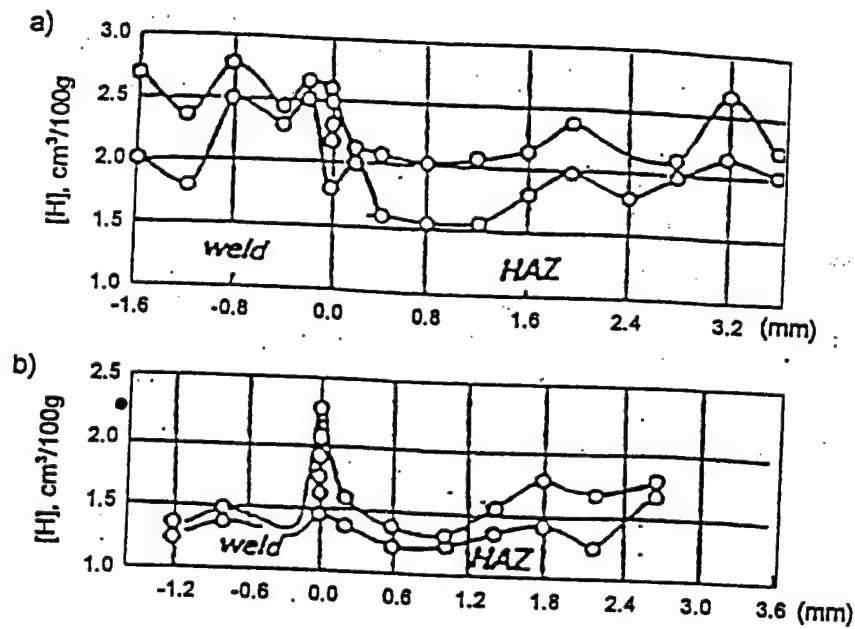


Figure 4. Distribution of hydrogen in a welded joint in 15Kh1M1F steel : (a). not heat treated after welding; (b). tempered at a high temperature (730° C) after welding [26].

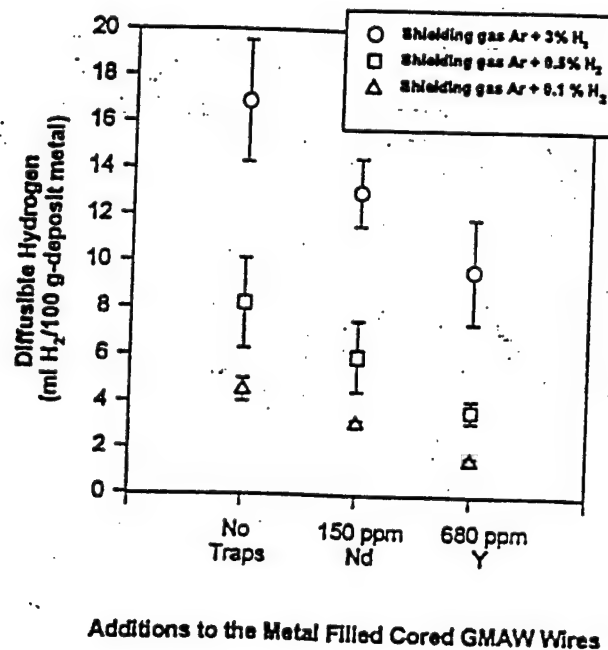


Figure 5. Effect of trap additions to the amount of diffusible hydrogen of weld samples welded with GMAW process at nominal heat input 1.5 kJ/mm

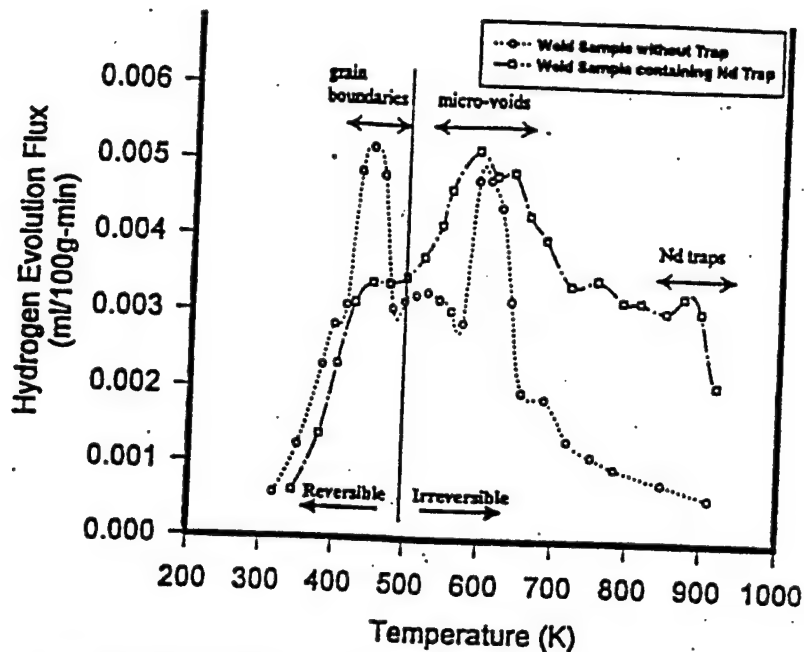


Figure 6. Hydrogen desorption at  $4^{\circ}\text{C/min}$  heating rate of iron weld sample free of deep traps and iron weld sample containing neodymium deep traps. The peak at 450 K is the hydrogen released from grain boundaries, at 600 K from micro-voids and at 873 K from neodymium associated trap sites

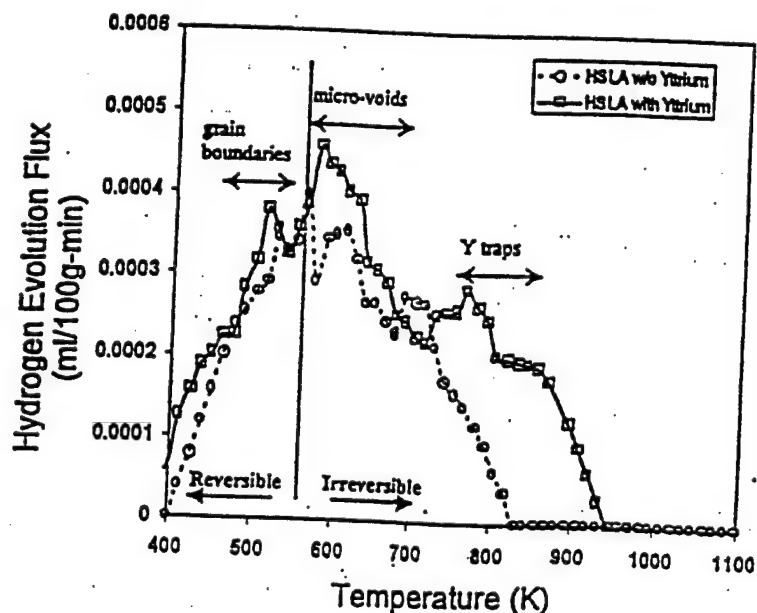


Figure 7. Hydrogen desorption at  $3^{\circ}\text{C/min}$  heating rate of HSLA weld sample free of deep traps and HSLA weld sample containing yttrium deep traps. The peak at 450 K is the hydrogen released from grain boundaries, at 600 K from micro-voids and at 800 K from yttrium associated trap sites.

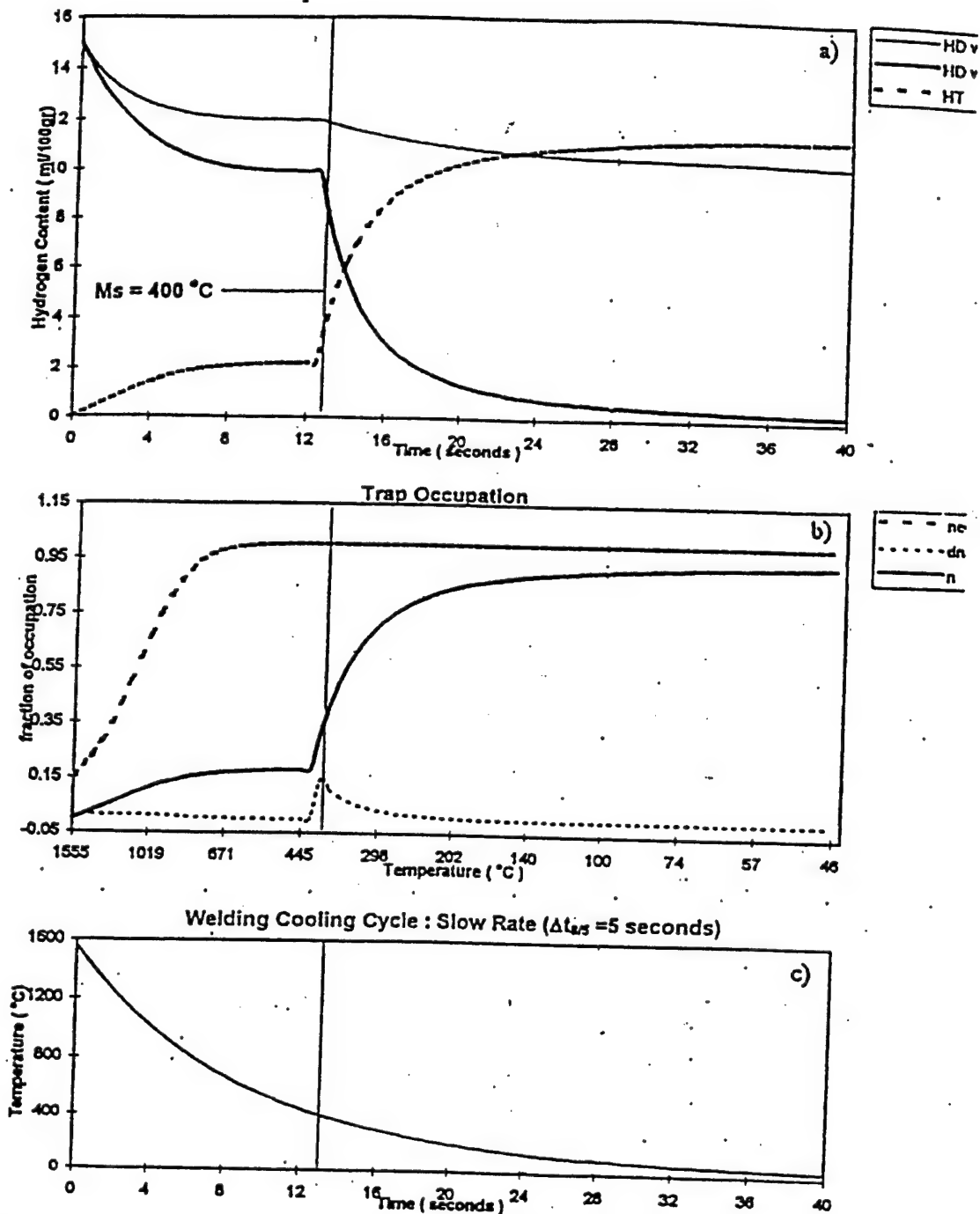


Figure 8. Theoretical evaluation on the performance of hydrogen trapping during welding cooling cycle. Initial diffusible hydrogen in weld metal is 15 ml/100g. In (a), the notation HD stand for diffusible hydrogen, HT is the trapped hydrogen. In (b),  $\phi$  is the fraction of trap occupation by hydrogen and  $\phi_0$  is the equilibrium fraction of occupation determined by the Fermi-Dirac distribution [11].

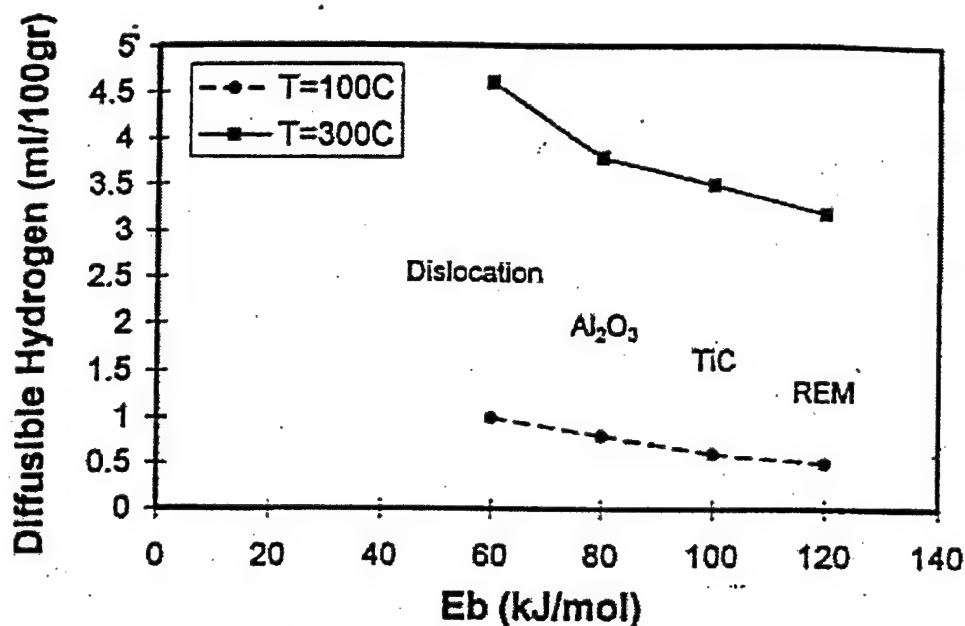


Figure 9. Summary of diffusible hydrogen content at 100 and 300° C during cooling cycle, as a function of Hydrogen-trap binding energy. Initial diffusible hydrogen content is 15 ml/100g.  $M_s=400^\circ\text{C}$ ,  $\Delta t_{25} = 5$  seconds, trap density  $N_t = 5 \times 10^{19}/\text{cc}$  [11].

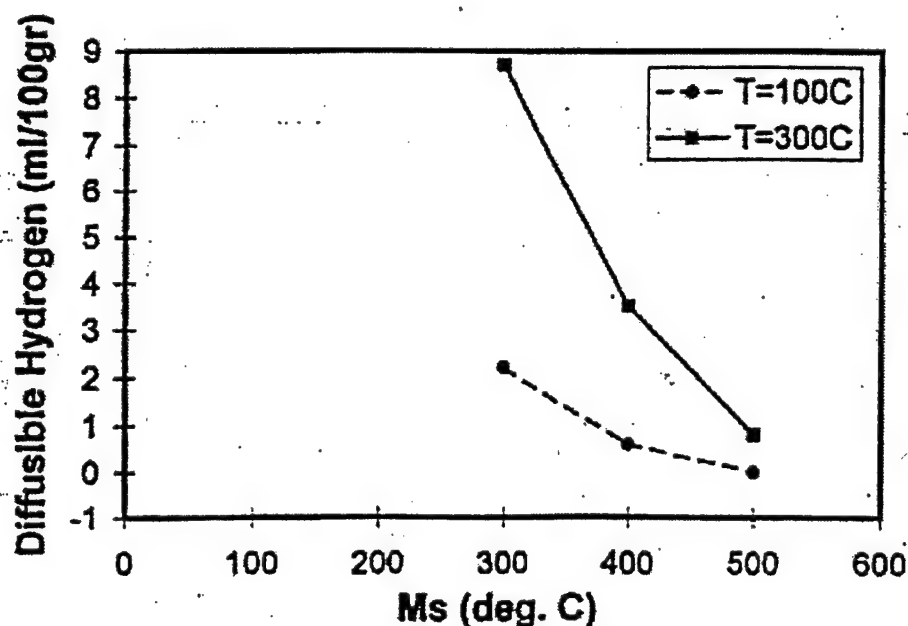


Figure 10. Summary of diffusible hydrogen content at 100 and 300° C during cooling cycle, as a function of Martensite start temperature. Initial diffusible hydrogen content is 15 ml/100g,  $E_B=100$  kJ/mol-H,  $\Delta t_{25} = 5$  seconds, trap density  $N_t = 5 \times 10^{19}/\text{cc}$  [11].

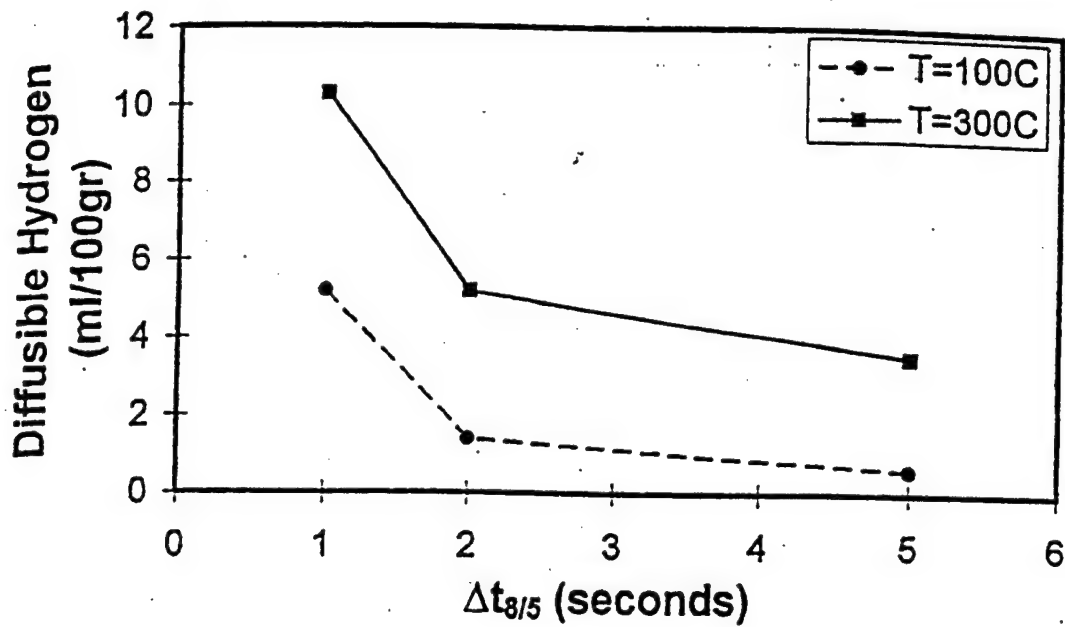


Figure 11. Summary of diffusible hydrogen content at 100 and 300° C during cooling cycle, as a function of cooling rate. Initial diffusible hydrogen is 15 ml/100g,  $M_s = 400^\circ\text{C}$ ,  $E_B = 100\text{ kJ/mol-H}$ , trap density  $N_t = 5 \times 10^{19}/\text{cc}$  [11].

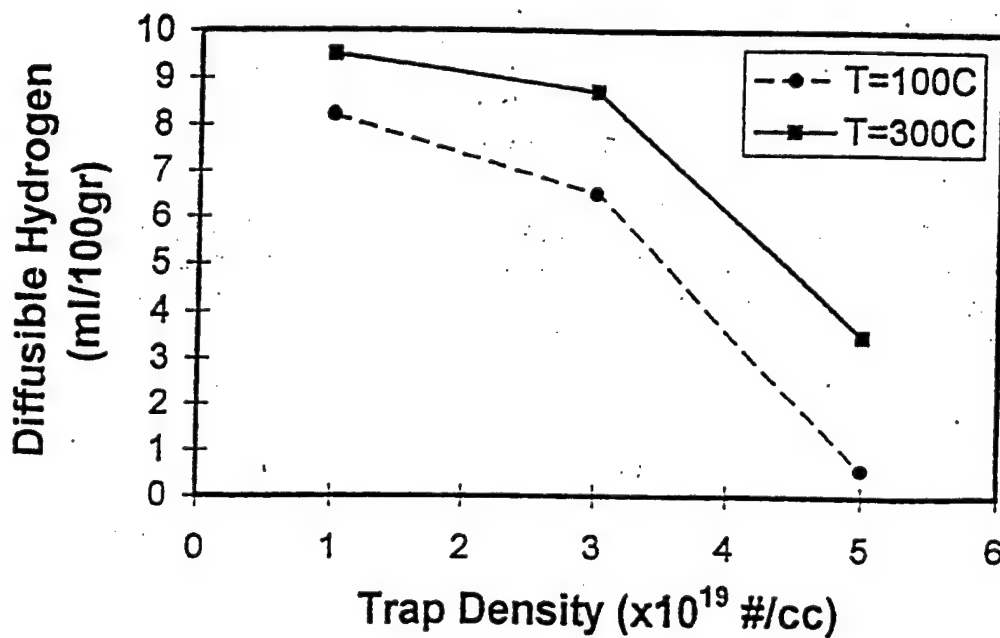


Figure 12. Summary of diffusible hydrogen content at 100 and 300° C during cooling cycle, as a function of trap density. Initial diffusible hydrogen is 15 ml/100g,  $M_s = 400^\circ\text{C}$ ,  $E_B = 100\text{ kJ/mol-H}$  [11].

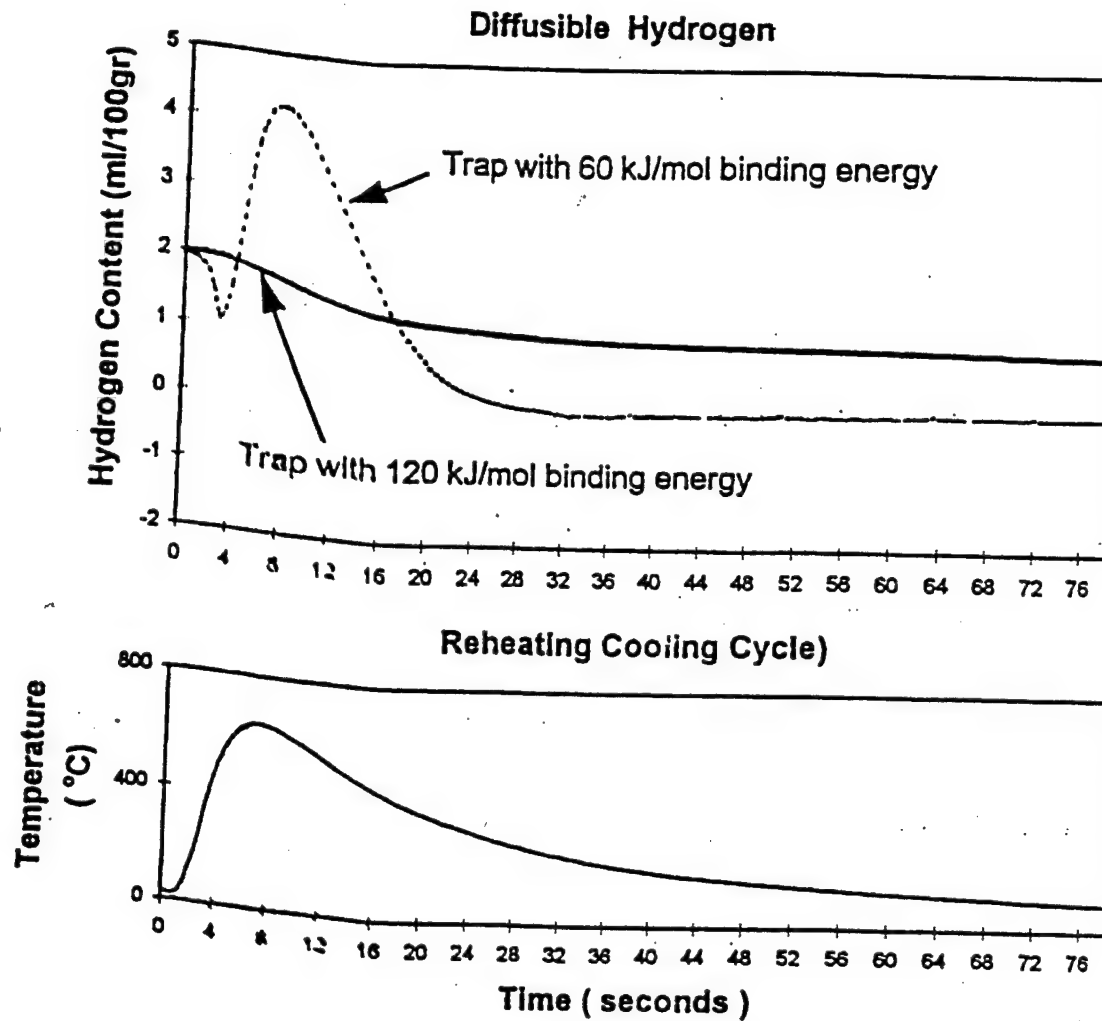


Figure 13. Theoretical evaluation on the performance of hydrogen trap during multipass welding. (a). Diffusible hydrogen (HD) of weld metal containing trap with  $E_A = 100$  kJ/mol and  $E_B = 60$  kJ/mol (c). Thermal cycle during multipass welding

**C. Evaluation of Hydrogen Trapping for Hydrogen Management in Ferrous Alloy Welding,**  
*by I. S. Maroef, C. A. Lensing, and D. L. Olson, Colorado School of Mines*

Research efforts to prevent hydrogen cracking in high strength steel welding have been focused on the prevention of hydrogen localization at regions of stress concentration. This task is achieved by reducing the amount of diffusible hydrogen and controlling the hydrogen distribution in weld joints. Neodymium and yttrium have been introduced to the weld metal to form hydrogen trap sites, which serve two major functions. The first function is to accelerate reduction of diffusible hydrogen during cooling cycle and the second is to provide a more uniform distribution of hydrogen in welded joints. The trap sites were introduced during GMA welding of steel samples with different levels of hydrogen in the argon shielding gas. A reduction of diffusible hydrogen by more than 50 percent (from 4.5 to 1.5 ml/100 g-deposit metal) has been demonstrated when approximately 600 ppm of trapping elements are present in the weld metal.

The evaluation of hydrogen trap sites in rapid reduction of diffusible hydrogen is based upon several hydrogen trapping parameters, including the hydrogen-trap binding energy; the rate of hydrogen capture; and the density of trap sites. These parameters have been assessed by a hydrogen thermal desorption analysis which uses a gas chromatograph-ramping furnace setup to release trapped hydrogen during a constant-rate heating. The trap sites associated with neodymium and yttrium additions were shown to release the hydrogen at high temperature ranges (400 to 600°C), an indication of the trap sites having high binding energies with hydrogen, and thus are the preferred trap sites. The amount of hydrogen released from these trap sites, which is equal to the density of these trap sites, was shown to be proportionally related to the reduction of diffusible hydrogen in the corresponding weld sample. Further identification of these trap sites was done through the use of electron microscopy to correlate the density of trap sites to the density of inclusions in the weld metal, as well as to correlate the binding energy to the various forms of these inclusions (oxide or carbo-nitride).

The effect of accelerated reduction of diffusible hydrogen by trap sites to hydrogen localization has been investigated in the light of a micro-printing technique with silver-bromide photographic emulsion. Hydrogen transport to regions of stress concentration, both by stress assisted diffusion and by dislocation sweeping, has been shown to be affected by the presence of trap sites. The distribution of hydrogen around a region of stress concentration has been correlated to the binding energy and the density of the trap sites.

The performance of hydrogen trap sites has been evaluated based on their trapping parameters and their effectiveness in reducing hydrogen transport to stress concentration regions. This research continues to assess a larger selection of trapping additions and welding conditions. It will ultimately provide a guidance for better welding consumables and practices to manage hydrogen cracking problems in high strength steel.



# The Role of Retained Austenite in the Hydrogen Management of High Strength Steel Welds

Y. D. Park, A. Landau, G. R. Edward and D. L. Olson

Colorado School of Mines  
Center for Welding, Joining and Coating Research  
Golden, CO. 80401

## Introduction

High Strength Low Alloy (HSLA) steels are known to be susceptible to hydrogen cracking problems. As the strength is increased, so is the risk of hydrogen assisted cracking (HAC) after welding. Hydrogen assisted cracking (HAC) is defined as the hydrogen induced reduction of the fracture toughness of a metallic alloy or steel. The risk of hydrogen assisted cracking has been greatest in the heat affected zone of the parent metal, where susceptible microstructures can form as a result of the rapid cooling rate experienced during the welding thermal cycle,<sup>(1,2)</sup> but can also occur in the weld metal. The purpose of this paper is to evaluate the retained austenite as a trap site and to understand the potential role of retained austenite in hydrogen cracking in high strength steel welding.

**Hydrogen Trapping** There are several well-known methods to solve the HAC problems. Common practice to reduce cold cracking in high strength steel welding is the pre- or post- weld heat treatment. Heat treatment is performed to control the cooling rate and to ensure sufficient time for removal of hydrogen from the weld metal. The suppression of diffusible hydrogen can also be achieved by the introduction of selected rare earth metal and transition metal additions to the weld metal to serve as hydrogen traps. These traps, in the form of oxides or carbo-nitrides have high binding energies with hydrogen. They are capable of immobilizing hydrogen at temperature ranges much higher than 100 °C, before the risk of cold cracking emerges.<sup>(3)</sup>

The ability of trap site to hold a hydrogen atom is associated with the hydrogen trap binding energy. A trapped hydrogen atom must acquire an energy substantially greater than the lattice migration energy to escape the trap and to contribute to the measured diffusivity. Trapping parameters such as the trap binding energy and peak temperature of trap are examined by using the thermal analysis. Since HAC depends on hydrogen diffusivity, hydrogen trapping may serve a beneficial role by hindering the hydrogen cracking mechanism.

The hydrogen will be found in different types of trap sites which can be atomic and microstructural imperfections such as vacancies, solute atoms, dislocations, bulk microstructure (FCC

and BCC), grain boundaries, voids, and second phase particles<sup>(4)</sup>. These sites are sinks which retain the hydrogen atom even during thermo-mechanical loading. There are two types of trap sites. If binding energy is small, the corresponding traps are referred to as reversible traps and can act either as hydrogen sinks, which deposit hydrogen atoms to stronger traps. On the other hand, large binding energy give rises to traps which are termed irreversible traps. These traps normally will not release hydrogen even at higher temperatures<sup>(5)</sup>.

**Retained Austenite** The retained austenite resulting from the thermal cycle of strength steel welding is a concern due to the significant differences in hydrogen solubility and diffusion coefficients of the austenite and the ferrite. The transport aspect becomes important because of the higher hydrogen solubility but lower hydrogen diffusion rate in austenite (FCC crystal structure), in contrast to ferrite and martensite that have orders of magnitude higher hydrogen diffusion coefficients than austenite. As a result of the difference a non-uniform distribution of hydrogen may result in weld. It is well known that HSLA steels will have some amount of retained austenite microstructure in weld metal after welding. Consequently some of the hydrogen will be dissolved in the retained austenite microstructure. This retained austenite is unstable relation to the thermodynamic equivalent and may transform to martensite with changes in service temperature and plastic strain.

## Experimental

**Sample Preparation** The samples that were used for thermal analysis were type 304 stainless steels ( 100 pct. austenite phase ), super duplex stainless steels ( 50 pct. austenite phase ), dual-phase steel ( 12 pct. retained austenite ) and HSLA weld metal respectively. HSLA weld metal cooled in air ( 4 pct. retained austenite ) and quenched in liquid nitrogen ( 0 pct. Retained austenite ). These materials were selected to achieve a matrix of materials with different amounts of austenite in the steel. The chemical compositions are shown in Table 1. The super duplex stainless steel was alloy SAF2507, and had a sample size of 120 X 20 X 3 mm. The isothermally transformed sheet steels was heat treated to obtain the 12 pct. retained

**Table 1- Chemical composition of the each sample for thermal analysis (wt-%)**

	Cr	Ni	Mo	C	Mn	Si	Al	N	Cu	V
Type 304 Stainless Steels	19	8	—	0.08	2.0	—	—	—	—	—
Super Duplex Stainless Steels	24.72	6.95	3.09	0.013	0.44	0.29	0.029	0.26	0.26	—
12% Retained Austenite Sample	—	—	—	0.138	1.567	1.126	0.027	0.0035	—	—
Welded HSLA sample	0.04	2.92	0.49	0.063	0.94	0.23	—	—	0.065	0.010

austenite. Cold-rolled sample was maintained at intercritical annealing temperature (770°C) to produce a certain amount of austenite. After annealing, the specimens were isothermally transformed for one hour in 440°C. The isothermal heated sample was cooled by oil-quenched to room temperature. The 4 pct. retained austenite containing sample was taken from the HSLA steel weld metal which is GMA welded sample. To achieve the smooth surface, all samples are mechanically polished onto 1000-grit emery paper.

**Experimental Apparatus and Methods** All four specimens were charged with 100 pct. hydrogen at 130 °C for 24 hours. The hydrogen charged specimens were transferred to the thermal analysis system, Figure 1, and held for six hours at room

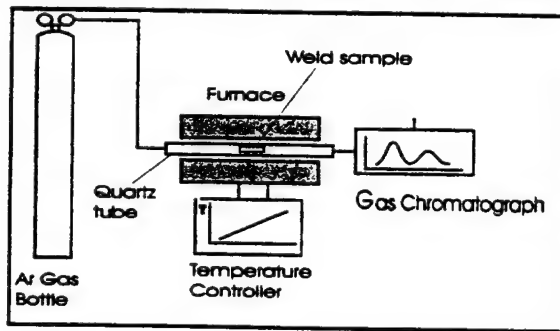


**Fig. 1- Hydrogen thermal desorption analysis aperture**

temperature to remove diffusible hydrogen, so that only trapped hydrogen remained in the specimen. As each specimen was heated at 4 °C/min heating rate and the trapped hydrogen starts to evolve. The super duplex stainless steels and type 304 stainless steels specimens were welded with Gas Tungsten Arc (GTA) welding (1pct. hydrogen + 99pct. argon shielding gas) and quenched in ice water first and then kept in the liquid nitrogen for fifteen minutes. These two samples also transferred to thermal analysis chamber and were heated at 4°C/min heating rate. The position and heights of the peaks for the evolution rate as function of temperature were assumed to be determined by the interaction energy between hydrogen and trapping sites and the amount of hydrogen in trapping sites, respectively. The binding energy of hydrogen evolution was calculated by monitoring change of peak temperature position with various heating rates from 2 to 4 °C/min. TEM, SEM, X-ray and optical micrograph were taken for each specimens to identify the microstructure.

## Results

**Thermal Analysis** A typical thermal analysis curve is shown in Figure 2 for pure iron welded sample which is GTA welded with 1 pct. hydrogen plus 99 pct. argon in the shielding gas. There are three relatively small peaks are observed at 180, 410 and 570°C, indicating that at least three types of trapping sites, which are dislocation, microvoid and oxides inclusion from weld metal, exist in this material. The heights of each peak are different, indicating the relative amount of hydrogen in each trapping site is different. Figure 3 shows the thermal analysis result for wrought type 304 stainless steels. The peak

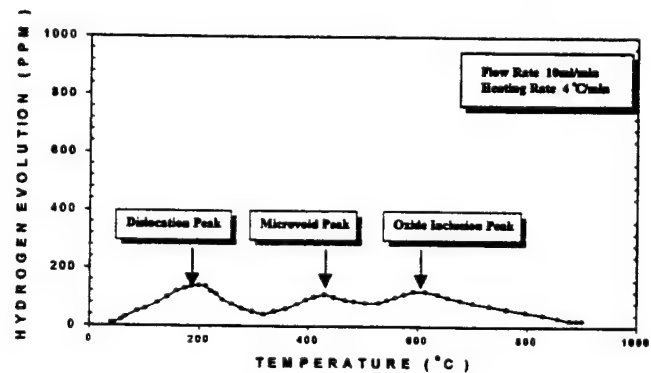


**Fig. 2- Typical thermal analysis results for pure iron cold rolled steels**

temperature is at 600°C and the range of the peak is wide from about 250°C up to 800°C ( $\Delta T=550^\circ\text{C}$ ). The microstructure for the type 304 stainless steels is 100 pct. austenite (FCC). The height of hydrogen peak for the type 304 stainless steels indicates the amount of hydrogen trapped in the bulk austenite trapping site. The thermal analysis for the GTA welded type 304 stainless steels sample is shown in Figure 4. Welded sample also has wide and high temperature peak. Cold rolled sample has slightly low peak temperature than annealed sample.

Thermal analysis curve of super duplex stainless steel sample which is shown in the Figure 5 is showing one broad peak at about 600°C with 4°C/min heating rate. The peak temperature was almost same comparing with type 304 stainless steels sample. The peak temperature range was from about 380 to 780°C ( $\Delta T=400^\circ\text{C}$ ). The SEM and TEM microstructure and thermal analysis peaks for super duplex stainless steels, which are composed with 50 pct. ferrite and 50 pct. austenite, are shown in Figure 6 (a) and (b). The white region in the SEM micrograph is ferrite phase and the darker region is austenite

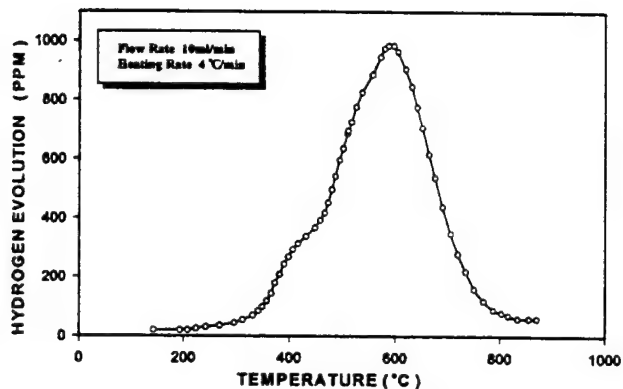


Fig. 3- Typical thermal analysis results of type 304 stainless steel sample

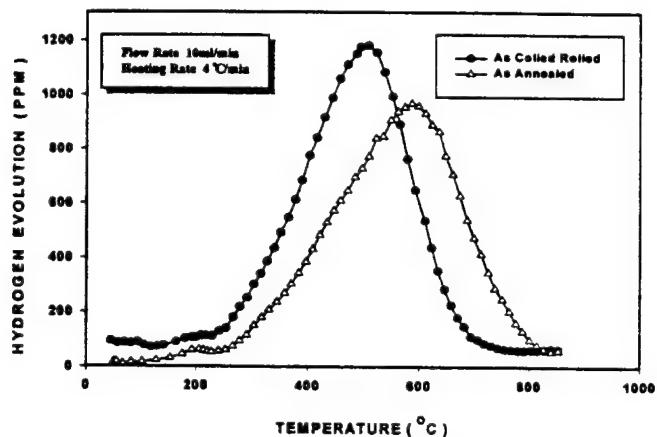


Fig. 4- Thermal analysis of GTA welded type 304 stainless steel sample

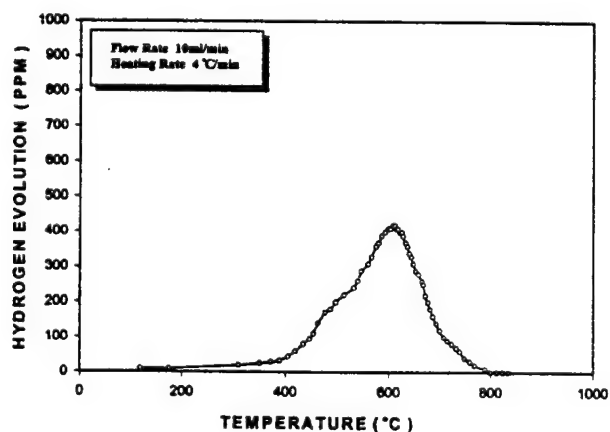


Fig. 5- Thermal analysis of super duplex stainless steel sample

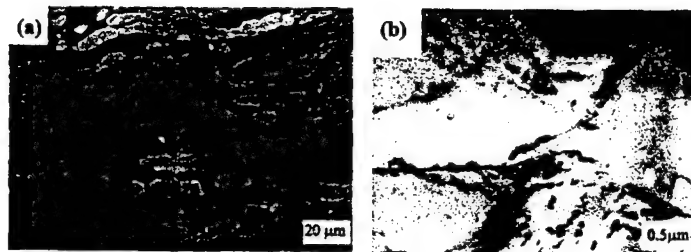


Fig. 6- Microstructure of super duplex stainless steel : (a)SEM  
b)TEM

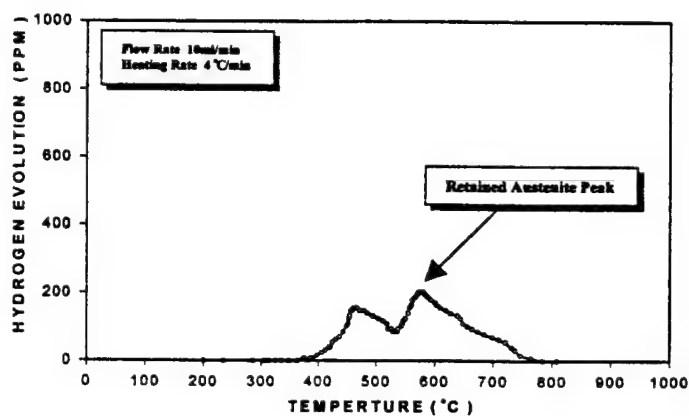


Fig. 7- Thermal analysis of 12pct. retained austenite sample

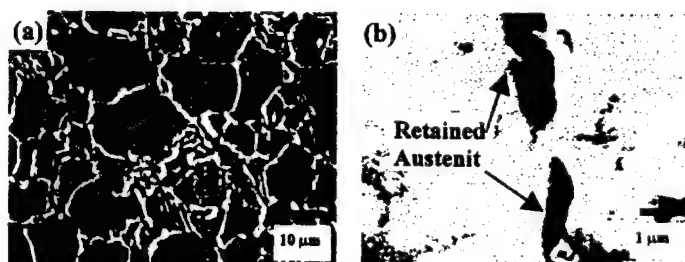


Fig. 8- Microstructure of intercritically heat treated steel which contains 12pct. retained austenite: (a) SEM (b) TEM

phase. The TEM micrograph is also showing the ferrite and austenite microstructure, the dislocations are primarily located in austenite phase.

Thermal analysis was performed for cold-rolled, intercritically annealed, and isothermally transformed sheet steels containing 12 pct. retained austenite. The thermal analysis result is shown in Figure 7. There are two wide peak temperature. The peak temperature for the 12 pct. retained austenite sample were 480°C and 730°C. This result is showing higher peak temperature has same peak temperature range with austenite bulk trapping in the type 304 stainless steels sample. The peak temperature range starts from about 480 to 770°C

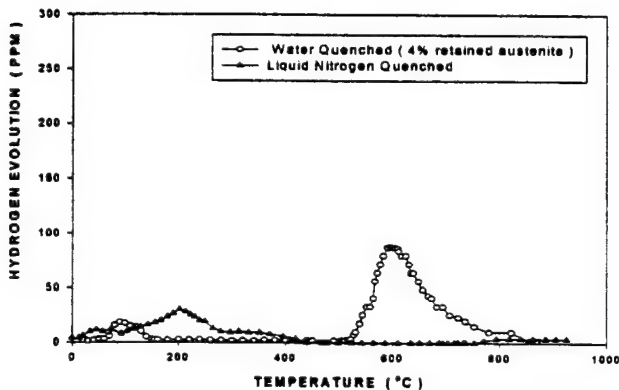


Fig. 9- Thermal analysis of HSLA weld metal which contains 4pct. retained austenite

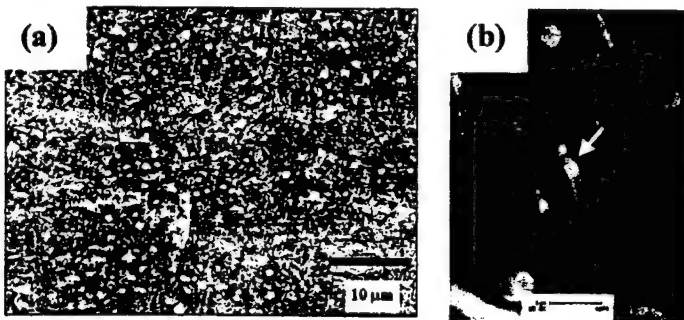


Fig. 10- Microstructure of HSLA weld metal which contains 4 pct. retained austenite : (a) SEM (b) TEM

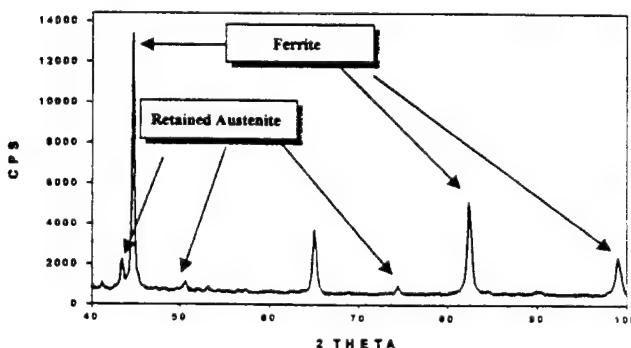


Fig. 11- Thermal analysis of HSLA weld metal which contains 4pct. retained austenite

( $\Delta T=250^\circ\text{C}$ ). The micrograph is shown in Figures 8 (a) and (b). The SEM and TEM micrograph shows that most of the retained austenite is present at the ferrite-austenite interfaces formed by intercritical annealing. The TEM micrograph shows retained austenite which is surrounded with ferrite.

Two thermal analysis for HSLA steel weld metal, which is cooled in air (4 pct. retained austenite) and quenched in liquid nitrogen 0 pct. retained austenite), were also performed which are shown in Figure 9. The peak temperature for water quenched (4 pct. retained austenite) sample is observed at 590°C. This curve indicates the peak temperature of the 4 pct. retained austenite sample is similar to the type 304 stainless steel peak. But the hydrogen evolution is smaller. The peak temperature range is from about 520 to 690°C ( $\Delta T=170^\circ\text{C}$ ). The microstructure in Figure 10 is showing the retained austenite and acicular ferrite in the weld metal of HSLA. The X-ray analysis, Figure 11, is showing the HSLA steel weld metal that has austenite peak and the content is 4 pct. retained austenite by calculation from the X-ray diffraction pattern. The liquid nitrogen quenched weld metal sample is showing no high temperature bulk austenite peak because it has 0 pct. retained austenite.

**Measurements of Trap Binding Energy** As the heating rate is increased from 2 to 4°C per minute, the peak temperature which corresponds to each trap site is increased. Using these data and Kissinger's equation (Eq 1), the trap binding energy ( $E_b$ ) for hydrogen evolution is obtained<sup>(6)</sup>.

$$\frac{\partial \ln(\phi / T_m^2)}{\partial (1/T_m)} = -\frac{E_a}{R} \quad (\text{Eq 1})$$

$\phi$  is the heating rate (K/min),  $T_m$  is the hydrogen evolution peak temperature, and  $R$  is the universal gas constant.  $E_a = E_B + E_L$  and is the activation energy for hydrogen release from trap site. The value of the trap binding energy for bulk austenite trap is 55 kJ/mol-H. The trap activation energy is the sum of the trap-hydrogen binding energy and lattice diffusion energy. Since the lattice diffusion energy is not known, it is assumed to be the same as the activation energy for normal lattice diffusion. The  $E_b$  of the austenite bulk trap is lower than the irreversible trap.

## Discussion

**Hydrogen trapping in austenite phase** A prominent effect of hydrogen trapping is to decrease the apparent hydrogen diffusivity in steel at temperatures below 200°C. The ability of a trap site to hold a hydrogen atom is associated with the hydrogen-trap binding energy. Thermal analysis results for the type 304 and super duplex stainless steel samples indicates that hydrogen is desorbed by volume diffusion rather than by lattice defects because the thermal analysis results is showing broad and high peak temperature. This results suggest that the hydrogen transport behavior including trapping and detrapping for austenite phase is rate controlled by the low diffusion coefficient. As a result, hydrogen is trapped in the austenite bulk trap site. Iino<sup>(7)</sup> reported influence of hydrogen diffusion parameters, heating condition and geometry of specimen on the

amount of local hydrogen available for cracking. This cracking will be apparent along the austenite-martensite interface.

**Table 2-Hydrogen trapping binding energies**

Trap Site	Binding Energy (kJ/mol-H)
H-Dislocation	26
H-Austenite bulk trap	55
H-TiC interface	87

### Conclusions

1. Retained austenite in high strength steel weld is a significant high temperature bulk hydrogen trap which must be considered for determining the hydrogen cracking susceptibility.
2. Austenite trapping is associate with a slow hydrogen transport in the austenite lattice and is not a defect hydrogen interaction.
3. The existence of retained austenite means low reported diffusible hydrogen values when using existing testing methodologies.
4. The amount of allowable retained austenite needs to be related to the amount of hydrogen and the expected service condition.

### Aacknowledgments

The authors acknowledge and appreciate the research and material support of the U.S. Army Research Office, the U.S. Welding Company, AB Sandvik Company, Mr. Marshal Clark, Mr. Iman Maroef, Mr. Chad Lensing and Mr. Bob McGrew.

### Reference:

1. N. Yurioka and H. Suzuki, *International Materials Review*, Vol. 35, No. 4, 217-249 (1990)
2. D.L. Olson, I. Maroef, C. Lensing, R.D. Smith, W.W. Wang, S. Liu, T. Wikleman and M. Eberhart, *Proceedings of the Joint Seminar, Hydrogen Management in Steel Weldments*, WTIA, Melbourne, Australia, 1-20 (1996)
3. J.L. Davidson, S.P. Lunch and A. Majumdar, *Hydrogen Management in Steel Weldments*, 21-34 (1996)
4. G.M. Pressouyre and I.M. Bernstein: *Metall. Trans*, 12A, 835-844 (1981)
5. I. Maroef, D.L. Olson, M. Eberhart, G.R. Edwards, and C. Lensing, *Weld Metal Hydrogen Trapping, Review paper*, Colorado School of Mines, (1998)
6. H.E. Kissinger, Reaction Kinetics in Differential Thermal Analysis, *Analytical Chemistry*, 1702-1706 (1957)
7. Makio Iino, Evaluation of Hydrogen-Trap Binding Enthalpy II, *Met. Trans A*, Vol. 29A, 1017-1021 (1998)

# **HYDROGEN ASSISTED CRACKING IN HIGH STRENGTH STEEL WELDMENTS**

**I. Maroef, D.L. Olson, and G.R. Edwards**

**Center for Welding, Joining, and Welding Research**

**Colorado School of Mines**

**Golden, CO 80401**

**USA**

Several issues on hydrogen assisted cracking (HAC) in high strength steel welding are reviewed. The concept of correlating martensite start temperature to hydrogen transport and distribution in a weld will be discussed. The model of utilizing hydrogen traps to reduce localization of hydrogen at regions of high stress concentration will be discussed. The role of carbide, oxide, and sulfide inclusions, as well as retained austenite as hydrogen traps is reviewed.

## 1. Introduction

Traditionally, hydrogen assisted cracking (HAC) in steel welding is considered to occur when all the necessary conditions for cracking are fulfilled simultaneously. These conditions encompass the combination of diffusible hydrogen content, restraint stress, hardness or susceptible microstructure, and temperature range between  $-100$  and  $100^{\circ}\text{C}$  [1]. An observation by Hart [2], on the heat-affected zone of various steels, led to a conclusion that controlling factors for hydrogen cracking fall into two conditions. For high concentrations of hydrogen (approximately  $10\text{ ml H}_2/100\text{ g}$  deposit metal), the resistance to cracking was primarily controlled by weld deposit hardness. The value of  $350\text{ HV}$  is often specified as the maximum allowable HAZ hardness to avoid hydrogen cracking [3]. At lower levels of hydrogen, less than  $5\text{ ml H}_2/100\text{ g}$ , resistance to cracking was determined more by microstructure than by hardness. In high strength steel welding, formation of martensite should be prevented and is commonly minimized by reducing the carbon content. The presence of oxides and sulfides, in optimal size and amount, also reduce hardenability of steel by facilitating the formation of tough acicular ferrite microstructures.

Common practices to prevent hydrogen cracking in high strength steel weldments are the pre- or post-weld heat treatment, the use of non-cellulosic electrodes with proper baking, and edge preparation. Heat treatment has been necessary to control the cooling rate after welding to allow for sufficient hydrogen removal, as well as to control the heat-affected zone (HAZ) hardness. The higher the strength of the steel, the lower the acceptable weld hydrogen content, even to levels as low as one to two  $\text{ml H}_2/100\text{ g}$  deposit metal [1,4]. With proper selection and use of welding consumables, a minimal hydrogen content can be introduced to the weld pool. However, considerations for hydrogen cracking in high strength steel welding involve further aspects. The high strength level of this class of steel results in high restraint stresses, which are non-uniformly distributed within the weld joint. High stresses are often accompanied by non-uniform hydrogen distribution in the weld joint, a condition which requires very low nominal hydrogen content [5]. Evidence of non-uniformity of hydrogen distribution has been shown by Olson et.al [6], using a laser induced breakdown spectroscopy, as shown in Figure 1. Non-uniform hydrogen



distribution will become more critical issue with the welding of even higher strength steels.

The concomitant effect of localized hydrogen concentration and high restraint stress gives rise to crack initiation at stress concentrations within the weld joint. Stress concentrations are located at inclusion interfaces and grain boundaries, and at the weld fusion line. These locations may be either in the heat-affected zone (HAZ) or in the fusion zone (FZ), depending upon how hydrogen, stress, and hardness are distributed within the weldment.

Non-uniform hydrogen distribution across the weldment can result from poorly matched welding consumables and base metal compositions [7]. Stress-induced hydrogen diffusion and hydrogen transport by dislocation sweeping are also factors generally considered to be responsible for localized accumulation of hydrogen at regions of stress concentration [3,5]. Dislocation sweeping in weld joints will be operative if the hydrogen cracking mechanism is dominated by localized plasticity [8]. Through implant tests of high strength steel, micro-void coalescence, which is a result of localized plasticity, has been shown to occur by Gedeon and Eagar [9]. Microstructural heterogeneities, can function as hydrogen traps. The type and distribution of hydrogen traps are also determining factors to the short range distribution of hydrogen, through partitioning of hydrogen atoms between lattice sites and various trap sites in the weldment. Such a partitioning of hydrogen atoms may significantly improve the resistance to HAC.

## **2. Hydrogen Distribution and Hydrogen Cracking in Weldments with Unmatched Fusion Zone and HAZ Chemical Composition.**

Commonly, hydrogen cracking occurs in the heat-affected zone (HAZ). The crack initiates near the fusion zone, at the regions with the highest stress intensity factor. However, in recent years, the development of cleaner HSLA steels (with ultra-low carbon content) led to HAC in the weld metal rather than in the HAZ [10]. To explain this situation, the locations of HAC in the weld joint have been related to the non-

Alternate hydrogen cracking location within weldments have also been illustrated by Matsuda et. al [15]. In their illustration, the variation of hydrogen concentration with time in the weld metal was assumed to be different than that variation in the HAZ, as shown in Figure 4. This difference may be caused by the difference in the thermal history of the weld metal as compared to the heat-affected zone. The corresponding time dependent critical stresses for HAC in both regions are shown in Figure 5. Figure 5 illustrated that, low weld metal hardness will cause crack to occur in the HAZ, since the critical stress for HAC in the weld metal will always be higher than the value of stress being applied to the weld joint. On the other hand, for high weld metal hardness, the crack will initiate in the weld metal, since the critical condition for HAC in the weld metal is satisfied before that condition is met in the HAZ.

### 3. Hydrogen Distribution in Weldment as a Result of Stress Assisted Diffusion and Dislocation Assisted Transport of Hydrogen Atoms

Moving dislocations can acts as rapid and efficient carriers or sweepers of hydrogen, as was experimentally verified by tritium release rate and penetration experiments of Donovan, Louthan, and co-workers [16,17,18], and also by permeation experiments of Kurkela and Latanision [19]. Dislocation sweeping has been thoroughly studied by Tien et. al [20,21], who also showed the close relationship between the kinetics of embrittlement, under strain loading, and the transport of hydrogen to critical failure sites within the material. Hydrogen atoms can follow the motion of dislocations with a velocity which was derived through the Einstein-Stokes relationship [22] :

$$v = \left( \frac{D_H}{kT} \right) F \quad (1)$$

where  $D_H$  is the effective diffusivity of hydrogen in the matrix and  $F$  is the effective driving force per atom of hydrogen carried by the dislocation. A critical velocity,  $v_c$ , for hydrogen to move along with a dislocation, was assumed for a critical driving force  $F_c$ , that correspond to a gradient of hydrogen-dislocation binding energy,  $E_B$ , assumed to be distributed over a distance of  $30b$ , where  $b$  is the dislocation's Burgers vector ( $F_c = E_B/30b$ ). Above  $v_c$ , or at a strain rate greater than  $\dot{\epsilon} = \rho \cdot b \cdot v_c$ , the

#### 4. Effect of Hydrogen Traps on the Hydrogen Partitioning within Weldments

In steel, hydrogen will be found not only in the host lattice, but also segregated to atomic and microstructural imperfections such as vacancies, solute atoms, dislocations, grain boundaries, voids, and second phase particles. In these localized regions, the mean residence time of a hydrogen atom is considerably longer than in a normal interstitial lattice site. In the extreme case, these regions are sinks, which retain the atom even during mechanical loading. The generic term for this phenomenon is trapping and these localized regions are hydrogen trap sites [28,29,30].

The strength of a trap site; i.e., the fraction of time a hydrogen atom resides in that trap site, depends upon the binding energy,  $E_B$ , of the hydrogen atom to the trap. The binding energy of 60 kJ/mol-H for a dislocation or a grain boundary is generally regarded as the limiting value for a reversible trap. With this energy level, a reversible trap becomes effective in capturing hydrogen around 400 K. A reversible trap with binding energy lower than 60 kJ/mol-H will not be able to prevent hydrogen cracking. The trapped hydrogen will be picked up by moving dislocations, and will eventually be delivered to crack initiation sites [31]. With regard to HAC, the preferred traps are consequently those traps having binding energies in excess of 60 kJ/mol-H. These traps are termed irreversible traps [32].

The presence of deep hydrogen traps in the weld metal may significantly alter hydrogen content and distribution during welding. A reduction of the concentration of diffusible hydrogen has been demonstrated by Pokhodnya [33] through the introduction of rare earth elements into the weld metal. Lensing et.al [34] have found similar results through the introduction of neodymium and yttrium. Their result for low carbon-low alloy steel welds is shown in Figure 8. Significant reduction of diffusible hydrogen by more than 50 percent (down from 4.5 to 1.5 ml H<sub>2</sub>/100g) when 600 parts per million of trapping elements were incorporated into the weld metal. In their study, hydrogen thermal desorption analysis has also been conducted. In this analysis, weld samples were heated with constant heating rate so that trapped hydrogen atoms were released at different temperature regimes, depending upon the

dislocation line can be expected to break away from its hydrogen cloud, so that dislocation sweeping is no longer effective.

Dislocation-assisted transport of hydrogen atoms contributes a major fraction of the HAC in high strength steels. The high strength level of this steel causes high restraint stresses, even when the weldment temperature is still high, and dislocations are very mobile. This situation leads to extensive dislocation-assisted hydrogen transport in the weldment. Theoretical study on role of dislocation-assisted hydrogen transport to localized hydrogen has been investigated by Kikuta et al [23, 24], using finite element analysis. Similar study has also been conducted by Yurioka et.al. [25,26] who considered not only the effect of dislocation assisted hydrogen transport but also the effect of stress assisted hydrogen diffusion due to triaxial stress. A finite difference method was used in theoretical study and a non-uniform hydrogen distribution, such as that shown in Figure 6, was obtained.

In many occasions, heat treatments to prevent HAC require very tight temperature control because they allow only narrow windows of time and temperature. While an extensive heat treatment is necessary for sufficient hydrogen degassing, limitations are necessary to maintain mechanical properties and to minimize hydrogen localization. Localized hydrogen accumulation in high strength steel has been shown to be enhanced after post weld heat treatment is imposed upon the weld joint [27]. Hydrogen distribution was measured in a welded joint without heat treatment (Figure 7.a) and with post-weld heat treatment (Figure 7.b). In Figure 7.b, local accumulation of hydrogen in a welded joint is developed after post weld heat treatment. This localized hydrogen accumulation occurred even though the average content of hydrogen is less than that of the weld joint prior to post weld heat treatment, as shown in Figure 7.a. This result implies that, for certain critical weld joints, high restraint stresses preclude recommending any acceptable heat treatment consistent with safe welding conditions. Prevention of hydrogen cracking in this situation would require an alternative solution to substitute the heat treatment procedure.

strength of the trap sites. In Figure 9, hydrogen release from weld metal containing neodymium additions is contrasted with hydrogen release from a weld metal free of deep traps. At high temperatures (800-900 K), a peak of hydrogen evolution was observed in the weld sample which contain neodymium, indicating that irreversible traps were present.

Hydrogen trapping offers the prevention of HAC during high strength steel welding by reducing the diffusible hydrogen without an extensive heat treatment. Hence, localization of hydrogen at stress concentration regions by dislocation-assisted transport can be minimized. A theoretical calculation of an accelerated reduction of hydrogen in weld metal due to the presence of hydrogen traps is shown in Figure 10. It was found through these calculations that any weld metal with low martensite start temperature requires trap sites with high binding energy to ensure rapid hydrogen capturing. On the other hand, decohesion at inclusions due to trapped hydrogen is also possible, depending upon the electronic bonding change which occur at the inclusion interfaces in the presence of hydrogen. While hydrogen trapping can prevent hydrogen cracking cause by localization of diffusible hydrogen, optimal trapping inclusions must be determined, based upon evaluation of both hydrogen capturing capabilities and mechanical properties.

Various inclusions which are effective as hydrogen traps in high strength steel have been reported. The results reported vary from advantageous effect (especially for strong irreversible traps), to detrimental effects (for weak traps), relative to weld joint mechanical integrity. Some of these reports may not accurately represent the performance of these traps in the real welding situation. To accurately evaluate trap sites, a comprehensive investigation that closely simulates both the actual steel welding and the weld joint function is required. Adequate simulations requires a meaningful level of hydrogen contamination, an actual welding cooling rate, measurement of hydrogen at critical temperatures (100° C -300° C), and an extensive mechanical testing.

## Oxide Inclusions as Hydrogen Traps

A number of oxide inclusions have been identified as relatively weak but irreversible trap sites, such as  $\text{Al}_2\text{O}_3$  ( $E_B = 79 \text{ kJ/mol-H}$ ) [35] and iron oxide ( $E_B = 50\text{--}70 \text{ kJ/mol-H}$ ) [36]. With longitudinal butt-tensile restraint cracking (LB-TRC) testing, Shinozaki et al. [37] investigated the effect of oxygen on the mechanical integrity of HY-100 and HSLA-100 steels samples, welded with hydrogen contamination in the shielding gas. Longitudinal Bead – Tensile Restraint Cracking (LB-TRC) test was used to enable the investigators to impose mechanical tensile loading on a weld bead when the temperature reach  $150^\circ \text{C}$  during cooling after welding. At a hydrogen level of 4.7 ppm, HY-100 steel welds, which consistently revealed a martensitic microstructure, experienced a reduction of the critical stress for HAC as the oxygen content was increased up to 200 ppm. With increasing oxygen content, the fracture mode was altered from quasy-cleavage to intergranular. Intergranular failure occurred via oxide-matrix decohesion at prior austenite grain boundaries. These oxide trap sites may be too weak and consequently, the rate of hydrogen trapping may not be sufficiently fast to prevent accumulation of hydrogen at grain boundary areas of high stress concentration.

Several oxide inclusions, such as  $\text{Al}_2\text{O}_3$  and  $\text{CaO-Al}_2\text{O}_3$ , are non-deformable. Within the regions of high stress concentration, these inclusions also act as a stress intensifier and promote a localized plastic deformation in steels [38,39]. Hydrogen concentration around the inclusion can be increased locally and the critical concentration for HAC can be reached earlier. In other inclusion situations, trapped hydrogen may relate to prevention of HAC by promoting decohesion and facilitate the formation of blunt crack at the inclusion-matrix interface. In this way, trapped hydrogen conversely could increase the critical stress for HAC because a crack initiation site is available without the need to fracture the oxide inclusions, otherwise sharp crack initiations are easily formed. Understanding of the relationship between inclusion-matrix decohesion and toughness as well as HAC needs to be further investigated.

The role of oxide inclusions in the HSLA-100 steel weld sample was thought to be overshadowed by the increasing formation of acicular ferrite or bainite structure as the oxygen content increase. An increase of critical stress with oxygen content, up to 638

ppm, was observed and thought to be a result of the formation of tougher microstructures. However, it has been known that, in the absence of hydrogen, the maximum toughness of weld metal usually occurs at an oxygen content of 250 ppm [40]. In this particular investigation, it is highly possible that the formation of acicular ferrite in HSLA-100 steel occurred at a higher temperature than the formation of martensite in HY-100 steel. In this situation, hydrogen capturing is more effective in HSLA-100 steel and contributes to the increase of critical stress for HAC. Reduction of diffusible hydrogen is faster in HSLA-100 steel than in HY-100 steel for the same welding cooling cycle.

### **Carbide Inclusions as Hydrogen Traps**

TiC precipitates in microalloyed HSLA steel has been of great interest for many investigators due to the high binding energy ( $E_b = 98 \text{ kJ/mol-H}$ ) [28]. Stevens and Bernstein [41] had attempted to evaluate the mechanical response of TiC-containing HSLA steel. Unfortunately, they could not exclude the deleterious effect of sulfur or phosphorous segregation to grain boundaries, which occurred during annealing heat treatments that were intended to vary the density of TiC precipitates. The presence of small and finely distributed TiC precipitates were shown to improve the resistance to HAC, since they compensated for the loss of resistance to HAC due to the segregation of sulfur or phosphor. It was thought that, without the presence of such deep and innocuous trap sites, the fracture toughness of the hydrogen-charged HSLA steel would decrease significantly.

Besides TiC, VC inclusions have been investigated as hydrogen traps to prevent disbonding of austenitic stainless steel cladding from 2 ¼ Cr -1 Mo steel base plates [42]. Disbonding usually occurs at the interface of the two steel layers when a hydrogen-containing pressure vessel is cooled down from an elevated temperature. While disbonding in ordinary steel started to occur when the specimen was cooled down from 450° C and 14.7 Mpa hydrogen pressure, disbonding in VC modified steel was not observed even after cooling from 500° C and 19.6 Mpa (containing higher level of hydrogen). The role of VC was thought to be that of a hydrogen trap and alleviated localization of hydrogen at the cladding interface.



Quite recently a more comprehensive evaluation of VC particles has also been done through both hydrogen measurement and notched tensile testing [43]. Two similar classes of steel, AISI 4340 and ASTM A723 steels, were modified to obtain the same vanadium and carbon content. These modifications promoted the formation of VC particles, which were shown to significantly improve the resistance to HAC relative to the base steel compositions. The embrittlement index for AISI 4340 steel was decreased by the VC particles formation from 61.2 percent down to 22.2 percent. A similar case was observed for the ASTM A723 steel ( from 5.8 percent down to 3.8 percent). Quantitative evaluation of the binding energy of VC particles has not been reported. Extraction studies that were performed in this investigation showed that the particles do not release the trapped hydrogen during sample reheating at 200° C, which implies that these particles are irreversible traps.

### **Sulfide Inclusions as Hydrogen Traps**

While sulfur content in steels has been reduced to improve mechanical properties, some papers have reported that a reduction of non-metallic inclusions, mainly sulfides, could increase the risk of HAC in the HAZ. Hirose, Araki and Kikuta [44] observed that, in quenched and tempered HSLA steels containing 10 ppm hydrogen, the critical stress for HAC increased with increasing sulfur content up to 300 ppm. The sulfur content was directly proportional to the MnS inclusion density, which was the main microstructural feature responsible for suppression of HAC. With the matrix of all the sample being martensite, these sulfides were thought not to reduce HAC by reducing the hardenability of steels. Instead, because of the fact that the apparent hydrogen diffusivity decreased with increasing MnS density, the above investigators concluded that MnS inclusions served as hydrogen trap sites, thus suppressing HAC. These investigators suggested that the presence of hydrogen at the interface of these inclusions did not become the initiation site for HAC because MnS inclusions are deformable. As a trap sites, manganese sulfide has been identified as a weak irreversible trap with a binding energy of 72 kJ/mol-H [45].

## 5. The Role of Retained Austenite as a Hydrogen Trap.

Austenite manifests a much larger solubility and much slower diffusivity of hydrogen than in ferrite. This phase, in the form of retained austenite, can behave as a three-dimensional hydrogen trap. Knowledge concerning retained austenite as an effective hydrogen trap has not been well established. Initially, retained austenite may assist in the accelerated reduction of diffusible hydrogen right after the formation of martensite. Hence, it can help reducing diffusible hydrogen without extensive dislocation assisted hydrogen transport. However, as the temperature drops, solubility of hydrogen in retained austenite decreases, and retained austenite begins to export hydrogen atoms to the adjacent martensite matrix. Furthermore, the slow diffusivity of hydrogen in this retained austenite may also increase the probability of HAC, since export of hydrogen atoms to the ferrite matrix would occur at low temperature, where the chance for HAC is high. The role of retained austenite, whether it helps to prevent or it increases the risk of HAC, strongly depends upon the welding thermal cycle, as well as upon the retained austenite density and its location with respect regions of high stress concentration. Theoretical predictions to determine the proper heat treatment for preventing HAC in high strength steel welding should also include the effect of retained austenite, in addition to the previously mentioned factors (stress-assisted hydrogen diffusion, dislocation-assisted hydrogen transport, and hydrogen trapping).

Evaluations for HAC-related issues in steel welding such as diffusible hydrogen measurements involve quenching weld specimens in iced water and storing in liquid nitrogen or dry ice – acetone solutions after completion of the welding process. This procedure does not represent the actual welding situation in steel construction, since the weld sample transform completely to martensite when its temperature drops as low as  $-70^{\circ}\text{C}$ . On the other hand, the slower cooling rate and much higher final welding temperatures in actual steel construction would yield significant amounts of retained austenite in many weldments. Investigations concerning retained austenite require better measurement techniques than the above mentioned conventional technique to get meaningful hydrogen concentrations as well as the appropriate mechanical responses.

## 6. Closure

In addition to the nominal amount of diffusible hydrogen, non-uniform distribution of hydrogen is a significant contributor to hydrogen cracking in high strength steel welding. This non-uniformity can be minimized when the martensite start temperature of the weld metal is slightly higher than that of the HAZ. Furthermore, localization of hydrogen at regions of high stress concentration should also be prevented by minimizing the amount of dislocation-assisted transport of hydrogen. Such a hydrogen transport may be facilitated by an extensive heat treatment imposed upon the weld joint. To avoid this, hydrogen traps may be incorporated, thus avoiding extensive heat treatment, while still reducing diffusible hydrogen concentration. Selection of hydrogen traps to prevent HAC requires further information than just their hydrogen trapping characteristics. Understanding the effect of these inclusions and their trapped hydrogen concentrations on the whole mechanical integrity of the weld joint is necessary. Finally, understanding the effect of retained austenite as a three-dimensional hydrogen trap with a temperature dependent trapping capacity should be carefully assessed, since actual welding of steel construction may involve a significant retained austenite volume fractions.

## 7. Acknowledgment

The authors acknowledge and appreciate the research support of the US Army Research Office and the Office of Naval Research.

## 8. References

1. N. Bailey, F.R. Coe, T.G. Gooch, P.M. Hart, N. Jenkins, and R.J. Pargeter, "Welding Steel without Hydrogen Cracking", 2<sup>nd</sup> Edition, Abington, 1993.
2. P.M. Hart, *Welding Journal*, Vol. 65, 1986, pp. 14-22s.
3. N.Yurioka and H.Suzuki, *Int. Mat. Rev.*, Vol. 35(4), 1990, pp. 216-249.
4. R. Wong, J. Blackburn, J. DeLoach, and R. DeNale, in "Hydrogen Management in Steel Weldments", DSTO and WTIA, Oct. 1996, Melbourne, Australia, pp. 35-48.
5. V.F. Musiyachenko and S.B. Kasatkin, *Automatic Welding*, Sept. 1985, pp. 22-26.
6. D.L. Olson, I. Maroef, C. Lensing, R.D. Smith, W.W. Wang, S. Liu, T. Wildeman, and M. Eberhart, in "Hydrogen Management in Steel Weldments", DSTO and WTIA, Oct. 1996, Melbourne, Australia, pp. 1-19.
7. W.Wang, S. Liu, and D.L. Olson: in Proc. Intl. Conf. 'Offshore Mechanics and Arctic Engineering - Materials Engineering', Vol. III, Florence, Italy, 1996, ASME, pp. 403-409.
8. J.P. Hirth: *Metal. Trans.*, 1980, 11A, pp. 861-890.
9. S.A. Gedeon and T. Eagar: *Welding Journal*, 1990, pp. 213-220s
10. J. Vuik, *An Update of the State-of-the-art of Weld Metal Hydrogen Cracking*, IIW document, IXJ-175-92, 1992, American Council, AWS, Miami, FL
11. Th. Bollinghaus, H. Hoffmeister, and A. Dangeleit, "A scatter Band for Hydrogen Diffusion Coefficients in Microalloyed and Low Carbon Structural Steels", IIW Document IX-1767-94, 1994).
12. H. Granjon, "Cold Cracking in Welding of Steels", Intl. Symposium on Cracking and Fracture in Welds, Conf. Proc. Japan Welding Society, (1971), IB, 1.1.
13. B. Gravile, "Hydrogen Cracking Sensitivity of HSLA Steels", The Metallurgy, Welding and Qualification of Microalloyed (HSLA) Steel Weldments, (1990), pp. 127-150.
14. W.W. Wang, R. Wong, S. Liu, and D.L. Olson, in Conf. Proc of 'Welding and Weld Automation in Shipbuilding', Oct 29- Nov. 2, 1995, eds R.DeNale, TMS, Warrendale PA, 1996, pp. 17-31.
15. F. Matsuda et.al., *Trans. of JWRI*, Vol. 12 (2), 1983, pp. 75 - 85.
16. J.A. Donovan, *Metall. Trans. A*, Vol. 7, 1976, pp. 1677-1683.
17. J.A. Donovan, *Metall. Trans. A*, Vol. 7, 1976, pp. 145-149.
18. M.R. Louthan, Jr., G.R. Caskey, Jr., J.A. Donovan, and D.E. Rawl, Jr., *Mat. Sci. and Eng.*, Vol. 10, 1972, pp. 357-368.
19. M. Kurkela and R.M. Latanision, *Sripta Metall.*, Vol. 13, 1979, pp. 927-932.
20. J.K. Tien, S.V. Nair and R.R., Jensen, in "Hydrogen Effects in Metals", eds. I.M Bernstein and A.W. Thompson, The Metall. Soc. of AIME, Pittsburgh, Pennsylvania, 1981, pp. 37-56.
21. S.V. Nair, R.R. Jensen, and J.K. Tien, *Metall. Trans. A*, Vol. 14, 1983, pp. 385-393.
22. J.K. Tien, A.W. Thompson, I.M. Bernstein and R.J. Richards, *Metall. Trans.A*, Vol. 7, 1976, pp. 821-829.
23. Y. Kikuta, in "Hydrogen Effects in Metals", eds. I.M. bernstein and A.W. Thompson, The Metall. Soc. of AIME, Pittsburgh, Pennsylvania, 1981, pp. 755-765.
24. Kikuta et. al., *Trans. Japan. Weld. Soc.*, Vol. 11 (2), 1980, pp. 36-44.
25. N. Yurioka and K. Kohira, "A Numerical Analysis of the Diffusion and Trapping of Hydrogen in Steel Welds", IIW Doc. IX-951-76, 1976.

26. N. Yurioka and S. Oshita, "An Analysis of Effect of Microstructure, Strain and Stress on the Hydrogen Accumulation in HAZ", IIW Doc. IX-1161-80, 1980.
27. Grivnyak I, in "Scientific Problems in Welding and Special Electrometallurgy Part 3", Kiev Naukova dumka, 1970, pp. 38-48.
28. G.M. Pressouyre and I.M. Bernstein, *Metall. Trans. A*, Vol. 9, 1978, pp. 1571-1580.
29. G.M. Pressouyre and I.M. Bernstein, *Metall. Trans. A*, Vol. 12, 1981, pp. 835-844.
30. I.M. Bernstein and G.M. Pressouyre, in "Hydrogen Degradation of Ferrous Alloys", ed. by R.A. Oriani, J.P. Hirth and M. Smialowski, Noyes Pub., 1985, pp. 641-685.
31. J.K. Tien, A.W. Thompson, I.M. Bernstein, and R.J. Richards, *Metall. Trans. A*, Vol. 7, 1976, pp. 821-829.
32. G.M. Pressouyre and I.M. Bernstein, *Metall. Trans. A*, Vol. 12, 1981, pp. 835-844.
33. I.K. Pokhodnya, in Sem. Proc 'Hydrogen Management in Steel Weldments', eds. J.L. Davidson and D.L. Olson, DSTO and WTIA, Oct. 1996, Melbourne, Australia, pp. 141-181.
34. C.A. Lensing, I. Maroef, and D.L. Olson, "Presentation at AWS Convention 1997", April 1997, Los Angeles.
35. K.Y. Lee, J.Y. Lee, and D.R. Kim, *Mat. Sci. Eng.*, Vol. 67, 1984, pp. 213-220.
36. J.L. Lee and J.Y. Lee, *Met. Trans. A*, Vol. 17, 1986, pp. 2183-2186.
37. Shinozaki and T. North, *Metall. Trans. A*, Vol. 21, 1990, pp. 1287-1298.
38. E. Pickering, *JISI*, Vol. 189, 1958, p. 148.
39. S. Rudnik, *JISI*, Vol. 204, 1966, p. 374.
40. D.J. Abson and R.J. Pargeter, *Int. Mater. Rev.*, Vol. 31(4), 1986, pp. 141-194.
41. M.F. Stevens and I.M. Bernstein, *Metall. Trans. A*, Vol. 20, 1989, pp. 909-919.
42. J. Shimomura, Y. Nakano, S. Nakano, and S. Ueda, *ISIJ Int.*, Vol. 31(4), 1991, pp. 379-386.
43. G.L. Spencer and D.J. Duquette, "The Role of Vanadium Carbide in Reducing the Susceptibility to Hydrogen Embrittlement of High Strength Alloy Steels", US. Army Benet Laboratories, Watervliet, NY, (1997).
44. Y. Kikuta, T. Araki, and A. Hirose, *Trans. Japan Welding Society*, Vol. 19 (1), April 1988, pp. 60-65.
45. S.M. Lee and J.Y. Lee, *Acta Metall.*, Vol. 35 (11), 1987, pp. 2695-2700.

## 9. Figures

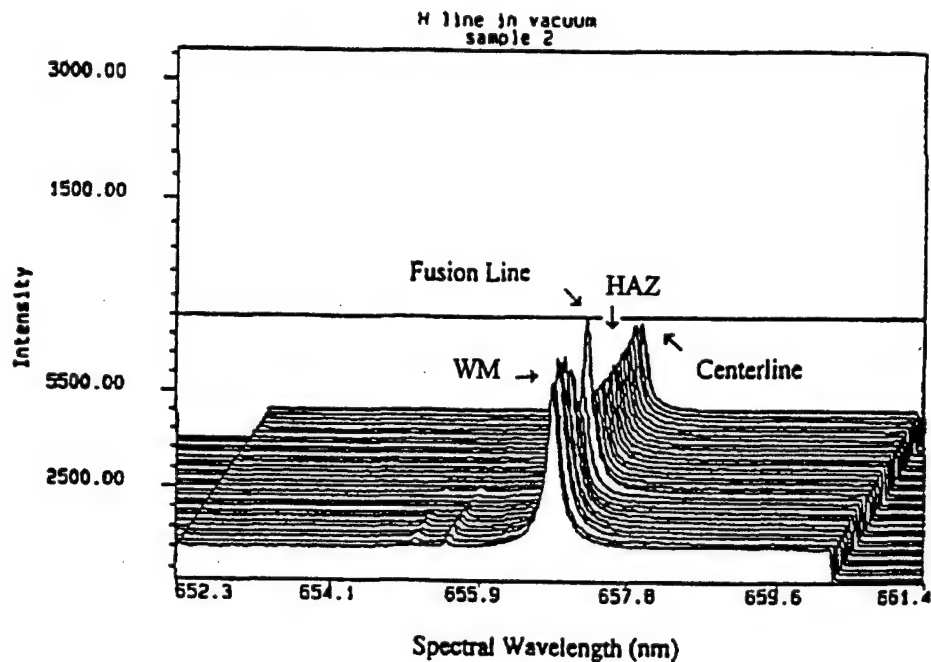


Figure 1. Non-uniform distribution of hydrogen across the center line of a weldment. Intensities of the hydrogen spectral emission are proportional to the hydrogen concentration [6].

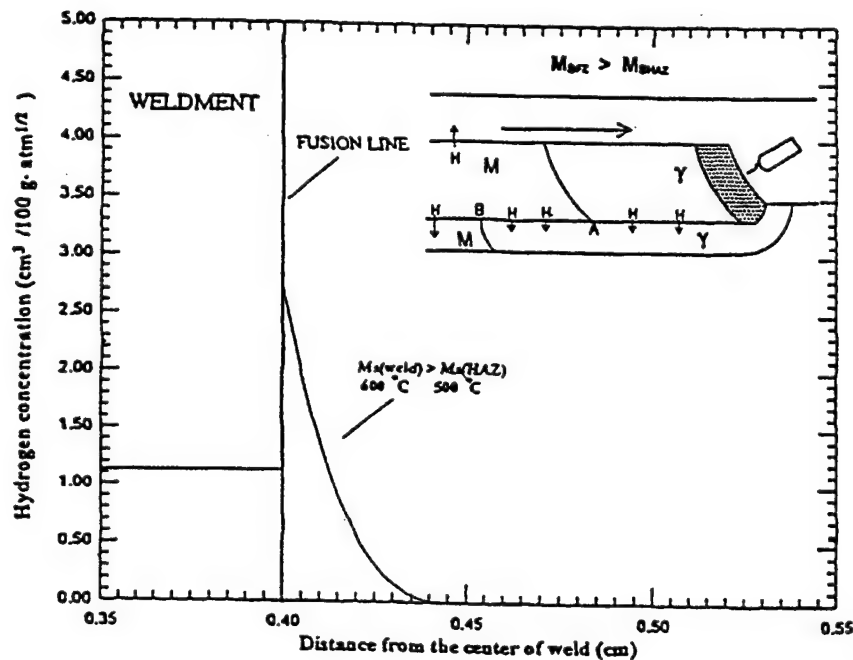


Figure 2. Hydrogen distribution across the fusion line of a steel weldment for  $M_{SWM}(600^{\circ}\text{C}) > M_{SHAZ}(500^{\circ}\text{C})$  [14].

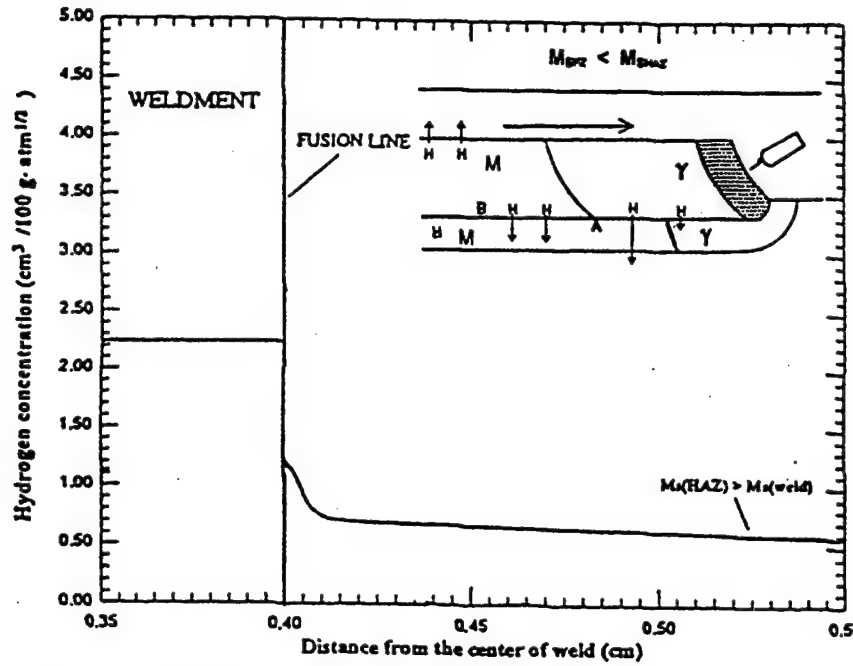


Figure 3. Hydrogen distribution across the fusion line of a steel weldment for  $M_{SWM} (500^{\circ} \text{C}) < M_{SHAZ} (600^{\circ} \text{C})$  [14].

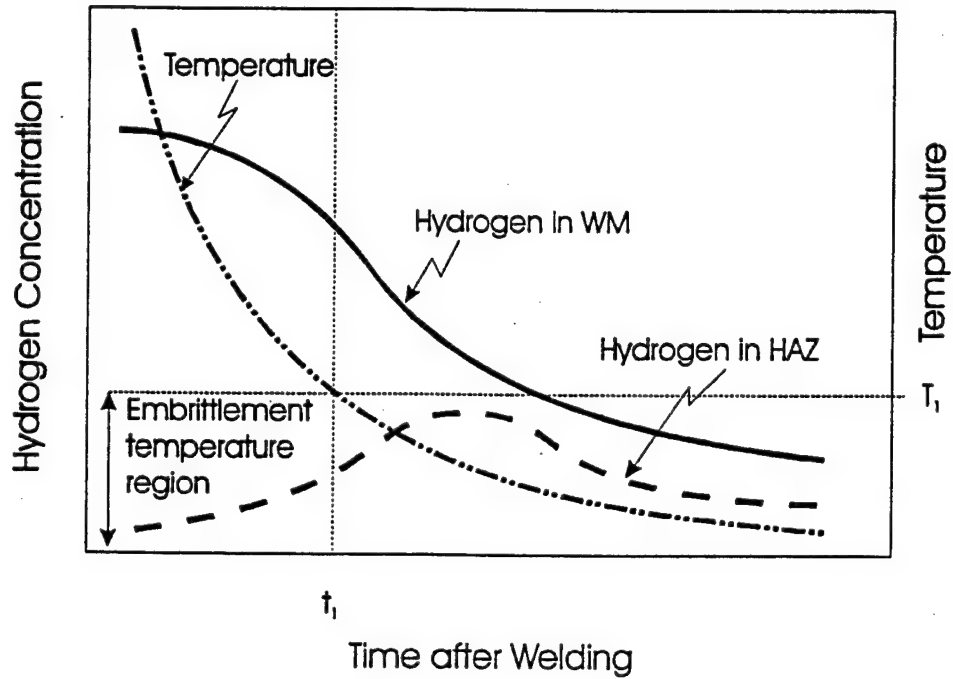


Figure 4. Variation of hydrogen concentration in the weld metal (WM) and the HAZ after completion of welding process [15]



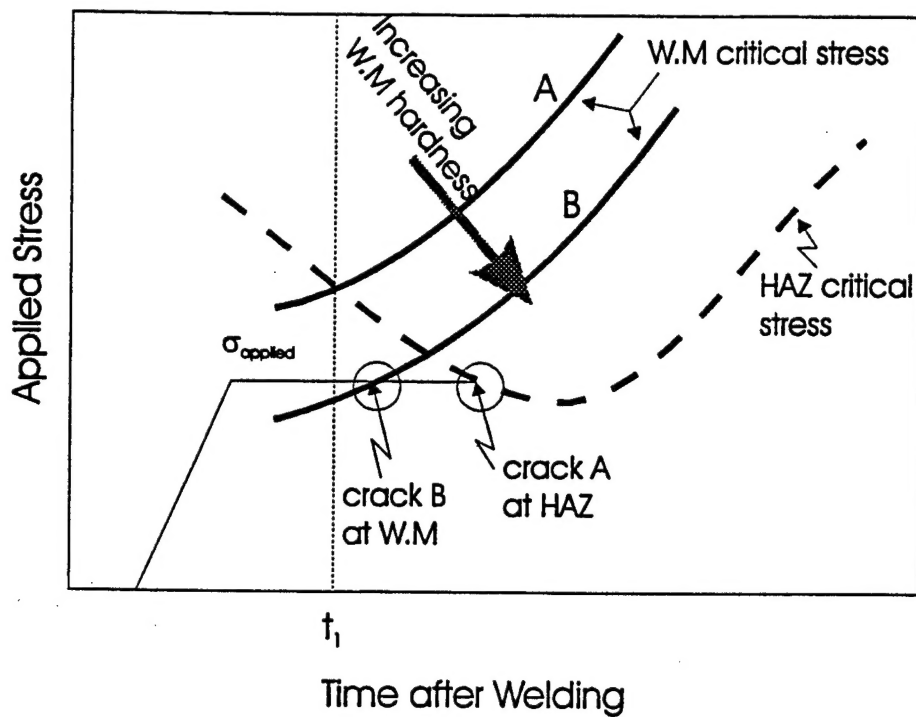


Figure 5. Variation in critical stress for HAC in weld metal (WM) and HAZ during cooling cycle. (A). low WM hardness: crack location is in HAZ. (B). high WM hardness: crack location is in WM [15].

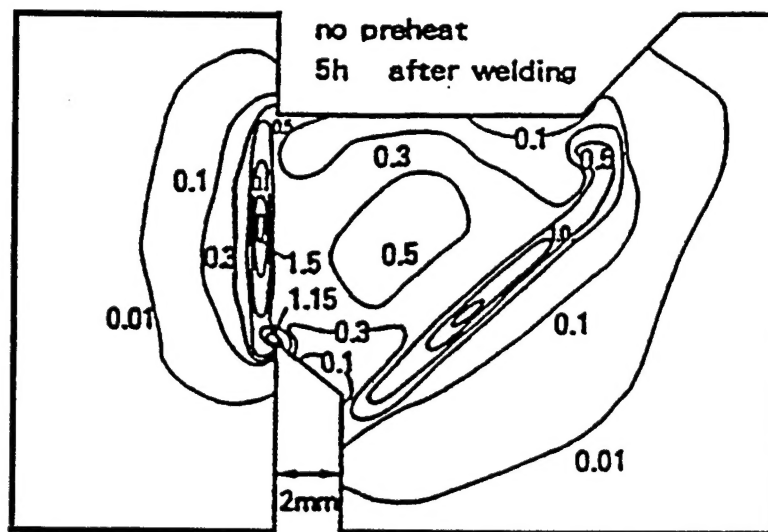


Figure 6. Distribution of hydrogen (non-dimensional concentration with respect to initial concentration in weld metal) in single bevel groove weld, 5 hrs. after welding [25,26]

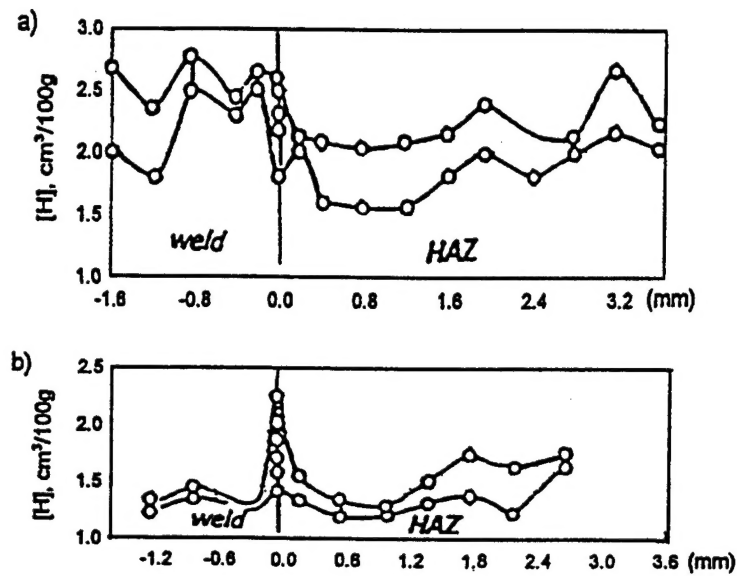


Figure 7. Distribution of hydrogen in a welded joint of 15Kh1M1F steel. (a). not heat treated after welding. (b). tempered at a high temperature (730° C) after welding [27].

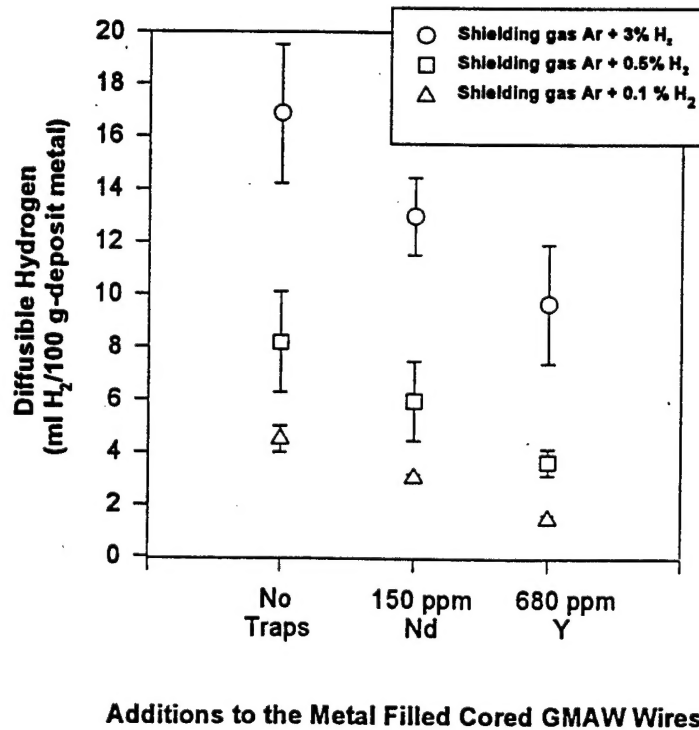


Figure 8. Effect of trap additions to the amount of diffusible hydrogen of weld samples welded with GMAW process at nominal heat input 1.5 kJ/mm [34].

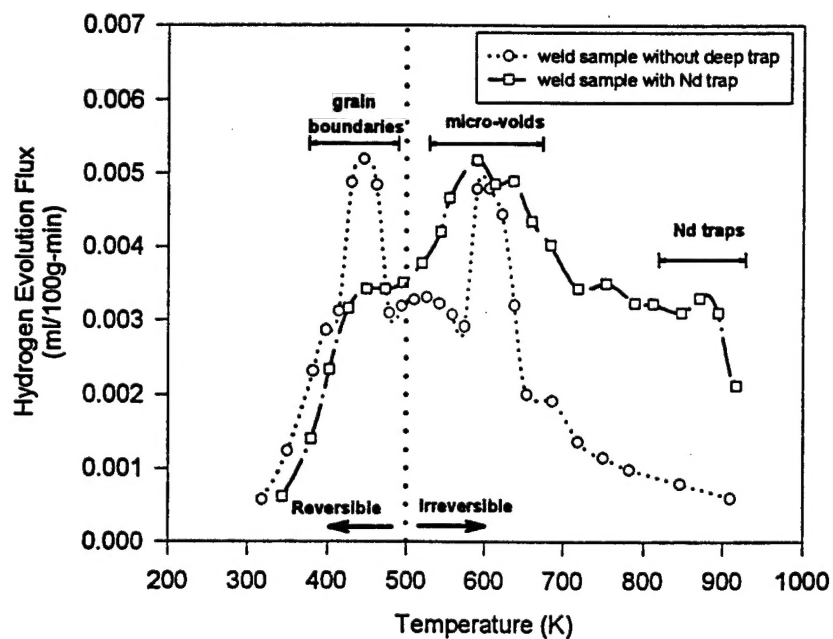


Figure 9. Hydrogen desorption at  $4^{\circ}\text{C/min}$  heating rate of iron weld sample free of deep traps and weld sample containing neodymium deep traps. The peak at 450 K is the hydrogen released from grain boundaries, at 600 K from micro-voids and at 873 K from neodymium associated trap sites [34].

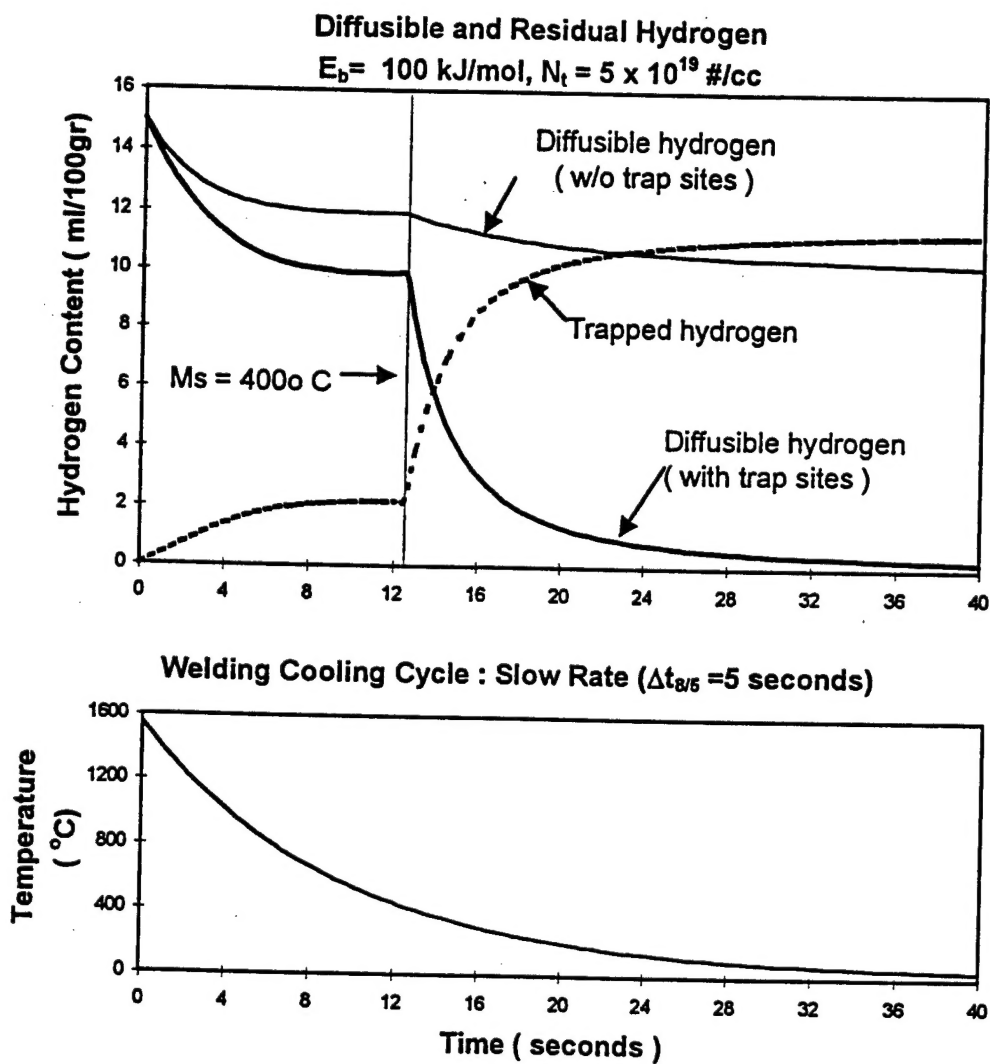


Figure 10. Theoretical evaluation on the performance of hydrogen trapping during welding cooling cycle. Initial diffusible hydrogen in the weld metal is 15 ml/100 g-deposit metal [6].